Nouvelle physique entre Cosmologie et le LHC : Axions, Neutrinos et Z'

M. Elmer

Thèse

présentée devant

l'Université Claude Bernard Lyon - I

École Doctorale de Physique et d'Astrophysique

pour l'obtention du

DIPLÔME de DOCTORAT

Spécialité : Physique Théorique / Physique des Particules

(arrêté du 7 août 2006)

par

Martin ELMER

Nouvelle physique entre Cosmologie et le LHC : Axions, Neutrinos et Z'

A soutenir publiquement le 18 Septembre 2014 devant la Commission d'Examen

M.	J.	Gascon	*Président du jury*	-	IPN Lyon
M.	J.	Lesgourgues	*Rapporteur*	-	CERN Genève, EPFL Lausanne
M.	G.	Raffelt	*Rapporteur*	-	MPP Munich
M.	M.	Frigerio	*Examinateur*	-	L2C Montpellier
Mme.	S.	Davidson	*Directeur de thèse*	-	IPN Lyon

PHD THESIS of the UNIVERSITY of LYON

Delivered by the UNIVERSITY CLAUDE BERNARD LYON 1

Subject:

THEORETICAL PHYSICS / PARTICLE PHYSICS

submitted by

Mr. MARTIN ELMER

for the degree of

DOCTOR OF PHILOSOPHY

New physics between Cosmology and the LHC: Axions, Neutrinos and Z'

To defend September 18th, 2014 in front of the following Examining Committee:

Mr.	J.	Gascon	*President*	-	IPN Lyon
Mr.	J.	Lesgourgues	*Reviewer*	-	CERN Genève, EPFL Lausanne
Mr.	G.	Raffelt	*Reviewer*	-	MPP Munich
Mr.	M.	Frigerio	*Examiner*	-	L2C Montpellier
Mrs.	S.	Davidson	*Supervisor*	-	IPN Lyon

Remerciements

First of all I would like to thank my PhD supervisor Sacha Davidson for all the advice and help during the last three years. Thank you for the interesting projects, for showing me how scientific work is done and also for giving me the liberty to do some research "on my own".

I would also like to thank Guillaume Drieu La Rochelle for our project among young scientists and for introducing me into the world of collider phenomenology and some of its tools in an incredibly short time. My thanks to Georg Raffelt for many useful discussions on the axion project as well as for hospitality during my stay in Munich at the beginning of that project.

I would also like to Julien Lesgourgues and Georg Raffelt for having accepted to be reviewer of my thesis and spending some of your precious time on reading my thesis, writing a report and numerous constructive remarks.

I also want to thank Jules Gascon for being the president of my examining committee and Michele Frigerio for having accepted to be examiner of my thesis.

Je tiens aussi à remercier l'ensemble du personnel de l'IPNL et plus particulièrement le groupe de physique théorique pour l'accueil sympathique qui m'a été réservé pendant ces trois dernières années. Je voudrais remercier Aldo, Giaccomo, Luca, Hubert, Jean-Marc, Dany et mon parrain Antoine pour leurs conseils et les conversations que nous avons eues au cours des ces trois derniers ans. Merci à Christopher pour les conseils scientifiques ainsi que pour me faire découvrir la vie d'un jeune chercheur. Un très grand merci au groupe de "manger à 11h40" pour la bonne ambiance apportée au quotidien et pour les soirées inoubliables.

Thanks to Jean-Baptiste, Guillaume, Nicolas, Ahmad, Daniel and Martin for the afternoon coffee breaks with an almost uncountable number of useful as well as useless discussions about physics, math and life!

Merci à Fosca et Tatjana pour les soirées ensembles, les rigolades et votre amitié. Vos visions de la vie en thèse m'ont beaucoup aidé à traverser les périodes désertes que l'aventure de la thèse réserve. Un très grand merci aussi à Julien, Catherine, Étienne et tous les autres qui ont rendu la vie à Lyon aussi splendide.

Je voudrais aussi remercier le "CAF dissident": Marie, Anne, Benoit, Céline, Julien, Clémence et ses autres membres associés pour m'avoir montré la beauté des alpes françaises, pour votre enthousiasme à organiser des soties ensembles ainsi que votre savoir vivre français.

Vielen Dank an Parcley, Paty, Chiller, Maria, Roman, Resi, Gattal, Gifti, Maxi und den Rest der "Hüttengemeinschaft" für die legendären Tage im Winter als auch für eure stete Freundschaft während der letzten vier Jahre.

Am meisten möchte ich meinen Geschwistern und meinen Eltern danken: ohne eure unermütliche Untertützung und euren Rückhalt wäre dieses Unterfangen schlicht unmöglich gewesen. Ich danke euch von ganzem Herzen.

Merci à Élisa pour simplement TOUT!

Abstract

During the three years as a PhD student I had the pleasure to work on three major projects which are united in the goal to better constrain new physics models between cosmology and the LHC.

The similar values of dark matter and baryon relic abundances raise the question whether there is a link between them. We attempt to explain the observed values by relating leptogenesis to the WIMP miracle which gives naturally the right relic abundance. If the baryon asymmetry is produced in electroweak-scale-out-of-equilibrium decays and dark matter is made of WIMPs, both relic densities are controlled by electroweak scale interactions going out of equilibrium. We construct a TeV-scale leptogenesis model using an inverse-seesaw extension of the SM with additional singlets. To produce a large enough asymmetry we require CP violation $\sim \mathcal{O}(1)$ which is difficult to achieve in our set-up.

Axions as well as WIMPs are well motivated dark matter candidates. It would be very useful to be able to tell them apart. Sikivie argues that if axions are in a Bose-Einstein condensate they could form a different galactic dark matter halo than WIMPs and that gravitational interactions drive axions into a Bose-Einstein condensate. However for the formation of such a condensate entropy generation is needed which leading order gravitational interactions do not provide. We explore the entropy generation of gravitational interactions by estimating a dissipation scale in the axion fluid due to the presence of a anisotropic stress. We cannot confirm a fast gravitational thermalisation rate.

New neutral gauge bosons like the Z' are generic extensions of the standard model which appear in many different models. Traditionally these particles are searched for in resonant searches at colliders, i.e. by producing the particles on-shell and looking for a resonance in the invariant mass spectrum of their decay products. However the presence of a Z' can also affect other kinematic observables without being actually produced on-shell, i.e. non-resonant searches. We compare compare resonant and non-resonant searches at the LHC and find that while for small couplings resonant searches are more sensitive, for larger couplings non-resonant searches are more efficient.

Résumé

Pendant mes trois ans de doctorat j'ai eu le plaisir de travailler sur trois projets très variés ayant un but commun: mieux contraindre certains modèles de nouvelle physique entre cosmologie et le LHC.

Le fait que les densités reliques de matière noire et de baryons sont similaires semble indiquer qu'il y a un lien entre les deux. Nous essayons d'expliquer les valeurs observées en reliant un modèle de leptogenèse au miracle des WIMPs, qui produit naturellement la bonne densité relique. Si l'asymétrie baryonique est produit dans des désintégrations hors équilibre à l'échelle électro-faible et si la matière noire est constituée de WIMPs, les deux densités reliques sont contrôlées par des processus électro-faibles hors équilibre. Je construis un modèle de leptogenèse à l'échelle du TeV en utilisant une extension du type seesaw inverse du modèle standard avec des singlets additionnels. Pour produire suffisamment d'asymétrie baryonique il faut une violation $CP \sim \mathcal{O}(1)$ qui est difficile à obtenir dans mon cadre.

Les axions, tout comme les WIMPs sont de bons candidats de matière noire bien motivés. Il serait très utile de pouvoir les distinguer. Sikivie argumente que si des axions sont dans un condensat de Bose-Einstein, alors ils forment des halos galactiques différents des halos de WIMPs. D'après Sikivie ce sont les interactions gravitationnelles qui thermalisent les axions et qui les condensent. La formation d'un condensat nécessite la génération d'entropie qui ne peut pas être fourni par les interactions gravitationnelles au premier ordre. J'étudie la génération d'entropie par les interactions gravitationnelles en estimant une longueur de dissipation dans le fluide d'axions qui vient de la présence d'une pression anisotrope. Je ne peux pas confirmer la thermalisation rapide d'axions causé par leurs interactions gravitationnelles.

Des nouveaux bosons de jauges comme le Z' apparaissent dans un grand nombre d'extensions du modèle standard. On les recherche le plus souvent comme une résonance dans le spectre de masse invariante de leurs produits de désintégration. Le Z' doit être produit sur couche de masse dans ces recherches résonantes. Mais la présence d'un Z' peut aussi influencer d'autres observables cinématiques sans être produit directement, ce qu'on peut utiliser dans des recherches non-résonantes. Je compare ces deux types de recherches au LHC et trouve que pour des petits couplages les recherches résonantes sont plus adaptées mais pour de plus grandes masses et couplages les recherches non-résonantes sont plus performantes.

Contents

Introduction 1

I Framework 5

1 The standard model of particle physics and beyond 7
1.1 The Standard Model of particle physics . . . 7
1.1.1 Gauge sector . . . 7
1.1.2 Fermion sector . . . 8
1.1.3 Higgs sector . . . 9
1.1.4 Yukawa sector . . . 10
1.2 Beyond the SM . . . 11
1.2.1 Signs for new physics . . . 11
1.2.2 New physics models . . . 13

2 Cosmology and its standard model 15
2.1 Geometry and matter content of our universe . . . 15
2.2 Thermal history . . . 18
2.2.1 Thermodynamics in an expanding universe . . . 18
2.2.2 Early stages . . . 21
2.3 Cosmological perturbation theory . . . 25
2.3.1 Theoretical treatment . . . 25
2.3.2 Large scale structure power spectrum . . . 28
2.3.3 CMB anisotropies . . . 30
2.4 Dark Matter . . . 33
2.4.1 Evidence for dark matter . . . 33
2.4.2 Candidates . . . 35
2.4.3 Search for DM . . . 38

3 Neutrino physics beyond the SM 41
3.1 Neutrino oscillations . . . 41
3.1.1 Dirac mass term . . . 41
3.1.2 Neutrino oscillation theory . . . 42
3.1.3 Neutrino oscillation experiments . . . 45
3.1.4 Cosmological neutrino constraints . . . 48
3.2 Seesaw mechanism . . . 50
3.2.1 Majorana mass term . . . 50
3.2.2 Seesaw . . . 52

II Leptogenesis project **55**

4 Baryogeneis through leptogenesis **57**
4.1 Introduction . . . 57
4.2 Thermal leptogenesis . . . 59
4.2.1 C and CP violation . . . 60
4.2.2 Out-of-equilibrium dynamics: η_α . . . 60
4.2.3 Lepton number and $B+L$ violation . . . 62
4.3 CP violation . . . 64
4.3.1 General properties . . . 64
4.3.2 Calculating CP violation rates . . . 65

5 Relating leptogenesis to the WIMP miracle **67**
5.1 Introduction . . . 67
5.2 Review, Notation and Masses . . . 68
5.2.1 Observations . . . 68
5.2.2 Models . . . 69
5.2.3 Notation and Masses . . . 70
5.3 Thermal History . . . 72
5.3.1 $\psi\overline{\psi} \to \phi\overline{\phi}$ annihilations . . . 72
5.3.2 Decays and the CP asymmetry . . . 73
5.3.3 Washout of the asymmetry by inverse decays and scattering . . . 75
5.3.4 Putting it all together in the Majorana case . . . 77
5.3.5 Dirac limit . . . 77
5.4 Discussion . . . 79

III Axion project **83**

6 Introduction to axions **85**
6.1 Strong CP problem and axions . . . 85
6.1.1 Generic axion features . . . 86
6.1.2 Axion as Nambu-Goldstone Boson . . . 86
6.1.3 Different axion models . . . 89
6.2 Axions in Cosmology . . . 89
6.2.1 Thermal production . . . 90
6.2.2 Misalignment angle mechanism . . . 91
6.2.3 Cosmic strings and domain walls . . . 92
6.3 Bounds on axions . . . 92
6.3.1 Astrophysical bounds . . . 92
6.3.2 Experimental axion searches . . . 93
6.3.3 Cosmological bounds . . . 93

7 Observable axion WIMP difference? **99**
7.1 The initial idea . . . 99
7.2 Do axions form a Bose-Einstein condensate in cosmology? . . . 100
7.2.1 Bose-Einstein condensation . . . 101
7.2.2 Axions and Gravity, the standard picture . . . 101
7.2.3 Axion viscosity estimate . . . 108

7.2.4 Discussion . . . 110
7.2.5 Summary . . . 112

IV Z' project **113**

8 Heavy Z': resonant versus non-resonant searches **115**
8.1 Introduction . . . 115
8.2 Framework . . . 116
8.3 Analysis . . . 118
8.3.1 t-channel: Dijet angular spectrum . . . 118
8.3.2 t-channel: Inclusive jet p_T spectrum . . . 118
8.3.3 s-channel: Dijet resonance . . . 119
8.3.4 s-channel: $t\bar{t}$ resonance . . . 119
8.4 Results . . . 119
8.4.1 Observed results . . . 119
8.4.2 Projections at higher luminosities . . . 121
8.5 Conclusion . . . 122
8.6 Appendix: Details on analysis recasts . . . 124
8.6.1 t-channel: Dijet angular spectrum . . . 124
8.6.2 t-channel: Inclusive jet p_T spectrum . . . 124
8.6.3 s-channel: Dijet resonance . . . 125
8.6.4 s-channel: $t\bar{t}$ resonance . . . 126

Conclusion & outlook **127**

Introduction

What are we made of? Where do we come from? These are two questions that have concerned humanity for a very long time. Modern physics is unable to answer these philosophic questions but one can find partial answers to them by rephrasing the questions in a more scientific way: What are the elementary constituents of matter? What is the history of our universe? Physics has developed two domains that try to answer these questions: particle physics and cosmology. It is quite surprising to see that both questions are actually related to each other: in the early history of the universe the elementary constituents of matter describe the evolution of the universe. It is impossible to answer the second question without having a good understanding of the first one. The other way around by studying the second question one can establish the existence of new constituents that have not yet been identified by particle physics, like e.g. dark matter.

The two domains are governed by the two most fundamental theories of modern physics: Particle physics is formulated in the language of quantum mechanics (or quantum field theory). Cosmology is only possible in the context of Einstein's theory of general relativity. These two theories have been my motivation to start the long and difficult adventure of studying physics at university and later to launch into a PhD that is situated at the interface of the two domains.

In particle physics the standard model (SM) has proven to be very successful in accurately predicting observables that have been verified by a very large number of measurements. The SM describes the fundamental constituents of matter, their interactions with each other and how they finally form the non-elementary bricks of matter that we call atoms. In cosmology the Λ Cold Dark Matter model provides an excellent fit to the observed data. It states that the universe today is dominated by a cosmological constant and non-relativistic matter. However most of the non-relativistic matter comes from a still unknown source, called dark matter. Only $\sim 15\%$ of the observed non-relativistic matter can be explained using the matter content of the particle physics SM.

Even if both models are very successful it is clear that neither is complete. In cosmology different issues, e.g. the flatness problem, the horizon problem and the origin of perturbations ask for an extension of the cosmological standard model. Until today the most likely extension seems to be inflation (there are several indirect evidences in favor of inflation, a first direct one was recently announced by the BICEP2 collaboration, subject to confirmation). The SM of particle physics can neither explain the nature of dark matter nor the baryon asymmetry of the universe that is observed in cosmology. Furthermore neutrino oscillations, the hierarchy problem and the strong CP problem tell us that also in particle physics extensions of the SM are needed. On the theoretical side we are still badly in need of a theory that unites both quantum field theory and general relativity in one "theory of everything".

Current experiments like the LHC, the PLANCK satellite or numerous other experiments further test the standard models and measure their parameters with unprecedented precision. But they also have the potential to discover what is called new physics, extensions to the stan-

dard models, or to constrain these possible extensions. In this context it is the theorists role to infer to new models that can explain as many observed phenomena as possible while keeping the models as simple as possible. However it is not enough to create new models, a lot of theoretical work is done to derive observables that constrain new models with already existing measurements and to develop ways how to test new models in the most efficient way.

This thesis, which is situated somewhere between particle physics and cosmology, makes a very small contribution to both parts of theoretical work: constructing a new model and examining new and efficient ways to test existing extensions of the SM. The work done during the three years of PhD can easily be structured according to the four publications. The first project, which was mainly done during the master thesis, concentrated on the constraints on a simple supersymmetric seesaw extension [1]. We used a supersymmetric type I seesaw model with two, three or four singlets and examined the possibility of reconstructing the high energy parameters from observations at low energies. To estimate the rate of rare decays we used a "minimal-flavour-violation-like" ansatz for supersymmetry. As this work has already been presented in the master thesis it is not included in this thesis.

In the second project we were trying to relate the dark matter relic density to the baryon relic density by using an extended leptogenesis model at the TeV-scale [2]. The basic idea is to relate the baryon relic density to the WIMP relic density which is naturally of the right order. This can be established if the baryon-parent particle freeze-out density is of the same order as the WIMP density and if the CP violation in the parent decays is of order 1. We construct such a leptogenesis model using a inverse seesaw model containing extra light singlets and scalars that creates the baryon asymmetry prior to electroweak phase transition.

The third project concentrated on Sikivie's new idea on how to distinguish between WIMP and axion cold dark matter [3]. Sikivie's idea states that if axions are in a Bose-Einstein condensate they form a different galactic dark matter halo than WIMPs. We claim that leading order gravitational interactions are fast but do not contribute to a Bose-Einstein condensation of axions because they do not create entropy. We estimate the gravitational entropy creation by calculating the dissipation rate of axions due to anisotropic stress. We cannot confirm that axions produce enough entropy in their gravitational interactions to form a Bose-Einstein condensate.

The fourth and final project examined possible collider search strategies for an additional neutral gauge bosons like the Z' [4]. New heavy gauge bosons are usually searched for in resonant searches where the new particle is created on-shell and shows itself as a peak in the invariant mass spectrum. However an off-shell Z' exchange can leave an imprint on other kinematic distributions, leading thus to non-resonant searches. We show that non-resonant searches are less sensitive for small couplings but can give stronger constraints than resonant searches when couplings are large.

To present the work accomplished during the three years of PhD, the thesis is divided into four parts:

- Part I
  The first part reviews the framework of this thesis. The first chapter gives a very condensed review of the SM of particle physics as a gauge theory. In the second chapter one finds a short description of cosmology containing the geometry of space-time, the thermal history and linear perturbation theory as well as some details on dark matter. The theory and experimental status of neutrino oscillations are shown in chapter 3. It also contains an introduction to the seesaw mechanism that gives a natural explanation for the smallness

of neutrino masses.

– Part II
The second part of this thesis is dedicated to the project on leptogenesis. Chapter 4 contains an overview of the general idea of leptogenesis and how it works in its simplest realization. In chapter 5 one can find our attempt to link baryon abundance to the WIMP miracle using a TeV-scale leptogenesis model that is based on a inverse seesaw mechanism with additional singlets. Chapter 5 consists of the published article [2].

– Part III
The third part contains the axion project. In chapter 6 a review of axions is given. It contains an explanation of the strong CP problem, the Peccei-Quinn mechanism as a solution predicting the presence of axions, the role of axions in cosmology and constraints on the axion parameter space from direct searches, astrophysics and cosmology. Chapter 7 introduces Sikivie's idea of an observable difference in the galactic dark matter halo between axions and WIMPs as dark matter constituents. Then follows our estimate on the Bose-Einstein condensation of dark matter axions through gravitational interactions based on [3] but presented in a slightly different way.

– Part IV
The last part of this thesis is used to present the work on the ideal search strategy for additional neutral gauge bosons at the LHC [4]. It compares resonant and non-resonant searches for a Z' model and finds that for small coupling the resonant searches are stronger whereas for large couplings it is more efficient to use non-resonant searches to constrain such models.

Part I

Framework

Chapter 1

The standard model of particle physics and beyond

1.1 The Standard Model of particle physics

The standard model (SM) of particle physics is a renormalizable quantum field theory that describes the interactions between the elementary constituents of matter. The basic properties of the SM are fixed by its symmetry groups: in addition to the Poincaré group, the SM is invariant under the gauge groups $SU_C(3) \times SU_W(2) \times U_Y(1)$. The latter two symmetries describe the electroweak (EW) interactions while the $SU(3)$ symmetry describes strong interactions, also called quantum chromo dynamics (QCD). The complication of QCD compared to EW interactions is that quarks are confined into hadrons at low energy and that they are no free initial or final states.

Matter fields have charges under these symmetries that describe their transformation under the three gauge symmetries. They restrict the possible combinations of fields in the Lagrangian and determine so the possible interactions between particles. The interactions are mediated by the gauge bosons that correspond to the symmetry: the strong interactions contain 8 gluons G^A_μ with $A \in 1, .., 8$, the electroweak interactions involve four bosons, W^a_μ with $a \in 1, 2, 3$ and B_μ. When the EW symmetry is broken into electromagnetic symmetry $U(1)_{\text{EM}}$ by the Brout-Englert-Higgs mechanism [5, 6] the electroweak vector bosons transform into three massive vector bosons $W^\pm, Z$ and the massless photon γ. The charges of all SM fields are summarized in table 1.1.

The Lagrangian of the SM can be divided into four different parts: the gauge sector $\mathcal{L}_G$, the Higgs sector $\mathcal{L}_H$, the fermion or matter sector $\mathcal{L}_F$ and the Yakawa sector $\mathcal{L}_Y$. In order to introduce the used notations all four parts will be reviewed quickly. More pedagogic introductions to the SM and gauge field theories in general can be found in many books, e.g. [7, 8, 9].

$$\mathcal{L} = \mathcal{L}_G + \mathcal{L}_H + \mathcal{L}_F + \mathcal{L}_Y \tag{1.1}$$

1.1.1 Gauge sector

The kinetic terms of the gauge fields are

$$\mathcal{L}_G = -\frac{1}{4} B^{\mu\nu} B_{\mu\nu} - \frac{1}{4} \sum_{a=1}^{3} W^{a\mu\nu} W^a_{\mu\nu} - \frac{1}{4} \sum_{A=1}^{8} G^{A\mu\nu} G^A_{\mu\nu} \tag{1.2}$$

where $B^{\mu\nu}$, $W^{a,\mu\nu}$ and $G^{A,\mu\nu}$ are the field strength tensors of the gauge fields associated to the symmetries $U(1)_Y$, $SU(2)_W$ and $SU(3)_C$. They are given by the following combination of gauge

fields

$$\begin{aligned} B^{\mu\nu} &= \partial^\mu B^\nu - \partial^\nu B^\mu \\ W^{a\mu\nu} &= \partial^\mu W^{a\nu} - \partial^\nu W^{a\mu} + g_w \epsilon^{abc} W^{b\mu} W^{c\nu} \\ G^{A\mu\nu} &= \partial^\mu G^{A\nu} - \partial^\nu G^{A\mu} + g_\mathrm{s} f^{ABC} G^{B\mu} G^{C\nu} \quad . \end{aligned} \tag{1.3}$$

The coupling constants for the three symmetry groups are called g_Y, g_w, and g_s. The structure constants for the non-abelian groups $SU(2)$ and $SU(3)$ are ϵ^{abc} and f^{ABC} respectively. Gauge fixing terms and ghost terms are not specified here because they are not need throughout this thesis.

1.1.2 Fermion sector

The fermion sector contains kinetic terms of all matter fields. To make the kinetic terms invariant under the local gauge symmetries one has to introduce covariant derivatives. The covariant derivatives induce the gauge interactions of fermions according to the charge of the fermion field. The SM is a chiral theory, gauge interactions do not couple in the same way to left as to right-handed fields (as can be seen from table 1.1). Therefore we write separate terms for left and right-handed Dirac spinors.

$$\mathcal{L}_F = i\,\overline{\ell_{Li}} \not{D} \ell_{Li} + i\,\overline{e_{Ri}} \not{D} e_{Ri} + i\,\overline{q_{Li}} \not{D} q_{Li} + i\,\overline{u_{Ri}} \not{D} u_{Ri} + i\,\overline{d_{Ri}} \not{D} d_{Ri} \tag{1.4}$$

Field	Notation	$SU(3)_C$	$SU(2)_W$	$U(1)_Y$	$U(1)_\mathrm{EM}$	t^3
Quarks($s=1/2$)	$q_{Li} = \begin{pmatrix} u_L \\ d_L \end{pmatrix}, \begin{pmatrix} c_L \\ s_L \end{pmatrix}, \begin{pmatrix} t_L \\ b_L \end{pmatrix}$	3	2	1/6	$\begin{pmatrix} 2/3 \\ -1/3 \end{pmatrix}$	$\begin{pmatrix} 1/2 \\ -1/2 \end{pmatrix}$
	$u_{Ri} = u_R, c_R, t_R$	3	1	2/3	2/3	0
	$d_{Ri} = d_R, s_R, b_R$	3	1	$-1/3$	$-1/3$	0
Leptons($s=1/2$)	$\ell_{Li} = \begin{pmatrix} \nu_e \\ e_L \end{pmatrix}, \begin{pmatrix} \nu_\mu \\ \mu_L \end{pmatrix}, \begin{pmatrix} \nu_\tau \\ \tau_L \end{pmatrix}$	1	2	$-1/2$	$\begin{pmatrix} 0 \\ -1 \end{pmatrix}$	$\begin{pmatrix} 1/2 \\ -1/2 \end{pmatrix}$
	$e_{Ri} = e_R, \mu_R, \tau_R$	1	1	-1	-1	0
Gauge($s=1$)	g	8	1	0	0	0
	$W^3, W^\pm$	1	3	0	$0, \pm 1$	$\{1, 0, -1\}$
	B	1	1	0	0	0
Higgs($s=0$)	$H = \begin{pmatrix} \phi^+ \\ \phi_0 = \frac{1}{\sqrt{v}}(v + h + i\varphi_0) \end{pmatrix}$	1	2	1/2	$\begin{pmatrix} 1 \\ 0 \end{pmatrix}$	$\begin{pmatrix} 1/2 \\ -1/2 \end{pmatrix}$

Table 1.1: The SM fields with their representations under $SU(3)_C$ and $SU(2)_W$, their charges under $U(1)_Y$ and $U(1)_\mathrm{EM}$ and their weak isospin projection t^3. The electric charge is given by $Q = t^3 + Y$

The family index i is summed over. Colour indices have been removed for more readability. The covariant derivative is defined as

$$D_\mu = \partial_\mu - i\ g_\mathrm{s}\theta_\mathrm{s}G^A_\mu T^A - i\ g_\mathrm{w}\theta_\mathrm{w}W^a_\mu t^a - i\ g_Y Y B_\mu \ . \tag{1.5}$$

The generators of the $SU(3)_C$ and $SU(2)_W$ groups are called T^A and t^a [1] respectively. Y is the weak hypercharge, $\theta_\mathrm{s} = 0, 1$ for colour singlets or triplets, and $\theta_\mathrm{w} = 0, 1$ for singlets or doublets under the weak symmetry group.

1.1.3 Higgs sector

The Higgs sector is an essential part of the SM, it is responsible for the spontaneous breaking of the electroweak symmetries to the electromagnetic symmetry by giving mass terms to three gauge bosons. In order to break the EW symmetries spontaneously one introduces a $SU(2)_W$ doublet scalar field that respects all symmetries of the SM in its interactions. However its vacuum expectation value does not respect all symmetries:

$$\langle H \rangle = \frac{1}{\sqrt{2}}\begin{pmatrix}0\\ v\end{pmatrix} \ . \tag{1.6}$$

The Higgs being a singlet under colour symmetry, we will only consider its transformation under the electroweak symmetry groups: $H \to e^{i\alpha^a t^a}e^{i\beta/2}H$. The transformations leave the vacuum expectation value $\langle H \rangle$ invariant only if $\alpha^1 = \alpha^2 = 0$ and $\alpha^3 = \beta$. Consequently the theory will contain one massless gauge boson corresponding to this particular combination of generators. The other three gauge bosons will acquire mass. The kinetic and potential terms for the Higgs field are

$$\mathcal{L}_H = |D_\mu H|^2 + \mu^2 H^\dagger H - \lambda (H^\dagger H)^2 \ . \tag{1.7}$$

This is one of the easiest possible potentials that provides a vacuum expectation value for the Higgs field. The minimum of the potential occurs at $v = \sqrt{\frac{\mu^2}{\lambda}}$. The covariant derivative for the Higgs field is given by

$$D_\mu H = (\partial_\mu - i\ g_\mathrm{w}W^a_\mu t^a - i\ \frac{1}{2}g_Y B_\mu)H \ . \tag{1.8}$$

The mass terms for the gauge bosons have their origin in the kinetic energy term evaluated for the vacuum expectation value of the Higgs field. The relevant terms can be obtained by using the explicit form of the generators $t^a = \sigma^a/2$ in terms of the Pauli matrices:

$$\begin{aligned}\mathcal{L}_\Delta &= \frac{v^2}{8}\left[g^2_\mathrm{w}(W^1_\mu)^2 + g^2_\mathrm{w}(W^2_\mu)^2 + (-g_\mathrm{w}W^3_\mu + g_Y B_\mu)^2\right] \\ &= \frac{v^2}{4}g^2_\mathrm{w}W^+_\mu W^{-\mu} + \frac{v^2}{8}(g^2_\mathrm{w} + g^2_Y)Z_\mu Z^\mu \ .\end{aligned} \tag{1.9}$$

In the last step we have diagonalized the mass term using the linear combinations

$$W^\pm_\mu = \frac{1}{\sqrt{2}}(W^1_\mu \mp iW^2_\mu) \qquad \text{with mass} \qquad m_W = g_\mathrm{w}\frac{v}{2} \tag{1.10}$$

$$Z_\mu = \frac{1}{\sqrt{g^2_\mathrm{w} + g^2_Y}}(g_\mathrm{w}W^3_\mu - g_Y B_\mu) \qquad \text{with mass} \qquad m_Z = \sqrt{g^2_\mathrm{w} + g^2_Y}\frac{v}{2} \tag{1.11}$$

1. For $SU(2)$ the generators can be written as $t^a = \sigma^a/2$ with σ^a being the Pauli matrices.

The fourth gauge field, orthogonal to Z_μ, is the photon which is given by

$$A_\mu = \frac{1}{\sqrt{g_{\rm w}^2 + g_Y^2}}(g_Y W_\mu^3 + g_{\rm w} B_\mu) \ . \tag{1.12}$$

After spontaneous symmetry breaking three gauge bosons become massive and only the gauge boson of the new $U(1)_{\rm EM}$, the photon, is massless. The interactions of the "new" gauge bosons can be derived by simply rewriting the covariant derivative. For this aim one defines $t^\pm = (t^1 \pm i t^2)$.

$$D_\mu = \partial_\mu - i\frac{g_{\rm w}}{\sqrt{2}}(W_\mu^+ t^+ + W_\mu^- t^-) - i\frac{1}{\sqrt{g_{\rm w}^2 + g_Y^2}} Z_\mu (g_{\rm w}^2 t^3 - g_Y^2 Y) - i\frac{g_{\rm w} g_Y}{\sqrt{g_{\rm w}^2 + g_Y^2}} A_\mu (t^3 + Y) \tag{1.13}$$

From the coupling constant in front of the photon the electron charge and the electric charge operator Q can be found to be

$$e = \frac{g_{\rm w} g_Y}{\sqrt{g_{\rm w}^2 + g_Y^2}} = g_{\rm w} \sin(\theta_W) \qquad \text{and} \qquad Q = t^3 + Y \tag{1.14}$$

where we have introduced the Weinberg angle θ_W which is defined by $\sin(\theta_W) = \frac{g_Y}{\sqrt{g_{\rm w}^2 + g_Y^2}}$.

At the end, only the Higgs boson h (see table 1.1) remains physical. The fields φ_0 and $\phi^\pm$ are Goldstone bosons associated to the symmetry breaking. In unitary gauge they will be "eaten" by the Z, $W^\pm$ to create the longitudinal polarization of the heavy gauge fields. The mass of the remaining Higgs boson is $m_h = \sqrt{2}\mu = \sqrt{2\lambda}v$. The CMS [10] and Atlas [11] collaborations found a new particle that seems to be the predicted Higgs boson. The mass of the observed resonance is at $m_h \approx 125$ GeV.

1.1.4 Yukawa sector

Until now all matter fields are massless. Normal mass terms mix left and right-handed components of fermion fields and therefore violate gauge invariance. To write a gauge invariant mass term one uses the Higgs doublet field. Then mass terms violate gauge invariance only spontaneously when the Higgs field takes its vev. The fermion-Higgs couplings are called Yukawa couplings

$$\mathcal{L}_Y = -Y_d'^{ij} \overline{q_L}^i \cdot H d_R^i - Y_u'^{ij} \overline{q_L}_a^i (i\sigma_2)^{ab} H_b u_R^i - Y_\ell'^{ij} \overline{\ell_L}^i \cdot H e_R^j \tag{1.15}$$

The Yukawa matrices are general, not necessarily symmetric or Hermitian complex-valid matrices. To diagonalize the mass matrices we can define six unitary matrices so that

$$Y_u' = U_u Y_u W_u^\dagger \quad \text{and} \quad Y_d' = U_d Y_d W_d^\dagger \quad \text{and} \quad Y_\ell' = U_\ell Y_\ell W_\ell^\dagger \tag{1.16}$$

where Y_u,Y_d and Y_ℓ are real diagonal matrices. We now change variables, starting with right-handed quarks

$$u_R^i \to W_u^{ij} u_R^j \quad \text{and} \quad d_R^i \to W_d^{ij} d_R^j \tag{1.17}$$

The three families of right-handed quarks have the same gauge couplings and do not mix u_R and d_R terms, so that the W matrices commute with the covariant derivatives and cancel out of the theory. For the left-handed quarks we do the same change in variables

$$u_L^i \to U_u^{ij} u_L^j \quad \text{and} \quad d_L^i \to U_d^{ij} d_L^j \tag{1.18}$$

Using these variables the Yukawa couplings for quarks are diagonal. The strong gauge interactions commute with the U matrices so that strong interactions are not modified. However the $SU(2) \times U(1)$ interactions mix u_L and d_L in the couplings to $W^{\pm}$. The change in variable lets a mixing matrix appear

$$g_{\mathrm{w}} W_{\mu}^{+} \frac{1}{\sqrt{2}} (\overline{u_L}^{i} \gamma^{\mu} d_L^{i}) \rightarrow g_{\mathrm{w}} W_{\mu}^{+} \frac{1}{\sqrt{2}} (\overline{u_L}^{i} (U_u^{\dagger} U_d)^{ij} \gamma^{\mu} d_L^{j}) \ . \tag{1.19}$$

The appearing matrix $U_{\mathrm{CKM}} = U_u^{\dagger} U_d$ is called the Cabbibo-Kobayashi-Maskawa matrix. In the SM it is the only term that mixes quarks of different families. The CKM matrix can be parametrized by three mixing angles and a CP violating phase, which are all very precisely measured [12]. The couplings to photons A^{μ} and Z_{μ} are not affected by the change of variables.

For leptons the same diagonalisation procedure can be done. The transformations of right-handed leptons cancel out and the transformations of the left-handed charged leptons appear in the couplings to $W^{\pm}$. However the appearing matrix can be absorbed in a redefinition of the left-handed neutrino field that has no mass term in the SM. In the end all gauge interactions stay unchanged and the letpon mass matrix is diagonal. This is only due to the fact that neutrinos are massless in the SM. Massive neutrinos change this situation so that a second mixing matrix appears, as seen in chapter 3.1.1.

1.2 Beyond the SM

1.2.1 Signs for new physics

The SM model is one of the best tested theories in physics today. It has been tested on a large range of energies: from the atomic structures (eV -range) to high energy colliders up to the TeV scale. In almost all cases the predictions are in very good agreement with observed values, especially the electroweak precision tests are in spectacular agreement with data (e.g. table 10.5 of [12]). However today we can be sure that the SM is not the end of the story of particle physics. Several issues give very clear indications for physics beyond the SM. Here we will give a short and not exhaustive list of signs for physics beyond the SM.

Theoretical puzzles

First let us start by mentioning theoretical puzzles of the SM. These problems are not consistency problems of the SM but they are, at least from a theoretical point of view, unsatisfying. It is obvious that the SM cannot be the whole theory of particle interactions because it describes only three of the four elementary interactions of matter. Gravitational interactions are not included in the SM and until today it is unclear how to quantize gravity and "add" it to the interactions of the SM. Another issue is the large hierarchy of fermion masses: from 0.5 MeV to 174 GeV the masses span over 5 orders of magnitude and the SM does not provide an explanation for the large differences.

A famous problem is the hierarchy problem. It has many different formulations, but it finally boils down to the question why are electroweak interactions so much stronger than gravitational interactions. Equivalently one can ask why is the scale of the electroweak theory ~ 100 GeV so small compared to the Planck scale $m_{\mathrm{Pl}} = 1.2 \times 10^{19}$ GeV. To illustrate this problem we turn to the Higgs boson mass $m_h \approx 125$ GeV. The Higgs potential is very sensitive to any new physics that couples directly or indirectly to the Higgs field: virtual loop effects give enormous

contributions to the Higgs boson mass. Consider a fermion f and a scalar field S with couplings $\mathcal{L} \sim -Y_f H \bar{f} f - \lambda_s |H|^2 |S|^2$. Self energy diagrams involving the additional particles (c.f. figure 1.1) give large contributions to the Higgs mass

$$\Delta m_h^2 \sim \frac{1}{16\pi}(-2|Y_f|^2 + \lambda_s)\Lambda_{\mathrm{UV}}^2 + \mathcal{O}\left((m_f^2 - m_s^2)\log(\Lambda_{\mathrm{UV}})\right) \tag{1.20}$$

where Λ_{UV} is the ultraviolet cut-off used to regularize the loop. It is at least of the order of the scale at which new physics alter the high energy behaviour of the theory. If the scale is set to the Planck scale, the Higgs boson mass should be 15 orders of magnitude larger than the observed value. Even if one wants to ignore the physical meaning of the cut-off and uses dimensional regularization of the loop integral, the Higgs mass still receives contributions proportional to the mass squared of any particle that couples directly or indirectly to it. So if there are additional particles at high energies it is difficult to understand why the Higgs boson mass is so small.

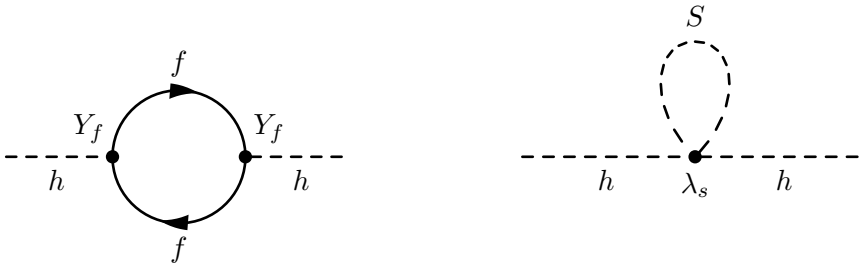

Figure 1.1: Self energy diagrams contributing to the mass of the Higgs boson. The right diagram shows the loop of a fermion coupling to the Higgs whereas the right shows the loop contribution of a scalar.

A very important issue of the SM is called the strong CP problem. In the gauge sector of strong interactions a CP violating term $\theta \frac{\alpha_s}{8\pi} G^{\mu\nu}\tilde{G}_{\mu\nu}$, with $G^{\mu\nu}$ being the gluon field strength and $\tilde{G}_{\mu\nu} = \frac{1}{2}\epsilon_{\mu\nu\rho\sigma}G^{\rho\sigma}$ its dual, is allowed by all symmetries and should therefore be present. However from observations we know that the term is not present or has at least a very small coefficient in front $|\theta| < 10^{-9}$. Within the framework of the SM it is impossible to explain why this CP violating term is so small. More details on the strong CP problem can be found in section 6.1.

Direct observational shortcomings

Neutrino oscillations are today the most evident and best measured sign of physics beyond the SM. In a large number of experiments the appearance or disappearance of neutrino flavours have been detected. At the origin of these observations are neutrino oscillations which require at least two massive neutrinos, in contrast to the prediction of the SM. Many more details on neutrino oscillations will be mentioned later in section 3.1. Additionally a small number of tensions between experiments and SM predictions have been observed, like e.g. the anomalous magnetic moment of the muon. However many of these deviations could be explained by experimental issues or are not very significant.

Cosmological signs to new physics

Cosmology is a very important test for and an application of particle physics. Even if the SM content can describe large parts of the observed phenomena in cosmology, it is clear that some ingredients are missing. Observations on different length scales show that gravitationally bound objects (e.g. galaxies, or clusters) are dominated by non-baryonic matter, dark matter. The SM falls short in providing a stable, very weakly interacting dark matter candidate. Furthermore the SM cannot explain the baryon abundance observed today. Baryons should have annihilated completely with antibaryons when they became non-relativistic in the thermal history of the universe. At some moment a baryon asymmetry must have been created to explain the presence of baryons today. In the SM CP violating processes are probably not strong enough to explain the observed asymmetry. The SM can also not explain the nature of dark energy that is dominating our universe today.

1.2.2 New physics models

Many models for new physics have been proposed in order to solve the above mentioned problems. Some of them are even able to explain more than one of the shortcomings of the SM. Here a non-exhaustive and slightly biased list of physics beyond the SM is given.

- **Supersymmetry**
  Supersymmetry (SUSY) is an additional symmetry between fermions and bosons. It states that for every fermionic degree of freedom there is a bosonic degree of freedom and vice versa. Supersymmetry is the only possible extension to Poincaré symmetry and internal symmetries of a 4 dimensional quantum field theory. It naturally provides a solution to the hierarchy problem because the bosonic and fermionic contributions to the Higgs mass (see equation 1.20) cancel exactly if their couplings and masses are related to each other. SUSY predicts the same masses and couplings for fermions and its bosonic partners. This is obviously in contradiction with observations. Consequently SUSY must be broken at a scale that is not too far above the electroweak scale in order to be able to solve the hierarchy problem. If SUSY is extended by an R-parity, the lightest supersymmetric particle is stable and can be a good dark matter candidate.
- **Extra dimensions**
  Another possible extension is to add additional dimensions to the 4 dimensional Minkowski space-time. It is possible to add compact extra dimensions that only affect physics at high energy scales, related to the size of the extra dimension. One can then define the Planck mass on the $4+N$ dimensional space, which is much smaller than the Planck mass observed in 4 dimensions. In this way one can solve the hierarchy problem. Additional compact dimensions can also give rise to an infinite tower of excitations of known particles. These additional particles with heavy masses can be stable and can be good dark matter candidates.
- **Axions**
  Axions are a very elegant solution of the strong CP problem. The solution replaces the constant in front of the CP violating QCD term by a pseudoscalar field, the axion, which is dynamically driven to zero. In some part of their one dimensional parameter space they can also be excellent dark matter candidates. Section 6 gives more details on the strong CP problem, an introduction to axions as well as their role in cosmology as dark matter.
- **Right-handed neutrinos**
  In order to explain neutrino masses one has to introduce right-handed neutrinos. The seesaw mechanism provides a very natural explanation for the smallness of neutrino masses by giving large Majorana mass terms to the right-handed neutrinos (c.f. section 3.2.2).

The heavy right-handed neutrinos can also provide a new source of CP violating couplings which can produce a lepton and baryon asymmetry in the thermal history of the universe. These models are called leptogenesis models (c.f. section 4). Right-handed neutrinos with keV masses can also be dark matter candidates. It is astonishing how a small extension of the SM can solve three major problems at once. Today we are almost sure that right-handed neutrinos exist but experimentally it will be very difficult to observe them because in the minimal picture they are singlets under all gauge groups and do only interact via Yukawa couplings with the SM.

Chapter 2

Cosmology and its standard model

This chapter will give a short introduction to the cosmological standard model, called the Λ Cold Dark Matter model (ΛCDM). We will review the geometry of our universe, look at its thermal history, describe the evolution of small perturbations that give rise to structure formation and then give a small review on dark matter. For a more detailed introduction to cosmology I recommend the reader to have a look in one of these excellent works [13, 14, 15] or in [16] for an additional introduction to GR.

2.1 Geometry and matter content of our universe

To describe the evolution of the universe, cosmology makes the fundamental assumption that on large enough scales the universe is homogeneous and isotropic, called the cosmological principle. It states that on a sufficiently large scale the universe should have the same properties for all observes. Experimentally this assumption is (mostly) true for scales larger than 100Mpc. Due to charge neutrality the universe is dominated by gravity on large length scales so that Einstein's theory of general relativity should give an appropriate description of the dynamics. Using this assumption Einstein's field equations have an exact solution that was found by Friedman, Robertson, Walker and Lemaitre in the 1920s and 1930s. The resulting metric is called Friedman-Robertson-Walker-Lemaitre (FRWL) metric

$$ds^2 = dt^2 - R(t)^2 \left(\frac{dr^2}{1-kr^2} + r^2(d\theta^2 + \sin^2\theta d\phi^2) \right) \quad . \tag{2.1}$$

The variables r, θ, ϕ are polar coordinates. All physical length scales are multiplied by $R(t)$, the scaling factor that describes the expansion of the universe. k is a constant number that describes the spatial curvature. For $k = 0$ the universe is Euclidean (flat universe), for $k > 0$ it has positive curvature (closed universe) and for $k < 0$ the universe is negatively curved (open universe). The dynamics of the universe are encoded in the evolution of $R(t)$. The rate of change of R is called the expansion rate, or the Hubble parameter

$$H(t) \equiv \frac{1}{R}\frac{dR}{dt} = \frac{\dot{R}}{R} \quad . \tag{2.2}$$

The value of the Hubble parameter today H_0 is often parametrized like $H_0 = h \times 100 \text{kms}^{-1}\text{Mpc}^{-1}$. Its measured value today is roughly $h \sim 0.7$.

The evolution of $R(t)$ depends on the matter content of the universe and can be calculated using Einstein's field equations which relate the geometry of space time to the matter (energy)

content,

$$R_{\mu\nu} - \frac{1}{2}R + g_{\mu\nu}\Lambda = 8\pi G T_{\mu\nu} \tag{2.3}$$

where $R_{\mu\nu}$ is the Ricci curvature tensor, $R = R^{\mu}_{\mu}$ the Ricci scalar and Λ a constant (often called the cosmological constant). The energy momentum tensor of the cosmological matter content $T_{\mu\nu}$ in a homogeneous and isotropic universe has the form

$$T^{\mu}_{\nu} = \begin{pmatrix} \rho & 0 & 0 & 0 \\ 0 & -p & 0 & 0 \\ 0 & 0 & -p & 0 \\ 0 & 0 & 0 & -p \end{pmatrix} \tag{2.4}$$

where ρ is the energy density and p is the pressure of the cosmological fluid. The $0,0$ component of the Einstein equation is the famous Friedmann equation in the presence of a cosmological constant

$$H^2 = \left(\frac{\dot{R}}{R}\right)^2 = \frac{8\pi G}{3}(\rho_M + \rho_R) - \frac{k}{R^2} + \frac{\Lambda}{3} \tag{2.5}$$

One sees that only a positive curvature term decreases the expansion of the universe, all other terms ehance the expansion rate. The differentiation between non-relativistic matter ρ_M and ultra-relativistic matter ρ_R is for pure pedagogical reasons. Both contribute in the same way to the expansion rate of the universe, but their evolution with time is slightly different. Consider the energy momentum conservation for a fluid with energy momentum tensor given in equation (2.4) in an expanding universe

$$T^{\nu}_{0;\nu} = 0 \quad \Leftrightarrow \quad \dot{\rho} = -3\frac{\dot{R}}{R}(\rho + p) \ . \tag{2.6}$$

Non-relativistic matter has negligible kinetic energy and therefore also negligible pressure $p \sim 0$.

$$\dot{\rho}_m = -3\frac{\dot{R}}{R}\rho_m \quad \Rightarrow \quad \rho_m \propto R^{-3} \tag{2.7}$$

The energy density of non-relativistic matter depends only on the particle density which gets diluted $\propto R^{-3}$ because the volume expands like R^3.

For ultra-relativistic matter like photons the kinetic energy is dominant and therefore the pressure is not negligible. From statistical thermodynamics we know that $p = \rho/3$. This implies

$$\dot{\rho}_r = -4\frac{\dot{R}}{R}\rho_r \quad \Rightarrow \quad \rho_r \propto R^{-4} \ . \tag{2.8}$$

Not only the number density gets diluted but also the energy per particle is redshifted when the universe expands. Both effects sum up to a faster dilution of an ultra-relativistic fluid compared to a non-relativistic fluid. The curvature contribution to H gets diluted like $\propto R^{-2}$, while the contribution of a cosmological constant stays constant and does not scale with R. Non-relativistic matter is often simply called "matter", whereas ultra-relativistic matter is often called "radiation".

As the components of the universe dilute differently with time it is possible that at different times the universe is dominated by different fluids. It is also clear that the fastest diluting components should dominate at early times whereas the slowly diluting components dominate at later times. The evolution of H during different phases of domination is:

– Radiation domination

$$H^2 \propto R^{-4} \;\Rightarrow\; R(t) \propto t^{1/2} \;\Rightarrow\; H(t) = \frac{1}{2t} \tag{2.9}$$

During radiation domination the expansion is decelerating.

– Matter domination

$$H^2 \propto R^{-3} \;\Rightarrow\; R(t) \propto t^{2/3} \;\Rightarrow\; H(t) = \frac{2}{3t} \tag{2.10}$$

During matter domination the expansion is also decelerating but slower than during radiation domination.

– negative curvature domination

$$H^2 \propto R^{-2} \;\Rightarrow\; R(t) \propto t \;\Rightarrow\; H(t) = \frac{1}{t} \tag{2.11}$$

During a potential domination of curvature the universe is expanding linearly with time.

– Cosmological constant

$$H^2 = \frac{\Lambda}{3} \;\Rightarrow\; R(t) \propto e^{\sqrt{\frac{\Lambda}{3}}t} \;\Rightarrow\; H(t) = \sqrt{\frac{\Lambda}{3}} \tag{2.12}$$

When the cosmological constant is dominating the expansion is accelerating.

If the universe does not only contain a cosmological constant, it seems that at some moment in the past the scale factor goes to zero, called the initial singularity or the "Big Bang". However the physical treatment that we used here does not hold until this moment. At times smaller than the Planck time, Einstein's description of gravity is not valid any more because gravitational quantum effects should be taken into account.

A very economic description of the matter content in the universe today can be found by dividing the Friedman equation by H_0^2 and defining

$$\Omega_r = \frac{8\pi G}{3H_0^2}\rho_R(t_0) \tag{2.13}$$

$$\Omega_m = \frac{8\pi G}{3H_0^2}\rho_M(t_0) \tag{2.14}$$

$$\Omega_k = \frac{k}{R_0^2 H_0^2} \tag{2.15}$$

$$\Omega_\Lambda = \frac{\Lambda}{3H_0^2} \;. \tag{2.16}$$

The Friedman equation today now reads

$$1 = \Omega_r + \Omega_m - \Omega_k + \Omega_\Lambda \;. \tag{2.17}$$

As the value of H_0 is not perfectly well known, experiments measuring the energy densities of different components of the universe often publish their results as $\Omega_x h^2$ in order to relate the

results directly to the energy density, without adding the uncertainty on H_0 to the uncertainty of the measured value.

The most precise values for the matter content have been measured by the PLANCK collaboration [17]. They measure temperature fluctuations in the cosmic microwave background (CMB). The temperature of the CMB today is $T = 2.7255$ K. The energy density of this radiation is negligible compared to the other densities in the universe today, but at earlier stages the radiation density was dominating. The contribution to the energy density from the curvature term is $\Omega_k = -0.0003 \pm 0.0065$ (1σ) which is perfectly compatible with 0. In the following we will only consider the case of a flat universe and set $k = 0$. Today's expansion rate with its 68% Confidence Level (CL) is

$$H_0 = 67.0 \pm 1.2 \text{ kms}^{-1}\text{Mpc}^{-1} \quad . \tag{2.18}$$

The matter density and the cosmological constant are measured with their 1σ error to be

$$\Omega_M = 0.3183^{+0.016}_{-0.018} \tag{2.19}$$

$$\Omega_\Lambda = 0.6817^{+0.018}_{-0.016} \quad . \tag{2.20}$$

The baryon mass density can be measured to be $\Omega_B h^2 = 0.02205 \pm 0.00028$ (1σ) which is only $\sim 15\%$ of the total non-relativistic matter density in the universe. The nature of the remaining matter density is currently unknown and is called dark matter. The dark matter density is $\Omega_{\text{DM}} h^2 = 0.1199 \pm 0.0027$ (1σ). More about the evidence for dark matter and possible candidates can be found in section 2.4 of this chapter.

2.2 Thermal history

2.2.1 Thermodynamics in an expanding universe

In this section we will describe the history of the universe at high temperatures and high densities before structure formation starts. At high temperatures the universe was filled by a soup of particles that were interacting with each other through strong and electroweak interactions. The only effect of gravity during the early stages of the universe is to drive expansion.

The cosmic fluid consists of different species that are described by their phase space density f_i. In a homogeneous and isotropic universe the phase space density can only depend on the absolute value of the momentum and time: $f_i(p, t)$. The number density, the energy density and the pressure of one species are then given by

$$n_i(t) = \frac{g_i}{(2\pi)^3} \int d^3p f_i(p, t) \tag{2.21}$$

$$\rho_i(t) = \frac{g_i}{(2\pi)^3} \int d^3p E_i f_i(p, t) \tag{2.22}$$

$$p_i(t) = \frac{g_i}{(2\pi)^3} \int d^3p \frac{p^2}{3E_i} f_i(p, t) \tag{2.23}$$

where g_i is the number of quantum degrees of freedom. We consider antiparticles as independent particles and do not include them in the count of g_i.

Thermal equilibrium

If two particle species a and b have frequent interactions (e.g. elastic scattering $a+b \to a+b$) they can exchange momentum randomly and reach kinematic equilibrium, they are in thermal

equilibrium. If there are many species in thermal equilibrium they form a "thermal bath". In this case the distribution functions f_i for all species in the bath depend on the same parameter T, the temperature of the bath. A species a is in thermal equilibrium with another species if its interaction rate is larger then the expansion rate of the universe $\Gamma_a(t) > H(t)$.

In thermal equilibrium the phase space distribution is given by the Fermi-Dirac distribution $(+)$ for fermions or by the Bose-Einstein distribution $(-)$ for bosons.

$$f_{i\pm}^{\rm eq} = \frac{1}{e^{(E_i-\mu_i)/T} \pm 1} \tag{2.24}$$

where μ_i is the chemical potential of species i. We can calculate the number density and energy density in two different limiting cases:

– ultra-relativistic particles ($E \gg m$) with negligible chemical potential $\mu_i \ll T$.

$$n_{i\pm}^{\rm eq} = \frac{g_i T^3}{\pi^2}\zeta(3) \quad \left(\times\frac{3}{4} \quad \text{for fermions}\right) \tag{2.25}$$

$$\rho_{i\pm}^{\rm eq} = \frac{\pi^2 g_i}{30}T^4 \quad \left(\times\frac{7}{8} \quad \text{for fermions}\right) \tag{2.26}$$

$$p_i^{\rm eq} = \frac{1}{3}\rho_{i\pm}^{\rm eq} \tag{2.27}$$

– non-relativistic particles $m \gg T$

$$n_{i\pm}^{\rm eq} = g_i\left(\frac{m_i T}{2\pi}\right)^{3/2}\exp\left[-\frac{m_i-\mu_i}{T}\right] \tag{2.28}$$

$$\rho_{i\pm}^{\rm eq} = m_i n_{i\pm}^{\rm eq} \tag{2.29}$$

$$p_i^{\rm eq} = T n_{i\pm}^{\rm eq} \ll \rho_{i\pm}^{\rm eq} \tag{2.30}$$

Comparing the number densities of a relativistic particle with a non-relativistic particle one sees that the ratio $n_i^{\rm non-rel}/n_i^{\rm rel} \sim e^{-m_i/T}$ is exponentially suppressed. If a particle stays in thermal equilibrium even when it gets non-relativistic its number density falls rapidly and can soon be neglected.

In the limiting cases we have observed that the differences between Bose-Einstein statistics and Fermi-Dirac statistics are relatively small. One can therefore often use Boltzmann statistics

$$f_{\rm MB}^{\rm eq} = e^{-(E_i-\mu_i)/T} \quad . \tag{2.31}$$

This gives very similar values in the relativistic case

$$n_{i\,\rm MB}^{\rm eq} = \frac{g_i T^3}{\pi^2} \tag{2.32}$$

$$\rho_{i\,\rm MB}^{\rm eq} = \frac{3g_i}{\pi^2}T^4 \tag{2.33}$$

$$p_i^{\rm eq} = \frac{1}{3}\rho_{i\,\rm MB}^{\rm eq} \tag{2.34}$$

In the non-relativistic case the results are the same as for the exact phase space densities. It is often a sufficiently good approximation to use Maxwell Boltzmann statistics.

Chemical equilibrium

In inelastic scattering reactions particles do not only exchange momentum but can be created or annihilated. The dynamics of the rate of change of a particle density are controlled by Boltzmann equations, which are of the form

$$\dot{n} + 3Hn = \frac{g}{(2\pi)^3}\int C[f]\frac{d^3p}{E} \tag{2.35}$$

The time evolution of the number density is given by dilution due to the expansion of the universe and by creation or annihilation due to collisions. The collision integral for a process $a + b + \cdots \leftrightarrow i + j + \cdots$ is given by [13]

$$\frac{g_a}{(2\pi)^3}\int C[f]\frac{d^3p_a}{E_a} = -\int d\Pi_a d\Pi_b \cdots d\Pi_i d\Pi_j \cdots \times (2\pi)^4\delta^4(p_a + p_b + \cdots - p_i - p_j \cdots)$$
$$\times\Big[|\mathcal{M}|^2_{a+b+\cdots\to i+j+\ldots} f_a f_b \cdots (1 \pm f_i)(1 \pm f_j)\cdots - |\mathcal{M}|^2_{i+j+\cdots\to a+b+\ldots} f_i f_j \cdots (1 \pm f_a)(1 \pm f_b)\cdots\Big] \tag{2.36}$$

where f_k is the phase space density of particle k and $(+)$ applies to bosons, $(-)$ to fermions and $d\Pi = \frac{g}{(2\pi)^3}\frac{d^3p}{2E}$. Boltzmann equations give a coupled set of differential equations for the phase space distributions of all involved species. Consider a simple example of a reaction $a+b \to i+j$. For the moment one can neglect CP violation, which means that

$$|\mathcal{M}|^2_{a+b\to i+j} = |\mathcal{M}|^2_{i+j\to a+b} = |\mathcal{M}|^2 \ . \tag{2.37}$$

Furthermore consider that all involved particles are in thermal equilibrium and their phase space density is given by Maxwell Boltzmann statistics and neglect $(1 \pm f) \approx 1$. Thus one can rewrite the Boltzmann equation

$$\dot{n}_a + 3Hn_a = \int d\Pi_a d\Pi_b d\Pi_i d\Pi_j \times (2\pi)^4\delta^4(p_a + p_b - p_i - p_j)|\mathcal{M}|^2\left[f_i f_j - f_a f_b\right] \ . \tag{2.38}$$

Using conservation of energy and the equilibrium distributions for f one can rewrite

$$[f_i f_j - f_a f_b] = f_a f_b\left(e^{(-\mu_a-\mu_b+\mu_i+\mu_j)/T} - 1\right) \ . \tag{2.39}$$

If one defines the thermally averaged cross section to be

$$\langle\sigma|v|\rangle \equiv \int d\Pi_a d\Pi_b d\Pi_i d\Pi_j \times (2\pi)^4\delta^4(p_a + p_b - p_i - p_j)|\mathcal{M}|^2$$
$$\times\, e^{-(E_a+E_b)/T}\left(\int\frac{d^3p_a}{(2\pi)^3}e^{-E_a/T}\int\frac{d^3p_b}{(2\pi)^3}e^{-E_b/T}\right)^{-1} \tag{2.40}$$

one can rewrite equation (2.38)

$$\dot{n}_a + 3Hn_a = \langle\sigma|v|\rangle n_a n_b\left(e^{(-\mu_a-\mu_b+\mu_i+\mu_j)/T} - 1\right) \ . \tag{2.41}$$

If the interaction rate is fast $n_b\langle\sigma|v|\rangle \gg H$, one can neglect the expansion of the universe and the equilibrium condition is given by

$$\mu_a + \mu_b = \mu_i + \mu_j \ . \tag{2.42}$$

This means the number densities cannot be arbitrary but must obey the chemical equilibrium condition. In the other extreme case of very slow interactions $n_b\langle\sigma|v|\rangle \ll H$ the number density gets only depleted due to the expansion of the universe $n_a \propto R^{-3}$.

Entropy conservation

From the laws of thermodynamics one can show that the total entropy in a comoving volume is conserved. The entropy is given by

$$s = \frac{\rho + p}{T} \tag{2.43}$$

where ρ and p are the total density and total pressure of all species in thermal equilibrium. As we have seen above the energy density is mostly dominated by relativistic species, whereas non-relativistic species give negligible contributions. Using equation (2.26) for the energy density and $p = \frac{1}{3}\rho$ one can simplify the entropy to

$$s = \frac{4}{3}\frac{\pi^2}{30} g_* T^3 \quad . \tag{2.44}$$

Here g_* counts all relativistic degrees of freedom in thermal equilibrium with an additional factor $\frac{7}{8}$ for fermions

$$g_* = \sum_{\text{rel.bosons}} g_i + \frac{7}{8} \sum_{\text{rel.fermions}} g_i \quad . \tag{2.45}$$

The conservation of the total entropy then implies that $g_* T^3 R^3 = \text{const}$. Most of the time the product TR is constant. However in moments when g_* changes, e.g. when a species becomes non-relativistic, the temperature has to scale differently to ensure the conservation of entropy.

2.2.2 Early stages

We will review very briefly the various stages of thermal evolution of the universe starting from the earliest period until photon decoupling. After photon decoupling the universe is subject to structure formation which will be treated in the next section. The earliest stages in the evolution of the universe are still rather unknown and no complete theory has yet been proven to be true. However a kind of standard picture seems to emerge. The earliest moment we can treat is at Planck time $t_P \sim 10^{-36}$ ss when gravity became a classical theory which is very well described by Einstein's theory of general relativity. Shortly after it seems to be likely that the universe went through a phase of accelerated expansion, called inflation. During inflation the Hubble parameter was almost constant so that $\dot{R}(t) = H_{\text{inf}} R(t)$ and therefore the universe was expanding exponentially

$$R(t) \propto \exp(H_{\text{inf}} \cdot t) \quad . \tag{2.46}$$

The phase of inflation is usually described by the domination of the potential energy of a scalar field (inflaton) with negligible kinetic energy (slow roll). At the end of inflation the inflaton oscillates rapidly around the minimum of its potential and decays into SM particles. The SM particles are produced with high kinetic energy so that they form a thermal bath of relativistic particles. The initial temperature of the bath after inflation is called reheat temperature. After inflation the universe is dominated by radiation and the temperature scales like $T \propto R^{-1}$, except for the moments when g_* changes.

At this stage SM particles are still massless and quickly interacting with other particles from the bath. Quarks are free particles and not yet confined into hadrons. At around $T \sim 100$ GeV the electroweak symmetry is spontaneously broken by the vacuum expectation value of the Higgs field (electroweak phase transition). Consequently SM particles acquire their mass and heavy particles become quickly non-relativistic and their number density falls exponentially compared to the number density of photons. At $T \sim 100$ MeV the QCD phase transition occurs: quarks

are confined into hadrons (baryons and mesons) so that all coloured objects disappear from the bath.

Let us mention here a very important issue of the thermal history of our universe: baryon asymmetry. To illustrate the problem consider only one particle b with baryon number $B = 1$ and mass m_b. If baryon number is conserved at the end of inflation, as many particles as antiparticles have been created $n_b = n_{\bar{b}}$. The baryons can annihilate into n photons

$$b + \bar{b} \leftrightarrow n\gamma \tag{2.47}$$

At temperatures $T > m_b$ they are relativistic as well as in thermal and chemical equilibrium with the bath because photons have enough energy to produce pairs of $b\bar{b}$. However when the temperature drops below m_b, photons do not carry enough energy to recreate $b\bar{b}$. The number of baryons and antibaryons drops rapidly until there are practically no more particles left. As we observe a non negligible amount of baryons today $Y_B = \left.\frac{n_B - n_{\bar{B}}}{s}\right|_0 \approx 10^{-10}$, baryon number must be violated at some point. Models that create a baryon asymmetry dynamically are called baryogenesis. In chapter 4 of this thesis a general class of baryogenesis models, called leptogenesis will be introduced.

Consider now the matter content of the universe around $T \sim 10$ MeV. Assume that some mechanism produced a baryon asymmetry and that all antibaryons have annihilated with baryons and only the over-density of baryons is left. The universe contains protons and neutrons that are both non-relativistic. Protons are stable and neutrons can decay into protons by β decay $n \to p + e^- + \nu_e$. However the inverse reaction is still quick so that the proton to neutron ratio is constant. Both baryons are in thermal equilibrium through weak and electromagnetic interactions. Further more there are electrons and anti-electrons that are still relativistic. The charge neutrality ensures that

$$n_e - n_{\bar{e}} = n_p \ . \tag{2.48}$$

The thermal bath contains also 3 families of neutrinos and anti-neutrinos, that are still in thermal equilibrium due their weak interactions, as well as photons and potentially dark matter particles. The relativistic degrees of freedom can be summed up to $g_*(T \sim 10 \text{ MeV}) = 10.75$.

The next step in the evolution of the thermal plasma is the decoupling of neutrinos. The charged current and neutral current interactions of neutrinos are of the order of $\langle \sigma_\nu |v| \rangle \sim G_{\text{F}}^2 T^2$ where G_{F} is Fermi's constant. The interaction rate is then $\Gamma_\nu = n_e \langle \sigma_\nu |v| \rangle \sim G_{\text{F}}^2 T^5$. Comparing the interaction rate to the Hubble expansion rate one finds

$$\frac{H}{\Gamma_\nu} \sim \left(\frac{T}{1 \text{ MeV}}\right)^3 \ . \tag{2.49}$$

Neutrinos leave thermal equilibrium around $T \sim 1$ MeV and their phase space distribution freezes in while being relativistic. From this moment on the neutrino density gets only diluted by the expansion of the universe. Even if they become non-relativistic their number density stays $n_\nu \sim T^3$ because they are decoupled.

When the temperature drops further electrons become non-relativistic and start to annihilate. The electron and anti-electron density drops dramatically compared to the photon number density. The annihilations stop only when no more anti-electrons are left and the electron number density is $n_e = n_p$. The electron annihilations create an excess in photons which implies and increase in the product TR. During the annihilations the total entropy of the bath is conserved $sR^3 \propto g_*(TR)^3 = \text{const}$ which implies

$$\frac{11}{2}(TR)^3_{\text{before}} = 2(TR)^3_{\text{after}} \tag{2.50}$$

where we have used that $g_*(\text{before}) = 2 + \frac{7}{8}(2+2) = \frac{11}{2}$ and $g_*(\text{after}) = 2$. If electron annihilation is an abrupt process, the photon temperature increases by a factor $\left(\frac{11}{4}\right)^{1/3}$. During electron annihilation the neutrino temperature decreases simply like $T_\nu \propto R^{-1}$ and is completely unaffected by what happens to the photon temperature. The neutrino to photon temperature ratio after electron annihilation is therefore

$$\left(\frac{T_\nu}{T}\right)_{\text{after}} = \left(\frac{4}{11}\right)^{1/3} \tag{2.51}$$

After electron annihilation photons are the only relativistic species in the "bath" and the photon temperature scales until today in the same way as the neutrino temperature, so that the relation between both temperatures is still the same today. We expect the cosmic neutrino background to have a slightly lower temperature than the cosmic microwave background.

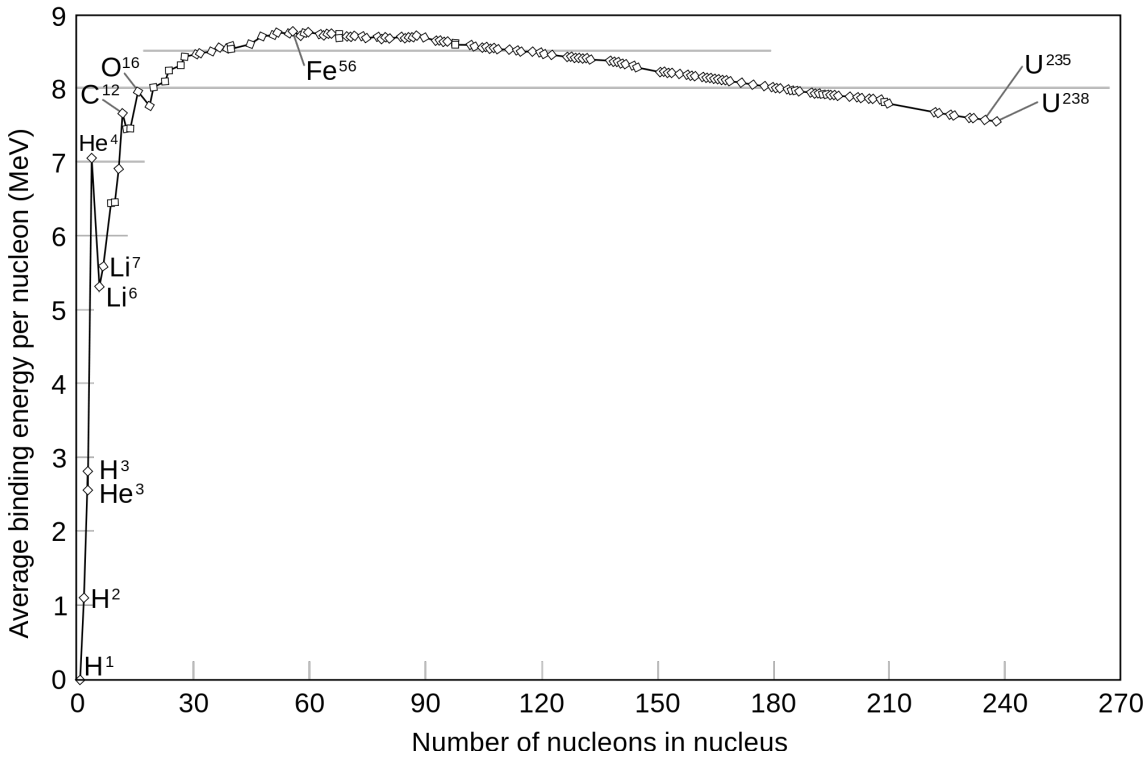

Figure 2.1: The average binding energy per nucleon in a nucleus as a function of the number of nucleons. The most strongly coupled nucleus is Fe^{56}.

We will now come to the next stage, the primordial formation of light elements, called nucleosynthesis. The average binding energy per nucleon in a nucleus is shown in figure 2.1. From a purely energetic point of view one expects that when the temperature drops below the binding energy of deuterium $B_D \sim 2$ MeV it is energetically more advantageous to form deuterium for the protons and neutron. As the photons do not have enough energy to destroy

the formed deuterium further reactions can take place. Typical nuclear reactions are

$$\begin{aligned} p + n &\leftrightarrow \mathrm{D} + \gamma \\ \mathrm{D} + \mathrm{D} &\rightarrow {}^3\mathrm{He} + n \\ {}^3\mathrm{He} + \mathrm{D} &\rightarrow {}^4\mathrm{He} + p \end{aligned} \tag{2.52}$$

$$\cdots \tag{2.53}$$

However the number density of photons is much larger than the number density of baryons $n_B \sim 10^{-10} n_\gamma$, so that even for $T \lesssim B_D$ there is still a large number of photons in the high energy tail of the photon distribution that can destroy formed deuterium. Only when the temperature is significantly smaller then B_D ($T \sim 0.07$ MeV) the formed deuterium is stable for long enough to continue the nuclear reaction chain. At the end of the chain is Fe^{56} which has the highest binding energy per nucleon. However to reach Fe a long chain of nuclear reactions is needed and the number densities of intermediate nuclei are not high enough for the reactions to happen. The formation of ^{4}He from deuterium is rather efficient so that most of the produced D is converted into helium. However in figure 2.1 one sees that the binding energy has a local maximum at ^{4}He and reaches higher values only for ^{12}C. To cross the gap a three body reaction is needed $3 \times {}^4\mathrm{He} \rightarrow {}^{12}\mathrm{C}$. Nucleosynthesis stops around ^{4}He, only very few Li and heavier elements are formed.

The details of big bang nucleosynthesis (BBN) are rather complicated and will not be reviewed here. A nice review can be found in [18]. Recent results of theoretical predictions and experimental observations are shown in [12]. Globally the predictions and observations for the abundances of D, ^{3}He and ^{4}He are in very good agreement and are one of the most solid confirmations of the big bang model. One can use BBN to constrain new physics, like e.g. the number of relativistic neutrino species (or more generally any additional relativistic degree of freedom) $N_\nu < 4.2 (95\% CL)$ [12], compared to SM prediction $N_\nu \approx 3$. However the stellar measurements of Li/H abundances in metal poor stars in the spheroid of our galaxy and the predictions from BBN show a discrepancy with a 5.3σ significance. Further details on the "lithium problem" can be found in [19]. The discrepancy could point towards new physics, e.g. some supersymmetric models or a varying fine structure constant could explain the discrepancy.

The next step in the evolution of the universe is the matter-radiation equality. We have seen above that the energy density of radiation is diluted faster than the energy density of stable matter. At some moment the matter energy density will become comparative to the radiation energy density and then dominate the Friedmann equation. This is the case around $T \sim 1$ eV.

After nucleosynthesis the electromagnetic interactions are still fast so that photons, electrons, protons and He are in thermal equilibrium. The interactions remain efficient as long as H and He are ionized. For H the important reaction is

$$p + e^- \leftrightarrow \mathrm{H} + \gamma \ . \tag{2.54}$$

For the inverse reaction the photon has to carry at least 13.6 eV. Once again the large number of photons compared to protons ensures that the reaction stays in equilibrium even for $T \lesssim 13.6$ eV. But around $T \sim 0.25$ eV protons and electrons start to combine and form stable atoms, so that the universe does not contain any charged particles any more. This is called "recombination". Recombination triggers the decoupling of photons: there are no more charged particles to interact with, so that the photon distribution, like the neutrino distribution, gets frozen in and is from then on only changed by the expansion of the universe. The remaining photons form a background radiation that can still be observed today with a temperature $T \approx 2.7$ K, it is the famous CMB.

2.3 Cosmological perturbation theory

Until now we have assumed that the universe is homogeneous and isotropic. The aim of this section is to introduce small perturbations to the homogeneity and describe their evolution. The inhomogeneities are responsible for the formation of gravitational bound structures in today's universe. We know from the temperature anisotropies in the CMB that in the early universe the perturbations are 10^5 times smaller than the background quantities. The density perturbations grow and finally collapse into bound objects on small length scales due gravitational instability. It is therefore possible to treat the perturbations to linear order in the early universe and at late times on large length scales. A nice review on cosmological perturbation theory can be found in [20].

2.3.1 Theoretical treatment

In order to write down the theory of perturbations one has to introduce perturbations to the background metric in equation (2.1) and background energy momentum tensor in equation (2.4). The flat perturbed metric can be written like

$$ds^2 = (1+2\psi)dt^2 + B_i dx^i dt - R^2(t)\left[(1-2\phi)\delta_{ij} + H_{ij}\right] dx^i dx^j \quad . \tag{2.55}$$

Where the vector $\vec{B}$ can be decomposed into longitudinal and transverse part

$$\vec{B} = \vec{\nabla} b + \vec{\nabla} \times \vec{b} \quad . \tag{2.56}$$

The tensor H_{ij} can be decomposed into three traceless parts

$$H_{ij} = \left(\partial_i \partial_j - \frac{1}{3}\delta_{ij}\nabla^2\right)\mu + (\partial_i a_j + \partial_j a_i) + h_{ij} \tag{2.57}$$

The perturbations are divided into scalar perturbations (ϕ, ψ, b, μ), vector perturbations (b_i, a_i) and tensor perturbations (h_{ij}). The three types of perturbations evolve independently and can therefore be considered separately. One can show that vector perturbations decay quickly in an expanding universe. Gravitational waves can be important, but we will focus here on scalar perturbations because they exhibit instability and could lead to formation of structures. Using this parametrisation one can construct gauge invariant variables [20], which can be extremely useful to compare between different gauges. We choose to use the longitudinal gauge which leaves only two scalar parameters ϕ, ψ, so that the metric looks like

$$ds^2 = (1+2\psi)dt^2 - R^2(t)(1-2\phi)\delta_{ij}dx^i dx^j \tag{2.58}$$

One also needs to specify the perturbations of the energy momentum tensor. For each species there are four additional scalar degrees of freedom [21]. First the perturbation in the energy density

$$\delta_0^0 = \delta\rho \quad . \tag{2.59}$$

The energy flux that is 0 in the homogeneous case has one longitudinal degree of freedom

$$\sum_i \partial_i T_i^0 = (\bar{\rho} + \bar{p})\theta \quad . \tag{2.60}$$

The remaining parts of the energy momentum tensor contain an isotropic pressure δp and a contribution from an anisotropic pressure σ, defined by

$$\begin{aligned} \delta T^i_j &= -\delta p \delta^i_j + \Sigma^i_j \\ \sum_{ij} \left(\partial_i \partial_j - \frac{1}{3}\delta_{ij} \right) \Sigma^i_j &= (\bar{\rho} + \bar{p}) \Delta\sigma \end{aligned} \tag{2.61}$$

where we have used $\Sigma^i_j = T^i_j - \delta^i_j T^k_k/3$ the traceless component of T^i_j. With these definitions one can use Einstein's field equations to determine the evolution equations of the small perturbations. One can work to linear order in the perturbed quantities. The perturbed Einstein equations read like

$$\begin{aligned} -3H^2\psi - 3H\dot{\phi} + \frac{\Delta}{R^2}\phi &= 4\pi G \delta\rho \\ \Delta(H\psi + \dot{\phi})R &= 4\pi G R^2 (\bar{\rho} + \bar{p})\theta \\ \left(2\frac{\ddot{R}}{R} + H^2 \right)\psi + H\left(\dot{\psi} + 3\dot{\phi} \right) + \ddot{\psi} + \frac{1}{3}\frac{\Delta}{R^2}(\psi - \phi) &= 4\pi G \delta p \\ \frac{\Delta}{R^2}(\phi - \psi) &= 12\pi G(\bar{\rho} + \bar{p})\sigma \end{aligned} \tag{2.62}$$

Here we have used $\dot{X} = \frac{dX}{dt}$. One can show that a perfect fluid has to first order an anisotropic stress $\sigma = 0$ [21]. Before recombination photons, baryons and electrons are in thermal equilibrium and form a perfect fluid. Cold dark matter is a pressure less fluid and has $\delta p = \sigma = 0$. So only neutrinos contribute to the anisotropic stress. Its effect is usually small so we will neglect it for this short review. This implies that $\phi = \psi$, so that the perturbations in the metric are described by one single variable.

In addition to Einstein equations that provide a link between the geometry of the universe and its matter content we need the equations of motion of the fluid. They are obtained from $\nabla_\mu T^\mu_\nu = 0$. To simplify these equations we assume that for each fluid a liner equation of state holds, $p/\rho = w$, with $\dot{w} = 0$. The equation of state holds for the homogeneous quantities $\bar{p}/\bar{\rho} = w$ as well as for the perturbed quantities $\delta p/\delta\rho = w$, which gives the seed of sound $c_s^2 = w$. The conservation of energy, obtained from $\nabla_\mu T^\mu_0 = 0$, holds for every species s [21, 15]

$$\dot{\delta_s} = (1 + w_s)(R\theta_s + 3\dot{\phi}) \tag{2.63}$$

where we defined $\delta_s = \frac{\delta\rho_s}{\bar{\rho}_s}$. The spatial components $\nabla_\mu T^\mu_i = 0$ imply the equivalent of the Euler equation

$$\frac{1}{R}\dot{\theta}_s = \frac{H}{R}(3w - 1)\theta_s + \Delta\phi + \frac{w}{1 + w}\Delta\delta_s \ . \tag{2.64}$$

A first simplification comes from Fourier transforming the Einstein equations and the equations of motion. The effect of the Fourier transform on this equations is to replace $\Delta \to -k^2$ where k is the comoving wave vector. The physical wavelength of a perturbation scales like $\lambda(t) = R(t)\frac{2\pi}{k}$ and grows proportional to the scale factor. The horizon of the causal universe today is $r_h(t_0) \sim 1/H_0$. This implies that all observable perturbations must have a wavelength $\lambda(t_0) < 1/H_0$. We have seen that during matter or radiation domination

$$\begin{aligned} \lambda \propto R &\propto t^m \quad \text{with } m < 1 \\ H &\propto t \end{aligned} \tag{2.65}$$

The casual horizon of the universe grows faster than the physical wavelength of a perturbation. Fourier modes that have been outside the horizon in the past enter and can be observed. Smaller

wavelengths enter first. But this implies a problem because wavelengths outside the casual horizon cannot be produced by physical processes. This problem was striking cosmologists for some time but can be explained by inflation. All wavelengths have been inside the casual horizon before inflation. During the epoch of accelerated expansion the wavelength grows quickly whereas the horizon of the universe stays almost constant. Most wavelengths become larger than the horizon and re-enter later during radiation or matter domination, c.f. figure 2.2. Fluctuations outside the casual horizon are not affected by any physical mechanism so they do not evolve with time except for red-shifting, they are frozen in.

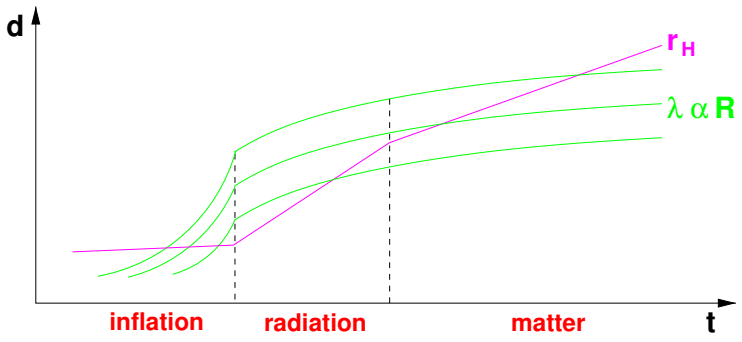

Figure 2.2: The evolution of the physical wavelengths λ and of the casual horizon r_H as a function of time, from [15]. At the beginning of inflation all modes are inside the horizon but they leave the casual horizon quickly because of the exponential expansion. During radiation or matter domination modes re-enter the horizon.

Before one can start to solve the evolution equations for perturbations one has to fix the initial conditions for perturbations before they enter the horizon. One distinguishes between two types of fluctuations, adiabatic (curvature) and isocurvature (isothermal) fluctuations. Adiabatic perturbations are fluctuations in the energy density due to temperature fluctuations. The equivalence principle implies that all species participate in such fluctuations [13]

$$\frac{\delta n_i}{\bar{n}_i} = 3\frac{\delta T}{\bar{T}} \tag{2.66}$$

with $i \in \{\gamma, \nu, b, CDM, s\}$ (s being the entropy). This equation holds in physical space $(\vec{x}, t)$ as well as in momentum space $(\vec{k}, t)$. Adiabatic fluctuations are also characterized by $\delta(n_i/s) = 0$. The fluctuations in the energy density for non-relativistic species is the same as for the number density whereas for relativistic components a factor $4/3$ appears

$$\delta_b = \delta_{\mathrm{CDM}} = \frac{3}{4}\delta_\gamma = \frac{3}{4}\delta_\nu = 3\frac{\delta T}{\bar{T}} \quad . \tag{2.67}$$

Adiabatic fluctuations can be characterized in a gauge invariant way as fluctuations in the local curvature, therefore the name curvature fluctuations. Isocurvature (isothermal) fluctuations are not fluctuations in the local total energy density $\delta\rho = 0$ (at least not as long as the modes are outside the Hubble radius) but are merely fluctuations in the local equation of state, which implies $\delta(n_i/s) \neq 0$. Imagine a small isocurvature fluctuation in the energy density of a non-relativistic particle X on a super horizon scale: $\delta\rho_X$. As the total energy density is unchanged this implies a fluctuation in the temperature so that $\delta\rho_r + \delta\rho_X = 0$. But as $\rho_r \gg \rho_X$ the fluctuation in the temperature is negligible small, therefore such fluctuations can be called

isothermal. Isocurvature modes have not yet been detected and are therefore neglected in most models of cosmological perturbations. However we will see that some axion models can develop isocurvature fluctuations and their non-observation constrains these models.

The origin of classical cosmological fluctuations lies in inflation. The inflation field has, as any scalar field in de Sitter space, quantum fluctuations with a nearly scale invariant spectrum. The fluctuations in the inflaton field give rise to energy density fluctuations because of the potential energy of the inflaton. A very robust outcome of inflation is that the spectrum of fluctuations in the energy destiny is nearly scale invariant

$$\langle |\delta_i(\vec{k}, t)|^2 \rangle \sim k^{-3} \tag{2.68}$$

Where the $\langle \cdots \rangle$ means an average over all Fourier modes with a fixed wave number $k = |\vec{k}|$. The k dependence is often written as k^{n_s-4} with n_s being the spectral index which is supposed to be close to one. It is a major reason for inflation that this scale invariant spectrum of initial perturbations is exactly the one that is needed to explain the observed CMB fluctuations and the large scale structure power spectrum. More details on how inflation generates the initial perturbations can be found in [22, 13]

We will now review the outcome of cosmological perturbation theory: the time evolution of fluctuations. A nice presentation with analytic approximations can be found in [15]. The final results are that during radiation domination all modes that are outside the horizon are frozen and therefore keep their initial conditions $\delta_b = \delta_{\text{CDM}} = \frac{3}{4}\delta_\gamma$. When a mode of the photon fluctuations enters the horizon during radiation domination the perturbation starts to oscillate as a consequence of the interplay between pressure and gravitational attraction. Baryons are still in thermal equilibrium with photons and follow the oscillations of photons $\delta_b = \frac{3}{4}\delta_\gamma$. Dark matter is a pressure-less fluid and is not coupled to photons so it does not participate in the oscillations. During radiation domination the dark matter density feels the attraction of the gravitational potential but does not influence it because of its small energy density compared to photons. Due to gravitational instability the dark matter perturbations grow but only logarithmically with time because the expansion rate counter balances most of its growth.

During matter domination the gravitational potential is driven by the matter distribution of dark matter and baryons. Fluctuations in the matter density inside the horizon during matter domination grow, linearly with R

$$|\delta_m| \propto t^{2/3} \propto R(t) \tag{2.69}$$

which implies that the gravitational potential ϕ is constant in time [1]. One observes that during matter domination structures grow until they leave the regime of small perturbations and their behaviour becomes non-linear.

2.3.2 Large scale structure power spectrum

We will now turn to observable predictions of the cosmological perturbation theory. The two major observations that we treat are the power spectrum of large scale structures and the anisotropies in the CMB. For the large matter power spectrum one measures the galaxy distribution. With it one reconstructs the distribution of luminous galactic matter perturbations $\delta_{\text{lgm}}(\vec{x}, t)$. The fluctuations are then Fourier transformed and an average over all Fourier modes with a fixed wave vector k is done. This gives the power spectrum

$$P_{\text{lgm}}(k) = \langle |\delta_{\text{lgm}}(\vec{k})|^2 \rangle \ . \tag{2.70}$$

1. Knowing that $\bar{\rho} \propto R^{-3}$ one can determine $\delta\rho \propto R^{-2}$. Using the limit of length scales much smaller than the size of the horizon, the first equation of equation (2.62) give the Poisson equation $\frac{k^2}{R^2}\phi = 4\pi G\delta\rho$. This implies that ϕ is constant with time.

Models of galaxy formation show that the distribution of luminous matter follows the distribution of matter (baryons and dark matter) on scales larger than galaxies, so that we can assume $\delta_{\text{lgm}} \approx b\delta_m$, where b is a undetermined parameter called the light-to-mass bias.

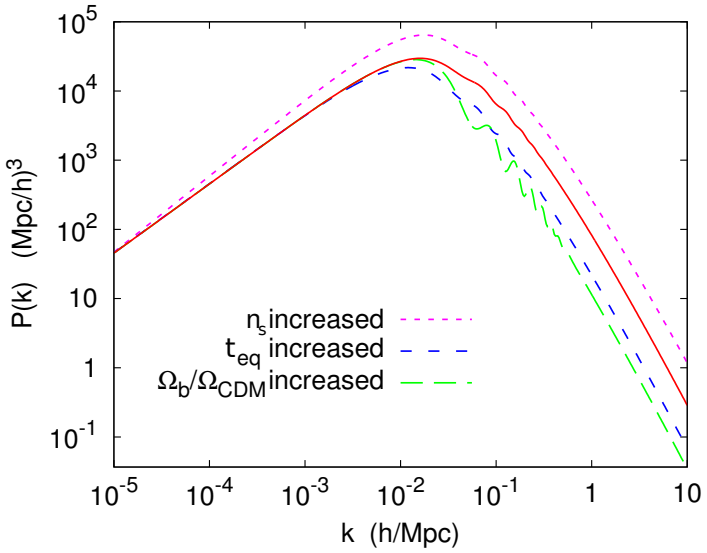

Figure 2.3: The figure shows the theoretical large scale structure power spectrum. The red solid line corresponds to the domination of cold dark matter over baryonic matter. One observes that an increase in n_s changes the slop of the spectrum. A change in t_{eq} shifts the maximum of the spectrum. An increase in the baryon density with respect to the dark matter density increases the small oscillations and sharpens the spectrum. Adapted from [15].

We will first assume that the matter density in the universe is completely dominated by cold dark matter and that the baryonic contribution is negligible. At the moment of matter radiation equality, some of the today's observable modes are still outside the Hubble horizon. They are characterized by $kt_{\text{eq}} \ll R(t_{\text{eq}})$ and are frozen in with their initial spectral distributions. Other modes have already entered the horizon, $kt_{\text{eq}} \gg R(t_{\text{eq}})$, and started to grow logarithmically with time. After matter radiation equality all relevant scales enter the horizon and grow in the same way, i.e. they grow linearly with R. One can show that the predicted matter power spectrum is [15]

$$P_m \propto \begin{cases} k^{n_s} & \text{for } kt_{\text{eq}} \ll R(t_{\text{eq}}) \\ \log\left(\frac{kt_{\text{eq}}}{R(t_{\text{eq}})}\right)^2 k^{n_s-4} & \text{for } kt_{\text{eq}} \gg R(t_{\text{eq}}) \end{cases} \tag{2.71}$$

Recall that the spectral index is supposed to be close to 1. For baryon perturbations the story is a little bit different. The modes that entered during radiation domination did not grow but were subject to damped acoustic oscillations. For baryons the power spectrum falls more sharply for large k and small oscillations are imprinted to power spectrum (so called baryon acoustic oscillations). For the modes that were frozen during radiation domination no difference to a pure CDM density is observable. The power spectrum is influenced by the following quantities

- the slope depends on the spectral index n_s
- the position of the maximum k_{max} depends on the time of matter radiation equality and therefore on the ratio of ρ_m/ρ_r. As the amount or radiation today is fixed by the temperature of the CMB, this constrains the matter density today.

– the shape for $k > k_{\max}$ depends on the ratio of ρ_b/ρ_{CDM}.

Their effect on the power spectrum can be seen in figure 2.3. The SDSS collaboration measured the large scale structure power spectrum by their search for luminous red galaxies up to red-shifts $z \approx 5$. Their result is shown in figure 2.4.

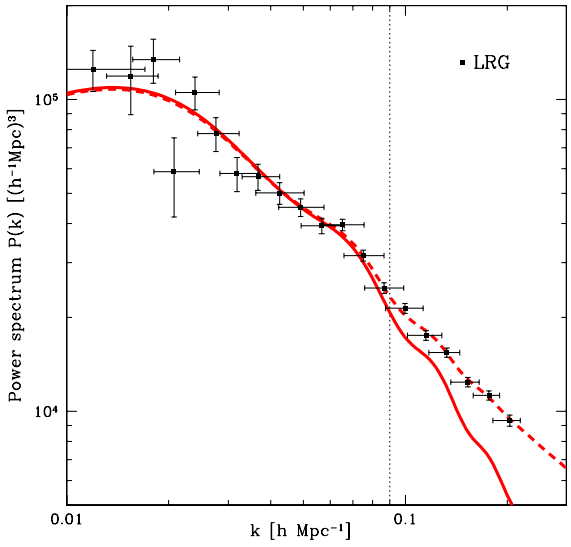

Figure 2.4: The observed power spectrum measured by the SDSS collaboration [23]. The results for the luminous red galaxies survey are shown. The solid curve shows the predictions using the best fit of WMAP3 parameters. The dashed line contains non-linear corrections to the predictions for small length scales.

2.3.3 CMB anisotropies

We will now turn to the power spectrum of the CMB anisotropies. If decoupling is a fast process the small fluctuations in the photon temperature before decoupling are frozen in. Photons propagate freely until today and their spectrum still contains the fluctuations of the moment of decoupling. We can measure the temperature anisotropy $\left.\frac{\delta T}{\bar{T}}\right|_{\text{obs}}(\vec{n})$ in a given direction $\vec{n}$. These fluctuations can be expanded in terms of spherical harmonics

$$\left.\frac{\delta T}{\bar{T}}\right|_{\text{obs}}(\vec{n}) = \sum_{\ell m} a_{l,m} Y^{\ell,m}(\vec{n}) \quad . \tag{2.72}$$

The statistic isotropy of the universe implies that all ms are equivalent, i.e. there is no preferred direction in the sky. The statistical properties of fluctuations depend only on the angular separation between two points and not their orientation in the sky. The power summed over all ms for a given ℓ is $(2\ell+1)C_\ell/(4\pi)$ [12], where

$$C_\ell = \langle |a_{\ell m}|^2 \rangle \tag{2.73}$$

Calculating its average value over all ms for a given ℓ allows one to compare the observed mean value to the predicted value. However this implies that for small ℓ only very few m values can be observed and the average is not necessarily very close to the predicted value because of

simple statistical uncertainties. This limitation is due to the fact that we can observe only one universe but our theory makes statistical predictions. This principle is called cosmic variance. An anisotropy with multipole ℓ corresponds approximately to an angle $\theta \sim \frac{\pi}{\ell}$ on the sky.

Before turning to the predicted spectrum, let us recall that the CMB is an almost prefect black body with temperature $T_\gamma = 2.7255 \pm 0.0006$ K (1σ) [17] with only very small asymmetries. It has its maximal anisotropy in the first multipole $\ell = 1$ (a dipole). The dipole is a result of the velocity of our laboratory reference frame with respect to the reference frame of the photon fluid. The relative velocity is a result of the velocity of our solar system in the galaxy and of the velocity of the galaxy in the local group. The dipole is normally subtracted from the CMB power spectrum.

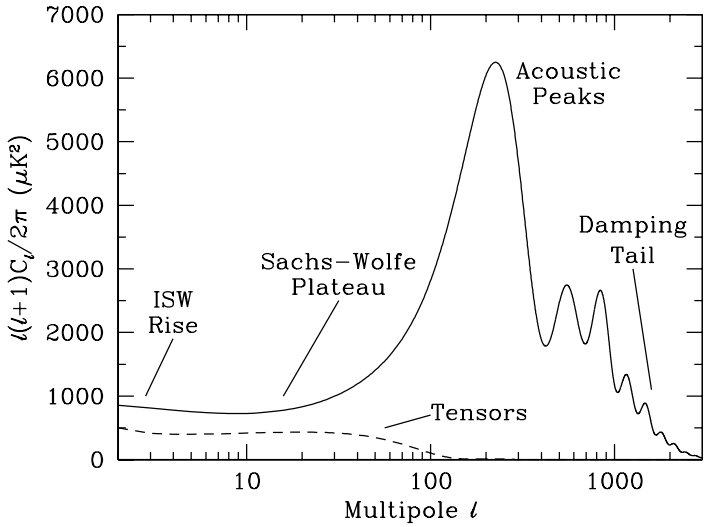

Figure 2.5: A sketch of the CMB anisotropy power spectrum, from [12]. The solid line is for scalar modes with adiabatic initial conditions. It shows the mains features described in the text: integrated Sachs-Wolf effect, Sachs-Wolfe plateau, acoustic oscillations and the Silk damping tail. The tensor modes are also shown, with an arbitrary normalization.

We will now discuss the main features of the CMB power spectrum. For the moment we will only consider adiabatic initial conditions. The CMB power spectrum is divided into three regions.

– **Sachs-Wolfe plateau and ISW rise for $\ell \lesssim 100$**
The horizon scale at the moment of last scattering is seen at multipoles of the order of $\ell \sim 100$. Anisotropies on larger scales, i.e. with $\ell < 100$, have not yet entered the horizon before photon decoupling and have therefore only been redshifted by expansion so that they have simply the initial perturbation spectrum imprinted.
The photon spectrum is not only redshifted because of expansion but also contains a shift due to the gravitational Doppler effect. The difference between the local value of the gravitational potential at emission and detection shifts the wavelength of photons. The gravitational Doppler effect is called the Sachs-Wolfe effect. Imagine a point at the last scattering surface (LSS) with a positive temperature fluctuation and consequently a photon over-density. The over-density creates a gravitational potential which redshifts the photons that leave it. The total effect on the photon wavelength is that it is redshifted,

i.e. it appears as a cold spot on the CMB anisotropy map. A nearly scale invariant initial spectrum predicts a constant power spectrum $\ell(\ell+1)C_\ell \sim$ const for small ℓ, the so called Sachs-Wolfe plateau [24].
For small ℓ the time dependence of the gravitational potential is also important. During its journey from the LSS to us the photon travels through the gravitational potential and gets red- and blue-shifted. If the potential is static, only the difference between initial and final potential is important. However if the potential is time dependent the photon can accumulate additional red or blue-shift. During matter domination the gravitational potential is constant in time. Time variations can occur just after decoupling when radiation density is not yet completely negligible or at late times during the domination of a cosmological constant. The first effect, called early-integrated-Sachs-Wolf effect (EISW), enhances mainly the power in $20 < \ell < 200$. At late times if the equation of state is different from $p/\rho = w = 0$, i.e. not an exact cosmological constant, then this effect raises the power spectrum at lowest ℓ above the Sachs-Wolfe plateau. This rise due to a time dependent potential at late times is called (late-)integrated-Sachs-Wolfe (ISW) rise. However such a rise is hard to discover because of cosmic variance.

– **Acoustic oscillations for $100 \lesssim \ell \lesssim 1000$**
The rich structure in the intermediate range of the power spectrum is due to acoustic oscillations. The modes that entered the horizon during radiation domination underwent acoustic oscillations because of the interplay of gravity and pressure. When the photon fluid decouples from baryons the oscillations remain frozen in the spectrum. The first and main peak in the spectrum is formed by modes that entered shortly before decoupling and went through 1/4 of an oscillation period, when the amplitude of the oscillation is maximal. Even peaks in the spectrum correspond to maximal under-densities in the photon fluid.

– **Damping tail for $\ell \gtrsim 1000$**
For large multipoles the spectrum is suppressed by Silk damping. If decoupling was a instantaneous process a photon observed in direction $\vec{n}$ would only carry information about the local temperature variation on the LSS in the same direction. However the mean free path of photons does not jump instantaneously to infinity at the moment of decoupling but grows in a continuous way. When photons leave equilibrium they can still scatter elastically and change the direction of their trajectory. When we observe a photon from direction $\vec{n}$ it does not exactly carry the information from the same direction but from a point a little bit around it. The incertanty is of the order of the mean free path after decoupling. This implies that correlations on smaller scales are erased and the power spectrum drops asymptotically to zero for large ℓ.
Another effect on small length scales is due to gravitational lensing. When photons travel to us they cross regions with large matter densities at late times (when structure growth has already reached the non-linear regime). However this is a second order effect and we will not consider it in more detail here.

Figure 2.5 shows a sketch of the CMB power spectrum for scalar adiabatic perturbations with the different effects discussed in the text. The most recent measurement of the CMB power spectrum was done by the PLANCK satellite [25]. Its result is shown in figure 2.6.

Isocurvature perturbations give rise to a different spectrum of the CMB (c.f. figure 6.5). As the spectrum of adiabatic fluctuations looks exactly like the data, isocurvature perturbations are strongly disfavoured. Only a small admixture of about 4% isocurvature modes is allowed [12].

Inflation predicts not only scalar perturbations but also tensor modes (gravitational waves). Their amplitude is proportional to the potential of the inflaton $A_t \propto V$. A larger gravitational

wave contribution is predicted when inflation takes place at a higher energy. The tensor ratio r is usually defined by the ratio of the scalar to tensor power spectrum at small ℓ. It is hard to detect tensor modes in the CMB power spectrum because they simply add to the spectrum of scalar modes a low ℓ and there is no way to disentangle them from the scalar modes. However measuring the polarization of the CMB the BICEP2 experiment recently announced the discovery of gravitational waves in the CMB [26]. A tensor contribution $r = 0.20^{+0.07}_{-0.05}$ was found.

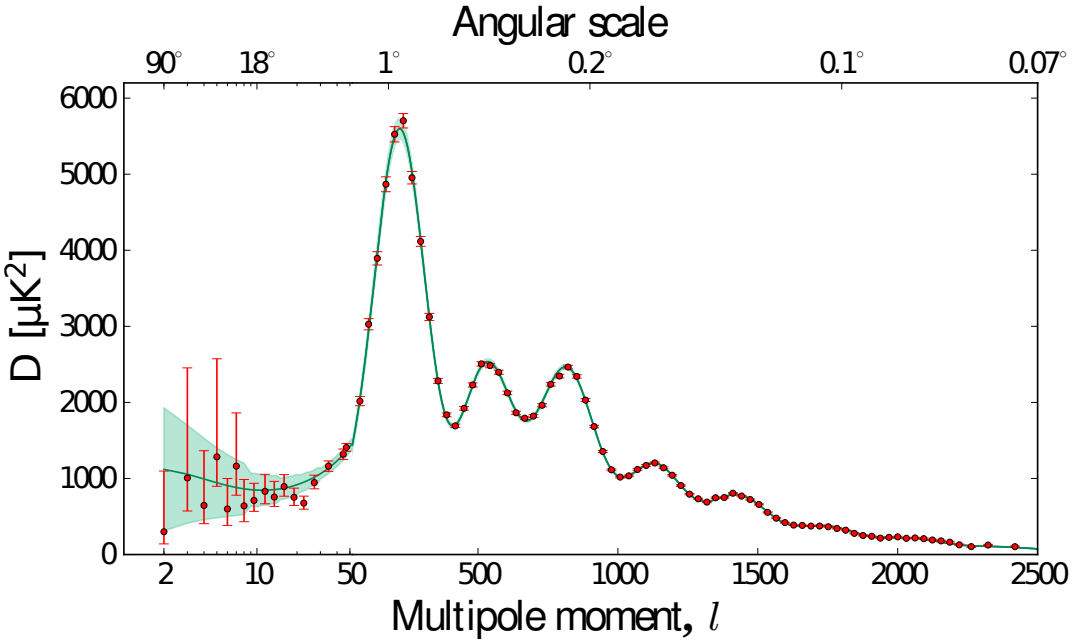

Figure 2.6: The power spectrum obtained by the PLANCK collaboration [25]. The green band indicates the uncertainty due to cosmic variance. The solid green line is the predicted power spectrum using the best fit values. The agreement is astonishing!

2.4 Dark Matter

As we have seen before cosmology tells us that the matter density in our universe does not only consist of baryonic matter but that most of the matter density is due to some unknown source, called dark matter. SM particles cannot provide such an additional source of matter, so that the observation of dark matter is a clear indication to physics beyond the SM and a very active topic of current research. Until today the particle physics origin of dark matter remains an open question. Here we will review evidences for dark matter on different scales, possible particle candidates as well as current experimental searches.

2.4.1 Evidence for dark matter

A first indication for dark matter was found by the Dutch astronomer J. H. Oort in 1932 [27]. Oort measured the Doppler shifts of stars in the Milky Way and determined their velocities. He

found that some stars moved with velocities larger than the escape velocity of the gravitational potential of luminous matter. He concluded that the Milky Way must contain at least one additional invisible species of matter. Almost at the same time Fritz Zwicky studied the velocity distribution of individual galaxies in the Coma galaxy cluster [28]. Using the Virial theorem he estimated the gravitational mass of the cluster and compared it to the mass distribution which he could extract by the observation of the luminosity of nebulae in the cluster. He found that the luminous matter was only a fraction of the gravitational matter. Since then a large number of evidences for dark matter have been observed on different length scales. Some examples are given in the following.

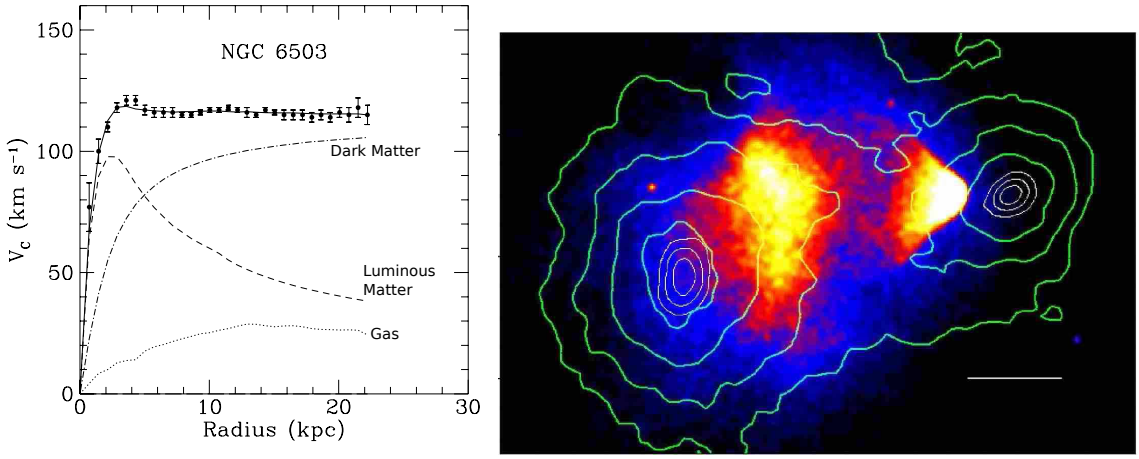

Figure 2.7: (**Left**) A typical example of the rotation velocity in a spiral galaxy, adapted from [29]. Considering luminous matter and gas one would expect the rotation velocity to fall down for large distances from the galactic centre. But observations show that the rotation curve is practically flat, which can only be explained if additional matter is present. (**Right**) The bullet cluster from [30]. The yellow and red colours show X-ray emission of the gas. The green lines show the gravitational potential. It is clear that maximum of gas density and total matter density do not coincide with each other.

Galaxy scale

The most important evidence for dark matter on galactic scales comes from rotation curves in galaxies. Measuring Doppler shift of the 21 cm line one can reconstruct the rotation velocity as a function of the radius in a spiral galaxy. Using Newtonian dynamics one can show that the rotation velocity at a given radius r is

$$v(r) = \sqrt{\frac{GM(r)}{r}} \tag{2.74}$$

where $M(r)$ is the mass enclosed within the radius r: $M(r) = 4\pi \int \rho(r) r^2 dr$. If luminous matter was the only source of matter, one would expect that the rotation curve falls like $r^{-1/2}$ beyond the visible disk R_{vis}. However the observations indicate that the rotation curve stays constant for $r > R_{\text{vis}}$, c.f. figure 2.7. To explain a constant rotation cure, the enclosed matter must grow linearly with the radius, $M(r) \propto r$, which implies a dark matter density profile like $\rho(r) \propto r^{-2}$. Only additional matter can explain the observed rotation curves.

Galaxy cluster scale

The most famous example for dark matter evidence on galaxy cluster scales is the bullet cluster. A smaller sub cluster is colliding with a galaxy cluster (1E 0657-558). During the collision the galaxies do not collide but simply pass by each other and are only slowed down by gravitational interactions. The baryonic mass of both clusters is dominated by a gas which interacts much more and which is heated up by the collision. The gas emits a large amount of X-rays that were observed by NASA's Chandra-X observatory. The gas corresponds to the red, yellow and bright colours in figure 2.7 (right). Using weak lensing of objects behind the bullet cluster one can measure the gravitational mass distribution, given by the green contours in the picture. It is obvious that the centre of baryonic mass and of gravitational mass do not coincide. Only an additional invisible matter contribution can explain this discrepancy. One can also see that the dark matter halo of both galaxies do not seem to have been influenced by the collision. Dark matter is a collision-less fluid. Another famous examples of a galaxy cluster that shows the existence of dark matter is MACS J0025.4-1222.

Cosmological scale

On galactic scales we have seen that evidence for dark matter is provided by the fluctuations in the CMB and by the large scale structure power spectrum. The CMB tells us that even at the moment of decoupling dark matter was already present and even dominating the universe. The large scale structure power spectrum shows that during structure formation dark matter played a very important role.

Altogether the evidence for dark matter is extraordinary: from very early in the thermal history until today and from scales as small as the size of individual galaxies until the size of the observable universe today. Parts of the observed phenomena can be explained using alternative theories of gravity [31] but until today it is not possible to explain the observational evidence on all length scales with one coherent theory of modified gravity.

2.4.2 Candidates

Until now the particle physics nature of dark matter has not yet been discovered. A large range of theoretical candidates exist and are actively searched for. Before giving a short list of possible candidates we have to distinguish between to possible classes of dark matter: hot and cold dark matter. Hot dark matter is made of particles that became non-relativistic just before matter-radiation-equality or even later and have still quite large velocities during structure formation whereas cold dark matter particles have negligible velocities during structure formation.

The large velocities of hot dark matter erase perturbations on structures smaller then the free-steaming length of the DM particles. The best example of a hot dark matter candidate are neutrinos with masses $m_\nu \sim 30$ eV. For neutrinos the cut-off in the perturbation spectrum is [13]: $\lambda_D = 40 \left(\frac{m_\nu}{30 \text{ eV}}\right)^{-1}$ Mpc. This means that the smallest scales initially formed are of the size of superclusters. When these structures go non-linear they condense into bound objects within which baryons collide with each other and can dissipate energy away until they form gravitationally bound objects on smaller scales, like galaxies. The formation of structures in a hot dark matter model is said to be "top down".

In models of hot dark matter, galaxies form only quite late, $z \leq 1$. Which is contradictory with the observation of a large number of galaxies with larger redshifts $z \lesssim 3$. Another problem

of hot dark matter is the mismatch of scales: the typical size on which the galaxy correlation function shows non-linearity is $r \approx 5h^{-1}$ Mpc. Hot dark matter predicts non linearity at scales $\lambda_D = 40 \left(\frac{m_\nu}{30 \text{ eV}}\right)^{-1}$ Mpc. One can reconcile the two scales by adjusting the neutrino mass but then the neutrino relic density is too large $\Omega_\nu h^2 \sim 2$. Today hot dark matter is almost completely excluded by CMB precision measurements, e.g. the PLANCK collaboration gives an upper limit on the neutrino mass $\sum m_\nu \leq 0.23$ eV (95% CL) .

Cold dark matter also has a cut-off in its perturbation spectrum but it is irrelevantly small ($\ll 1$ pc). As smaller fluctuations start to grow earlier, the first objects that are formed are of sub-galactic size. These objects virialize into gravitationally bound objects with a radial density profile like galactic DM halos. Baryonic matter can lose energy through dissipative interactions and condenses further. In cold dark matter models structures form "from the bottom up". Cold dark matter seems to fit all current observations so that the cosmological standard model today is called the Λ Cold Dark Matter model.

The requirements for a good dark matter candidate are the following:
- it must have the right relic abundance $\Omega_{\text{CDM}} h^2 \approx 0.012$
- it must be very weakly interacting with SM particles, it is even possible that dark matter has only gravitational interactions with SM particles
- during structure formation, it must be non-relativistic with negligible velocities = CDM
- the lifetime of the particle must be at least as long as the age of the universe today

However these are not the only constraints on dark matter candidates. Direct and indirect detection experiments, collider searches and astrophysical observations can further constrain dark matter candidates and reduce the available parameter space. A large number of candidates has been proposed and here we will only give a short list of the best motivated [2] possible candidates.

Weakly interacting massive particles

The most commonly cited candidate is a WIMP (weakly interacting massive particle). It is a whole class of candidates with similar properties. WIMPs are very popular candidates because their relic density is naturally of the right order when their annihilation cross section that controls the freeze-out is of the order of a electroweak process.

To illustrate the freeze-out of a particle species consider a stable particle χ that annihilates into SM model particles X: $\chi + \bar{\chi} \leftrightarrow X + \bar{X}$ with a thermally averaged cross section $\langle \sigma |v| \rangle$, which is of the order of a typical (electro-) weak process. The Boltzmann equation can be written as

$$\dot{n}_\chi + 3Hn_\chi = -\langle \sigma |v| \rangle (n_\chi^2 - (n_\chi^{\text{eq}})^2) \tag{2.75}$$

where n_χ^{eq} is the equilibrium number density of χ. At high temperature χ is in thermal equilibrium because its interactions with the thermal bath are fast. When the temperature drops $T \lesssim m_\chi$, the number density of χ gets exponentially suppresses, as long as $\langle \sigma |v| \rangle n_\chi^{\text{eq}} > H$. However when the number density becomes too small, the annihilation rate becomes smaller than the expansion rate H, and the number density freezes in. If χ is stable, from the moment of freeze-out on the number density gets only depleted by expansion. The freeze out temperature is almost independent of the exact WIMP properties, $T_F \approx m_\chi/20$. The relic density of the

2. The judgment of the motivation of a candidate is certainly a highly subjective one.

WIMP can be obtained by solving the Boltzmann equation numerically [12]

$$\Omega_\chi h^2 \approx \text{const}\frac{T_0^3}{m_{\text{Pl}}^3\langle\sigma|v|\rangle} \approx \frac{0.1 \text{ pb}}{\langle\sigma|v|\rangle} \tag{2.76}$$

where T_0 is the CMB temperature today. If the annihilation cross section is larger, the WIMPs stay longer in thermal equilibrium and their relic density is smaller, as shown in figure 2.8.

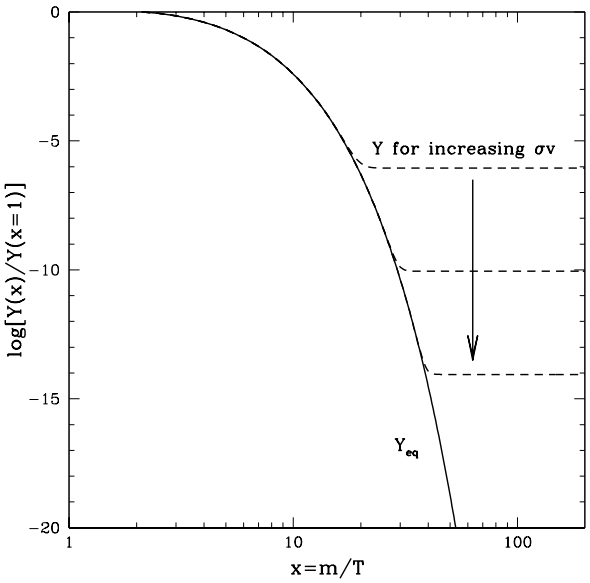

Figure 2.8: The figure from [32] shows the evolution of the relative WIMP number density $Y(x) = n_\chi(x)/s(x)$ as a function of $x = m_\chi/T$. As long as the annihilation rate is fast, the χ number density traces the equilibrium density which is exponentially suppressed. When the annihilation rate becomes slow, the number density freezes-out. The larger the annihilation cross section the longer χ is in thermal equilibrium and the smaller the relic density.

Many extensions of the SM predict the existence of WIMPs, some examples are

– Supersymmetry
  In SUSY theories one often introduces a discrete $\mathcal{Z}_2$ symmetry, called R-parity, to suppress operators that harm the stability of the proton. Supersymmetric particles are differently charged under this symmetry than SM particles. Therefore R-parity implies that the lightest supersymmetric particle (lsp) is stable. For a long time sneutrinos have been considered as dark matter candidates however their expected scattering rate with nucleons is already excluded by direct detection experiments. Other possible candidates are neutralinos or gravitinos. Gravitinos might be very difficult to detect because they have only gravitational interactions with SM particles.
– Kaluza-Klein candidates
  Models with extra spatial dimensions can also provide a dark matter candidate. In particular in models with universal extra dimensions, i.e. SM fields are free to propagate in the bulk (= extra dimension + usual 4 dimensions), the lightest Kaluza-Klein particle can be stable and can be a dark matter candidate. Extra dimensions compacted on an orbifold often have some geometric symmetry which is a subgroup of the higher dimensional Poincaré group. The momentum conservation in the extra dimensions can be broken down

to some discrete symmetry, KK-parity, which ensures the stability of the lightest Kaluza-Klein particle. The Kaluza-Klein decomposition of the $4+N$ dimensional field gives an infinite tower of 4 dimensional fields with growing masses. If the lightest Kaluza-Klein excitation is neutral and charged under KK partiy, it is a viable dark matter candidate. Potential candidates are KK gauge bosons, KK neutrinos, KK scalars or KK gravitons [33]

Neutrinos

We have already seen above that SM neutrinos with small masses cannot be the dominant dark matter component. However right-handed neutrinos with order keV masses can be viable dark matter candidates. Sterile neutrinos can be produced by mixing with standard neutrinos [34]. But the mixing also introduces a loop decay into a standard neutrino and a photon. The lifetime of the sterile neutrino depends on its mixing angle with neutrinos. The non-observation of an X-ray line restricts the production mechanism. Such constraints can be circumvented if the production is enhanced due to the MSW effect or if the dominating production mechanism is the decay of a gauge singlet boson. Very recently a X-ray line at about 3.5keV has been discovered from various galaxy clusters and the Andromeda galaxy [35, 36]. This could be a first sign of sterile neutrino dark matter.

Axions

Axions were originally introduced to solve the strong CP problem. However it turns out that axions are also perfectly suitable clod dark matter candidates. A major research part of this thesis is dedicated to axions. More details on axions can be found in chapter 6.

2.4.3 Search for DM

Dark matter candidates are actively searched for. The search strategy depends very much on the candidate one is looking for. Experiments looking for axions are reviewed in chapter 6. To search for WIMPS, one often uses direct detection experiments. Indirect detection experiments are sensitive to a large range of models.

Direct detection

Direct detection experiments try to detect the nuclear recoil produced by a dark matter particle that hits a nucleus. The source of dark matter particles is the galactic halo. The recoil energy depends on the velocity of the DM particles. In the standard halo model the mean velocity is $v_0 \approx 220$ km/s [12]. WIMPs with masses between 10 GeV and 10 TeV produce nuclear recoil energies of the order $1-100$ keV. The rate of the events depends on the local dark matter density, which is given in the standard halo model by 0.39 GeV/cm^3. Using this value, the expected rate depends only on two unknown parameters: the DM mass and the interaction cross section. As the expected rates are very low, of the order of 1 event kg^{-1}day^{-1}, the reduction of background events is of highest priority for experiments. Most of these experiments are situated in underground laboratories to shield themselves against cosmic rays. Another important issue is the energy threshold: if one wants to study low mass WIMPs (below 10 GeV) one needs to be able to detect nuclear recoils with energies below 1 keV. A WIMP signal shows two important signatures: the direction of the nuclear recoil has strong asymmetry from day to night because of the rotation of the earth. Furthermore a few percent annual modulation of the signal is expected from the speed of the earth that is added to or subtracted from the speed of the sun.

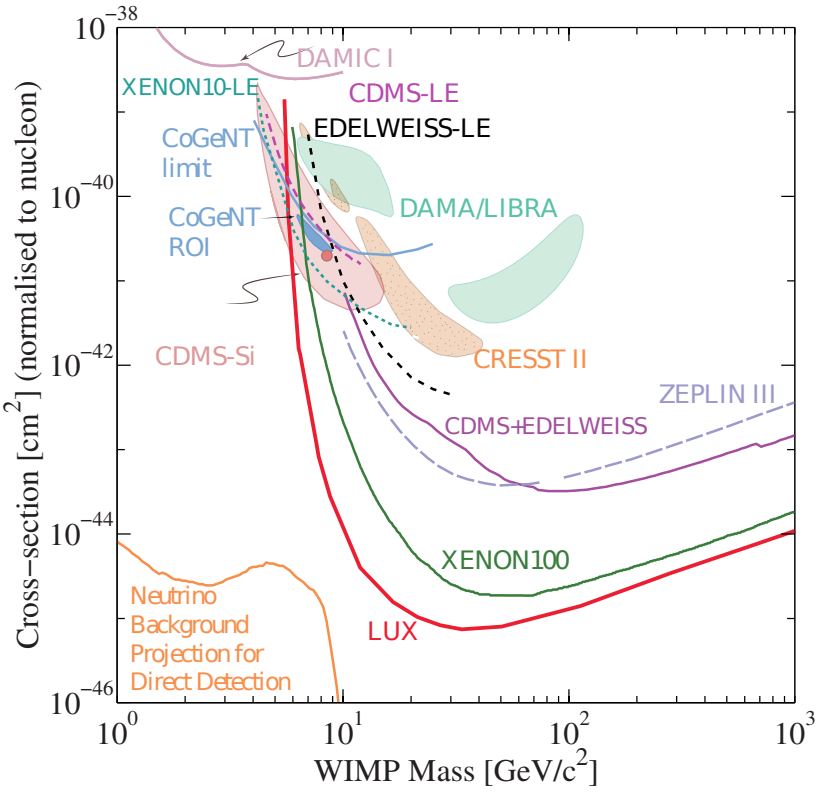

Figure 2.9: The figure shows observed exclusion lines and detection ranges by different experimental searches. The different experiments with references are described in the text. Adapted from [12].

A brief overview of the most important experiments and their results is given in the following.

The CoGeNT experiment used Germanium detectors with a low energy threshold 400 eV. They claim to see a signal at low recoil energies that could be compatible with a WIMP mass $7-11$ GeV and a cross section 3×10^{-5} pb [37]. They see an annual modulation of their signal [38] but the amplitude of the modulation is much stronger than what is expected for such a WIMP.

The DAMA collaboration used sodium iodide scintillators and has reported the observation of a signal after 6 years of data taking. They observe an annual modulation of the signal at 8.9σ [39]. The observation can either be explained by a WIMP with mass ~ 50 GeV and cross section 7×10^{-6} pb or a lighter WIMP with mass of $6-10$ GeV and cross section $\sim 10^{-3}$ pb.

The EDELWEISS [40] and CDMS [41] collaborations use semiconductor detectors (Ge or Si) which are operated at very low temperatures so that they can simultaneously measure the phonon and ionization signal and are able to discriminate between nuclear and electric recoil. Both groups have performed a special low energy analysis [42, 43] which give comparable exclusions. They exclude a large part of the DAMA region and cut a part of the CoGeNT region of interest. The combined CDMS and EDELWEISS data give currently the second best exclusion on spin independent cross sections for $m_\chi > 80$ GeV [44]. The CDMS collaboration has recently reported [45] an excess of events that are best fit by a WIMP with mass 8 GeV and a cross section $\sim 10^{-7}$ pb. The EDELWEISS experiment does not only look for WIMPs but is also sensitive to axions [46]. They are building a new detector with around 30 kg of detector material which should

start to operate soon.

Noble gas detectors have a similar advantage as semiconductor detectors because one can measure both the primary scintillation and the ionization electrons, which can be used for background reduction. The XENON100 experiment took data for 225 days and did not find any excess of events [47]. The collaboration has set very strong bonds for large WIMP masses. The LUX detector is also a Xenon detector which has recently published its exclusion limits after 85 live days [48]. It sets the most stringent limits on the WIMP cross section for masses larger then 8 GeV. It excludes completely the CoGeNT region of interest. A summary of the all mentioned experiments is found in figure 2.9.

Indirect detection

Indirect searches look for the annihilation products of WIMPs. As the annihilation rate depends strongly on the local DM density, one should look at regions with large DM concentrations. DM can be locally trapped in large gravitational potentials like the earth, the sun or the centre of our galaxy. The most frequent decay products are photons, neutrinos and antimatter particles like antiprotons and positrons. Some DM candidates can also decay with a lifetime comparable to the age of the universe. An example is a possible photon line that would be emitted by sterile neutrinos in the keV region.

Photons can be produced with a continuous spectrum when DM particles annihilate to a quark and an antiquark. The jets can then emit photons of different energies and produce a spectrum of photons. If DM candidates can annihilate into a pair of photons, or a photon and a Z boson (via one loop) then a γ line is expected at an energy corresponding to half of the WIMP mass. By re-analysing the data of the FERMI satellite, Weniger found a γ ray line at 130 GeV in the spectrum coming from the centre of our galaxy [49]. The FERMI collaboration confirmed the existence of this line but with a lower significance [50]. The cross section needed to explain this line is larger than the normally predicted cross section of a thermal WIMP. This hint has triggered a large amount of speculation about the interpretation as a dark matter signal.

Neutrinos from dark matter annihilations could be created in the sun or in the earth. The annihilations would be a source of muon neutrinos which could be observed by neutrino experiments like IceCube [51] or SuperKamiokande. Until now no excess that can be related to dark matter has been observed.

Antimatter is an excellent way to detect dark matter because it is quite rare and astrophysical processes producing antimatter are well understood (as long as the energy is not too high). However positrons and antiprotons are charged and are therefore deflected by magnetic fields or interactions with the CMB, so that information about their source is lost. The PAMELA [52] and AMS02 [53] experiments measured the positron flux and found a rise in the positron spectrum for $10 - 200$ GeV. To explain this rise in terms of a WIMP annihilation one needs to evoke rather large annihilation cross sections or a very clumpy dark matter halo. PAMELA measured also the antiproton flux and found no excess [54]. This sets even stronger constrains on models that try to interpret the asymmetry in the $e^{\pm}$ spectrum as WIMP annihilations.

In summary dark matter is actively searched for using different types of experiments. For direct detection experiments the situation is not clear because of claimed signals in regions where other experiments exclude the existence of a signal. Indirect searches show several excesses but they cannot easily be explained simultaneously in terms of dark matter and point in different directions. Only further experimental efforts can clarify the situation and reveal the origin of dark matter.

Chapter 3

Neutrino physics beyond the SM

Neutrinos masses are probably the most model independent and clearest sign of physics beyond the standard model. In 1968 the Homestake experiment by Ray Davis was the first to measure electron neutrinos coming from the sun and observed a deficit compared to the predictions of the solar standard model. This difference can be explained by neutrino oscillations. Since neutrino oscillations have been observed for the first time, a large number of experiments established and tested the picture of neutrinos oscillating from one flavour to another. These oscillations are only possible if at least two of the tree neutrinos are massive, even if their masses are tiny compared to other masses in the SM. A very elegant way of explaining small neutrino masses naturally is the seesaw mechanism. It describes neutrino masses as a low energy effect suppressed by the high scale of new physics.

This chapter will briefly review the theory of neutrino masses and oscillations, their experimental status and then explain the seesaw mechanism, which will be important for leptogenesis. The introduction of neutrino physics is very much inspired by [55] which contains not only a very complete picture of role of neutrinos in cosmology but also a very nice introduction to the physics of neutrinos.

3.1 Neutrino oscillations

3.1.1 Dirac mass term

To explain neutrino oscillations one has to introduce a neutrino mass term which is absent in the SM. Like for the electron one needs a right-handed $SU(2)$ singlet to introduce a Yukawa coupling between the Higgs field and the neutrino which then forms a Dirac mass term after spontaneous symmetry breaking. The right-handed neutrino $N_{R\alpha}$ is a singlet under all three SM gauge groups. It has therefore almost no interactions with other SM particles and is called sterile. The lepton Yukawa part of the Lagrangian is given by

$$\mathcal{L}_L = -Y'^{\ell}\bar{\ell}_L H e_R - Y'^{\nu}\bar{\ell}_L(i\sigma_2 H^*)N_R \tag{3.1}$$

where family indices are suppressed. After electroweak symmetry breaking these two terms give rise to mass terms for charged leptons and neutrinos. The Yukawa matrices are not diagonal but can be diagonalized using biunitary transformations

$$V_L^{\ell\dagger} Y'^{\ell} V_R^{\ell} = Y^{\ell} \tag{3.2}$$

$$V_L^{\nu\dagger} Y'^{\nu} V_R^{\nu} = Y^{\nu} \tag{3.3}$$

where Y^ℓ and Y^ν are diagonal matrices. The transformation matrices $V^\ell_{L,R}$ and V^ν_R can be absorbed in a redefinition of the fields ℓ_L, e_R and N_R. However, like in the case of massive quarks, there is one transformation matrix too much. The matrix V^ν_L cannot be adsorbed in a redefinition of ℓ_L because this would change the first term in the Lagrangian. This means that for neutrinos, the flavour basis in which electroweak interactions are diagonal is not the same basis that diagonalises the mass matrix. The unitary transformation matrix between mass eigenstates and interaction eigenstates is called the PMNS matrix [56, 57, 58]

$$U \equiv V_L^{\ell\dagger} V_L^\nu \quad \text{and} \quad \nu_{L\alpha} = U_{\alpha k}\nu_{Lk} \ . \tag{3.4}$$

It is the analogue of the CKM matrix in the leptonic sector. From now on Greek indices stand for the interaction basis $\alpha \in \{e, \mu, \tau\}$ whereas Latin indices imply the mass eigenstates $k \in \{1, 2, 3\}$. The neutrino mass eigenvalues are given by $m_k = Y^\nu_k v$ where $v = \langle H \rangle \approx 174$ GeV is the vacuum expectation value of the Higgs field.

A convenient parametrisation of the PMNS matrix is given in terms of three angles θ_{12}, θ_{13}, $\theta_{23} \in [0, \pi/2]$ and one phase $\delta \in [0, 2\pi]$

$$\mathbf{U} \quad = \quad \begin{bmatrix} c_{13}c_{12} & s_{12}c_{13} & s_{13}\ e^{-i\delta} \\ (-s_{12}c_{23} - s_{23}s_{13}c_{12}\ e^{i\delta}) & (c_{23}c_{12} - s_{23}s_{13}s_{12}\ e^{i\delta}) & s_{23}c_{13} \\ (s_{23}s_{12} - s_{13}c_{23}c_{12}\ e^{i\delta}) & (-s_{23}c_{12} - s_{13}s_{12}c_{23}\ e^{i\delta}) & c_{23}c_{13} \end{bmatrix} \tag{3.5}$$

The matrix breaks lepton flavour conservation but still conserves total lepton number. A non-zero value of δ leads to CP violation which is actively searched for in upcoming neutrino experiments like NoνA.

This simple extension of the SM is sufficient to explain all data obtained from neutrino oscillations (except for the so called anomalies). However theoretically it is not very appealing because in order to explain the smallness of neutrino masses, the Yukawa couplings need to be tiny $Y^\nu_k \lesssim 10^{-12}$. The question is: why are neutrino Yukawa couplings so small, compared to the top quark Yukawa coupling $Y_{\text{top}} \sim 1$? One way to explain this is the seesaw mechanism which will be introduced in the next section.

3.1.2 Neutrino oscillation theory

Oscillations between different neutrino flavours are a result of the fact that the mass eigenstates are not identical with the interaction eigenstates. Neutrinos are produced as interaction eigenstate which is a superposition of several mass eigenstates which all propagate differently in time and give therefore rise to flavour oscillations.

We will consider the mixing of three neutrino flavours with a 3 mixing matrix U. The effect of additional n_s sterile neutrinos can easily be taken into account by using a $(3+n_s)\times(3+n_s)$ mixing matrix. We assume that at $t = 0$ a neutrino of flavour α is created. It can be written as a superposition of mass eigenstates

$$|\nu_\alpha\rangle = \sum_k U^*_{\alpha k}|\nu_k\rangle \tag{3.6}$$

The complex conjugate matrix U^* is used here because one has to use the creation operators to construct the initial states out of the vacuum. The mass eigenstates ν_k propagate as free waves

$$|\nu_\alpha(t, \vec{x})\rangle = \sum_k U^*_{\alpha k} e^{-ip_k\cdot x}|\nu_k\rangle \tag{3.7}$$

where p_k is the four-momentum of neutrino state k. Using the unitary of U one can invert equation (3.6) $|\nu_k\rangle = \sum_\beta U_{\beta k}|\nu_\beta\rangle$. This can be plugged into the previous equation to eliminate the mass eigenstates

$$|\nu_\alpha(t,\vec{x})\rangle = \sum_{\beta,k} U^*_{\alpha k} e^{-ip_k\cdot x} U_{\beta k}|\nu_\beta\rangle \tag{3.8}$$

The probability of measuring a neutrino of flavour β at time t and position $\vec{x}$ when at $t=0$ and $\vec{x}=0$ a neutrino of flavour α was produced can then be evaluated to

$$P_{\nu_\alpha\to\nu_\beta}(t,\vec{x}) = |\langle\nu_\beta|\nu_\alpha(t,\vec{x})\rangle|^2 = \sum_{k,j} U^*_{\alpha k}U_{\beta k}U_{\alpha j}U^*_{\beta j}e^{-i(p_k-p_j)\cdot x} \tag{3.9}$$

In all relevant cases neutrinos are ultra-relativistic. Furthermore for most experimental setups the distance L between creation and detection is the crucial variable and not the time of flight t. Using natural units one can therefore replace t by $\frac{L}{c} = L$. This simplifies the propagation $p_k\cdot x = E_k t - \vec{p}_k\cdot\vec{x} \approx (E_k - p_{zk})L$ where we have chosen our reference frame so that neutrinos travel in positive z direction. One can expand the energy as $E_j = p_z + \frac{m_i^2}{2p_z}$. Defining the mass squared difference $\Delta m^2_{kj} = m^2_k - m^2_j$ one can simplify

$$P_{\nu_\alpha\to\nu_\beta}(L) = \sum_{k,j} U^*_{\alpha k}U_{\beta k}U_{\alpha j}U^*_{\beta j}e^{-i\frac{\Delta m^2_{kj}}{2E}L} \tag{3.10}$$

It should not be surprising that for $L=0$ the probability becomes diagonal $P_{\nu_\alpha\to\nu_\beta}(L\to 0) = \delta_{\alpha\beta}$. To simplify equation (3.10) consider a case where two flavours participate in the mixing, e.g. ν_e and ν_μ. They are related to the two mass eigenstates via one single mixing angle

$$|\nu_e\rangle = \cos\theta|\nu_1\rangle + \sin\theta|\nu_2\rangle \tag{3.11}$$
$$|\nu_\mu\rangle = -\sin\theta|\nu_1\rangle + \cos\theta|\nu_2\rangle \tag{3.12}$$

In this case equation (3.10) gives the famous oscillation probability

$$P^{2\times2}_{\nu_e\to\nu_\mu}(L) = \sin^2(2\theta)\sin^2\left(\frac{\Delta m^2}{4E}L\right) \tag{3.13}$$

where Δm^2 is the mass squared difference between the two mass eigenvalues. Consequently oscillations are observable if $\frac{\Delta m^2}{4E}L = \mathcal{O}(1)$. If the distance between creation and detection is known with a much larger uncertainty than the occurring oscillation length $L^{\text{osc}}_{k,j} = 4\pi E/\Delta m^2_{kj}$, then one can simply average over the distances $L^{\text{osc}}_{k,j}$ and obtain

$$\langle P_{\nu_\alpha\to\nu_\beta}(L)\rangle = \sum_k |U_{\alpha k}|^2|U_{\beta k}|^2 \tag{3.14}$$

which is then independent of the distance L. In the opposite case of very short distances $L \ll L^{\text{osc}}_{k,j}$ the probability to observe a transition goes to zero.

Using oscillation experiments in vacuum one can determine the three neutrino mixing angles θ_{kj} and the mass squared differences but not the overall neutrino mass scale. One can also extract information about CP violation by comparing the oscillations of neutrinos and anti-neutrinos. The CPT symmetry that should be conserved in every quantum field theory implies $P_{\nu_\alpha\to\nu_\beta}(L) = P_{\bar\nu_\beta\to\bar\nu_\alpha}(L)$. However CP violation would manifest itself in the difference

$$P_{\nu_\alpha\to\nu_\beta}(L) - P_{\bar\nu_\alpha\to\bar\nu_\beta}(L) \neq 0 \quad \text{if } \delta \neq 0,\pi \ . \tag{3.15}$$

CP violation has not yet been observed but thanks to the large value of θ_{13} current experiments are coming very close to the needed sensitivity [59].

Neutrino oscillations in matter can significantly differ from neutrino oscillations in vacuum because the interactions between neutrinos and the particles forming the background matter change the propagation of different mass eigenstates. Because interactions couple to flavour eigenstates they significantly change the propagations of mass eigenstates which are not any more eigenstates of the Hamiltonian. If the typical oscillations length scale is much larger then the background inter particle spacing, one can define a neutrino refraction index n_ν which takes into account matter effects in the neutrino propagation.

$$n_\nu = \frac{p_{\text{matter}}}{p} \quad . \tag{3.16}$$

Here p_{matter} is the linear momentum of neutrinos in matter and p the momentum in vacuum. For ultra-relativistic neutrinos they can be related by

$$p_{\text{matter}} = p - V_{\text{CC}} - V_{\text{NC}} \ , \tag{3.17}$$

where V_{CC} (V_{NC}) is the effective potential that neutrinos feel due to their charged current (neutral current) interactions with the medium.

Normally the background medium (e.g. the sun) consists of electrons, protons and neutrons. Only electron neutrinos can have charged current interaction with the electron density. In [55] it is shown that the charge current effective potential can be written as

$$V_{\text{CC}} = \sqrt{2} G_{\text{F}} n_e \ , \tag{3.18}$$

where n_e is the electron density in the medium and G_F is the effective Fermi coupling constant. All three neutrino flavours take part in neutral current interactions with all three components of the medium. The neutral current effective potential is [55]

$$V_{\text{NC}} = \sqrt{2} G_{\text{F}} \left(n_e g_V^e + n_p g_V^p + n_n g_V^n \right) = -\frac{1}{2} \sqrt{2} G_{\text{F}} n_n \tag{3.19}$$

where $g_V^f = g_R^f + g_L^f$ is the vector coupling constant of fermion f induced by electroweak interactions. In the last step we used that $g_V^e = -g_V^p$ and that due to charge neutrality $n_e = n_p$.

Neutrinos in matter behave like they had an effective mass different from the vacuum mass. As neutrino oscillations only depend on the differences in masses, only different refractive indices for different flavours change their behaviour. In the three flavour mixing scenario the neutral current interactions change all three neutrino masses in the same way so that the net effect is zero. But if one considers sterile neutrinos one has to take them into account.

To see the effect of matter on neutrino oscillations concretely consider again the case of only two neutrinos ν_e and ν_μ with two mass eigenstates ν_1 and ν_2 as described in equation (3.12). The effective mixing angle in matter can be related to the vacuum mixing angle θ by [55]

$$\tan 2\theta_M = \tan 2\theta \left(1 - \frac{2|\vec{p}| V_{\text{CC}}}{\Delta m^2 \cos 2\theta} \right)^{-1} \quad . \tag{3.20}$$

The effective mass squared difference is then

$$\Delta m_M^2 = \sqrt{(\Delta m^2 \cos 2\theta - 2|\vec{p}| V_{\text{CC}})^2 + (\Delta m^2 \sin 2\theta)^2} \ . \tag{3.21}$$

In [60, 61] it was realised that the transition from one flavour to another is resonantly enhanced for

$$\Delta m^2 \cos 2\theta = 2|\vec{p}|V_{\mathrm{CC}} \tag{3.22}$$

If this condition is verified the effective mixing is maximal $\theta_M = \frac{\pi}{2}$ and the transition is the largest. This is called the MSW effect. It can play an important role in astrophysical environments like the sun or type II supernovae where the radial profile of the matter density can provide the right matter density for resonant enhancement of flavour oscillations at some point of the radial distribution.

3.1.3 Neutrino oscillation experiments

Neutrino oscillation experiments can be classified by the used neutrino sources. Natural neutrino sources like solar neutrinos and atmospheric neutrinos as well as artificial neutrinos from nuclear reactors or neutrino beams are used in experiments. They all have in common that the neutrino energy E and the distance between source and detection L must be chosen so that

$$\frac{\Delta m^2}{4E} L = \mathcal{O}(1) \tag{3.23}$$

in order to be able to detect neutrino oscillations. Experiments generally measure either the appearance of a neutrino flavour absent in the initial neutrino beam (appearance experiments) or the depletion of a flavour relative to its initial proportion (disappearance experiments).

Nuclear reactions in the sun like $p+p \to d+e^+ +\nu_e$ produce electron neutrinos with energies between 0.1 MeV and 10 MeV. In 1968 Ray Davis succeeded for the first time to detect solar neutrinos with his chlorine experiment in the Homestake mine. The experiment was based on the production of Ar through the reaction $\nu_e + {}^{37}\mathrm{Cl} \to {}^{37}\mathrm{Ar} + e^-$. The produced Ar was chemically separated from the chlorine and detected by its nuclear decay. The production reaction is only possible if the incoming neutrinos have a energy higher than 0.8 MeV. So a large part of the neutrino spectrum could not be measured. The experiment measured a large deficit in the electron neutrino flux relative to the expected one [62]. Other experiments like GALLEX/GNO [63] which measured also neutrinos with lower energy, forming the largest part of the solar spectrum, or the Super-Kamiokande experiment [64] confirmed the deficit and improved the precision on the neutrino flux. The proof that neutrino oscillations are responsible for the neutrino deficit pas given by the SNO experiment [65] which used a heavy water Cherenkov detector in the Sudbury Mine with 10000 t of D_2O. The experiment was sensitive to charged current, neutral current and elastic interactions

$$\nu_e + d \;\to\; p + p + e^- \quad \mathrm{CC} \tag{3.24}$$

$$\nu_\alpha + d \;\to\; p + n + \nu_\alpha \quad \mathrm{NC} \tag{3.25}$$

$$\nu_\alpha + e^- \;\to\; e^- + \nu_\alpha \quad \text{elastic} \tag{3.26}$$

It was therefore possible to measure the total solar neutrino flux of all three flavours which was found to be in agreement with the prediction of the solar standard model. It proofed that neutrinos did not simply disappear but change their flavour while travelling to earth. Solar neutrino experiments are sensitive to Δm^2_{21} and θ_{12}. The sign of Δm^2_{21} is fixed due to matter effects in the sun.

Atmospheric neutrinos are created when cosmic rays hit the atmosphere. These interactions create, among other particles, a large amount of pions which in their decays create neutrinos

and muons which themselves decay and produce a second generation of neutrinos.

$$\pi^+ \to \mu^+ + \nu_\mu \qquad \pi^- \to \mu^- + \bar{\nu}_\mu \tag{3.27}$$

$$\mu^+ \to e^+ + \nu_e + \bar{\nu}_\mu \qquad \mu^- \to e^- + \bar{\nu}_e + \nu_\mu \tag{3.28}$$

From this on can infer that the muon neutrino flux should be about two times the electron neutrino flux. The first sign of atmospheric neutrino oscillations was observed by the Super-Kamiokande experiment [66]. Atmospheric neutrinos should be produced uniformly around the earth. The experiment observed a deficit of up-going muon neutrinos which was compatible with neutrino oscillations between ν_μ and ν_τ. The difference comes from the fact that L, the distance between creation and detection, depends on the direction of the neutrinos. For down-going neutrinos it is minimal whereas for up-going neutrinos it is maximal. In this way the experiment could measure for the first time θ_{23} and $|\Delta m^2_{23}|$.

Reactor neutrinos are produced in the β decays of heavy nuclei used in nuclear power plants. The produced neutrinos are electron anti-neutrinos with typical energies of order MeV. The sensitivity to a certain Δm^2 depends on the baseline L. Short baseline experiments ($L \sim 10$ m) are sensitive to $\Delta m^2 \sim 0.1$ eV^2, experiments with a baseline around $L \sim 1$ km) can measure $\Delta m^2 \sim 10^{-3}$ eV^2. The (very) long baseline experiments ($L \sim 100$ km) measure consequently $\Delta m^2 \sim 10^{-5}$ eV^2. Very recently the three experiments DoubleCHOOZ [67], Daya Bay [68] and RENO [69] have measured for the first time θ_{13} by observing an electron antineutrino disappearance in the neutrino fluxes from nuclear reactors. To be able to measure the disappearance one has to know the initial number of produced neutrinos very exactly. Therefore these experiments used a near detector and a far detector and compared the two observed rates in order to cancel out uncertainties on the initial anineutrino flux.

From the seven parameters that characterise the neutrino mixing (three mass eigenvalues, three mixing angles and one phase) already five have been measured: all three mixing angles $\{\theta_{12}, \theta_{13}, \theta_{23}\}$ and two mass differences $\{\Delta m^2_{21}, |\Delta m^2_{31}|\}$. For the solar mass difference the sign is known whereas for the atmospheric mass difference the sign is still unknown. Depending on this sign one distinguishes two cases: normal hierarchy (NH) $m_1 < m_2 < m_3$ or inverted hierarchy (IH) $m_3 < m_1 < m_2$. The CP violating phase and the neutrino mass scale are still unknown. It is still possible that only two neutrinos are massive and that the third one is massless. The values of all measured parameters are given in table 3.1.

The three flavour neutrino mixing is a very successful theory that describes almost all observations of neutrino experiments. However there are also some observed phenomena that the three flavour neutrino mixing cannot explain, so called anomalies. If one wants to explain the observed data using neutrino mixing, one has to include additional neutrinos with quite a large mass $\Delta m^2 \sim 1$ eV^2 compared to the observed neutrino mass differences. But the measurement of the invisible width of the Z boson by the LEP experiment constraints the number of neutrinos to [71] $N_\nu = 2.9840 \pm 0.0082$ (1σ). The additional neutrinos, called sterile neutrinos, can therefore not be sensitive to electroweak interactions.

A first evidence was observed by the LSND experiment [72] which is a SBL experiment that uses an $\bar{\nu}_\mu$ beam and looks for the appearance of $\bar{\nu}_e$ in their beam. They observed an excess in anti neutrino events of more than 3σ above background that points to a mass difference $\Delta m^2 \sim 1$ eV^2 which is much higher than the mass differences observed by solar and atmospheric neutrinos. The MiniBooNE experiment was designed to check the LSND results and found no evidence for such oscillations in the neutrino mode $\nu_\mu \to \nu_e$. But in the antineutrino mode $\bar{\nu}_\mu \to \bar{\nu}_e$ an excess of $\bar{\nu}_e$ was observed [73]. The observed excess is compatible with the LSND results.

Parameter	best fit $\pm 1\sigma$	3σ range
$\sin^2\theta_{12}$	$0.302^{+0.013}_{-0.012}$	0.267 to 0.344
$\sin^2\theta_{23}$	$^*0.413^{+0.037}_{-0.025}$	0.342 to 0.667
$\sin^2\theta_{13}$	$0.0227^{+0.0023}_{-0.0024}$	0.0156 to 0.00299
$\delta/1^\circ$	300^{+66}_{-138}	0 to 360
$\frac{\Delta m^2_{21}}{10^{-5}\text{ eV}}$	$7.50^{+0.18}_{-0.19}$	7.00 to 8.09
$\frac{\Delta m^2_{31}}{10^{-3}\text{ eV}}$(NH)	$+2.473^{+0.070}_{-0.067}$	$+2.276$ to $+2.695$
$\frac{\Delta m^2_{32}}{10^{-3}\text{ eV}}$(IH)	$-2.427^{+0.042}_{-0.065}$	-2.649 to -2.242

Table 3.1: Best fit values with 1σ errors and 3σ range for all neutrino mixing parameters, from [70]. * For the value of $\sin^2\theta_{23}$ a second local minima at $0.594^{+0.021}_{-0.022}$ exists.

Another anomaly appeared recently. The re-evaluation of the antineutrino fluxes at nuclear reactors estimated the flux to be 3% higher than the fluxes predicted by previous calculations. This means that data from reactor neutrino experiments at very short distances can be interpreted as a deficit of 6% in the flux of $\bar{\nu}_e$. The so called reactor anomaly can also be explained by the presence of a sterile neutrino with $\Delta m^2 \sim 1$ eV^2 [74]. Another anomaly was announced by the GALLEX and SAGE experiment which observed evidence for ν_e disappearance at very short baselines [75]. Unfortunately no coherent picture that can fit all three anomalies has yet been found. It is clear that further investigation is needed to check these anomalies and to bring them in agreement with each other.

As seen above neutrino oscillation experiments can measure mass differences but cannot determine the absolute neutrino mass scale. The best way to measure the neutrino mass scale is to use the kinematic effects of neutrino masses on the β decays of nuclei ${}^A Z \to {}^A(Z+1)+e^-+\bar{\nu}_e$. Thereby one looks at the endpoint of the spectrum of the emitted electron. The maximal kinetic energy of the electron is given by

$$E^e_{\text{Max}} = M_i - M_f - m_e - m_{\nu_e} \tag{3.29}$$

where M_i (M_f) is the mass of the initial (final) nucleus. The principle effect is shown in figure 3.1. The difference is best measurable for nuclei with a small mass difference $M_i - M_f$. Therefore tritium is often used for these measurements. As the electron neutrino is not a mass eigenstate, the measured mass is a superposition of all mass eigenvalues

$$m^2_\beta = \sum_{k=1}^{3+n_s} |U_{ek}|^2 m^2_k \tag{3.30}$$

where N_s is the number of sterile neutrinos. The present bound on the neutrino mass is [12]

$$m_\beta \lesssim 2 \text{ eV} . \tag{3.31}$$

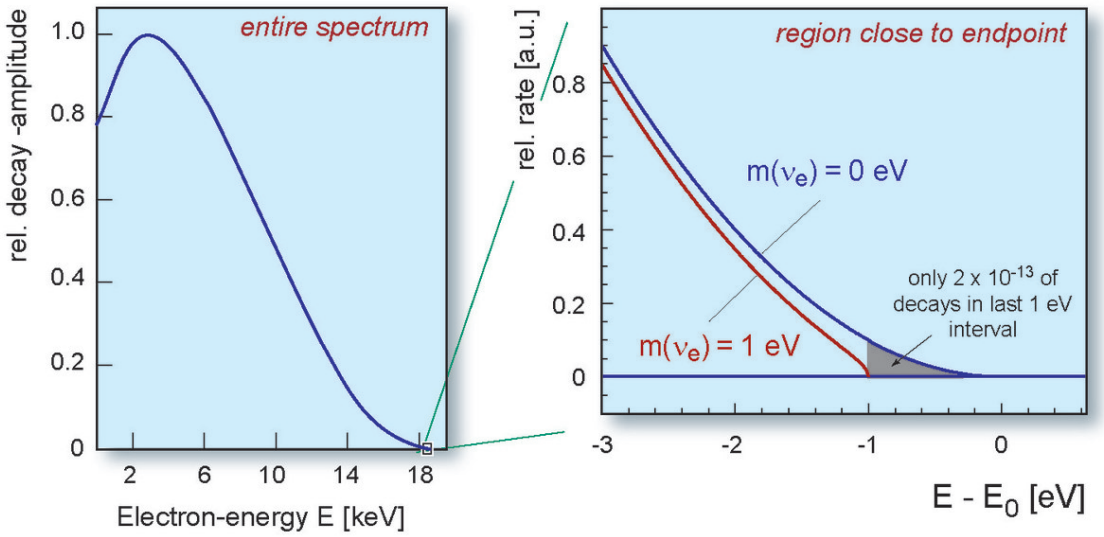

Figure 3.1: The effect of a non zero neutrino mass on the spectrum of the emitted electron in a β decay, from [76]. The endpoint of the spectrum is shifted by the neutrino mass

The upcoming Karlsruhe Tritium Neutrino experiment (KATRIN) should be able to find a new lower bound which is smaller by one order of magnitude.

3.1.4 Cosmological neutrino constraints

Neutrinos play only a sub leading role in cosmology but have nevertheless some impact on observables so that their properties can be constrained by cosmological observations. However it is important to keep in mind that cosmological bounds are very model dependent. They depend on the basic cosmological model that is used (one normally uses the ΛCDM model) and on the way extensions of this model are introduced. To get constraints one adds generally an additional parameter, like e.g. the number of neutrinos or the neutrino mass, to the basic model and then fits the cosmological data sets. In doing so one can extract information about the new parameter without falling into regions of very low probability of the parameter space.

Number of neutrinos

The neutrino energy density in the thermal bath can be parametrized relative to the photon energy density

$$\rho_\nu = N_{\text{eff}} \frac{7}{8} \left(\frac{4}{11}\right)^{4/3} \rho_\gamma \tag{3.32}$$

For three SM neutrinos one obtains $N_{\text{eff}} = 3.046$. A fully thermalized additional neutrino (sterile or not) would enhance N_{eff} by one if it has the same temperature as normal neutrinos. The best way to constrain additional neutrinos in cosmology is to use CMB data. The main effect of increasing neutrino number on the CMB power spectrum is that the additional radiation density increases the expansion rate at recombination. The diffusion length of a photon during recombination scales like $\sim \sqrt{t_{eq}}$. However the horizon at decoupling scales like $\sim t_{eq}$. Consequently the

angular scale of the photon diffusion length increases. The power for a given ℓ in the damping tale is therefore reduced [55]. The PLANCK collaboration's most stringent bound is obtained by combining CMB data with data from baryonic acoustic oscillation measurements [17]

$$N_{\text{eff}} = 3.30^{+0.54}_{-0.51} \quad . \tag{3.33}$$

The errors are approximate 1σ bounds. One additional thermalized massless neutrino is therefore not excluded but more are not allowed.

Neutrino masses

The basic cosmology model that the PLANCK collaboration uses assumes a minimal mass model, i.e. neutrinos with normal hierarchy and one massless neutrino. The heaviest neutrino has a mass $m_\nu \sim 0.06$ eV whereas the mass of the second massive neutrino (controlled by the solar mass splitting) ~ 0.009 eV is neglected. We will see shortly that even a mass of $m_\nu \sim 0.06$ eV is beyond current sensitivity of the experiment so that there is effectively no difference to a model with massless neutrinos. To study the effect of heavier neutrinos one defines the total mass M_ν of all three neutrino species. As cosmology has rather few sensitivity to mass splitting one can also assume that all three neutrinos have degenerate masses $m_\nu = M_\nu/3$.

Massive neutrinos change the moment of matter - cosmological constant equality and influence the CMB spectrum via the late integrated Sachs-Wolfe effect. The ISW rise for $\ell < 20$ is depleted. They also influence the evolution of the gravitational potential just after decoupling by adding some more mass density. This follows in a depletion of the spectrum in the range $20 < \ell < 200$ via the early ISW effect. The depletion is of the order [55]

$$\frac{\Delta C_\ell}{C_\ell} \sim -\frac{m_\nu}{10 \text{ eV}} \quad . \tag{3.34}$$

Another way to constrain neutrino masses is to measure the distortion of the CMB spectrum due to gravitational lensing when CMB photons travel though regions in space where structure formation has gone non-linear. Massive neutrinos enhance the expansion rate during matter domination and therefore suppress the clustering of matter. They only affect scales smaller than the horizon at the moment when neutrinos became non-relativistic. This decreases the gravitational lensing potential and therefore the weak lensing effect. For PLANCK this should be the dominating effect of massive neutrinos. The PLANCK limit on the total mass of neutrinos using CMB data and baryonic acoustic oscillation data is [17]

$$M_\nu = \sum m_\nu < 0.23 \text{ eV} \quad \text{at } 95\% \quad . \tag{3.35}$$

Including the weak lensing data has the effect of weakening the bound on the total neutrino mass. The weak lensing data seems to indicate a non-zero total mass of neutrinos of the order $M_\nu = 0.46$ eV. Similar effects have been observed in lensing data from SPT [77] and ACT [78].

Additional massive sterile neutrinos

We have seen that to explain the LSND anomaly and the reactor anomaly one or two sterile neutrinos with mass $m \sim 1$ eV are needed. To constrain them using cosmological data one has to extend the cosmological standard model by N_{eff} and M_ν at the same time. In [79] it is was shown that additional sterile neutrinos with $m \sim 1$ eV are strongly disfavoured by cosmology if they are fully thermalised because they contribute too much to hot dark matter. Changing the equation of state of dark energy or including additional radiation can improve the situation.

In [80] a model containing three light neutrinos with total mass $\sum m_\nu$ and one additional massive sterile neutrino with effective mass $m_s^{\text{eff}} = (T_s/T_\nu)^3 m_s$, T_s being the current temperature of the sterile neutrino, is considered. N_{eff} contains the contributions of the sterile neutrino to the radiation density. They find that at 95% CL the allowed values are

$$m_s^{\text{eff}} < 0.14 \text{ eV} \qquad \sum m_\nu < 0.27 \text{ eV} \qquad N_{\text{eff}} = 3.28^{+0.22}_{-0.21} \ . \tag{3.36}$$

The limits are quite strong and reduce the possibilities of explaining the observed anomalies using sterile neutrinos and a standard cosmological scenario.

3.2 Seesaw mechanism

As we have seen almost all data from neutrino oscillation experiments can be explained by simply giving neutrinos a Yukawa coupling to the Higgs field which then generates neutrino masses after the electroweak symmetry breaking. Therefore one needs to introduce right-handed neutrinos, which turn out to be gauge singlets. However the Yukawa couplings must be unnaturally small to explain the tiny neutrino masses. So at least from a theoretical point of view, this situation is not very satisfying. A solution to this problem is given by the seesaw mechanism [81, 82, 83, 84]. In its simplest version it adds a Majorana mass term for the right-handed neutrinos to the Lagrangian in equation (3.1). We will first review general Majorana mass terms, emphasise the differences to Dirac mass terms and then introduce the seesaw mechanism which explains in a natural way why neutrino masses are so small by adding a Majorana mass term to the SM. At the end we will review the basic idea of an experimental test of the Majorana hypothesis.

3.2.1 Majorana mass term

Using the projection operators $P_{R/L} = \frac{1}{2}(1 \pm \gamma_5)$ one can decompose the Dirac spinor in its two chiral components $\psi = \psi_L + \psi_R$. In this notation the Dirac equation is

$$i\partial\!\!\!/ \psi_L = m\psi_R \tag{3.37}$$
$$i\partial\!\!\!/ \psi_R = m\psi_L \ . \tag{3.38}$$

The Dirac equation mixes the two chiral components if the mass is non-zero. For $m = 0$ the two components are completely independent and can be treated separately. In the case of massless neutrinos there is no need for both chiralities, because only the left-handed neutrinos participate in electroweak interactions. Indeed in the SM only left-handed neutrinos exist. If the left and the right-handed components of a particle are only related to each other via their dynamics (the Dirac equation) the particle is called a Dirac particle. All fermions in the SM are Dirac particles. However the left and right-handed components can also be related by another condition, like the Majorana condition [85]. To write it down we first have to define charge conjugation

$$\psi(x) \xrightarrow{C} \psi^C(x) = \zeta \mathcal{C} \overline{\psi}^T(x) = i\zeta\gamma^2\gamma^0\overline{\psi}^T(x) \tag{3.39}$$
$$\overline{\psi}(x) \xrightarrow{C} \overline{\psi^C}(x) = -\zeta^* \psi^T(x)\mathcal{C}^\dagger \tag{3.40}$$

where $|\zeta|^2 = 1$. One can show that $\psi_L^C = \mathcal{C}\overline{\psi_L}^T$ behaves as a right-handed field. To show this, one uses the fact that the charge conjugation matrix and the projection operator commute $P_L\mathcal{C} = \mathcal{C}P_L$. So one has

$$P_L \mathcal{C} \overline{\psi_L}^T = \mathcal{C}(\overline{\psi_L} P_L)^T = \mathcal{C}\left((P_R\psi_L)^\dagger\gamma^0\right)^T = 0 \tag{3.41}$$

The analogue equation holds for the right-handed component. A Majorana fermion is then constructed by using only one helicity state and adding the charge conjugate to obtain the other helicity component, like

$$\psi = \psi_L + \psi_L^C \tag{3.42}$$

so that the Majorana fermion is its own antiparticle $\psi = \psi^C$. This is the Majorana condition. Of course this is only possible if the fermion is neutral. The Dirac equation now reads

$$i\partial\!\!\!/\psi_L = m\mathcal{C}\overline{\psi_L}^T \tag{3.43}$$

Majorana fermions are only then distinguishable from Dirac fermions if they are massive. In the massless case the two parts of the Dirac equation decouple and the right-handed component becomes inert.

For simplicity we will now consider only one neutrino. The mass term mixes left and right-handed components so that in the Majorana case it reads like

$$\mathcal{L}^M_{\text{mass}} = -\frac{1}{2} m \overline{\nu_L^C} \nu_L + h.c. \tag{3.44}$$

The factor $\frac{1}{2}$ is there to compensate the double counting of degrees of freedom. We have chosen to write the mass term in terms of the left-handed fermions because for the SM we are looking for a mass term of left-handed neutrinos. However we could have also written down in the same way a Majorana mass term for right-handed neutrinos. The kinetic terms in the Majorana case are the same as for Dirac fermions. The most important difference to the Dirac mass term is that a neutrino Majorana mass term breaks lepton number conservation. But as neutrino masses are very small one can treat the problem perturbatively. One can still define lepton number and all processes that do not involve the neutrino mass term conserve lepton number. In addition to the usual lepton number conserving SM processes one can look for processes that violate lepton number by two units. A famous example is the neutrinoless double β decay that is actively searched for by various experiments.

It is not easy to construct a Majorana mass term. One can show that the Majorana mass term is a weak isospin triplet (instead of a singlet in the Dirac case) and that it carries weak hypercharge $Y = -2$. It is therefore not possible to construct it using gauge invariant Yukawa interactions with the Higgs. There is a possibility to construct the Majorana mass term using two Higgs bosons, but then the operator is of dimension 5 and not renormalizable. It can be treated as the low energy effective Lagrangian of a high energy theory. We will see in a minute how the seesaw mechanism constructs a low energy Majorana mass terms for neutrinos.

In the case of three neutrinos the Majorana mass term can be written as

$$\mathcal{L}^M_{\text{mass}} = -\frac{1}{2} \nu^T_{\alpha L} \mathcal{C}^\dagger M^L_{\alpha\beta} \nu_{\beta L} + h.c. \tag{3.45}$$

In contrast to the Dirac mass case the Majorana mass matrix is diagonalised using one unitary transformation.

$$(V^\nu_L)^T M^L_{\alpha\beta} V^\nu_L = M \;\text{ with }\; M_{k,j} = m_{\nu_k}\delta_{kj} \tag{3.46}$$

After the diagonalization the Majorana mass term is

$$\mathcal{L}^M_{\text{mass}} = -\frac{1}{2} \sum_{k=1}^{3} m_{\nu_k} \nu^T_{kL} \mathcal{C}^\dagger \nu_{kL} + h.c. \;\; . \tag{3.47}$$

The mixing matrix is defined as in the Dirac case, but in the Majorana case it contains three phases which cannot be removed instead of only one phase.

$$U_M = V_L^{\ell\dagger} V_L^{\nu} = U D^M \quad \text{with} \quad D^M = \text{diag}(1, e^{i\lambda_1}, e^{i\lambda_2}). \tag{3.48}$$

The matrix U is the PMNS mixing matrix of the Dirac case, given in equation (3.5).

3.2.2 Seesaw

As already mentioned the seesaw mechanism provides a Majorana mass term for the left-handed neutrinos of the SM. The neutrino mass scale is naturally small because the Majorana mass term is the low energy effect of a new high energy theory at some high energy scale and because the effective operator giving neutrino masses is suppressed by the new high energy scale. Depending on the nature of the additional particle in the seesaw mechanism one can distinguish three types

- Type I: $SU(3) \times SU(2) \times U(1)$ singlet fermions
- Type II: $SU(2)$ triplet scalar
- Type III: $SU(2)$ triplet fermion

For brevity we will only concentrate on the type I seesaw mechanism and a very interesting variation of it, the inverse seesaw mechanism. We introduce n_s gauge singlet fermions N_{sR} with $n = 1, \cdots n_s$ which we will call right-handed neutrinos. Using the right-handed neutrinos we can write down a Dirac mass term M^D for neutrinos. But as the right-handed neutrinos are gauge singlets one can write down a Majorana mass term for them M^R. The mass Lagrangian can then be written

$$\mathcal{L}_{\text{mass}} = -\overline{\nu_{\alpha L}} M^D_{s\alpha} N_{sR} + \frac{1}{2} \nu^T_{sR} \mathcal{C}^\dagger M^R_{ss'} N_{s'R} + h.c. \tag{3.49}$$

The Dirac mass matrix $M^D_{s\alpha}$ is a $(n_s \times 3)$ matrix. It comes from the usual Yukawa couplings of fermions to the Higgs field. The Majorana mass matrix $M^R_{ss'}$ is a $(n_s \times n_s)$ matrix . The whole system of mass matrices can be written using a $(n_s + 3) \times (n_s + 3)$ complex symmetric matrix

$$M^{D+M} = \begin{pmatrix} 0 & (M^D)^T \\ M^D & M^R \end{pmatrix} \tag{3.50}$$

The matrix is written in the basis of row vector $N_L^T \equiv (\nu_{eL}, \nu_{\mu L}, \nu_{\tau L}, N^C_{s_1 R} \cdots N^C_{s_{n_s} R})$. Using this basis one can sum up both mass terms in one single expression

$$\mathcal{L}_{\text{mass}} = \frac{1}{2} N_L^T \mathcal{C}^\dagger M^{D+M} N^L + h.c. \tag{3.51}$$

This is just a Majorana mass term for the left-handed field N_L. It can be diagonalised using a unitary transformation matrix W. We will assume that M^R is a high mass scale because it is related to new physics. The mass eigenvalues split then into three light eigenvalues and three heavy eigenvalues

$$M_{\text{light}} \approx -(M^D)^T \frac{1}{M^R} M^D \quad \text{and} \quad M_{\text{heavy}} \approx M^R \tag{3.52}$$

The corresponding eigenvectors are $\nu_L + \nu_L^C$ and $N_R + N_R^C$. The active neutrinos as well as the heavy sterile neutrinos are Majorana particles. To get a feeling for the orders of magnitude involved in the neutrino mass eigenvalues consider only one generation. The active neutrino mass is then given $m_{\text{light}} = (M^D)^2/M = (Y^\nu)^2 u^2/M$. The Dirac mass term is naturally for

$Y^\nu \sim 0.1$ and therefore of the order u, the expectation value of H. To have neutrino masses of the order $m_{\text{light}} \sim 1$ eV, one obtains the scale of right-handed neutrino masses $M \sim 10^{14}$ GeV. For such high scales the neutrino masses are naturally very small, even for order one Yukawa couplings. This is theoretically a very satisfying answer to the smallness of neutrino masses, but the predicted scale of new physics is out of reach for every direct search experiment. However one can hope to detect the Majorana nature of the active neutrinos by looking for neutrinoless double beta decay.

To bring the scale of right-handed neutrinos down to observable scales ~ 1 TeV is the aim of a extension of the inverse seesaw mechanism [86]. It introduces not only three right-handed singlets ν_R but also three new left-handed singlets s_L. In the basis of (ν_L, N_R, s_L) the mass matrix is 9×9

$$\mathcal{M} \quad = \quad \begin{pmatrix} 0 & M^D & 0 \\ (M^D)^T & 0 & M \\ 0 & M^T & \mu \end{pmatrix} \tag{3.53}$$

which contains two Dirac mass matrices M^D and M as well as one Majorana mass matrix μ. In the limit $M \gg M^D, \mu$ one obtains by diagonalising a light mass matrix

$$M_{\text{light}} = (M^D)^T (M^T)^{-1} \mu M^{-1} M^D \tag{3.54}$$

for the active neutrinos. The remaining ν_R and s_L form three quasi Dirac leptons with mass M. The scale M is still a high energy scale but now the neutrino masses are suppressed by M^2. If one wants to have $M = \mathcal{O}(\text{TeV})$ within the reach of the LHC and keeping $Y^\nu = \mathcal{O}(1)$ one obtains that $\mu = \mathcal{O}(\text{keV})$ in order to have sub-eV neutrino masses.

Let us now turn to a potential experimental test of the seesaw mechanism. We have seen that within the seesaw mechanism active neutrinos are Majorana particles, so they are their own antiparticles. One way to test the hypothesis of Majorana particles is the double beta decay of nuclei,

$$N(A, Z) \to N(A, Z+2) + 2e^- + 2\overline{\nu}_e \ . \tag{3.55}$$

It is second order in G_{F} and therefore only appears for nuclei that cannot make a single beta decay. The double beta decay emits two electrons and two neutrinos. The neutrinoless double beta decay is the same transition process but without emitting two neutrinos. It is clearly forbidden by lepton number conservation. But when neutrinos are Majorana particles, lepton number is broken and the process is allowed. Figure 3.2 shows one Feynman diagram of the neutrinoless double beta decay.

As the normal double beta decay contains four outgoing particles the spectrum of the electrons is continuous. In the case of the neutrinoless double beta decay the electron spectrum is monochromatic, so that one can distinguish both processes by looking at the electron spectrum. The decay rate of the neutrinoless decay can be parametrised like

$$\Gamma_{2\beta 0\nu} = \langle m_{ee} \rangle^2 |\mathcal{M}|^2 F^{2\beta 0\nu} \ . \tag{3.56}$$

The $F^{2\beta 0\nu}$ stands for the phase space factor of the decay which can be calculated quite exactly. The $\mathcal{M}$ is the nuclear structure matrix element which is much harder to evaluate theoretically. The decay rate depends quadratically on a linear combination of neutrino mass eigenvalues and Majorana phases

$$\langle m_{ee} \rangle = |U_{e1}|^2 m_1 + e^{2i\lambda_2} |U_{e2}|^2 m_2 + e^{i(\lambda 3 - \delta)} |U_{e3}|^2 m_3 \ . \tag{3.57}$$

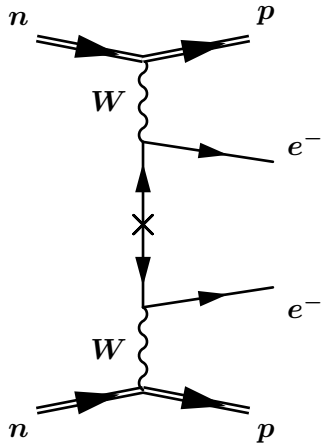

Figure 3.2: Sketch of the neutrinoless double beta decay. The cross symbolises the Majorana mass insertion.

In the case of normal hierarchy one can encounter the situation that even for three non-zero neutrino mass eigenvalues there is a combination of the phases $\delta, \lambda_1, \lambda_2$ so that $\langle m_{ee} \rangle$ vanishes. This means that even if neutrinos are massive Majorana particles it is not sure that a neutrinoless double beta decay is observable. However this combination of phases is not preferred over any other combination is therefore not very likely to be chosen by nature. On the other hand an observation of neutrinoless double beta decay would once and for all answer the question of Majorana masses and at the same time give the absolute scale of neutrino masses. Several experiments have already been looking for the neutrinoless decay and efforts continue to enhance the sensitivity of these experiments. See [87] for an overview of theory of the double neutrinoless beta decay and upcoming experiments.

Part II

Leptogenesis project

Chapter 4

Baryogeneis through leptogenesis

In the previous chapter on cosmology (section 2.2.2) we have seen that our standard picture of cosmology is not able to explain the observed value of the baryon relic density. A completely unrelated problem that we have discussed in some detail in chapter 3 are neutrino masses. Even if both problems are very different, they can both be explained by a very small extension of the SM. As we have seen introducing right-handed Majorana neutrinos explains neutrino masses very elegantly via the seesaw mechanism. The same right-handed neutrinos can also produce a lepton asymmetry in the early universe which can be converted into the baryon asymmetry observed today. As the baryon asymmetry is created via a lepton asymmetry these kind of scenarios are part of the leptogenesis models. In this chapter we will introduce the basic idea and the relevant mechanisms of baryogenesis through leptogenesis

4.1 Introduction

Current observations of our universe indicate that all structures contain only matter (baryons and electrons) and dark matter but only very few antimatter (antibaryons and positrons). It seems that the universe contains much more baryons than antibaryons. This is quite intriguing because our "Big bang" models indicate that at early times, at high temperatures, the number of baryons should be equal to the number of antibaryons. Let us assume an equal number of baryons and antibaryons throughout the whole evolution of our universe and only one baryon b with baryon number $B = 1$. Conserving baryon number the baryons can annihilate into n photons:

$$b + \bar{b} \longleftrightarrow n\gamma \tag{4.1}$$

At high temperature baryons are in thermal equilibrium with the thermal bath and have a relativistic number density density $n_b \sim T^3$. When the temperature drops below $T \sim m_b$ the photons from the thermal bath cannot produce baryons any more and the baryon density drops with $n_b \sim T^{3/2} \exp(-m_b/T)$. If baryons stay in equilibrium for a long time their relic density drops to 0 and no more baryons or antibaryons should be left. However if after $T \sim m_b$ the interaction becomes slow compared to the expansion rate of the universe, a baryon relic density can be left. Using the nucleon-anti nucleon annihilation cross section $\sigma \sim m_\pi^{-2}$, where $m_\pi = 135$ MeV one can show that the hypothetic baryon and antibaryon relic density would be [13]

$$Y_{\bar{b}}(t_0) = Y_b(t_0) = \frac{n_b}{s} \sim 10^{-19} \tag{4.2}$$

where the s is the entropy density given in equation 2.44. However the actual value for the

baryon asymmetry in the universe (BAU) is measured by Planck [17] to be

$$Y_{\Delta B} = \left.\frac{n_B - n_{\bar{B}}}{s}\right|_0 = (8.59 \pm 0.13) \times 10^{-11} \tag{4.3}$$

which contains the 1σ error.

In our toy model the baryon number density $Y_B = 0$ because we assumed a symmetric universe. The baryon density in our toy model is much too small to explain the measured value. In order to prevent that almost all baryons annihilate one has to introduce a baryon asymmetry. One can argue that this baryon asymmetry is just an initial asymmetry or one can try to explain it through a dynamical process. The first option has two problems: first the initial asymmetry must be very small, fine tuned, 6000001 baryons for every 6000000 antibaryons. Second if inflation took place in some early stage of the universe it would have completely erased an initial asymmetry. We are therefore looking for a possible dynamical generation of the baryon asymmetry. Such a scenario is called baryogenesis.

Sakharov showed that to create an asymmetry dynamically three conditions have to be verified [88]:

- **Baryon number** must be violated: in order to go from a state with $Y_{\Delta B} = 0$ to a state with $Y_{\Delta B} \neq 0$ baryon number must be violated.
- ***C* and *CP* violation:** It is clear that if C is not violated all processes involving baryons have the same rate as those involving antibaryons and no net difference between baryons and antibaryons is created. For CP violation, consider a process from an initial state i and some final state f where baryon number is produced. Call p_i (p_f) the momentum of particles in the initial (final) state and s_i (s_f) their spins. The conservation of CP implies (via the conservation of CPT) also conservation of time reversal T which would then imply
$$\Gamma(i \to f; p_i, s_i; p_f, s_f) = \Gamma(f \to i; -p_f, -s_f; -p_i, -s_i) \tag{4.4}$$
The baryon number produced in those two processes is opposite. Integrating over all possible momenta and spins we get no net asymmetry. A net baryon asymmetry can only be produced if C and CP are broken.
- **Out of equilibrium**: in chemical equilibrium no asymmetry is created in a quantum number even if it is not conserved. To see this one can write the mean value of the baryon number using the density matrix ρ, that describes your system
$$\langle B \rangle = \frac{\mathrm{Tr}(\rho B)}{\mathrm{Tr}(\rho)} \tag{4.5}$$
In thermal equilibrium the density matrix can be written like $\rho = e^{-\beta H}$. H is the Hamiltonian that commutes with the CPT operator Θ but not with B. The CPT operator anticommutes with baryon number $B\Theta = -\Theta B$ [1]. We use this and the invariance under cyclic permutations of the trace to show that
$$\langle B \rangle = \frac{\mathrm{Tr}(\Theta^{-1}\Theta e^{-\beta H} B)}{\mathrm{Tr}(\rho)} = \frac{\mathrm{Tr}(\Theta^{-1} e^{-\beta H}\Theta B)}{\mathrm{Tr}(\rho)} = -\frac{\mathrm{Tr}(\Theta^{-1} e^{-\beta H} B\Theta)}{\mathrm{Tr}(\rho)} = -\langle B \rangle \tag{4.6}$$
This implies that $\langle B \rangle = 0$ as long as thermal equilibrium holds.

1. Consider a process $a \to b$ with a given baryon number B. The CPT conjugate process is $\bar{b} \to \bar{a}$ has opposite baryon number $-B$.

It is very interesting to see that in the SM all three conditions are verified. Baryon number is violated by the triangle anomaly that leads to processes that involve nine left-handed quarks and three left-handed leptons. A selection rule for such processes is

$$\Delta B = \Delta L = \pm 3 \ . \tag{4.7}$$

At low temperature this process is suppressed but at high temperatures this process can be fast. Furthermore weak interactions violate C maximally and violate CP via the Kobayashi-Maskawa mechanism. However it is very difficult to produce the asymmetry observed today using only the CP violation from the SM because it is generally not strong enough [89]. New sources of CP violation are therefore needed if one wants to explain the BAU. At last the SM also provides departure from thermal equilibrium at the electroweak phase transition. As this phase transition is not strongly of first order as required by baryogenesis one also needs to provide a new departure from thermal equilibrium.

One of the first models that was proposed is GUT baryogenesis [90, 91]. In this model the asymmetry is created by out of equilibrium decays of heavy bosons in grand unified theories (GUT). The non-observation of proton decay seriously constrains GUTs to very large energy scales. This gives a lower bound on the reheating temperature after inflation. However simple inflation models do not give such a high reheating temperature which might also create unwanted relics. Furthermore the simplest GUTs violate $B + L$ while conserving $B - L$. Sphalerons that violate $B + L$ can destroy the produced asymmetry. Other models are electroweak baryogenesis [92] or Affleck-Dine mechanism [93].

A very interesting and attractive model explaining the BAU is given by leptogenesis. Leptogenesis was first proposed by Fukugita and Yanagida [94] and uses the heavy right-handed neutrinos introduced in the see-saw mechanism to explain neutrino masses and to create the BAU at the same time. The right-handed neutrinos are created at high temperatures and can create a lepton asymmetry in their decays. The new sources of CP violation are the Yukawa couplings of the right-handed neutrinos. Departure from equilibrium is provided by their slow decay and inverse decay rates. The produced lepton asymmetry is then transformed into a baryon asymmetry by non perturbative sphaleron processes.

4.2 Thermal leptogenesis

In this section we will give an introductory review to leptogenesis, following [89]. The following assumptions are made in order to simplify the analysis and to concentrate on the most important points of leptogenesis: The lepton asymmetry is produced in one single flavour α. The right-handed neutrino masses are hierarchical with the lightest mass being much lower then the other masses $M_1 << M_2, M_3$. We will assume that only the lightest right-handed neutrino N_1 is thermally produced. The other right-handed neutrinos are too heavy and their number densities will be neglected.

At very high temperatures $T > M_1$, s- or t-channel scattering processes involving top quarks of the form $q_L + t_R \to \ell_\alpha + N_1$ or $\ell_\alpha + t_R \to q_L + N_1$ populate the N_1 density. When the temperature drops below M_1, the right-handed neutrinos decay and the number density decreases according to $n_{N_1} \propto e^{-M_1/T}$. Due to the CP violating Yukawa couplings of N_1 its decays produce an asymmetry in lepton flavour α if the interactions are out of equilibrium. This asymmetry can then be reprocessed into a baryon asymmetry by $B + L$ violating sphaleron processes. However during the production of the N_1 density, an asymmetry equal in magnitude but opposite in sign to the asymmetry form N_1 decay was produced if interactions were not in thermal equilibrium. This

suggests that at leading order no asymmetry survives. But the anti-asymmetry gets depleted by scatterings, decays and inverse decays. This depletion is called washout and is a critical feature to thermal leptogenesis.

The baryon asymmetry created by leptogenesis can be parametrized in the following way

$$Y_{\Delta B} = \frac{135\zeta(3)}{4\pi^4 g_*} \sum_\alpha \epsilon_{\alpha\alpha} \times \eta_\alpha \times C \tag{4.8}$$

The sum is over all flavours but in the model considered here, only one flavour α produces an asymmetry. The fraction on the right hand side is the ratio of the N_1 number density at thermal equilibrium for $T > M_1$ and the entropy. A thermal equilibrium density for N_1 can occur at high temperatures only when the Yukawa coupling $\lambda_{\alpha 1}$ is sufficiently large. In the SM this fraction is of order $\mathcal{O}(4\times10^{-3})$ if the number of relativistic degrees of freedom in the plasma is $g_* \approx 106$. If the N_1 do not achieve a thermal distribution, the asymmetry produced is smaller, which is parametrised by the factor η_α. The three parameters after the fraction describe the following effects:

- ϵ_α describes how much CP violation is produced in the N_1 decays. Every $\frac{1}{\epsilon_\alpha}$ decay, one more ℓ_α than $\bar{\ell}_\alpha$ is produced.
- η_α is the efficiency factor. Inverse decays, washout processes or inefficiencies in the N_1 production reduce the asymmetry created. In the limit of N_1 interactions in perfect equilibrium, no asymmetry is produced and $\eta_\alpha = 0$. The maximal value is $\eta_\alpha = 1$.
- C describes a further reduction due to the redistribution of the asymmetry from lepton doublets to other particles or the inefficiency of $B + L$ violating processes that transform the lepton asymmetry into the final baryon asymmetry.

Estimating these three parameters is the aim of the following paragraphs.

4.2.1 C and CP violation

For the decay process of N_1 the amount of CP violation in flavour α can be defined as

$$\epsilon_\alpha = \frac{\Gamma(N_1 \to \ell_\alpha H) - \Gamma(N_1 \to \bar{\ell}_\alpha \overline{H})}{\Gamma(N_1 \to \ell_\alpha H) + \Gamma(N_1 \to \bar{\ell}_\alpha \overline{H})} \tag{4.9}$$

where $\bar{\ell}$ means the anti particle of ℓ and H is the Higgs field. As the right-handed neutrino is supposed to be a Majorana particle, one has $\bar{N}_1 = N_1$. The CP asymmetry is normalized by the total decay rate of N_1. By definition $|\epsilon_\alpha| \leq 1$. Usually it is much smaller than 1. However in the case of quasi degenerate N_i [95, 96] it can get close to 1. We will have a closer look at CP violation in section 4.3.

4.2.2 Out-of-equilibrium dynamics: η_α

Out-of-equilibrium dynamics can be provided by the expansion of the universe. Processes with an interaction rate slower than the expansion rate of the universe H cannot equilibrate particle distributions and are out-of-equilibrium. For analytical estimates processes that are much faster than the expansion rate can be treated by imposing their chemical and kinetic equilibrium conditions, processes that are slow can simply be neglected.

The production of N_1 is a crucial ingredient to our simple leptogenesis toy model. A full thermal number density can be produced only if the reheat temperature is high enough $T_{\text{reheat}} \gtrsim M_1/5$ and if the production rate is larger than the expansion rate of the universe $\Gamma_{\text{Prod}} > H$. In the early universe the most important production modes are inverse decays $H\ell_a \to N_1$ and

even more efficient scattering processes involving top quarks $q_L t_R \to \ell_a N_1$ and $\ell_a t_R \to q_L N_1$. The production rate can be estimated to (by dimensional analysis)

$$\Gamma_{\text{prod}} \sim \sum_\alpha \frac{h_t^2 |\lambda_{\alpha 1}|^2}{4\pi} T \tag{4.10}$$

The total decay rate of N_1 into leptons and Higgs is given by

$$\Gamma_D = \sum_\alpha \Gamma(N_1 \to \ell_\alpha H, \bar{\ell}_\alpha \bar{H}) = \frac{\left[\lambda^\dagger \lambda\right]_{11} M_1}{8\pi}. \tag{4.11}$$

If the production was fast at some moment, then from $h_t \sim 1$ one can infer that also the total decay rate was in thermal equilibrium at $T = M_1$. It is very useful to approximate the expansion rate of the universe during radiation domination by

$$H(T) \approx 1.66 \sqrt{g_*} \frac{T^2}{m_{\text{Pl}}} \tag{4.12}$$

where $m_{\text{Pl}} \approx 1.22 \times 10^{19}$ GeV is the Planck mass.

Knowing the decay and production rate of N_1 one can distinguish three different scenarios for the lepton asymmetry production as a function of whether the decay and production rates are fast or not.

– Strong washout
  The scenario of fast total decay rate $\Gamma_D > H$ and fast partial decay rate $\Gamma_\alpha > H$ in flavour α is called strong washout. At $T \sim M_1$ a thermal number density of N_1 is created without producing a lepton asymmetry because any asymmetry produced would be washed out immediately. When the temperature drops, the N_1 start to decay but do not produce a lepton asymmetry because inverse decays are still fast and wash out any asymmetry. The N_1 can produce an asymmetry in their decays only when the inverse decays fall out of equilibrium ($\Gamma_{ID\alpha} < H$). The inverse decay rate can be estimated to be

$$\Gamma_{ID\alpha} \equiv \Gamma(H\ell_\alpha \to N_1) \approx \frac{1}{2}\Gamma_\alpha e^{-M_1/T} \tag{4.13}$$

  The temperature for which $\Gamma_{ID\alpha}(T_\alpha) \approx H(T_\alpha)$ is called T_α. From T_α on, the N_1 decay out of equilibrium and create an asymmetry in flavour α, but the N_1 density is already suppressed by a factor $\sim e^{-M_1/T_\alpha}$. We can estimate the efficiency factor in this scenario

$$\eta_\alpha \approx \frac{n_{N_1}(T_\alpha)}{n_{N_1}(T >> M_1)} \sim e^{-\frac{M_1}{T_\alpha}} \sim \frac{H(T = M_1)}{\Gamma_\alpha} \tag{4.14}$$

– Intermediate washout
  The case where the total N_1 decay rate is fast $\Gamma_D > H$ but the partial decay rate is slow $\Gamma_\alpha < H$ is called intermediate washout regime. At high temperature a N_1 equilibrium number density is formed by the coupling $\lambda_{\beta 1}$ with $\beta \neq \alpha$. The production of N_1 produces an (anti-) asymmetry in flavour α of order $\sim -\epsilon_\alpha n_\gamma$. When the temperature drops, the out of equilibrium decays of N_1 produce an asymmetry of the same order but opposite in sign $\sim \epsilon_\alpha n_\gamma$. This implies that at leading order no net asymmetry is produced. However a small part of the anti-asymmetry from N_1 production is washed out before the N_1 start to decay. This fraction can be estimated to be of order $\sim \frac{\Gamma_\alpha}{H(T=M_1)} \epsilon_\alpha n_\gamma$ yielding an efficiency factor

$$\eta_\alpha \approx \frac{\Gamma_\alpha}{H(T = M_1)} \tag{4.15}$$

– Weak washout
If the N_1 total decay rate is slow one speaks about weak washout. The N_1 never achieve a thermal distribution because their couplings to SM particles are too small. Their production is most efficient at $T \sim M_1$ when the age of the universe is $t_U \approx 1/H$. The number density of N_1 is estimated $n_{N_1} \sim \Gamma_{\text{prod}} t_U n_\gamma$. The production of N_1 creates an anti-asymmetry that is erased by the asymmetry created in N_1 decays, as in the previous regime. The efficiency factor is therefore

$$\eta_\alpha \approx \frac{\Gamma_a \Gamma_D}{H^2(T = M_1)} \tag{4.16}$$

4.2.3 Lepton number and $B + L$ violation

To create a lepton asymmetry, the lepton number must be violated. This job is done by N_1. If one assumes N_1 has lepton number $L(N_1) = 1$, the Yukawa coupling involving N_1 conserves L but the Majorana mass term violates L. In the case where $L(N_1) = 0$ the Majorana mass term conserves L but the Yukawa coupling term violated L. Consequently the N_1 decays into leptons can produce a net lepton asymmetry. This asymmetry is then partially transferred into baryon asymmetry by $B + L$ violating non perturbative processes.

The question of anomalies and their role in cosmology is a very interesting but also difficult one. I will only give a very brief description of the most important properties. More details can be found in [97, 98, 99]. The SM Lagrangian conserves B and L_α but due to the chiral anomaly [100] there are non-perturbative gauge field configurations which can act as sources for $B + L_e + L_\mu + L_\tau$ violation, while conserving $B - L_e - L_\mu - L_\tau$. At low temperatures these processes are very slow and negligible but at in early universe at $T > T_{\text{EPT}}$ such configurations can occur frequently and lead to a rapid $B + L$ violation.

For our purposes the chiral anomaly of the $SU(2)$ symmetry of the SM is the one that gives $B + L$ violation. The Lagrangian for $SU(2)$ gauge interactions is

$$\mathcal{L} = \sum_i \bar{\psi}^i_L \gamma^\mu (\partial_\mu - i\frac{g_w}{2}\sigma^a W^a_\mu)\psi^i_L \tag{4.17}$$

where $\{\psi^i_L\} = \left\{q^{A,\beta}_L, \ell^\alpha_L\right\}$ with A colour index, α, β generation index and b $SU(2)$ index. W^a_μ is the gauge field and σ^a is the generators of the symmetry (the Pauli matrices). This Lagrangian has 12 global chiral $U(1)$ symmetries (one for each fermion field) of the form $\psi^i_L \to e^{i\beta}\psi^i_L$. The chiral currents associated to these symmetries are

$$j^i_\mu = \bar{\psi}^i_L \gamma_\mu \psi^i_L \tag{4.18}$$

The currents should be conserved because of the Noether theorem. However it turns out that the are only conserved at tree level but not on the quantum level. Due to the regularization of loops, which introduces an energy scale which breaks the chiral symmetry like a fermion mass, the divergence of the chiral current does not vanish (it is anomalous)

$$\partial^\mu j^i_\mu = \frac{1}{64\pi^2} W^a_{\mu\nu} \tilde{W}^{\mu\nu a} \quad . \tag{4.19}$$

Here $W^a_{\mu\nu}$ is the field strength of the $SU(2)$ gauge field and $\tilde{W}^{\mu\nu a}$ its dual. The right hand side can be related to the topology of gauge fields: it counts the winding number n_{CS} (Chern-Simons number) of the field configuration. This means that there is an infinite number of degenerate ground states with different n_{CS} which are separated by a potential barrier (figure 4.1).

The current associated to baryon number is the sum over all quark currents from equation (4.18)

$$j^B_\mu = \frac{1}{3}\sum_q \bar{q}\gamma_\mu q \ . \tag{4.20}$$

The baryon current is anomalous, as all individual currents. The current associated to lepton number is the sum over all lepton currents. Both currents are anomalous

$$\partial^\mu j^L_\mu = \partial^\mu j^B_\mu = \frac{N_f}{64\pi^2} W^a_{\mu\nu}\tilde{W}^{\mu\nu a} \tag{4.21}$$

with $N_f = 3$ being the number of families. Baryon and lepton number are violated as well as $B + L$ but $B - L$ is conserved [100]. As the winding number changes in integer steps, baryon and lepton number are changed in steps of $\Delta L = \Delta B = \pm 3n$ and n being a positive integer. Consequently it does not harm proton stability. It implies an effective interaction of 12 fermions (9 quarks and 3 leptons).

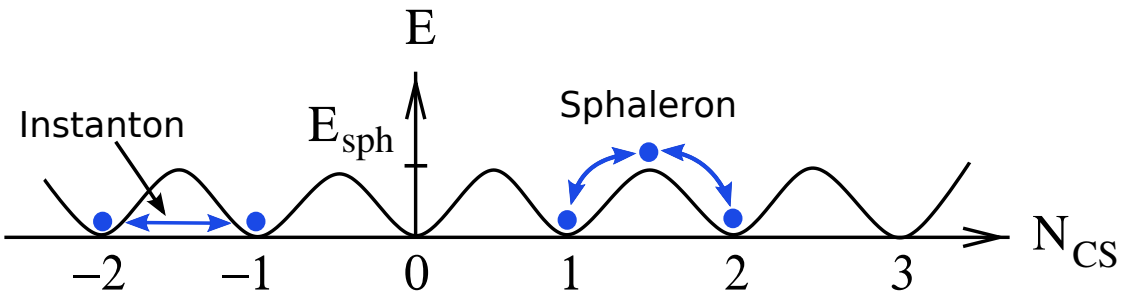

Figure 4.1: The figure shows the degenerate vacuum states with different winding number, separated by a potential barrier. Instanton effects are tunnelling process through the barrier. Sphaleron processes can be described as a "jump" over barrier due to thermal excitations.

At $T = 0$ one can go from one field configuration to another one by tunnelling through the potential barrier that separates the two ground states. This tunnelling is called the instanton effect. However its rate is exponentially suppressed by $\Gamma \sim e^{4\pi/\alpha_W}$ [100], so that instanton effects can safely be neglected at low temperatures. At high temperatures, thermal fluctuations can climb over the barrier and then fall into the neighbour ground state. These processes are called sphalerons. Their rate can be estimated to be $\Gamma_{\rm Sph} \propto e^{-E_{\rm Sph}/T}$ where $E_{\rm Sph} = 2Bm_W/\alpha_W$ is the height of the barrier at $T = 0$ and $B \sim 2$ a parameter of order one [101]. Above the electroweak phase transition all SM particles are massless and so the potential barrier disappear. The transitions occur frequently and also the $B + L$ violating rate is fast for $T >> M_W$. The associated rate of $B + L$ violation is estimated to be [102]

$$\Gamma_{\not{\rm B+L}} \sim 25\alpha_W^5 T \tag{4.22}$$

This rate exceeds the Hubble expansion rate H for $T_{\rm EPT} < T < 10^{12}$ GeV. It can therefore transform the lepton asymmetry in flavour α into a baryon asymmetry [89]

$$Y_{\Delta B} \approx \frac{12}{37}\sum_\alpha Y_{\Delta\alpha} \tag{4.23}$$

4.3 CP violation

CP violation is a crucial and highly non trivial ingredient to leptogenesis which deserves a more detailed view. At the beginning several general features of CP violation will be explained: why can CP violation only occur in the interference between a tree process and its loop correction, why does the total decay rate of any particle not violate CP and finally why is in leptogenesis a quite special treatment of on-shell intermediate states used? Then some more details about how to actually calculate the amount of CP violation are given.

4.3.1 General properties

The general features of CP violation can be obtained by simply using two fundamental principles: unitarity of the S matrix and CPT invariance of the quantum theory. It is useful to write the S matrix as

$$S = 1 + iT \ . \tag{4.24}$$

T is called the transition matrix. The S matrix unitarity condition gives

$$1 = SS^\dagger = (1 + iT)(1 - iT) \quad \Rightarrow \quad iT_{ab} = iT^*_{ab} - \left[TT^\dagger\right]_{ab} \tag{4.25}$$

Multiplying this equation by its complex conjugate one gets

$$|T_{ab}|^2 - |T_{ba}|^2 = -2Im\{\left[TT^\dagger\right]_{ab} T^*_{ba}\} + |\left[TT^\dagger\right]_{ab}|^2 \tag{4.26}$$

If one can expand the transition matrix T pertubatively in some coupling constant, then one can interpret this as if a difference between the tree level process $a \to b$ and its inverse $b \to a$ only arises in loop corrections. This implies that CP violation in a tree level process occurs to lowest order in the interference of the tree level process and its loop correction. However some caution is at order when considering this for the heavy right-handed neutrinos N_i: the S matrix is only defined for asymptotic states. As the N_i decay they can not always be considered as asymptotic states. This approximation will be examined further below.

The CPT symmetry that should be a symmetry of every quantum field theory implies

$$|\mathcal{M}(a \to b)|^2 = |\mathcal{M}(\bar{b} \to \bar{a})|^2 \tag{4.27}$$

where the matrix element is related to the transition matrix by

$$i\mathcal{M}(a \to b)(2\pi)^4\delta^4\left(\sum_i^n p_i - \sum_f^m q_f\right) = iT_{ab} \ . \tag{4.28}$$

The initial state contains n particles with corresponding momenta $\{a_1(p_1), \cdots a_n(p_n)\}$ and the final state contains m particles $\{b_1(q_1), \cdots b_m(q_m)\}$. Using this and the unitarity of the S matrix one can show [103] that the total decay rate of a particle and its anti-particle are identical

$$\sum_{\{b\}} |\mathcal{M}(X \to b)|^2 = \sum_{\{b\}} |\mathcal{M}(\bar{X} \to b)|^2 \tag{4.29}$$

where we used that one can define $\{b\} = \{\bar{b}\}$. This implies that CP violation does not occur in the total decay rate of a particle. Only the partial decay rates can violate CP.

The N_i can only be treated as asymptotic states if their lifetime is long compared to the time scale of the S matrix. For a $2 \to 2$ scattering process this time scale can be estimated by

$\tau = 1/\sqrt{s}$ where s is the centre of mass energy squared. Processes containing N_1 in the final or initial state can be treated with a unitary S matrix when $\Gamma_D << \sqrt{s} \sim M_1$.

One has to be careful when using N_1 as a final state in Boltzmann equations. Even if N_1 is stable on the timescale of the scattering process, on larger timescales N_1 decays. One encounters the problem of double counting. The N_1 appears as a intermediate on shell state as well as a real asymptotic state. Consider, e.g. the case of $H\ell_\alpha \to$ anything. It contains an on-shell contribution from the process $H\ell_\alpha \to H\ell_\beta$ where N_1 is exchanged in the s-channel diagram but also a contribution form $H\ell_\alpha \to N_1$ where the N_1 finally also decays. To fix the double counting one can subtract the on-shell contribution of the scattering rate:

$$\begin{aligned} |\mathcal{M}(H\ell_\alpha \to \text{anything})|^2 &= |\mathcal{M}(H\ell_\alpha \to N_1)|^2 \\ &+ \sum_\beta \Big[|\mathcal{M}(H\ell_\alpha \to H\ell_\beta)|^2 - |\mathcal{M}^{\rm OS}(H\ell_\alpha \to H\ell_\beta)|^2 \\ &+ |\mathcal{M}(H\ell_\alpha \to \bar{H}\bar{\ell}_\beta)|^2 - |\mathcal{M}^{\rm OS}(H\ell_\alpha \to \bar{H}\bar{\ell}_\beta)|^2 \Big] \end{aligned} \tag{4.30}$$

The on-shell part can be calculated via

$$|\mathcal{M}^{\rm OS}(H\ell_\alpha \to H\ell_\beta)|^2 = |\mathcal{M}(H\ell_\alpha \to N_1)|^2 B^{N_1}_{H\ell_\beta} \tag{4.31}$$

Where $B^{N_1}_{H\ell_\beta}$ is the branching ratio of N_1 to $H\ell_\beta$.

4.3.2 Calculating CP violation rates

To calculate the CP asymmetry one has to consider loop corrections to the tree level decay process. The leading order contribution arises from the interference of tree (subscript 0) and loop level (subscript 1) diagrams. The matrix elements can be separated into coupling constants and amplitude parts

$$\mathcal{M} = \mathcal{M}_0 + \mathcal{M}_1 = c_0\mathcal{A}_0 + c_1\mathcal{A}_1 \quad . \tag{4.32}$$

Here c_0, c_1 contain coupling constants and $\mathcal{A}_0, \mathcal{A}_1$ are the amplitude parts. The matrix element for the conjugate process is denoted

$$\bar{\mathcal{M}} = c_0^*\bar{\mathcal{A}}_0 + c_1^*\bar{\mathcal{M}}_1 \tag{4.33}$$

where in $\bar{\mathcal{A}}_0$ the Dirac spinors for external fermions u_ℓ is replaced by v_ℓ. The CP asymmetry given in equation (4.9) can then be rewritten following [89] to be

$$\begin{aligned} \epsilon_\alpha &= \frac{\int |c_0\mathcal{A}_0 + c_1\mathcal{A}_1|^2 \tilde{\delta} d\Pi_{\ell,H} - \int |c_0^*\bar{\mathcal{A}}_0 + c_1^*\bar{\mathcal{A}}_1|^2 \tilde{\delta} d\Pi_{\ell,H}}{2\sum_\beta \int |c_0\mathcal{A}|^2 \tilde{\delta} d\Pi_{\ell H}} \\ &= \frac{Im\{c_0c_1^*\}}{\sum_\beta |c_0|^2} \frac{2\int Im\{\mathcal{A}_0\mathcal{A}_1^*\}\tilde{\delta} d\Pi_{\ell H}}{\int |\mathcal{A}_0|^2 \tilde{\delta} d\Pi_{\ell H}} \end{aligned} \tag{4.34}$$

where $\tilde{\delta} = (2\pi)^4\delta^4(P_i - P_f)$ and $d\Pi_{\ell H} = d\Pi_\ell d\Pi_H = \frac{d^3p_\ell}{2E_\ell(2\pi)^3}\frac{d^3p_H}{2E_H(2\pi)^3}$ and P_i, P_f are respectively the incoming four momentum and outgoing four-momentum. The tree amplitude times loop amplitude has an imaginary part when intermediate particles are on-shell which arises when the H and ℓ_β are on-shell in the loops:

$$2Im\{\mathcal{A}_0\mathcal{A}_1^*\} = \mathcal{A}_0(N \to H\ell_a) \int \mathcal{A}_0^*(N \to \bar{\ell}'_\beta \bar{H}')\tilde{\delta}' d\Pi_{\ell',H'} \mathcal{A}_0^*(\bar{\ell}'_\beta \bar{H}' \to H\ell_\alpha) \tag{4.35}$$

The H' and ℓ' are the intermediate particles, taken to be massless and $d\Pi_{\ell',H'}$ the integration over their corresponding phase space.

In the model introduced above, where only N_1 have a thermal distribution and the asymmetry is created in its decay into $H\ell_a$, the CP asymmetry can be calculated to be [89]:

$$\epsilon_\alpha = \frac{3M_1}{16\pi v_u^2 \left[\lambda^\dagger\lambda\right]_{11}} Im\{[\lambda]_{\alpha 1}\left[m^*\lambda\right]_{\alpha 1}\} \tag{4.36}$$

where α is not summed over. This expression can be used to deduce an upper bound on ϵ_α.

$$|\epsilon_\alpha| \leq \frac{3M_1 m_{\max}}{16\pi v_u^2} \tag{4.37}$$

with $m_{\max}$ being the largest neutrino mass. This upper bound on the CP asymmetry can be used to derive a lower bound on right-handed neutrino mass M_1 in the case of a leptogenesis scenario with hierarchical right-handed neutrino masses. This lower bound on M_1 then implies a lower bound on the reheat temperature of the universe in order to produce the N_1 efficiently. For leptogenesis to produce the BAU one needs $\sum_\alpha \epsilon_\alpha \eta_\alpha \sim 10^{-7}$. Taking a typical value for the efficiency factor $\eta_\alpha \sim 0.1$ one obtains in the case where the asymmetry is produced in one single flavour

$$\epsilon_\alpha \gtrsim 10^{-6} \quad . \tag{4.38}$$

Using the atmospheric neutrino mass splitting for the largest neutrino mass, one obtains

$$M_1 \gtrsim 10^9 \text{ GeV} \quad \Rightarrow \quad T_{\text{reheat}} \gtrsim 10^9 - 10^{10} \text{ GeV} \tag{4.39}$$

The original derivation of this bound, called the Davidson-Ibarra bound, including a much more exact numerical evaluation of the lower bound on N_1 can be found in [104]. This bound is very restrictive, so it it worth recalling the assumptions of this bound:

- This bound only applies to non-degenerate right-handed neutrino masses. In the case of degenerate neutrino masses, the asymmetry can be much larger and the bound on M_1 as low as the TeV scale, e.g the model described in the following chapter is such a model.
- It only applies if there are no other additional particles than the SM particles and the right-handed neutrinos. A second Higgs, a fourth family or additional light singlets can change the situation completely.
- This bound was derived using hierarchical right-handed neutrino masses with one light mass $M_1 << M_{2,3}$.

In the supersymmetric version of leptogenesis the lower bound on the reheat temperature can conflict with the upper bound on the reheat temperature that comes from gravitinos. Gravitinos are abundantly produced at high temperatures by scattering in the thermal bath at a rate $\sim T^3/m_{\text{Pl}}$ and decay with a lifetime $m_{\text{Pl}}^2/m_{\tilde{G}}^3$. The decay products can disassociate light elements produced during BBN. To avoid this one has to restrict the amount of gravitinos that are produced and finds an upper bound on the reheat temperature [105]

$$T_{reh} \lesssim 10^9 - 10^{12} \text{ GeV} \tag{4.40}$$

If the first value of the bound holds, right-handed neutrinos are not sufficiently produced and leptogenesis does not work. However if 10^{12} GeV is the right bound (which is the case for relatively heavy gravitinos 3 TeV $\lesssim m_{\tilde{G}} \lesssim$ 10 TeV) then no conflict exists. Even in the first case there are still ways around the problem when right-handed neutrinos are produced in some non-thermal process. One such possibility would be a coupling of right-handed neutrinos to the inflaton, which produces enough right-handed neutrinos in inflaton decays [106].

Chapter 5

Relating leptogenesis to the WIMP miracle

This chapter presents my research work on leptogeneis together Sacha Davidson. We aim to link the generation of the Baryon Asymmetry of the Universe (BAU) to the WIMP miracle, which gives naturally the right number density for dark matter. We estimate the BAU produced in an inverse seesaw model containing extra light singlets, and with lepton number conservation prior to the electroweak phase transition. The number density of baryon parent particles is comparable to the WIMP number density when the efficient production of a CP asymmetry starts. A naturally large $\epsilon \sim \mathcal{O}(1)$ is required to obtain a large enough BAU and to link BAU to dark matter. The chapter is based on [2].

5.1 Introduction

In recent years, there has been some interest in relating the cosmological number density of baryons [88, 107, 97, 89], with the number density of dark matter particles [108]. A popular approach, refered to as Asymmetric Dark Matter (ADM) [109, 110, 111], is to implement a single mechanism that generates an excess of particles over anti-particles, which materialises both in the baryons and in the dark matter. However the relic density of a weakly interacting particle (WIMP) is naturally of order the observed dark matter density. So it is not clear what is gained by dropping the "WIMP miracle", to link the dark matter number density to the baryon asymmetry, which depends on an arbitrary CP violation parameter. Scenarios which implement the link in the inverse direction [112, 113], explaining the baryon number density from the dark matter density, could be more interesting. But they require a CP asymmetry that is naturally $\mathcal{O}(1)$. The aim of our model is to link the baryon asymmetry to the "WIMP miracle" density: we assume that the Dark Matter are WIMPs (so their observed relic abundance is already natural and requires no explanation), and attempt to build a baryogenesis model, which naturally generates, in a similar cosmology, the observed baryon asymmetry. If the parent particle, which produces the CP asymmetry in its decays, has a typical WIMP density at the moment when it starts to create a net asymmetry and if the CP violation is $\mathcal{O}(1)$, then similar relic abundances of DM and baryons are expected.

We consider an "inverse seesaw"-like model [86], extending the Standard Model (SM) with TeV-scale electroweak singlet Dirac neutrinos ψ, additional light singlet fermions s and a $L = 2$ singlet scalar ϕ. The ψ participate in Yukawa interactions with SM neutrinos, and the ϕ have (L conserving) interactions with ψ and s. For generic choices of couplings, lepton number violation

arises spontaneously when ϕ gets a vev, after the electroweak phase transition, giving Majorana masses to the doublet SM neutrinos. However, there is a particular limit where lepton number is conserved and the SM neutrinos are Dirac, whose baryogenesis prospects are explored in section 5.3.5. Section 5.2 reviews our model and notation. Since we are building a model, we would like it to exhibit as many interesting features as possible. Our model can fit the observed neutrino mass differences. However, the additional light singlets cannot fit the reactor neutrino anomaly [74] and Big Bang Nucleosynthesis; this is briefly discussed in section 5.2.

The Baryon Asymmetry of the Universe (BAU) is generated via leptogenesis [94] at the TeV scale. As the temperature of the Universe drops below the mass of the singlet ψs, their number density is depleted by annihilations and decays. We require this to occur prior to the electroweak phase transition. They can decay to SM neutrinos ν and a Higgs, or to light singlets s and ϕ, and CP asymmetries can arise in these decays. Since lepton number is conserved until ϕ gets a vev, these lepton asymmetries would be of equal magnitude and opposite sign in the doublets and singlets. The asymmetries can survive in the plasma, once "washout interactions", exchanging lepton number between the doublets and singlets, are out of equilibrium. Section 5.3.3 estimates that the co-moving number density of ψs remaining, when this occurs, is "naturally" of order that of WIMPs. So to "naturally" obtain similar relic densities of baryons and WIMPs would require to "naturally" obtain $\mathcal{O}(1)$ CP asymmetries in the ψ decays. As reviewed in section 5.3.2, large CP asymmetries can be arranged by taking the ψ masses to be quasi-degenerate [95]. The lepton asymmetry in Standard Model neutrinos then can be partially transformed to baryons by the non-perturbative SM sphaleron processes (as described above in section 4.2.3). Dark matter is assumed to be some other WIMP, with a "usual" relic abundance. So this scenario gives similar abundances of WIMPs and baryon-*parents*, but similar dark matter and baryon number densities only arise if there is an $\mathcal{O}(1)$ CP asymmetry in the parent decays. Unfortunately, such a large CP asymmetry is not easy to obtain in our model. We comment on this scenario's ability to relate the baryon and dark matter densities in section 5.4.

5.2 Review, Notation and Masses

5.2.1 Observations

The mass density of baryons B and cold dark matter in the universe today with their 1σ interval measured by the PLANCK satellite, using a canonical ΛCDM model are recalled here [17]

$$\Omega_B h^2 = 0.02205 \pm 0.00028 \qquad \Omega_{\rm CDM} h^2 = 0.1199 \pm 0.0027 \tag{5.1}$$

The ratio of dark matter particles to baryons is then given by

$$\frac{Y_{\rm CDM}}{Y_B} \sim 5 \frac{m_p}{m_{DM}} \quad , \tag{5.2}$$

where m_p is the proton mass. Since m_p mostly arises from QCD, and the dark matter should not have strong interactions, we assume that m_p and m_{DM} are unrelated, and focus on obtaining similar baryon and dark matter number densities today: $Y_B/30 \lesssim Y_{\rm CDM} \lesssim 30 Y_B$. This definition of "similar" allows a dark matter candidate in the mass range accessible to most direct detection experiments.

Notice that the ratio in equation (5.2) could be different in more complicated cosmological models, such as those with extra sterile neutrinos. The CMB data alone allows the dark matter density to increase with the number of relativistic species present at recombination (counted as the number $N_{\rm eff}$ of neutrino flavours): $\delta\Omega_{\rm CDM} \sim 0.4(\delta N_{\rm eff}\Omega_{\rm DM}/N_{\rm eff})$ [114]. PLANCK CMB

data combined with WMAP polarization data and baryon acoustic oscillation experiments gives [17] $N_{\rm eff} = 3.30^{+0.54}_{-0.51}$ which is compatible with the SM value $N_{\rm eff} \approx 3$ but does not exclude one additional relativistic species. An increase in $\Omega_{\rm CDM}$ would usefully increase the ratio in equation (5.2), various laboratory neutrino anomalies [74] could benefit from light neutrinos other than the three of the Standard Model, and here we construct a neutrino mass model with additional light singlets. However, cosmological data also constrains the light neutrino mass scale. An additional eV sterile neutrino that could address the reactor neutrino anomaly should respect cosmological bounds on hot dark matter. It was shown by [79] that such a eV-sterile is cosmologically consistent if there are additional lighter neutrino species to delay matter radiation equality, and an $\mathcal{O}(0.01)$ asymmetry in the ν_e density to allow Big Bang Nucleosynthesis (BBN) [115, 116] to produce the observed relic abundances of light elements. Our model allows several sterile species, but the baryon asymmetry is related to the asymmetry in SM neutrinos, so we do not obtain the large asymmetry in ν_e required by [79, 116]. Furthermore, if our extra steriles decouple prior to the Electroweak Phase Transition (EPT), their contribution to the radiation density at BBN is suppressed by a factor $g_*(T_{\rm BBN})/g_*(T_{\rm EPT})$, where $g_*(T)$ is the number of SM degrees of freedom in the plasma at T. [1]

5.2.2 Models

An explanation for the ratio (5.2), which has benefited from recent interest [110, 111] could be that a single asymmetry controls both the baryon and dark matter relic number densities. If this ratio, given in equation (5.2), should be exactly one, then a comparatively light cold dark matter candidate is required. The observed difference in mass densities could also be due to inequivalent cosmological histories after the formation of the asymmetry. Some early discussions of asymmetries in the dark matter density are [109, 117]; for a review of recent Asymmetric Dark Matter (ADM) scenarios, see *e.g.* [118]. ADM models explain why the dark matter and baryon number densities are similar, but not why they have have the observed value.

An alternative approach [112, 113], attaches importance to the "WIMP miracle" (see *e.g.* [108]): the relic abundance of a massive particle, which annihilates with its anti-particle via a weak cross-section, gives $\Omega_{\rm DM}h^2$ of order the observed value. To explain the ratio (5.2), one then only needs a natural scenario giving a relic number density of baryons minus anti-baryons, which is similar to the relic number density of WIMPS plus anti-WIMPS. We saw above (section 4.1) that to produce an asymmetry, CP violation and non-equilibrium are required, whereas only a departure from thermal equilibrium is required for the particle-antiparticle-symmetric relic density of WIMPs. So if the non-equilibrium is similar in the baryon and dark matter production, and the CP asymmetry for baryogenesis is one, then similar number densities could be expected. For instance, in [112], the baryon asymmetry is produced in the out-of equilibrium annihilations of the dark matter particle, which works for selected mass ranges of the particles involved. In our model, the lepton asymmetry is produced in decays. The parent particle of the asymmetry first annihilates, then decays out-of-equilibrium, at the TeV-scale. This freezes-

1. This comes from the fact that the temperature of the decoupled species continually decreases $T_s \propto R^{-1}$ due to the expansion of the universe. The photon temperature also scales as $T_\gamma \propto R^{-1}$ most of the time, expect when another species annihilates. When the temperature falls below the mass of some species X which is in thermal equilibrium and which annihilates to photons (or any other particles in thermal equilibrium), the number density of this species drops $\propto e^{-m_X/T}$ relative to the photon density. The number of relativistic degrees of freedom in the plasma changes, but total entropy is conserved. This implies that the photon temperature increases according to $g^* T_\gamma^3\big|_{\rm bef} = g^* T_\gamma^3\big|_{\rm aft}$. The additional photons that a higher photon temperature implies come from the annihilation of particle X. Consequently the number density of the decoupled species decreases relative to photon density.

in the baryon-parent and dark matter densities at a similar temperature, so the departures from thermal equilibrium in both processes may be similar. Indeed, the co-moving density of a weak-scale unstable particle, when inverse decays freeze out, is similar to the relic density of a weak-scale particle that annihilates. So an $\mathcal{O}(1)$ CP asymmetry is required to get similar baryon and dark matter densities today.

We construct a TeV-scale model of out-of-equilibrium-decay leptogenesis [94]. Various mechanisms have been studied for leptogenesis [2] in TeV-scale seesaw models [120], such as degenerate decaying singlets [95], or adding extra particles [121]. Heavy singlet fermions in the "inverse seesaw" pattern have been studied by various people [122, 123, 124]. A model where right handed neutrinos decay into right handed charged letpons that works at the TeV scale pas proposed by [125]. Our model differs from the usual inverse seesaw in that we have additional light singlets[126], so we can generate a non-zero asymmetry in SM leptons, despite that the model conserves lepton number. Our leptogenesis scenario therefore differs from that of [122], who also study a lepton number conserving scenario, but without extra light singlets. They obtain a sufficient baryon asymmetry by turning off the sphalerons before inverse decays go out of equilibrium, when various asymmetries are present and changing. Here, we explore whether the baryon asymmetry can be obtained in a more "dynamics-independent" way, due to the presence of extra singlets. The Lagrangians of [123] contain "hard" lepton number breaking, so the relevant interactions for leptogenesis are somewhat different, because a net lepton asymmetry is generated. An advantage of the hard breaking is that it can naturally provide the small mass splitting between the heavy decaying singlets [123]. We focus on a lepton number conserving model, because it is for such models that a "hidden sector" (as provided by the extra light singlets) is useful for storing an asymmetry.

The inverse seesaw (discussed in section 3.2.2) has received attention because it generates small neutrino masses due to new particles with TeV-scale masses and couplings of a "natural" size. Such new particles may therefore be kinematically accessible to the LHC [127], or induce detectable [128] non-unitarity and/or Lepton Flavour Violation. We wish to explore, in models where the small lepton number violation is spontaneous, the prospects of additional light singlets and leptogenesis. A careful study [122] (without additional light singlets s), showed that the baryon asymmetry can be generated by turning off the sphalerons during the decays. We had hoped that baryogenesis would be easier with additional light singlets, but the parameter space where we estimate that it could work is not large enough to be convincing.

Dark Matter has been studied in radiative inverse seesaw models [129, 130], where it can arise more naturally than in the inverse seesaw [131]. We recall that our model does not aim to provide a WIMP; we suppose that it arises in some other sector of the theory.

5.2.3 Notation and Masses

We consider a Lagrangian with several additional singlets, which can spontaneously violate lepton number. The SM doublet leptons ℓ have Yukawa couplings to (two or three) "right-handed neutrinos" N_R, there is some larger number of singlet left-handed leptons $\{S, s\}$, and an $L = -2$ singlet scalar ϕ. The left-handed singlets who participate in a mass matrix M with the N_R are refered to as $\{S\}$, and the remaining ss can acquire masses once ϕ develops a vev. Allowing all renormalisable interactions, the Lagrangian, written in two-component notation

2. Low temperature out-of-equilibrium-decay baryogenesis scenarios have also been considered; the analysis of [119] was useful to us.

with all the fermions left-handed, is:

$$\mathcal{L} = \mathcal{L}_{SM} + \{\lambda^*[\ell H]N^c + M^*\, N^c S + y^*\, \phi S s + \frac{Y^*}{2}\phi S S + \frac{X^*}{2}\phi s s + \frac{Z^*}{2}\phi^\dagger N^c N^c + h.c.\} + V(\phi) \ , \quad (5.3)$$

H is the Higgs, $[\ell H] = \nu H_0 - e H_+$, and N^c, S and s have lepton numbers $L = \{-1, 1, 1\}$. The potential $V(\phi)$ causes ϕ to develop a vev after the electroweak phase transition. We assume that such a potential can be constructed, and consider it no further. We also ignore the resulting majoron [132]. Generation indices are implicit; for simplicity, we suppose two generations of N, S and s, so the matrices λ, y, Y, X, Z and M are two by two. We denote the eigenvalues of λ as λ_1, λ_2 (and similarly for other matrices). We will see that $\lambda_1 \sim \lambda_2$, $y_1 \sim y_2$ and $M_1 \sim M_2$ to obtain a large enough CP asymmetry for leptogenesis.

Prior to the Electroweak Phase Transition, there are two gauge singlet Dirac fermions, ψ_1, ψ_2:

$$\psi_I = \begin{pmatrix} S_I \\ N_I \end{pmatrix} \ , \quad (5.4)$$

whose masses $M_I \sim$ TeV are the eigenvalues of M. The M_I will be taken degenerate to obtain a large enough baryon asymmetry, so when the mass difference is irrelevant, we write M_ψ.

In the presence of vacuum expectation values $v = \langle H \rangle = 174$ GeV and $u = \langle \phi \rangle \lesssim v$, the neutral Majorana mass matrix can be written, in two component notation, as

$$\mathcal{L}_{\text{mass}} = -\frac{1}{2}\,(\nu_L\, N^c\, S\, s) \begin{bmatrix} 0 & m_D & 0 & 0 \\ m_D^T & \mu_Z & M & 0 \\ 0 & M^T & \mu_Y & \mu_y \\ 0 & 0 & \mu_y^T & \mu_X \end{bmatrix} \begin{pmatrix} \nu_L \\ N^c \\ S \\ s \end{pmatrix} + h.c. \quad (5.5)$$

where $m_D = \lambda v$, $\mu_X = X u$, $\mu_y = y u$, $\mu_Z = Z u$, and $\mu_Y = Y u$ are two by two matrices.

We are interested in the limit where the eigenvalues of M are much larger than the other entries in the mass matrix. In the case of the usual inverse seesaw, which contains no light singlets s, the determinant implies that the light active neutrino mass matrix is $\sim m_D M^{-1} \mu_Y M^{T-1} m_D^T$. In the case where extra singlets are present, the determinant of the mass matrix in equation (5.5), in one generation, is $m_D^2(\mu_Y \mu_X - \mu_y^2)$. We neglect from now on the coupling Z, because its contributions to the mass matrix are unimportant, and its effects in the baryogenesis scenario are similar to those of Y, which will be unimportant. We will see in section 5.3.3 that the couplings in y and/or λ must be small [3] ($\lesssim 10^{-5}$), to prevent the washout of the lepton asymmetry. We focus on two simple limiting cases: $y_i \ll Y_i, X_i \lesssim 1$, which gives Majorana masses for the active neutrinos, and the case $Y_i = X_i = 0$, which gives Dirac masses between the ν_L and s.

In the Majorana case with $y_i \ll Y_i, X_i$, the active neutrinos have a usual-inverse-seesaw-like mass matrix $m_\nu \simeq m_D M^{-1} \mu_Y M^{T-1} m_D^T$, whose eigenvalues satisfy

$$\frac{m_{\text{atm}} m_{\text{sol}}}{\text{eV}^2} = 0.3 \left(\frac{\lambda_1 \lambda_2}{10^{-9}}\right)^2 \left(\frac{(3\ \text{TeV})^2}{M_1 M_2}\right)^2 \frac{Y_1 Y_2 \langle\phi\rangle^2}{v^2} \quad (5.6)$$

ϕ should have a mass and vev well below the Higgs vev $v = 174$ GeV, to ensure that lepton number is conserved prior to the electroweak phase transition. However, we will be forced to take the vev of order v (to allow λ_i small enough to give a sufficient abundance of ψs after freezeout

3. We therefore do not expect bounds on our model from lepton flavour violating processes such as $\mu \to e\gamma$, or non-unitarity [128].

of washout interactions). We will also require $\lambda_1 \simeq \lambda_2$, to obtain a large enough CP asymmetry, so we will suppose a mild hierarchy in Y to generate the atmospheric - solar splitting.

The light steriles s have a mass matrix $\sim \mu_X = X\langle\phi\rangle$. In the one generation case, s has a mixing angle with the active neutrino of order $\mu_y m_D/(M\mu_X)$, which allows the decay $s \to 3\nu$ at tree level. We focus on parameters[4] $X \lesssim Y$, such that the singlets are innocuous: their masses are $\lesssim$ GeV, they annihilate efficiently (to majorons), and otherwise can decay. Since the s decouple prior to the Electroweak Phase Transition, their temperature at $T \sim \mu_X$ is suppressed with respect to the photons, so they should not over-contribute to the radiation density.

The active neutrinos share Dirac masses $\sim m_D\mu_y/M$ with the singlets s, if $X = Y = Z = 0$ in the Lagrangian (5.3). We consider this limit only in section 5.3.5, because it allows more parameter space for our leptogenesis scenario[5]. By assigning $L = 0$ to ϕ, and $L = -1$ to s, lepton number clearly is conserved also after both ϕ and H get vevs. However, since ϕ was introduced to spontaneously break lepton number, it is peculiar to not give it lepton number. We nonetheless assume that ϕ does not mix with H, and do not discuss potential constraints from Higgs physics.

5.3 Thermal History

One of the roles of ψ is to generate the Baryon Asymmetry of the Universe (BAU). In its decays, it can generate an active versus sterile lepton asymmetry and the excess of active leptons will be partially transformed to baryons by sphalerons [101]. This is discussed in section 5.3.2. The asymmetries produced in ψ decay can survive in the plasma once "washout interactions" (such as inverse decays $\ell H \to \psi$ and $\overline{\phi}\overline{s} \to \psi$, and scattering $\ell H \to \overline{\phi}\overline{s}$) go out of equilibrium. This "freeze-out" temperature $T_{\rm BAU}$ is estimated in section 5.3.3. The baryon asymmetry present today will be generated in the decays of the ψs remaining at $T_{\rm BAU}$.

Decays and inverse decays are not the only interactions which change the ψ number density; $\psi + \overline{\psi}$ can also annihilate, via the coupling Y to $\phi + \overline{\phi}$. The annihilation rate is faster than the decay rate at temperatures just below the ψ mass, so we start by discussing annihilations below in section 5.3.1. Annihilations and inverse decays will freeze out at similar temperatures.

5.3.1 $\psi\overline{\psi} \to \phi\overline{\phi}$ annihilations

At temperatures $T \gtrsim M_I$, an equilibrium abundance of ψ_I and $\overline{\psi}_I$ will be present, because they can be produced via Yukawa interactions involving λ (for instance in $t_R\overline{t_L} \to H^* \to \ell\overline{\psi}$, at a rate $\Gamma \sim h_t^2\lambda^2 T/(4\pi)$, which is fast compared to the universe expansion H).

As the temperature T drops below their mass, the singlets can annihilate via their Y couplings, or decay to a light lepton and a scalar via their λ or y couplings:

$$\psi_I + \overline{\psi}_J \to \phi + \overline{\phi} \tag{5.7}$$

$$\psi_I \to \ell + H \ , \ \overline{s} + \overline{\phi} \tag{5.8}$$

We focus first on annihilations, because we envisage $1 \sim Y_i \gg y_j, \lambda_k \lesssim 10^{-4}$, which implies that initially, at $T \lesssim M_I$, the ψ_Is are more likely to annihilate than decay.

4. With $X \sim 10^{-10}$, we can obtain a singlet s with eV mass and $\sim 0.1 - 0.01$ mixing angle, that could fit the reactor neutrino anomaly. However, we do not explore this parameter space, because out model cannot give the large lepton asymmetry required to make it cosmologically acceptable.

5. Mixed scenarioscan be envisaged, for instance where the atmospheric mass is Dirac, and the solar mass is Majorana. We do not study this tuned example because we estimate that out-of-equilibrium-decay-leptogenesis does not occur.

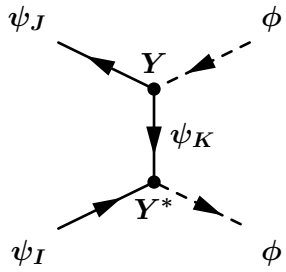

Figure 5.1: The figure shows the $\psi\overline{\psi} \to \phi\overline{\phi}$ annihilation process.

The non-relativistic annihilation cross-section in the centre of mass is

$$\sigma v(\psi_I + \overline{\psi}_J \to \phi + \overline{\phi}) = \frac{|[YY^\dagger]_{IJ}|^2}{128\pi M_\psi^2} \tag{5.9}$$

where all the singlet masses are approximated as M_ψ. We neglect the Sommerfeld enhancement due to ϕ exchange [6] because the ψs are almost relativistic; the enhancement can be estimated [133] to be a few percent. The number density of ψ_Is remaining when annihilations freeze out, and the freeze-out temperature $T_{\rm ann} \equiv M_\psi/z \simeq M_\psi/20$ can be determined from

$$n_\psi(T_{\rm ann})\sigma v \simeq H(T_{\rm ann}) \simeq \frac{1.7\sqrt{g_*(T_{\rm ann})}T_{\rm ann}^2}{m_{\rm pl}} \tag{5.10}$$

where $g_{\rm eff}$ is the number of degrees of freedom in the plasma, and $g_*({\rm TeV}) \simeq 100$ in our model.

5.3.2 Decays and the CP asymmetry

After the ψ annihilations freeze out, the number density of ψ and $\overline{\psi}$ will continue to drop, because they decay. The model conserves lepton number, so the total lepton asymmetry produced in these decays is zero. However, since the ψs decay both to SM particles H, ℓ, or to singlets $\overline{s}, \overline{\phi}$, equal but opposite lepton asymmetries in the singlet and doublet sectors could be produced. To obtain a baryon to dark matter ratio that is $\mathcal{O}(1)$, these CP asymmetries will need to be large, so we explore this limit below.

The ψ_Is, which carry $L = 1$, can decay at tree level to an ℓ_α and an H, or to a $\overline{\phi}$ ($L = 2$) and a $\overline{s}_\beta$, at partial rates

$$\Gamma(\psi_I \to \ell_\alpha + H) = \frac{|\lambda|^2_{\alpha I}}{16\pi}M_I \quad , \quad \Gamma(\psi_I \to \overline{s}_\beta + \overline{\phi}) = \frac{|y|^2_{\beta I}}{32\pi}M_I \tag{5.11}$$

See the first diagrams of figures 5.2 and 5.3. These decays are fast, compared to the expansion rate H, for $T \lesssim \{|\lambda|, |y|\}\sqrt{M_I m_{\rm Pl}}/20$, so at all temperatures relevant to us.

CP violating asymmetries for a given final state:

$$\epsilon_\alpha^{(I,\ell)} = \frac{\Gamma(\psi_I \to \ell_\alpha H) - \Gamma(\overline{\psi}_I \to \overline{\ell}_\alpha \overline{H})}{\Gamma(\psi_I \to all) + \Gamma(\overline{\psi}_I \to all)} \quad , \quad \epsilon_\alpha^{(I,s)} = \frac{\Gamma(\psi_I \to \overline{s}_\alpha \overline{\phi}) - \Gamma(\overline{\psi}_I \to s_\alpha \phi)}{\Gamma(\psi_I \to all) + \Gamma(\overline{\psi}_I \to all)} \tag{5.12}$$

can be obtained from the interference of tree with loop diagrams, if the couplings are complex and some particles in the loop can be on-shell. In figures 5.2 and 5.3, are drawn the subset

6. Sommerfeld enhancement is the enhancement of a annihilation cross section due to multiple exchange of a long range mediator particle. In our model the ϕ are effectively massless compared to the annihilating ψ: $m_\phi << M_\psi$. However this effect is only efficient if the colliding particles have small velocities. In our case at the moment of decoupling $T \sim \frac{20}{M_\psi}$ the incoming particles are still midly relativistic $v \sim 0.3c$. We thank Marco Cirelli for discussions of this issue.

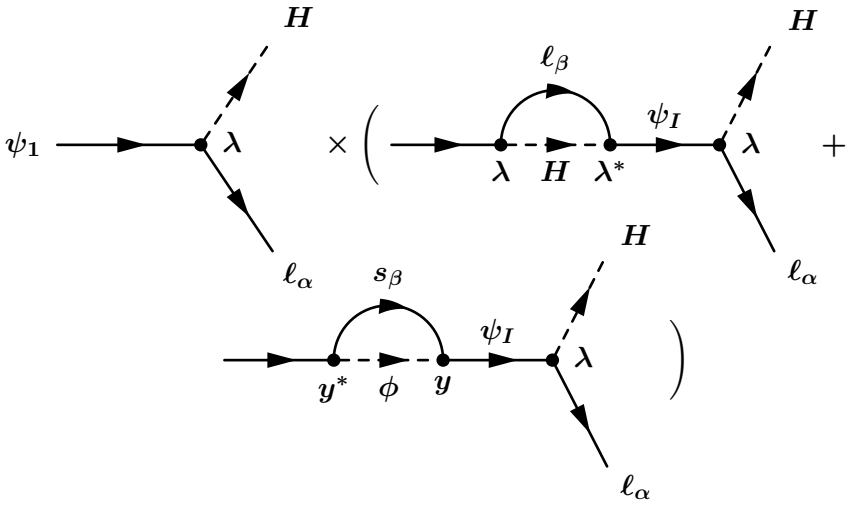

Figure 5.2: Diagrams contributing to the CP asymmetry with final state $\ell_\alpha + H$.

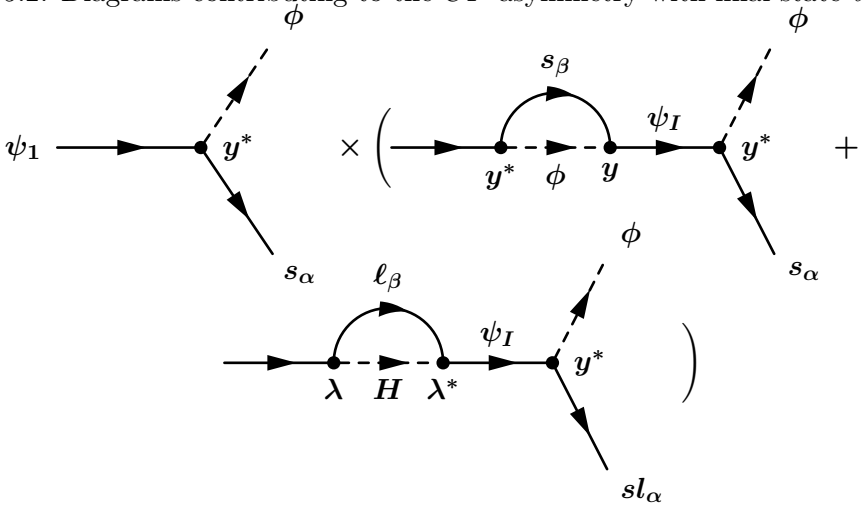

Figure 5.3: Diagrams contributing to the CP asymmetry with final state $s_\alpha + \phi$.

of one-loop diagrams which we include in our calculation. We are interested in $\epsilon \to 1$, which can be obtained in the decays of quasi-degenerate singlets from the illustrated wave-function renormalisation diagrams [95]. The vertex corrections diagrams are not enhanced by quasi degenerate singlets and are therefore neglected in the following.

We neglect the effects of X and Y couplings in the decay rate and CP asymmetries, despite the hierarchy in magnitudes: $X, Y \sim 1$, $y, \lambda \sim 10^{-4}$. This is because decays involving X and Y are suppressed by three-body final state phase space, and we were unable to find significant effects of X and Y in the CP asymmetries.

In the decay of ψ_I, the total asymmetry in the doublets, summed on lepton flavours α, is

$$\epsilon^{(I,\ell)} = \sum_\alpha \epsilon_\alpha^{(I,\ell)} = \sum_{\alpha,\beta,J} \frac{Im\{\lambda_{\alpha I}\lambda^*_{\alpha J} y_{\beta I} y^*_{\beta J}\}}{8\pi[2\lambda^\dagger\lambda + y^\dagger y]_{II}} \frac{\sqrt{x_J}}{1-x_J} \tag{5.13}$$

where $x_J = M_J^2/M_I^2$. This contribution arises from the interference of the tree decay with the last loop of figure 5.2. Similarly, the total asymmetry in the singlets is

$$\epsilon^{(I,s)} = \sum_\alpha \epsilon_\alpha^{(I,s)} = \sum_{\alpha,\beta,J} \frac{Im\{y^*_{\alpha I} y_{\alpha J} \lambda_{\beta J}\lambda^*_{\beta I}\}}{8\pi[2\lambda^\dagger\lambda + y^\dagger y]_{II}} \frac{\sqrt{x_J}}{1-x_J} \tag{5.14}$$

In both the doublet and singlet sectors, there can be asymmetries in the individual flavours α, which arise from the middle diagram of figures 5.2 and 5.3. The flavour sums of these two contributions are zero. We therefore neglect these contributions, and focus on the flavour-summed singlet and doublet asymmetries of equations (5.13) and (5.14), because its the total (=flavour-summed) doublet lepton asymmetry which the sphalerons transform to baryons

The asymmetries given are for the decays of any of the ψ_I. To obtain a large enough CP asymmetry, at least two of the ψ_I must be very degenerate: $M_I - M_J \sim \Gamma_I$, so the CP asymmetries in the decays of at least two of the ψ_Is will contribute to the baryon asymmetry. It is therefore fortunate that the CP asymmetries do not vanish when summed on I: in a two generation model, in the limit where $M_1 \to M_2$, the CP asymmetries are equal $\epsilon^{(1,\ell)} = \epsilon^{(2,\ell)}$, rather than opposite.

As anticipated, the sum of $\epsilon^{(I,\ell)}$ and $\epsilon^{(I,s)}$ vanishes because the model conserves lepton number. It will therefore be important that no interaction be fast enough to equilibrate the singlet and doublet sectors, as the asymmetries are produced and until the Electroweak Phase Transition. This is discussed in section 5.3.3.

It is helpful to be able to estimate the size of these CP asymmetries. This scenario of out-of-equilibrium decay leptogenesis at the electroweak scale requires a large CP asymmetry $\epsilon \gtrsim 0.1$. So from equation (5.13), all the elements $[\lambda]_{I\alpha}$ and $[y]_{I\beta}$ must be comparable, for all α, I, β, and the ψs degenerate :$M_1 - M_2 \gtrsim \Gamma$. For phases to maximise the asymmetry, large mixing angles, and comparable eigenvalues $\lambda_1 \sim \lambda_2$, $y_1 \sim y_2$,

$$\epsilon^I \sim \frac{1}{16\pi} \frac{y_1^2 \lambda_1^2}{y_1^2 + 2\lambda_1^2} \frac{M_I}{M_I - M_J} \leq \frac{1}{4D} \tag{5.15}$$

where the last approximation expresses the mass splitting in units of Γ_I

$$M_I - M_J = D\Gamma_I \tag{5.16}$$

and the coupling constant combination was maximised by taking

$$y_1 \sim \sqrt{2}\,\lambda_1 \quad . \tag{5.17}$$

Recall that the formulae in equations (5.13) and (5.14) are valid for $M_I - M_J > \Gamma_I$, so $\epsilon \sim 0.1$ is barely consistent. Since the mass M is the only interaction linking the singlet and doublet sector, loop corrections should not destabilise the small splitting.

5.3.3 Washout of the asymmetry by inverse decays and scattering

As the ψs decay, they produce an asymmetry in doublet leptons. This asymmetry will survive, and be redistributed throughout the plasma by the interactions in chemical equilibrium [134], if all the interactions which can destroy this asymmetry are out of equilibrium. Such destructive interactions are referred to as "washout interactions", and in our model we have to types: the inverse decays $\ell H \to \psi$ and $\overline{\phi}\overline{s} \to \psi$, which transfer lepton number back to the ψs, and the $H\ell \to \overline{\phi}\overline{s}$ scattering (see figure 5.4) which exchanges lepton number between the doublets and light singlets. As described above, we treat the on-shell-ψ part part of figure 5.4 as inverse decays, and including the remaining "Real Intermediate State -subtracted" part as scattering far below the ψ pole.

At first we will consider the inverse decays. We define the thermally averaged inverse decay rates as

$$\langle \Gamma(\ell_\alpha H \to \psi_I) \rangle \quad \simeq \quad \frac{n_\psi^{\rm eq}(T)}{n_\ell(T)} \Gamma(\Psi_I \to \ell_\alpha H) \tag{5.18}$$

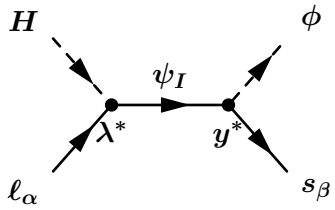

Figure 5.4: Dangerous scattering process $\ell + H \to \bar{s} + \bar{\phi}$ that could wash-out a created asymmetry.

where $n_\ell(T) \simeq g_\ell T^3/\pi^2$, the ψ decay rates are given in equation (5.11), and the equilibrium abundance of a non-relativistic particle X is

$$n_X^{\rm eq}(T) \simeq g_X \left[\frac{m_X T}{2\pi}\right]^{3/2} e^{-m_X/T} \tag{5.19}$$

where g_X is the number of spin degrees of freedom of X (notice that our number densities describe particles, not the particles + anti-particles). Comparing the inverse decay rate of equation (5.18) and the annihilation rate of equation (5.10) to the Hubble expansion, shows that they freeze out at a similar temperature

$$T_{\rm BAU} \simeq \frac{M_\psi}{20} \tag{5.20}$$

The annihilations $\psi\bar{\psi} \to \phi\bar{\phi}$, discussed in section 5.3.1, will freeze out first for

$$|[YY^\dagger]_{II}|^2 < \frac{M_\psi^3}{T^3} 2\pi^2 |y_{\beta I}|^2, 4\pi^2 |\lambda_{\alpha I}|^2 \quad . \tag{5.21}$$

We will see that this condition is satisfied, so annihilations stop depleting the ψ number density before the inverse decays allow a lepton asymmetry to survive.

The number density of ψs remaining when both inverse decays $\langle\Gamma(\ell H \to \psi_I)\rangle$ and $\langle\Gamma(\phi s \to \overline{\psi_I})\rangle$ are out of equilibrium is

$$n_\psi(T_{\rm BAU}) = \min\left\{\frac{H(T_{\rm BAU})}{\Gamma(\Psi_I \to \ell H)} n_\ell(T_{\rm BAU}) \ , \ \frac{H(T_{\rm BAU})}{\Gamma(\Psi_I \to \bar{\phi}\bar{s})} n_s(T_{\rm BAU})\right\} \tag{5.22}$$

where Γ and H are given in equations (5.11) and (5.10).

To protect a doublet lepton asymmetry, the inverse decays from the singlet and doublet sectors must both be out of equilibrium. To see this, recall that the heavy Dirac ψs have $L = 1$, and there are equal numbers of ψs and $\overline{\psi}$s to begin. As they decay, opposite lepton asymmetries develop in the doublet leptons and light singlet sector. Consider now the case that inverse decays from the doublets are out of equilibrium, but that the asymmetry in light singlets can be transfered back to the heavy Dirac leptons by $\phi s \to \overline{\psi_I}$. Then the anti-asymmetry from the light singlet sector is transfered to the ψs and $\overline{\psi}$s, who transmit it to the doublets via decays, which are always in equilibrium. Only when both inverse decays are out of equilibrium can the decays of ψ produce a net lepton asymmetry.

Now we will consider the scattering washout: $\ell + H \to \bar{s} + \bar{\phi}$. When this scattering process is still in equilibrium it can transfer the asymmetry from the singlet sector to the doublet sector and vice versa. As the asymmetries in both final states are equal in magnitude but opposite in sign, this process erases the asymmetry. Away from the ψ mass pole, the scattering cross-section is

$$\sigma(\ell_\alpha + H \to \bar{s}_\beta + \bar{\phi}) = \frac{|y_{\beta I}\lambda_{\alpha I}|^2}{32\pi} \frac{M_I^2}{(s - M_I^2)^2} \to \frac{|y_{\beta I}\lambda_{\alpha I}|^2}{32\pi M_I^2} \tag{5.23}$$

where, after the arrow, the internal line momentum is neglected. This is an acceptable approximation at temperatures $T \lesssim M_I/20$, where the inverse decays are out of equilibrium. With this approximation, the thermally averaged scattering rate $\Gamma \sim \sigma n_\ell$ is out of equilibrium for

$$|y_{\beta I}\lambda_{\alpha I}|^2 \lesssim 4 \times 10^{-11} \frac{M_I}{3\text{TeV}} \quad . \tag{5.24}$$

5.3.4 Putting it all together in the Majorana case

The "washout" interactions go out of equilibrium at T_{BAU} (given in equation (5.20)), after which an asymmetry in the SM leptons is produced. This should occur prior to the electroweak phase transition, which we take to occur at $T_{\text{EPT}} \sim 150$ GeV [102]. Requiring $T_{\text{BAU}} > T_{\text{EPT}}$, imposes a lower bound on the singlet mass scale

$$M \gtrsim 3 \text{ TeV} \quad . \tag{5.25}$$

There is also an upper bound on M, as a function of λ, $u = \langle\phi\rangle$ and Y, from requiring that the inverse seesaw give the observed neutrino mass differences. This condition was given in equation (5.6). Since a large enough CP asymmetry requires large mixing angles and comparable eigenvalues in λ and y, we can restrict to the one generation case:

$$m_{\text{atm}} = 0.59 \left(\frac{\lambda_2}{10^{-9}}\right)^2 \left(\frac{(3 \text{ TeV})}{M_2}\right)^2 \frac{Y_2\langle\phi\rangle}{v} \text{ eV} \tag{5.26}$$

And finally, the requirement that $\psi\bar{\psi} \to \phi\bar{\phi}$ annihilations freeze-out before the inverse decays $\ell_\alpha H \to \psi$, imposes the relation between Y and λ given in equation (5.21). Expressed in terms of eigenvalues, we obtain

$$Y_2^4 \lesssim 10^{-3} \left(\frac{\lambda_2^2}{10^{-9}}\right) \quad . \tag{5.27}$$

Electroweak sphalerons will partially transform the $B - L$ asymmetry produced in SM fermions, Y_{B-L}, to a baryon asymmetry[134] $Y_B = (12/37)Y_{B-L}$. So the baryon asymmetry produced in our model will be of order

$$Y_B \simeq \frac{12}{37}\frac{n_\ell - n_{\bar{\ell}}}{s} \simeq \frac{12}{37}\frac{4n_\psi(T_{\text{BAU}})}{s}\epsilon \simeq 4 \times 10^{-10}\frac{M_\psi}{3 \text{ TeV}}\frac{10^{-9}}{|\lambda_2|^2}\frac{1}{D} \quad , \tag{5.28}$$

where $4n_\psi = \Sigma_I(n_{\psi_I} + n_{\bar{\psi}_I})$, and we used equations (5.22) and (5.15). It is marginally possible to obtain the atmospheric mass difference and the observed baryon asymmetry, with $M = 3$ TeV, Y_2 saturating equation (5.27), and $\langle\phi\rangle \lesssim v$. In figure 5.5, the available parameter space is plotted in the plane $|y_1|^2/10^{-9}$ against the degeneracy defined in equation (5.16).

5.3.5 Dirac limit

As seen in the section above, for Majorana light neutrino masses, the parameter space of our model is very restricted. In this section, we explore the Dirac limit of the light neutrino mass matrix in equation (5.5), where all Majorana mass terms are zero, $\mu_A \to 0$, $A \in \{X, Y, Z\}$. Without Majorana mass terms one can redefine the lepton number of $\{N^c, S, s, \phi\}$ to be $\{-1, 1, -1, 0\}$ so that also after the phase transition of ϕ lepton number is conserved. Neutrinos become Dirac particles with s_I being their right handed Dirac partners. The light mass eigenvalue is

$$m_\nu^D = \frac{m_D\mu_y}{M} \tag{5.29}$$

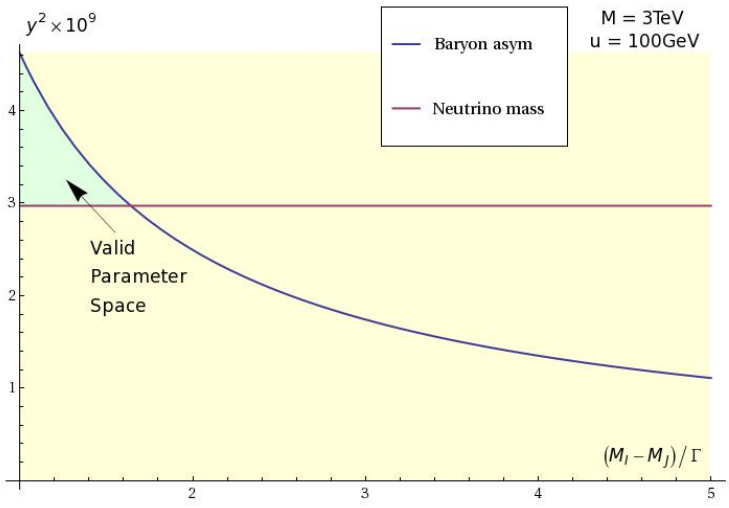

Figure 5.5: Available parameter space generating the observed baryon asymmetry and neutrino masses, of Majorana type, in the inverse seesaw model with extra light singlets, described by the Lagrangian (5.3).

which is only suppressed by $\frac{1}{M}$ compared to $\frac{1}{M^2}$ in the Majorana case. This will significantly enhance our allowed parameter space. But it is also clear that hirarchy in neutrino masses must now come from a hierarchy in the Yukawa eigenvalues $\lambda_1 < \lambda_2$, and/or the same for y.

Before looking at the parameter space in the Dirac model, we shall look at its thermal history, comparing to the Majorana case. The first thing to realize is, that annihilation processes $\psi\bar{\psi} \to \phi\bar{\phi}$ do not exist. The only processes that washout CP asymmetry are scattering, as in figure (5.4) and inverse decays which, like in the Majorana case, determine the moment of efficient CP violation. We assume the inverse decay rates from the various flavours are comparable, despite the mild hierarchy in λ and/or y. After the inverse decays become slow, all heavy parent particles will decay and produce a CP asymmetry that is not washed-out, so that the first part of equation (5.28) remains valid. Therefore the thermal history in the Dirac limit does not differ significantly from the Majorana case. The value of ϵ, however, will be reduced, because of the Yukawa hierarchy. To be concrete, in figure 5.6, we take $\epsilon = \frac{1}{16D}$ (compare to the Majorana case, equation (5.15)).

One should also have a careful look at Big Bang Nucleosynthesis because it restricts the number of thermalised neutrinos at $T \sim MeV$: $N_\nu \lesssim 4$. It was shown in [135] that right handed Dirac neutrinos are not in equilibrium at $T \sim MeV$ because their interaction rates are suppressed by a factor $\left(\frac{m_\nu}{T}\right)^2$ compared to that of left-handed neutrinos. Consequently the number of neutrinos in thermal equilibrium at BBN is not changed by our model with respect to the Standard Model.

Let us now turn to the parameter space of the Dirac limit. In the Majorana case the allowed parameter space is very small because asymmetry production favours small y, in order to produce a big density of ψ when inverse decays freeze out which can then be transformed into enough baryon asymmetry, even if $\epsilon < 1$. But neutrino masses prefer big y couplings, because the neutrino mass term is already suppressed by $1/M^2$. This forces us to take quite large values for u, the vev of ϕ in order to enhance neutrino masses without limiting asymmetry production. In the Dirac limit neutrino masses are less suppressed, so that the conflict between

baryon asymmetry and neutrino masses is less critical. We can realize our model with moderate values for $u \approx 6$ GeV, far away from electroweak phase transition, while parent masses are at $M = 3$ TeV and do not have to be more degenerate than $M_I - M_J \approx 5\Gamma(\psi_I \to \text{all})$. These values were obtained for a ideal constellation of our parameters, i.e. all phases in our Yukawa couplings λ and y are of order one and that $2\lambda_2^2 \sim y_2^2$. However in this Dirac limit small variations from these ideal conditions are possible as the parameter space is big enough to compensate for non ideal conditions. A plot of possible parameter space is given in figure (5.6).

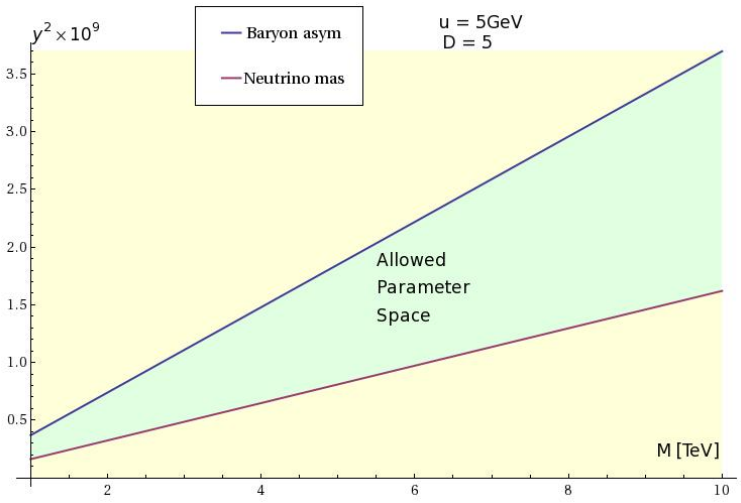

Figure 5.6: Constraints from the Baryon asymmetry and neutrino masses on y_2^2 as a function of the parent particle mass scale M_ψ give the allowed parameter space in the Dirac limit. The upper bound from Baryon asymmetry (solid line) varies with the degeneracy $M_I - M_J \approx D\Gamma(\psi_I \to \text{all})$. For less degenerate parent particles, the slope reduces and the allowed parameter space shrinks. The dashed line is the lower bound from neutrino masses and varies with the vacuum expectation value u. For smaller u, the slope rises and the parameter space shrinks.

5.4 Discussion

Our model considered baryogenesis at the electroweak scale, in an out-of-equilibrium decay scenario. This was implemented in an inverse seesaw model with extra light singlets s, described by the Lagrangian (5.3). The aim was to relate the baryon asymmetry to the dark matter abundance, and possibly fit various neutrino anomalies with the extra singlets. Similar Dark Matter and baryon abundances were supposed to arise, because, if the Dark Matter is made of WIMPs, and the baryon asymmetry produced in electroweak-scale out-of-equilibrium decay, then both relic densities are controlled by electroweak-scale interactions going out of equilibrium. The baryon asymmetry is also proportional to a CP asymmetry ϵ, see equation (5.28).

The scenario for generating the baryon asymmetry in our model is outlined at the end of the introduction. It does not work very well. The first difficulty is that it does not naturally give the large CP asymmetry that is required, contrary to models with explicit lepton number violation (reviewed in section 5.2.2). More importantly, the allowed parameter space where it produces a sufficient baryon asymmetry and correct neutrino masses is tiny (see figure 5.5), and unattractive. It requires a small mass splitting between the heavy singlets $M_2 - M_1 \simeq \Gamma$, but

the formula for ϵ, equation (5.13), becomes unreliable in this limit. Also, the inverse seesaw is attractive because it allows new LHC-scale singlet fermions with large Yukawa couplings, and spontaneous lepton number violation due to a small vev. However, our model requires small yukawas λ and y, to ensure that interactions which wash out the baryon asymmetry freeze out soon enough. This forces a large lepton number violating vev, of order the Higgs vev. The masses of the extra light singlets s are arbitrary, but would be $\lesssim$ GeV, unless a steep hierarchy is tuned into the couplings (see discussion after equation (5.6)). A larger successful parameter space is obtained (see figure 5.6), if the Majorana couplings of the inverse seesaw model are set to zero. Then the active neutrinos obtain Dirac masses with the light steriles. However, then the motivation for the singlet scalar (whose vev spontaneously broke lepton number in the Majorana case), is no longer clear. Since it no longer carries lepton number, it could mix with the Standard Model Higgs, and some analysis would be required to determine its experimental signatures.

Despite the flaws in our model, it could be unsurprising, if not natural, to obtain similar baryon and dark matter relic densities, when the dark matter are WIMPs, and the baryon asymmetry is produced in out-of-equilibrium decay. In such scenarios, the baryon asymmetry is produced after the freeze-out of washout interactions. This condition can be roughly estimated as

$$\Gamma(\text{all} \to \psi) \simeq \Gamma(\psi \to \text{all}) e^{-M/T} \lesssim H(T_{\text{BAU}}) \tag{5.30}$$

where ψ is the decaying parent of the BAU, of mass M, and H is the Hubble expansion rate. Notice that inverse decays are Boltzmann-suppressed, because the light decay products have difficulty to find, in the thermal bath, the energy to produce a heavy ψ.

This Boltzmann suppression is reminiscent of the freezeout of annihilations of a WIMP χ, which can be estimated to occur when

$$n_\chi(T_{\text{DM}}) \langle \sigma v \rangle \lesssim H(T_{\text{DM}}) \tag{5.31}$$

The $e^{-m/T}$ appears here in equilibrium number density of a non-relativistic particle, see equation (5.19).

From these two estimates, it is straightforward to estimate the ratio of co-moving densities [7] of BAU parents ψ to WIMPs χ as

$$\frac{Y_\psi}{Y_\chi} \simeq \frac{1}{(2\pi z)^{3/2}} \frac{g^4}{\lambda^2} \frac{M_\psi}{m_\chi} \sqrt{\frac{g(T_{\text{BAU}})}{g(T_{\text{DM}})}} \tag{5.32}$$

where the decay rates and annihilation cross-section were normalised to the relevant particle masses $\Gamma \equiv \lambda^2 M_\psi/(8\pi)$, and $\langle \sigma v \rangle \equiv g^4/(8\pi m_\chi^2)$, and we assume that the baryon-parents and WIMPs freeze out at comparable values of $z = m/T \simeq 25$. At a given mass scale, this shows that the co-moving number density of BAU-parents can be easily of the same order as that of particles which annihilate. So weak-scale BAU parents naturally have the same abundance as weak-scale dark matter.

However, all BAU parents do not necessarily produce baryons. On average, a parent produces ϵ baryons, where ϵ parametrises CP violation, and is suppressed by a loop factor, mixing angles and possibly small couplings. This could suggest that ϵ is naturally $\lesssim 10^{-3}$. Equation (5.32) predicts

$$\frac{n_B}{n_{\text{DM}}} \sim \epsilon \frac{Y_\psi}{Y_\chi} = C\epsilon \frac{M_\psi}{m_\chi} \tag{5.33}$$

7. Note that the WIMPs and BAU-parents may never simultaneously have this ratio of densities; the physically relevant ratio is n_b/n_χ.

where the coefficient C could be $\mathcal{O}(1)$, for $\lambda^2 \ll g^4$. So to obtain $n_B \sim n_{\rm DM}$ requires $\epsilon \sim 1$ for $m_\chi \sim M_\psi$, or $m_\chi < M_\psi$ for $\epsilon < 1$. It could be reasonable to suppose that the WIMP is an electroweak-scale particle, with gauge couplings g, and that the baryon-parent is a flavour-scale particle, with flavoured couplings λ, in which case, such a ratio of couplings could be credible. Then for "natural" values of the CP asymmetry $\epsilon \lesssim 10^{-3}$, and the flavour-scale $M_\psi \gtrsim 100$ TeV, the baryon and WIMP number densities today are "naturally" comparable.

Part III

Axion project

Chapter 6

From the strong CP problem to dark matter: the world of axions

We will now turn to the second project of this thesis that deals with axions. We have seen that many dark matter candidates exist, e.g. in the previous project we considered that dark matter was made of WIMPs. The axion is a very distinguished candidate because it can solve two problems of modern particle physics at the same time. Its existence was originally postulated to solve the strong CP problem and it was only later realized that axions could also be dark matter. In this chapter an introduction to axions is given. We start in section 6.1 by reviewing the strong CP problem and its solution involving axions. Section 6.2 introduces the role of axions in cosmology and section 6.3 gives a brief overview on axion constraints from cosmology, astrophysics and experimental searches.

6.1 Strong CP problem and axions

In this section we will loosely follow the extremely clear and pedagogic introduction given in [136]. The SM generally contains all possible renormalizable terms that are allowed by symmetries. In the QCD Lagrangian a term

$$\mathcal{L}_{\text{QCD}} \ni \Theta \frac{\alpha_s}{8\pi} G\tilde{G} \tag{6.1}$$

where $G_A^{\mu\nu}$ is the gluon field strength tensor, $\tilde{G}_{A\mu\nu} = \frac{1}{2}\epsilon_{\mu\nu\rho\sigma}G_A^{\rho\sigma}$ its dual, α_s is the fine structure constant of the strong interactions and Θ is a dimensionless constant, preserves all symmetries and should be present. The term violates CP and arises from the non trivial vacuum structure of QCD. There is even a second contribution to this CP violating term from generally complex Yukawa couplings which give rise to a complex quark matrix M_q. The phases of M_q can be rotated away by a chiral transformation of the quark fields [1]. With such a transformation one can make quark masses real but adds another contribution proportional to $\arg\det M_q$ to the CP violating term. The two contributions sum up to

$$\mathcal{L}_\Theta = \bar{\Theta}\frac{\alpha_s}{8\pi} G\tilde{G} \tag{6.2}$$

with $\bar{\Theta} = \Theta + \arg\det M_q$. This term leads to a neutron electric dipole moment of the order $|d_n| \approx |\bar{\Theta}|(0.004 - 2.0) \times 10^{-15} e$ cm [137, 138]. However an electric dipole moment is not

1. For leptons the phase can be absorbed by the massless neutrinos in the SM. If one quark was massless one could to the same for quarks and the strong CP problem would not exist.

observed until today and the upper limit restricts $|\bar{\Theta}|$ to be very small: $|\bar{\Theta}| < 10^{-9}$. The strong CP problem [139] is : Why is $|\bar{\Theta}|$ so small even though there is theoretical reason for it to be so small? [2]. One possibility to solve this problem was found by Peccei and Quinn [141, 142]. Their basic idea is to make $\bar{\Theta}$ a dynamical variable that is driven to zero by its potential.

6.1.1 Generic axion features

In order to explain the smallness of $\bar{\Theta}$ one introduces a new real scalar field, the axion $a(x)$. By construction it couples to gluons in the same way as in equation (6.2) but replacing $\bar{\Theta}$ by $-a/f_a$ and has the generic kinetic terms of a scalar field. If the axion is a pseudoscalar the term $aG\tilde{G}$ is CP conserving. The constant f_a must have dimension energy and is called axion decay constant. The axion must be massless so that a shift in the axion field $a(x) \to a(x) + a_0$ does not affect physics. This allows us to absorb $\bar{\Theta}$ in the definition of the axion field and write the axion Lagrangian

$$\mathcal{L}_a = \frac{1}{2}(\partial_\mu a)^2 - \frac{\alpha_s}{8\pi f_a} a G\tilde{G} \tag{6.3}$$

This Lagrangian conserves CP because the axion is a pseudoscalar field but does not yet explain the non-existence of an electric dipole moment. As axions couple to gluons they can undergo a transition to $\bar{q}q$ states (neutral pions, look at figure 6.1) which finally means that axions mix with pions and therefore obtain an effective mass of the order

$$m_a f_a \approx m_\pi f_\pi \tag{6.4}$$

even if axions were constructed to be massless [3]. Consequently after the QCD phase transition axions have a potential which can be expanded to lowest order as $V(a) \approx \frac{1}{2} m_a^2 a^2$. The axion field will finally have an average value $\langle a \rangle = 0$ which explains the smallness of the constant in front of the CP violating gluon term $G\tilde{G}$. If the axion field took a non-vanishing value a_0 in some region of space then neutrons would have an electric dipole moment in this region. Because of their mixing with pions axions do not only share their mass with them but also their couplings to photons and nucleons. The coupling strength is reduced by f_π/f_a. The coupling to photons is often used in axion search experiments.

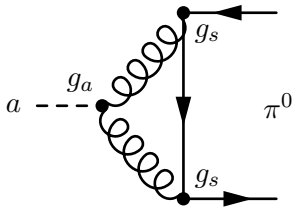

Figure 6.1: Through its coupling to gluons the axion can convert itself into a pion. The curly lines are gluons and solid lines are quarks

6.1.2 Axion as Nambu-Goldstone Boson

Let us now have a look at a concrete realization of the Peccei-Quinn mechanism, the KSVZ axion model (Kim [143], Shifman, Vainshtein and Zakharov [144]). As the axion Lagrangian is

2. A very comprehensible introduction to the strong CP problem and its solution in terms of the Peccei-Quinn mechansim is given in [140] by analogy to a pool table.
3. Before the QCD phase transition pions do not exist and the axion is actually massless.

invariant under the transformation $\Theta \to \Theta + 2\pi$ it seems to be a good idea to interpret the axion as the phase of a complex scalar field. One introduces a new complex scalar field Φ, singlet under the electroweak group $SU(2) \times U(1)$ and at least one new exotic quark field Ψ. In the Lagrangian one adds a potential V for the scalar field and a Yukawa term to the usual kinetic terms

$$\mathcal{L} = (\frac{i}{2}\bar{\Psi}\partial_\mu\gamma^\mu\psi + h.c.) + \partial_\mu\Phi^\dagger\partial^\mu\Phi - V(\Phi) - h(\bar{\Psi}_L\Psi_R\Phi + h.c.) \tag{6.5}$$

This Lagrangian is invariant under a chiral phase transformation

$$\Phi \to e^{i\alpha}\Phi\,, \qquad \Psi_L \to e^{i\alpha/2}\Psi_L\,, \qquad \Psi_R \to e^{-i\alpha/2}\Psi_R \tag{6.6}$$

This $U(1)$ transformation is called the Peccei Quinn symmetry. We impose that the potential has a Mexican hat form with an absolute minima at $|\Phi| = f_{\mathrm{PQ}}/\sqrt{2}$ where f_{PQ} is some large energy scale at which the symmetry is spontaneously broken. The ground state has therefore a non vanishing vacuum expectation value $\langle\Phi\rangle = f_{\mathrm{PQ}}/\sqrt{2}e^{i\varphi}$ with an arbitrary phase φ. The scalar field can be developed around its expectation value

$$\Phi = \frac{f_{\mathrm{PQ}} + \rho}{\sqrt{2}} e^{ia/f_{\mathrm{PQ}}} \tag{6.7}$$

Where ρ and a are two real scalar fields representing radial and angular excitations. The potential V provides the mass for the field ρ which will be chosen to be very high so that it is of no interest for the low-energy considerations. All terms involving ρ will be neglected in the following. The chiral symmetry implies that the theory is unchanged under a shift in the second scalar field $a(x) \to a(x) + a_0$. Therefore we conclude that a is massless and the Nambu-Goldstone boson of the PQ symmetry. Using equation (6.7) and defining $m = hf_{\mathrm{PQ}}/\sqrt{2}$ we can develop the Yukawa term in equation (6.5)

$$\mathcal{L}_{\mathrm{int}} = m\bar{\Psi}\Psi - i\frac{m}{f_{\mathrm{PQ}}}a\bar{\Psi}\gamma_5\Psi + \frac{m}{2f_{\mathrm{PQ}}^2}a^2\bar{\Psi}\Psi + ... \tag{6.8}$$

The dimensionless Yukawa coupling constant in front of the second term is $g_a = m/f_{\mathrm{PQ}}$. If the fermion Ψ is taken to have the usual strong interactions then a interacts with gluons to lowest order via a triangle diagram, shown in figure 6.2. Neglecting all external momenta with respect to m one can write the effective a-gluon interaction

$$\mathcal{L}_{\mathrm{aGluon}} = -\frac{g_a}{m}\frac{\alpha_s}{8\pi}aG\tilde{G} \tag{6.9}$$

where $\alpha_s = g_s^2/4\pi$ and $\frac{g_a}{m} = \frac{1}{f_{\mathrm{PQ}}}$.

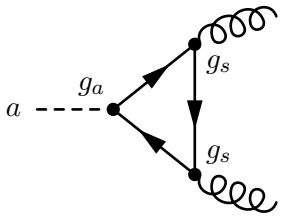

Figure 6.2: Axion gluon coupling through quark triangle diagram

In the more general case when one has different fermion fields Ψ^j, they will all participate in this interaction if they have the usual strong interactions. They are characterized by their PQ

charge X_j: $\Psi_L^j \to e^{iX_j\alpha/2}\Psi_L^j$. The total axion-gluon interaction includes the contributions from different fermions. The masses of the different fermions drop out because $g_{aj}/m_j = X_j/f_{\rm PQ}$. Defining

$$N = \sum_j X_j \quad \text{and} \quad f_a = f_{\rm PQ}/N \tag{6.10}$$

one finds the same interaction term as in equation (6.3). So we succeeded in introducing a real scalar field with exactly the right coupling to gluons, we introduced the axion! The only parameter that determines the axion mass and its couplings is the axion decay constant f_a.

At the QCD phase transitions instanton effects explicitly break the PQ symmetry by creating a potential for the axion with a minimum at $a = 0$. This explains the absence of the electric dipole moment. The potential gives the axion a mass as already explained in equation (6.4). A more detailed analysis gives the axion mass

$$m_a = \frac{z^{1/2}}{1+z}\frac{f_\pi m_\pi}{f_a} \approx 6\mu\text{eV}\frac{10^{12}\text{GeV}}{f_a} \tag{6.11}$$

where $z = m_u/m_d$. From their generic mixing with pions axions couple to photons according to

$$\mathcal{L}_{int} = -\frac{1}{4}g_{a\gamma}F_{\mu\nu}\tilde{F}^{\mu\nu}a = g_{a\gamma}\mathbf{E}\cdot\mathbf{B}a. \tag{6.12}$$

where F is the electromagnetic field strength. All charged leptons that carry Peccei-Quinn charge contribute to a triangle diagram like in figure 6.2 but replacing g_s with the electric charge of the leptons $Q_j e$. In analogy to the axion gluon coupling we get a coupling constant

$$g_{a\gamma} = -\frac{\alpha}{2\pi f_a}\xi \tag{6.13}$$

where ξ encodes the contributions of different leptons to the triangle and depends on the explicit assignment of PQ charges in a given model. For most estimates it is enough to assume $\xi \sim 1$.

The axion fermion interaction term in equation (6.8) is to lowest order a pseudo-scalar coupling. But there is a series of other interaction terms that sometimes have to be taken into account. For example the axion scattering on fermions is of second order in the pseudo-scalar interaction but of first order in the second term. This infinite series of interactions can be suppressed if one redefines the fermionic fields

$$\psi_L = e^{-ia/2f_{\rm PQ}}\Psi_L, \quad \psi_R = e^{ia/2f_{\rm PQ}}\Psi_R \tag{6.14}$$

The interaction now comes from the kinetic terms and takes the form

$$\mathcal{L}_{int} = \frac{1}{2f_{\rm PQ}}\bar{\psi}\gamma_\mu\gamma_5\psi\partial^\mu a \tag{6.15}$$

The interaction is of derivative nature and is linear in a without any higher order terms. Writing it in this way axions have basically the same interactions with fermions as pions have with nucleons. Pions are the Nambu-Godlstone bosons of the broken $U(2)_{L-R}$ symmetry of QCD.

One problem from which axion models suffer is due to gravity. The PQ symmetry like any other global symmetry will not be respected by quantum gravity. At scales below the Planck mass, quantum gravity should manifest itself by all sorts of effective interactions which are not forbidden by a symmetry and which are suppressed by inverse powers of $m_{\rm Pl}$. Such terms could give rise to a second mass term for the axion. In order to keep this additional mass term small compared to the QCD mass one has to take small values for f_a which are already excluded by experiments. However until now we do not know what quantum gravity looks like and if it influences our axion models in the described way (which is based more or less only on dimensional analysis).

6.1.3 Different axion models

Globally axions are described by one single parameter, f_a, but some freedom is left in their exact implementation. This gives rise to different axion models with slightly different couplings to quarks, leptons and photons. In the following a brief overview of the most important and most standard models of axions is given.

A first idea would be that the Higgs field is the scalar field of equation (6.7) whose phase is the axion. However in the standard model the Nambu-Goldstone boson of the spontaneous breaking of $SU(2) \times U(1)$ is interpreted as the third component of the Z boson. Therefore one has to extend the standard model by a second scalar doublet. The two Higgs fields H_1 and H_2 have different vacuum expectation values f_1 and f_2 which have to obey $f_1^2 + f_2^2 = f_{\mathrm{EW}}^2$. For the usual three families the axion decay constant is related to the weak-scale and therefore small $f_a \approx 43\,\mathrm{GeV}$. This is called the standard axion model (Peccei and Quin [141]) , Weinberg [145], Wilczek [146]). However this model is ruled out by experimental and astrophysical evidence.

In order to write down a viable axion model one has to use a scalar field that is not related to the electroweak scale. Therefore we introduce a $SU(2) \times U(1)$ singlet scalar field with vacuum expectation value $f_{\mathrm{PQ}}/\sqrt{2}$. Taking $f_{\mathrm{PQ}} \gg f_{\mathrm{EW}}$ gives small axion mass and very weak interactions. These models are called invisible axion models. The first invisible axion model has already been described above, the KSVZ model. The PQ mechanism decouples entirely from ordinary particles: at low energies axions interact with matter only by the two-gluon coupling. The simplest KSVZ model has only one additional fermion and so only one free parameter, f_a.

Another well known axion model is the DFSZ model, invented by Zhitnitskii [147] and Dine, Fischler and Srednicki [148]. It is like a mixture of the standard and the KSVZ axion model. It contains a electroweak singlet scalar field with vev $f_{\mathrm{PQ}}/\sqrt{2}$ and two electroweak doublet Higgs fields. However this model does not need the exotic quarks of the KSVZ model because the known fermions carry PQ charges. Therefore in this model axions couple also to charged leptons in addition to nucleons and photons. As the KSVZ model only couples to quarks it is called hadronic axion model.

The interaction of axions with a given fermion j (mass m_j) can be parametrised as

$$\mathcal{L}_{\mathrm{int}} = -i\frac{C_j m_j}{f_{\mathrm{PQ}}}\bar{\psi}_j\gamma_5\psi a \tag{6.16}$$

where C_j is an effective PQ charge, e.g. in the KSVZ model $C_e = 0$ at tree level (hadronic axions). Evidently $g_j = C_j m_j / f_{\mathrm{PQ}}$ plays the role of a Yukawa coupling constant.

6.2 Axions in Cosmology

Until now we have solved the CP problem but have not yet said anything about axions as CDM. Therefore we need to have a look at the thermal history of axions. Their cosmological history starts with the Peccei-Quinn phase transition at temperature $T \sim f_{\mathrm{PQ}}$. The complex scalar field named Φ takes a non-zero vacuum expectation value and the axion is the Nambu-Goldstone boson of the broken symmetry. Every value for f_{PQ} fixes the strong CP problem in an equally good way. However from experimental constraints we already know that the only viable values are some orders of magnitude around $f_{\mathrm{PQ}} \sim \mathcal{O}(10^{12}\mathrm{GeV})$ [4]. This could be of the order of the inflation scale. Consequently we will have to deal with two different scenarios: PQ symmetry breaking takes either place after inflation or before inflation. In both scenarios the

4. In the anthropic window the axion decay constant can also be much larger than 10^{12} GeV but this requires either fine-tuning of the initial misalignment value of the axion field or an additional symmetry.

axion is massless until temperature drops to $\Lambda_{QCD} \sim 200$ MeV (the temperature of the QCD phase transition). Below this temperature the axion has a small mass $m_a \approx m_\pi \frac{f_\pi}{f_a}$ from the mixing with pions. (Above the QCD phase transition pions are not stable.) Of course this is a smooth transition from $m_a = 0$ to its final value which makes the axion mass temperature dependent around $T \sim \Lambda_{QCD}$.

In Cosmology three distinct production mechanisms for axions are known and they give very different relic axions.

- thermal production → hot dark matter
- non-thermal misalignment angle mechanism → cold dark matter
- non-thermal axionic string decay → cold dark matter

We will now discuss these three production mechanisms and check their implications on cosmology.

6.2.1 Thermal production

Thermal production means that axions were produced by the thermal bath in the universe at high temperatures through processes involving axions and standard model particles. Prior to QCD phase transition axions interact mostly with quarks via Primakoff process $\gamma + q \leftrightarrow a + q$ (q is a quark) and with gluons via $q + \overline{q} \leftrightarrow g + a$. It is shown in [149] that for $m_a > 10$ μeV axions are in thermal equilibrium during some moment in the history of the universe. If the interactions are strong enough $m_a \sim$ eV, axions can be in thermal equilibrium after the QCD phase transition. The most relevant process is then "pion-axion conversion" $\pi + \pi \leftrightarrow a + \pi$ (π is a pion). It is then important to determine the temperature at which axions decouple from the thermal bath to determine the hot dark matter bounds on axions. An approximate integral expression for the axion interaction rate after the QCD phase can be found in [150]. In [151] a more precise numerical approach was done. They show that the axion absorption rate can be written as

$$\Gamma(T) = A \left(\frac{C_{a\pi}}{f_a f_\pi} \right)^2 T^5 h(m_\pi/T) \tag{6.17}$$

where $A = 0.215$ and $C_{a\pi}$ is the axion pion coupling constant, e.g. $C_{a\pi} = \frac{1-z}{3(1+z)}$ when ordinary quarks and leptons do not carry PQ charges. The function $h(m_\pi/T)$ decreases exponentially with decreasing temperature as an effect of the decreasing number density of pions. Comparing the interaction rate to the expansion rate of the universe $H \sim \frac{\sqrt{g_*} T^2}{m_{\rm Pl}}$ one can determine the freeze-out temperature and therefore the number density as a (numeric) function of the axion mass. Knowing that hot dark matter cannot be the dominant dark matter component one can put an upper bound on the axion mass. A recent study involving CMB anisotropy measurements, halo power spectrum data and Hubble constant measurements constrains the axion mass $m_a <$ 0.7 eV [152].

When estimating the thermal axion relic density it was assumed that axions where stable. However we saw above that axions have a generic coupling to photons and can therefore decay into two photons. The decay rate can be estimated by [153]:

$$\Gamma_{\rm decay} = \frac{g_{a\gamma}^2 m_a^3}{64\pi} \tag{6.18}$$

Comparing the decay rate with today's Hubble parameter we conclude that for $m_a \gtrsim 20$ eV axions decay fast on cosmic time scales. Consequently the limit hot dark matter limit on axions is only valid for masses up to 20eV. This means that big axion masses $m_a \gtrsim \mathcal{O}(100$ eV) do

not necessarily produce too much dark matter but they produce additional photons that are constrained by CMB measurements.

6.2.2 Misalignment angle mechanism

A non-thermal way to produce an axion population is the well known misalignment angle mechanism. In order to understand it we have to go back to the thermal history of axions before the QCD phase transition. As the axion potential is flat, the initial axion value chosen at the moment of PQ phase transition has no preferred value in the interval $-\pi \leq a_{\text{init}}/f_a \leq \pi$ and will therefore not already be at its future minimal value $a = 0$. When the Mexican hat potential tilts at QCD phase transition the axion field will "roll" towards 0 and overshoot, it will coherently oscillate around 0. The equation of motion for a homogeneous scalar field in an FRW universe is given by

$$\ddot{a} + 3H\dot{a} + m_a^2 a = 0 \tag{6.19}$$

When the axion mass is constant (some time after QCD phase transition) the approximate solution to this equation is

$$a \sim a_{\text{init}} \frac{1}{R^{3/2}} \cos(m_a t) \quad . \tag{6.20}$$

The energy density $\rho_a = \frac{1}{2}(\dot{a}^2 + m_a^2 a^2)$ scales with $1/R^3$ like non relativistic matter. This explains the interest in axions as dark matter candidate! Here we did neither take into account the temperature dependence of the axion mass around the QCD phase transition nor anharmonic effects in the potential.

The axion relic density depends further on when PQ symmetry breaking takes place. If it takes place before inflation then the axion field chooses one initial value within the causal horizon. This volume then gets expanded by inflation to a size much larger than the casual horizon so that in all different patches (causal connected volumes) of the universe the axion field has the same initial value. In this case the axion density depends on the initial value [12]:

$$\Omega_{\text{Mis}} h^2 \approx 0.4 \times 10^{\pm 0.6} \left(\frac{10\,\mu\text{eV}}{m_a}\right)^{7/6} \left(\frac{a_{\text{init}}}{f_a \pi}\right)^2 \tag{6.21}$$

Where $10^{\pm 0.6}$ takes into account the theoretical uncertainties on axions and cosmology [136]. If the initial value is very small, axions can have very small masses $m_a \ll \mu\text{eV}$ without producing to much dark matter. This is called the "anthropic axion window".

If PQ symmetry breaking happens after inflation the axion field will choose a different value in every Hubble patch. The total axion density can be calculated by assuming a flat probability distribution for initial values between $-\pi$ and π and calculating the root-mean squared: $(a_{\text{init}})_{\text{rms}} = \pi f_a/\sqrt{3}$. The axion density is then given by

$$\Omega_{\text{Mis}} h^2 \approx 0.2 \times 10^{\pm 0.6} \left(\frac{10\,\mu\text{eV}}{m_a}\right)^{7/6} \tag{6.22}$$

Comparing to the measured dark matter fraction $\Omega_{\text{DM}} h^2 \approx 0.13$ implies that axions with $m_a \sim 10\mu\text{eV}$ provide dark matter whereas smaller masses are excluded. The oscillating galactic dark matter axion field induces extremely small oscillating nuclear electric dipole moments that could perhaps be measured using experiments with cold molecules.

Axions produced by this mechanism have a typical momentum of the order

$$p(t) \sim H_{QCD} \frac{R(t_{QCD})}{R(t)} < m_a \tag{6.23}$$

and can therefore be considered as non-relativistic shortly after the QCD phase transition.

6.2.3 Cosmic strings and domain walls

In the case that PQ symmetry breaking occurs after inflation a third axion population arises from cosmic strings and domain walls. Domain walls appear when a symmetry is explicitely broken. For axions this is the case at the QCD phase transition: non perturbative QCD effects will break the $U(1)_{PQ}$ into the discrete $\mathcal{Z}_N$ subgroup: $\mathcal{Z}_N : \phi \to e^{i2\pi n/N}\phi$ and $n \in [0, N[$. N generally depends on the way PQ charge is assigned in different models, e.g. in the KSVZ model described above it is the number of quarks carrying PQ charge. That means that the axion potential has N degenerate minima. Different regions in space that are not causally connected are in different minima and have different field values. As the transition from one vacuum value to another must be smooth regions in space with non-minimal field values form. These regions are called domain walls. Their thickness depends on the form of the potential but it is generally small compared to their size in the other spatial directions. These domain walls are stable and can propagate in space. It is well known that domain walls are a disaster in cosmology because they dominate the universe soon after their formation and provide a relic density larger than the critical density, which contradicts present observations. There are at least two ways to circumvent such a disaster. Either PQ symmetry is broken before inflation so that the whole universe has the same axion field value or $N = 1$. In the latter case domain walls form but they are not stable and decay into axions.

Like domain walls, cosmic strings are also topological defects. But they appear when a symmetry is spontaneously broken. When $U(1)_{PQ}$ symmetry is spontaneously broken at $T \sim f_{\mathrm{PQ}}$ the phase φ of the complex scalar field Φ will take different values in causally disconnected regions of space. However Φ must be single valued, i.e. the total change in φ, $\Delta\varphi$ around any closed path must be an integer multiple of 2π. Shrinking a given path with $\Delta\varphi = 2\pi$ cannot continuously change $\Delta\varphi = 2\pi$ to 0. Therefore the path must contain a point in which the phase is not defined, i.e. $\Phi = 0$. The region where Φ does not take its minimal value constitutes a false vacuum in the form of a tube of either infinite length or of a closed tube. As their transverse dimension is far smaller than their length they can be treated as one dimensional objects, i.e. strings. The strings quickly decay into axions that are either non-relativistic or mildly relativistic. The later ones get red-shifted to non-relativistic velocities quickly. They constitute the third axion population. However it is not yet clear how much of these axions are produced. The authors of [154] estimate that the axion population produced from strings and domain walls

$$\Omega_{\mathrm{St}} h^2 \sim 0.9 \left(\frac{10\,\mu\mathrm{eV}}{m_a} \right)^{1.19} \tag{6.24}$$

is greater than from the misalignment angle mechanism. In [155] a smaller value for the axion density from string decay is estimated.

6.3 Bounds on axions

6.3.1 Astrophysical bounds

If axions exist they would be produced in hot astrophysical plasmas and transport energy out of these plasmas. They would open a new energy loss channel and therefore alter the time-scale for astrophysical processes. Measuring these time-scales and comparing them to the standard evolution theory constrains axion couplings from above. A very comprehensive introduction to astrophysical bounds on axions can be found in [136, 156]. Here I will only list the most stringent constraints for different axion couplings.

The axion electron coupling can best be constrained by low mass red giants where the emission of axions delays the helium ignition.

$$m_a C_e \lesssim 0.003 \text{ eV} \tag{6.25}$$

Axions that interact too strongly to escape freely from the interior of stars would still contribute to the radiative transfer of energy and consequently to the opacity of the star. For hadronic axions models this bound does not constrain the model.

The lifetime of horizontal branch stars constrains the axion photon coupling

$$m_a \xi \lesssim 0.4 \text{ eV}. \tag{6.26}$$

The best tests of the axion nucleon coupling are given by the supernova signal SN1987A. The duration of the neutrino signal excludes axions in the range $0,002 \text{ eV} \lesssim C_N m_a \lesssim 2$ eV. For large couplings axions are trapped and would have created additional neutrino events in detectors. This excludes axions for masses between 20 eV − 20 keV. The constraints from SN are subject to quite large uncertainties from the description of SN.

In summary, except for very special choices of model dependent parameters axions with masses above 0.01 eV are excluded by stellar evolution. Figure 6.3 includes a summary of all bounds on the axion parameter space.

6.3.2 Experimental axion searches

Axions are actively searched for in various experiments. The probably most promising way to detect axions is by its conversion into photons in an external electric or magnetic field. In "light shining through wall" experiments one uses this property. A laser beam is sent through an external magnetic field and then blocked by an optical barrier. In the magnetic field photons can convert into axions and traverse the barrier. In a second magnetic field on the other side of the barrier axions can reconvert into photons which can be detected. These experiments probe axion masses regions $m_a \lesssim$ meV and set an upper bound the axion photon coupling $g_{a\gamma} < 10^{-7}$ GeV^{-1} [157]. However this bound does not yet constrain axions because usual axion models predict $g_{a\gamma} \sim 10^{-13}$ GeV^{-1} for $m_a \sim$ meV.

Another type of experiments are axion helioscopes: they measure axions produced in the sun which can be registered on earth when they convert into photons in the magnetic field of the helioscope. The most recent CAST experiment could restrain $g_{a\gamma} \lesssim 10^{-12}$ GeV^{-1} for axion masses $m_a \lesssim 0,02$ eV which is still larger then the prediction. However for $m \approx 0,6$ eV CAST has reached the sensitivity needed to constrain axions [158].

Galactic dark matter halo axions are searched for by microwave cavity experiments. In a electromagnetic cavity permeated by a strong static B field, axions resonantly convert into a microwave signal. The ADMX experiment reached the axion line and excluded axions with masses between $1.9 - 3.3\,\mu$eV [160].

6.3.3 Cosmological bounds

Cosmological bounds on axions are strongly model dependent and should therefore be treated very carefully. If the PQ phase transition occurs after inflation the amount of axions produced by the misalignment mechanism depends only on the axion mass. In order not to produce too much dark matter the axion mass is restricted to

$$m_a \gtrsim 10\mu \text{ eV} \tag{6.27}$$

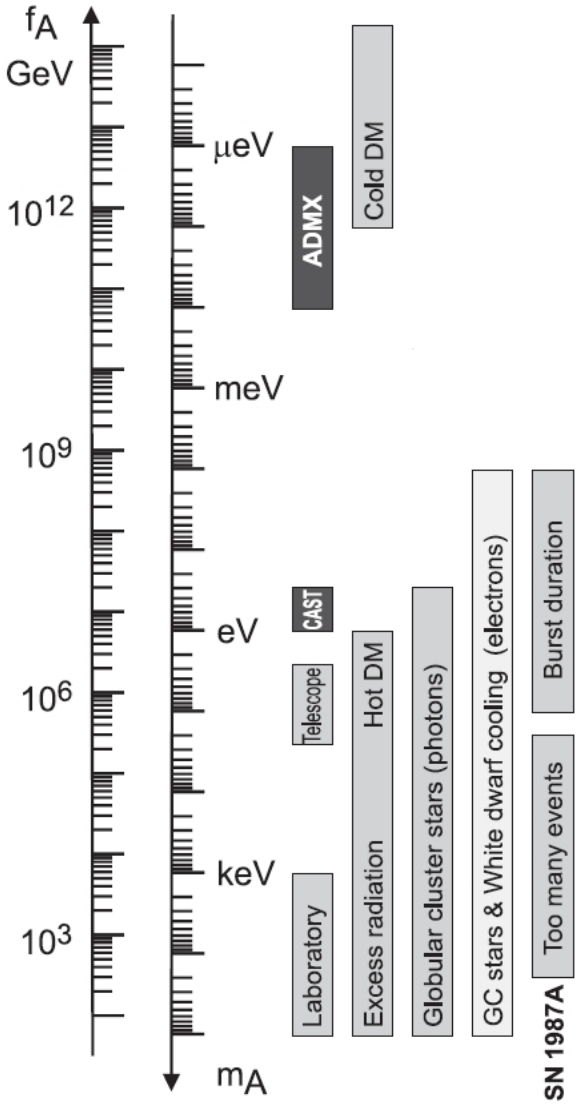

Figure 6.3: Summary of all bounds on axions from [12]. Cosmological constraints exclude low axion masses. Astrophysics by contrast exclude big axion masses. The dark intervals are the approximate CAST and ADMX search ranges. The "Laboratory" bar is a rough representation of the exclusion range for the standard axion model described above.

However one also has to take into account axions from string decays in this scenario which give a similar restriction on the axion mass as the misalignment angle mechanism. In the second case when PQ phase transition occurs before inflation the relic density of axions produced by the misalignment angle mechanism depends on the initial value of the axion field so that we cannot derive a bound on the axion mass. Axions from cosmic string decays after the PQ phase transition get depleted by inflation and domain walls do not form at the QCD phase transition because the axion field has the same value all over the universe. But in this case isocurvature perturbations can further constrain axions. If the axion field is present during inflation it will

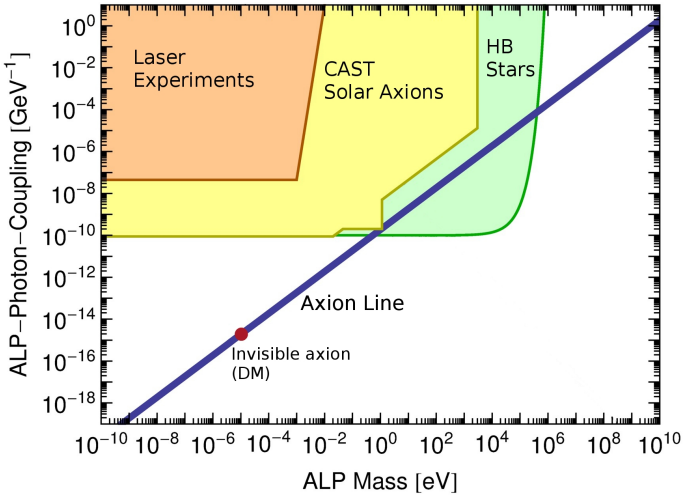

Figure 6.4: (adapted from [159]) Constraints on the axion - photon coupling from different sources: Laser experiments, the CAST experiment and horizontal branch stars. For axions the axion photon coupling is fixed by its mass (axion line). If one releases this constraint one has axion-like-particles (ALP) whose parameter space is shown here. In order to constrain axions the experiments have to reach the axion line for a given mass. The invisible axion model which provides all dark matter is not yet constraint.

have the same de-Sitter quantum fluctuations as the inflation [161]:

$$\langle|\delta a(k)|^2\rangle = \left(\frac{H_{\rm inf}}{2\pi}\right)^2 \frac{1}{k^3/2\pi^2} \tag{6.28}$$

$H_{\rm inf}$ is the Hubble parameter during inflation (where it is basically constant). These fluctuations δa do not perturb the total energy density because the potential energy is exactly zero before QCDPT and the gradient energy is negligible small. Consequently the fluctuations are of isocurvature type and are characterized by fluctuations in the ratio of number density to entropy $\delta\left(\frac{n_a}{s}\right) \neq 0$ and $\delta\rho_a = 0$. These isocurvature modes would leave their imprint on the CMB and their non observation by PLANCK puts a very stringent upper bound on the ratio of isocurvature power spectrum to adiabatic power spectrum [162]:

$$\beta_{\rm iso} < 0.039 \quad (95\%\text{CL, Planck + WMAP}) \tag{6.29}$$

where $\beta_{\rm iso} \approx \langle|\mathcal{S}_a(k)|^2\rangle/\langle|\mathcal{R}_(k)|^2\rangle$. The axion perturbation spectrum for the isocurvature modes is $\langle|\mathcal{S}_a(k)|^2\rangle = \langle|\frac{\delta n_a}{n_a}|^2\rangle$ and $\langle|\mathcal{R}_(k)|^2\rangle$ is the curvature power spectrum for the adiabatic mode.

The bound can be used to constrain the axion parameter space but the amount of isocurvature modes produced by axions also depends on the scale of inflation. If one assumes that (i) PQ symmetry is broken before inflation, (ii) that it is not restored by quantum fluctuations of the inflation nor by thermal fluctuations during reheating and (iii) that all of CDM consists of axions produced by the misalignment angle then one can derive an upper bound on the energy scale of inflation as [162]:

$$H_{\rm inf} \leq 0.87 \times 10^7 \text{ GeV} \left(\frac{f_a}{10^{11} \text{ GeV}}\right)^{0.408} \tag{6.30}$$

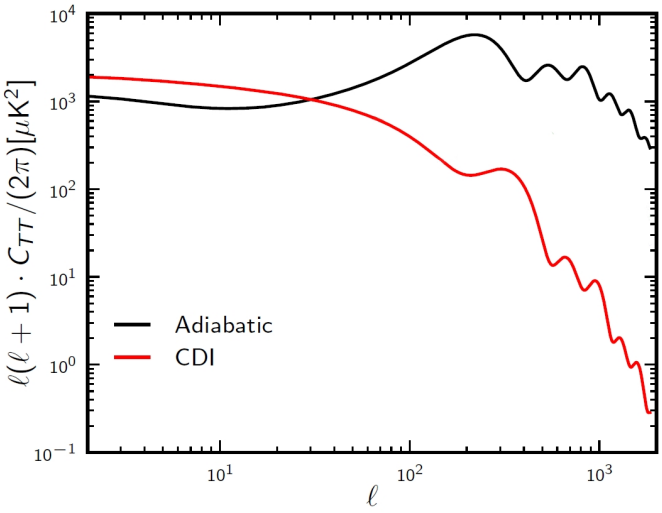

Figure 6.5: (adapted from [162]) Power spectrum of purely adiabatic modes and CDM isocurvature modes (CDI). For CDM isocurvature modes the power spectrum decreases rapidly with growing ℓ so that constraints are dominated by small ℓ. For small ℓ the peaks of acoustic oscillations are clearly not in phase. The very first amplitudes for $\ell < 20$ are difficult to constrain because of large statistical errors on big scales due to cosmic variance.

This does not exclude any value for the Peccei Quinn scale except one supposes something for the scale of inflation. But it indicates that under the given assumptions the scale of inflation has to be quite small. The recent BICEP2 measurement [26] indicates a larger inflation scale than compatible with allowed values of f_a in equation (6.30). If confirmed this would exclude the case that the PQ phase transition occurred prior to inflation unless there is some additional mechanism to reduce the amount of isocurvature perturbations for axions. The opposite case that the PQ symmetry breaking occurs after inflation is very well compatible with a high inflation scale.

It is important to distinguish the two possible cosmological scenarios for axions. If inflation occurs after PQ symmetry breaking then the axion field oscillates homogeneously over the entire universe after the QCD phase transition. Therefore the axion density from the misalignment angle mechanism depends on the initial field value chosen at the PQ phase transition. By consequence one can not put lower bound on the axion mass to prevent them from producing too much dark matter because the initial misalignment angle could be very close to zero. However in this case the axion field was present during inflation and has isocurvature fluctuations which are strongly bound by CMB data.

In the opposite case, when inflation occurs before PQ symmetry breaking, the axion density from the misalignment angle mechanism varies from one causal horizon to another. Its mean value is independent of the initial field values. One has therefore a lower bound on the axion mass. Furthermore cosmic strings are created that give a second cold axion population of comparable relic density. In order to circumvent the domain wall problem, $N = 1$.

To summarize this section on axion bounds one can see that the free parameter space for axions is already very restricted. Astrophysics exclude large couplings of axions to matter and therefore exclude large axion masses. Cosmology can exclude small axion masses because they

would produce too much dark matter. At the end the remaining axion window is

$$10\,\mu\text{eV} \lesssim m_a \lesssim 10\text{ meV} \tag{6.31}$$

Chapter 7

Observable axion WIMP difference?

7.1 The initial idea

This section will introduce the very interesting idea that Sikivie and Yang with Erken and Tam (ESTY) developed in [163, 164] about observable differences between axion dark matter and WIMP dark matter. The complete work on axions presented in this thesis is motivated by these previous works. The general idea is that cosmic axions produced by the misalignment angle mechanism form a Bose-Einstein condensate (BEC) due to gravitational thermalisation. As the axion BEC can support vortices it forms a different inner caustic structure in galactic halos than WIMPs and could therefore lead to observable differences between axions and WIMPS. Such differences would be very interesting as long as the nature of dark matter has not been explained by any particle detection.

Axions fulfil three important conditions for a BEC: they are bosons, their number is effectively conserved and their kinetic energy is clearly smaller than their critical temperature [163]

$$T_c = \left(\frac{\pi n_a^2}{\zeta(3)}\right)^{1/3} \approx 300\text{GeV}\left(\frac{f_{\text{PQ}}}{10^{12}\text{GeV}}\right)^{5/9}\frac{R(t_{\text{QCD}})}{R(t)}. \tag{7.1}$$

where $\zeta(3) \approx 1.20$ is the Riemann zeta function. According to ESTY the only condition for BEC formation that is not manifestly satisfied for axions is thermal equilibrium. The axion self interaction is shown to be insufficient to establish thermal equilibrium. However the gravitational interaction rate among axions is larger than the expansion rate of the universe and should therefore thermalise axions. Then they argue that a rethermalising BEC can have a galactic halo structure with a net overall rotation $\vec{\nabla}\times\vec{v} \neq 0$ as opposed to a WIMP halo structure that is irrotational $\vec{\nabla}\times\vec{v} = 0$. The different velocity fields give rise to different inner caustic structures. For the rest of this thesis we will only focus on the question of axion thermalisation and not on the resulting differences.

The important question is how to calculate the gravitational interaction rate of axions that changes the axion momentum distribution into the distribution with highest entropy, a BEC. The usual analysis using Boltzmann equations can not be used here because the axion modes are highly occupied and behave essentially as a classical field in contrast to a Boltzmann analysis that supposes a collection of particles. In [165] Saikawa and Yamaguchi calculated the gravitational interaction rate of axions in a Newtonian limit and obtain the same result as [163]. We will focus on [165] because its authors introduce very clearly the formalism used and provide a solid analytical analysis of this subject. I will try to give an overview of this calculation without going into to much detail. The reader is invited to look into the original work for more detail.

The axion state is described in Minkowski space time as a coherent state, i.e. a state with such a large occupation number that the application of the annihilation operator does not change the state: $\hat{b}_i|\alpha_i\rangle = \alpha_i|\alpha_i\rangle$. Usually coherent states are used to take the limit from quantum field theory to classical field theory. Axions from the misalignment angle mechanism are born as classical field oscillations and are therefore well described by coherent states. The axion interaction rate is given by the rate of change of the number operator $N_p = \langle\hat{N}_p\rangle = \langle\frac{\hat{b}_p^\dagger\hat{b}_p}{V}\rangle$:

$$\Gamma_{\rm SY} = \frac{1}{N_p}\frac{dN_p}{dt} \quad . \tag{7.2}$$

The time derivative of the number operator can be calculated by using the Heisenberg equation

$$\frac{d\hat{N}_p}{dt} = i[H_I, \hat{N}_p]. \tag{7.3}$$

The interaction Hamiltonian contains the Newtonian gravitational interaction.

$$H_I = -\frac{G}{2}\int d^3x d^3x' \frac{\rho(\vec{x},t)\rho(\vec{x}',t)}{|\vec{x}-\vec{x}'|} \tag{7.4}$$

With ρ being the axion energy density. The Hamiltonian can be expressed in terms of creation and annihilation operators in order to calculate the commutator with N_p. In this way the gravitational axion interaction rate can be shown to be [165, 163]

$$\Gamma_{\rm SY} \simeq \frac{4\pi G m_a^2 n_a(t)}{(\delta p(t))^2} \tag{7.5}$$

where $\delta p(t) \sim H_{\rm QCD}\frac{1}{R(t)}$ is the typical axion momentum for misalignment angle axions and n_a the axion density. The interaction rate exceeds the expansion rate of the universe H at $T \sim$ keV. Based on this fast interaction rate, the authors of [163, 164] claim that axions thermalise and form a Bose Einstein condensate.

In [166] the gravitational interaction rate of axions is calculated in a general relativistic framework. The obtained results agree with equation (7.5).

7.2 Do axions form a Bose-Einstein condensate in cosmology?

The above described scenario of axion Bose-Einstein condensation has one crucial ingredient: the thermalisation of axions through gravitational interaction. However it is not completely clear that a fast gravitational interaction rate is also a fast thermalisation rate. Therefore it seems to be a good idea to find a different and independent way to estimate the thermalisation rate of cold dark matter axions through gravitational interaction. The following section will present such an independent estimate by Sacha Davidson and myself, published in JCAP 13120(2013) 034. The following section presents (in slightly more detail) what we have done.

Using classical equations of motion during linear structure formation, we explore whether the gravitational interactions of axions can generate enough entropy to form a BEC. At linear order in G, we interpret that the principle activities of gravity are to expand the Universe and grow density fluctuations. To quantify the rate of entropy creation we estimate the axion viscosity and obtain a short dissipation scale for axions which does not confirm previous estimates of their gravitational thermalisation rate.

7.2.1 Bose-Einstein condensation

In the 1920s Bose and Einstein predicted the Bose-Einstein condensate (BEC) as a new state of matter. A conserved population of bosons at temperatures lower than their critical temperature exhibit a macroscopic population of one single quantum state, the zero momentum state. The BEC is the state of maximal entropy: most particles fall in the zero momentum mode to excite a few other particles that can occupy higher energy modes with a very large number of possible constellations. It is interesting to notice that the formation of a BEC does not require thermal equilibrium [167]. Even far from equilibrium a particle cascade towards the zero momentum state can form and create a macroscopic population of this state [168]. This behaviour is not a result of a finite number of scattering processes in the conventional kinetic theory but needs the summation of a infinite series of processes using the two particle irreducible effective action.

It is unclear which feature defines a BEC for dark matter axions, or especially which feature is crucial for the scenario evoked by Sikivie and collaborators: is it coherence of the axion field or is it the macroscopic occupation of the zero momentum mode? Axions from the misalignment angle mechanism, born as coherent oscillations of the classical axions field, can be described as a classical field and are therefore intrinsically coherent. So if coherence is the crucial feature then no axion thermalisation is needed and the following discussion is beside the point. However if a highly occupied zero momentum state is needed, the momentum distribution of the axion field must be changed. One must make sure that the used interaction actually shifts the axion population into the lowest energy state. Alternatively one can use the fact that Bose-Einstein condensation needs entropy creation (recall that a BEC is the state of highest entropy). The interaction that "thermalises" axions must create enough entropy to form a BEC. In the following we will only treat axions from the misalignment angle mechanism in the cosmological scenario that inflation occurs prior to PQ symmetry breaking and we will be looking for dissipative effects in gravitational interactions.

Finally, we raise a confusing issue about the definition of a BEC in cosmology. A BEC in statistical mechanics is a large number of particles in a δ-function at zero kinetic energy. However, in cosmology, it is unclear how narrow is the energy range for the axions making up the “zero mode”, or BE condensate. At the QCD phase transition, the axions of mass m_a and momentum $H_{\rm QCD}$, have kinetic energy $E_K = H_{\rm QCD}^2/2m_a \ll H_{\rm QCD}$. During radiation domination, the ratio

$$\frac{E_K}{H} \simeq \frac{H_{\rm QCD}}{2m_a} \ll 1 \tag{7.6}$$

remains constant; between matter-radiation equality and today, it increases by a factor $\sqrt{T_{\rm eq}/T_0}$, but does not attain one. Therefore, the Heisenberg uncertainty principle could imply that the age of the Universe is not long enough to distinguish that the axions are not in the zero mode. Does this imply that they are in a BE condensate? Notice that their three-momentum can be distinguished from zero, so if the condensate was defined as the zero-momentum state, then the axions are not in it.

7.2.2 Axions and Gravity, the standard picture

This section will treat the standard picture of gravitational interactions of axions using general relativity and show why we think that a fast gravitational interaction rate is not enough to condense axions into the zero mode. Two different scenarios are considered: axions in a homogeneous and isotropic universe with Friedman Robertson Walker Lemaitre metric (FRWL)

and axions in a universe with small perturbations around its homogeneous background.

Axions in FRWL universe

We will show that the only effect of gravity on the axion field in a homogeneous and isotropic universe is to redshift its momenta but not to change the form of the axion momentum distribution. We will describe the axion field as a massive scalar field in a coherent state on a homogeneous background. To first order this should be an appropriate description for the axion after the QCD phase transition during linear structure formation. The homogeneous and isotropic solution to Einstein's equation is given by the Friedman Robertson Walker Lemaitre metric (here we choose the flat case):

$$ds^s = dt^2 - R^2(t)(dx^2 + dy^2 + dz^2) \ . \tag{7.7}$$

The Lagrangian of a massive scalar field $a(x)$ in a FRWL universe is given by

$$\mathcal{L} = \frac{1}{2}\sqrt{-g}\left[\partial_\mu a \partial^\mu a - \left(m_a^2 + \xi\mathcal{R}(x)\right)a^2\right] \tag{7.8}$$

where the factor containing $g = det(g_{\mu\nu})$ is needed to ensure diffeomorphism invariance of the action. It describes the interaction of the scalar field with the metric, so the gravitational interaction of the scalar field in a general relativistic framework. $\mathcal{R}(x)$ is the Ricci scalar and the term $\xi\mathcal{R}(x)$ describes how the field couples to the curvature. In the following we will adopt the so called minimal coupled case where $\xi = 0$. The equations of motion can be obtained using the Euler-Lagrange equations

$$\partial_\mu\{\sqrt{-g(x)}g^{\mu\nu}(x)\partial_\nu a\} + \sqrt{-g(x)}m_a^2 a = 0 \ . \tag{7.9}$$

Introducing the Laplace operator in curved dimensions

$$\Box a = g^{\mu\nu}\nabla_\mu\nabla_\nu a = \frac{1}{\sqrt{-g}}\partial_\mu\left[\sqrt{-g}g^{\mu\nu}\partial_\nu a\right] \ . \tag{7.10}$$

The equations of motion can then be written

$$\left[\Box + m^2\right]\phi = 0 \ . \tag{7.11}$$

In the case of a homogeneous FRWL metric this simplifies to

$$\ddot{a} + 3H\dot{a} - \frac{1}{R^2(t)}\partial_i\partial_i a + m_a^2 a = 0 \tag{7.12}$$

where $\dot{a} = \partial_t a$. The axion field can be expanded in a set of orthonormal eigenmodes $u_{\vec{k}}(x)$. In a second quantization formalism this can be written as

$$\hat{a}(x) = \sum_{\vec{k}}\left(\hat{b}_{\vec{k}}u_{\vec{k}}(x) + \hat{b}^\dagger_{\vec{k}}u^*_{\vec{k}}(x)\right) \ . \tag{7.13}$$

The creation operators $\hat{b}_{\vec{k}}$ satisfy the canonical commutation relations $[\hat{b}_{\vec{k}}, \hat{b}^\dagger_{\vec{q}}] = \delta_{\vec{k},\vec{q}}$. The axions produced by the misalignment angle mechanism can be described as a coherent state

$$|a\rangle = \frac{1}{N}\exp\left(\sum_{\vec{p}}\tilde{a}(\vec{p},t)\hat{b}^\dagger_{\vec{p}}\right)|0\rangle \ . \tag{7.14}$$

Here N is a normalisation factor so that $\langle a|a\rangle = 1$. The coherent state is characterised by $b_{\vec{k}}|a\rangle = \tilde{a}(p,t)|a\rangle$. The classical axion field is then given by the expectation value of the field operator in the coherent state $a(x) = \langle a|\hat{a}(x)|a\rangle$. In the FRWL universe the eigenmodes can be written using the following ansatz [169]

$$u_{\vec{k}}(x) = \frac{1}{[R(t)L]^{3/2}} e^{i\vec{k}\cdot\vec{x}} \chi_{\vec{k}}(t) \quad . \tag{7.15}$$

The eigenmodes have been normalised to a box of physical volume $(R(T)L)^3$. This kind of separation into time dependent and $\vec{x}$ dependent part is only possible because the metric is homogeneous and isotropic. Plugging the eigenmodes into the equation of motion (7.12) one finds easily

$$\ddot{\chi}_{\vec{k}}(t) + \left[\frac{|\vec{k}|^2}{R^2(t)} + m_a^2 - \frac{3}{4}\left(\frac{\dot{R}}{R^2}\right)^2 - \frac{3}{2}\frac{\ddot{R}}{R}\right]\chi_{\vec{k}}(t) = 0 \quad . \tag{7.16}$$

One can now use the (i,i) component of Einstein's field equations for a perfect fluid with negligible pressure, like it is the case for cold dark matter:

$$2\frac{\ddot{R}}{R^2} + \left(\frac{\dot{R}}{R}\right)^2 \approx 0 \quad . \tag{7.17}$$

This simplifies the equation for χ to

$$\ddot{\chi}_{\vec{k}}(t) + \frac{|\vec{k}|^2}{R^2(t)}\chi_{\vec{k}}(t) + m_a^2\chi_{\vec{k}}(t) \approx 0 \quad . \tag{7.18}$$

Here we are interested in how gravity changes the spectrum of the axion field. It is known that gravity can create particles (e.g. black hole radiation) and change the momentum distribution of particles (e.g. red-shifting of momenta in FRWL cosmologies). These phenomena are normally described by defining two kind of states [169]: the **in** states $u^{\rm in}_{\vec{k}}(x)$ at $t \to -\infty$ and the **out** states $u^{\rm out}_{\vec{k}}(x)$ at $t \to \infty$. Both sets of modes are a complete set of orthogonal modes and can therefore be expanded one as a function of the other. These are the so called Bogolubov transformations:

$$u^{\rm out}_{\vec{k}} = \sum_{\vec{q}} \alpha_{\vec{k}\vec{q}} u^{\rm in}_{\vec{q}} + \beta_{\vec{k}\vec{q}} u^{\rm in,*}_{\vec{q}} \quad . \tag{7.19}$$

It is easy to see that the two sets of modes are different as long as $\beta_{\vec{k}\vec{q}} \neq 0$. For example consider as in state the in-vacuum $|0,{\rm in}\rangle$ which does not contain particles in the remote past. However in the far future the number of particles is determined by using the out-number operator $\hat{N}^{\rm out}_{\vec{k}} = \hat{b}^{\rm out\dagger}_{\vec{k}}\hat{b}^{\rm out}_{\vec{k}}$. The number of particles that a detector will register in the far future is therefore given by

$$N^{\rm out}_{\vec{k}} \;=\; \langle 0,{\rm in}|\hat{N}^{\rm out}_{\vec{k}}|0,{\rm in}\rangle \;=\; \sum_{\vec{q}} |\beta_{\vec{k}\vec{q}}|^2 \quad . \tag{7.20}$$

If this is non zero, particles have been created by gravity! The Bogolubov coefficients contain the information of how gravity modifies the axion spectrum. In our case we are interested in how the momentum distribution of out-state axions has changed compared to the axions in the in-state. We therefore define the **in** modes to be the eigenmodes shortly after QCD phase transition when axions have obtained their mass and started coherent oscillations and the **out** modes at the end of linear structure formation. Both in and out eigenmodes are orthogonal and therefore satisfy the following equations:

$$(u_{\vec{k}}, u_{\vec{q}}) = \delta^3_{\vec{k}\vec{q}}, \quad (u^*_{\vec{k}}, u^*_{\vec{q}}) = -\delta^3_{\vec{k}\vec{q}}, \quad (u_{\vec{k}}, u^*_{\vec{q}}) = 0. \tag{7.21}$$

The parentheses indicate the scalar product in the curved space time. These equations can be used to determine the Bogolubov coefficients from equation (7.19)

$$\alpha_{\vec{k},\vec{q}} = (u^{\text{out}}_{\vec{k}}, u^{\text{in}}_{\vec{q}}) \propto \delta_{\vec{k},\vec{q}} \quad , \quad \beta_{\vec{k},\vec{q}} = -(u^{\text{out}}_{\vec{k}}, u^{\text{in}}_{\vec{q}}) \propto \delta_{\vec{k},-\vec{q}} \ . \tag{7.22}$$

The fact that the Bogolubov coefficients are diagonal is a result of the homogeneous and isotropic metric that we use [169]. The number operator for axions at late times can be written as

$$b^{\text{out}\dagger}_{\vec{k}} b^{\text{out}}_{\vec{k}} = (\alpha_{\vec{k},\vec{k}} b^{\text{in}\dagger}_{\vec{k}} - \beta_{\vec{k},-\vec{k}} b^{\text{in}}_{-\vec{k}})(\alpha^*_{\vec{k},\vec{k}} b^{\text{in}}_{\vec{k}} - \beta^*_{\vec{k},-\vec{k}} b^{\text{in}\dagger}_{-\vec{k}}) \quad . \tag{7.23}$$

We follow that gravity does not change the shape of the axion momentum distribution in a homogeneous and isotropic universe but only redshifts the axion momentum and possibly creates particles. There is no evidence in this calculation that gravity can redistribute the axion momenta.

To estimate the amount of axions created by gravity we have to calculate $\beta_{\vec{k},-\vec{k}}$. However we expect that it is negligible because $H \ll m_a$. For a rough estimate we use the lowest order adiabatic approximation

$$\chi(t) = \frac{1}{\sqrt{2\omega}} e^{i\int^t \omega dt'} \tag{7.24}$$

with $\omega^2 = |\vec{k}|^2/R^2 + m^2$. For $|\vec{k}|^2 \ll m^2$, we obtain by calculating the scalar product of equation (7.22)

$$|\beta_{\vec{k},-\vec{k}}| \ll \frac{H(t_{\text{in}})}{m_a} \quad , \quad \alpha_{\vec{k},\vec{k}} \simeq 1 \tag{7.25}$$

where t_{in} is the starting time of our calculation, shortly after the QCD phase transition. One can therefore neglect gravitational particle production in our period of interest after the QCD phase transition because $H(t_{\text{in}}) \lesssim H_{\text{QCD}} \ll m_a$.

In summary in a homogeneous and isotropic universe there is no evidence that gravity redistributes axion momenta, except for red-shifting all momenta. Also gravitational particle creation is negligible so that the comoving particle density of axions is conserved.

Inhomogeneous universe

As in a homogeneous universe gravity only red-shifts momenta we will now have a look at a cosmological scenario with small fluctuations around the homogeneous case. As long as the perturbations are small gravity is linear in the perturbations. We want to investigate if gravitational interactions can create enough entropy so that axions can form a BEC.

This study starts once again a few Hubble times after the QCD phase transition when the axion mass has settled to its final value m_a. We look at axions from the misalignment angle mechanism and not from cosmic stings. The PQ phase transition will, if inflation happened before it, choose different initial values for the axion field in different Hubble volumes. When these volumes expand, still before the QCD phase transition, the gradient term in the axion energy will erase those differences within each Hubble volume. At the QCD phase transition the axion mass turns on and the axion field starts to oscillate coherently within a Hubble volume. The axion density in each Hubble volume depends on the initial axion value in this volume and will therefore vary from one volume to the other after the QCD phase transition. In the case when PQ phase transition occurs before inflation, the axion field oscillates coherently over the whole universe after QCD phase transition. In this case the axions are probably already in a BEC and further thermalisation is not needed. Therefore we consider the more interesting first case. The axion is described as a classical field which varies randomly from one Hubble

volume to another. It oscillates quickly in time with frequency m_a and more slowly in space with co-moving momentum $H_{\rm QCD}$. It can be expanded in Fourier modes

$$a(\vec{x},t) = \frac{1}{\sqrt{2m_a V R^3(t)}} \sum_p \left[\tilde{a}(\vec{p},t)\exp\{i(\vec{p}\cdot\vec{x}-\omega t)\} + \tilde{a}^*(\vec{p},t)\exp\{-i(\vec{p}\cdot\vec{x}-\omega t)\}\right] \quad (7.26)$$

where $\vec{p}$ is the co-moving three-momentum and the field is normalized in a comoving box of volume V. This is compatible with the description above that the classical axion field is the expectation value of the field operator in the coherent axion state. The fast time dependence $e^{-i\omega t}$ can be approximated by $e^{-im_a t}$ and will be averaged [170, 171] when the much slower spatial evolutions are considered [1]. $\tilde{a}(\vec{p},t)$ can evolve in time on a longer time scale of spatial evolution. Recall that $a(x,t)$ has mass dimension one, so that $\tilde{a}(\vec{p},t)$ is dimensionless. As the axion is a real scalar field, the Fourier coefficients have to satisfy $\tilde{a}(\vec{p},t) = \tilde{a}^*(-\vec{p},t)$. The Fourier transformations are performed in a comoving box $V = L^3$ and defined to be "dimensionless" to simplify dimensional analysis

$$\frac{d^3x}{V} \quad , \text{ and } \quad \sum_p = V\int \frac{d^3p}{(2\pi)^3} \quad . \quad (7.27)$$

The density fluctuations of axions are of $\mathcal{O}(1)$ from one Hubble volume to another. Within one volume the density is constant. We therefore expect the Fourier coefficients $\tilde{a}(\vec{p},t)$ to go to 0 for $|\vec{p}| > H_{\rm QCD}$ and to be constant for $|\vec{p}| < H_{\rm QCD}$ because the Fourier transform of a random distribution is a constant.

Often the axion field is described as a homogeneous field with small fluctuations around its mean value [171]. Such a description can be obtained by averaging the field in equation (7.26) over the universe and considering only fluctuations on large structure scales. For linear structure growth the differences between the two descriptions are negligible.

To describe the behaviour of axions in linear perturbation theory we start by specifying the perturbed metric. We consider only scalar perturbations and choose to write these in Newtonian gauge

$$ds^2 \quad = \quad (1+2\psi)dt^2 - R^2(t)(1-2\phi)\delta_{ij}dx^i dx^j \quad (7.28)$$

where $\psi \approx \phi$ is the Newtonian potential inside the horizon. The scale factor is dimensionless and is set to 1 at the QCD phase transition. To write down Einstein's equations one also needs to specify the energy stress tensor. In the homogeneous case it is described by a perfect fluid

$$T^\alpha_\beta = \text{diag}(\overline{\rho}, -\overline{P}, -\overline{P}, -\overline{P}) \quad (7.29)$$

where $\overline{\rho}$ and $\overline{P}$ are the homogeneous energy density and pressure of the cosmic fluid. Fluctuations around the homogeneous energy momentum tensor can be parametrized using four scalar degrees of freedom.

$$\begin{aligned} \overline{\rho}(t) \to \overline{\rho}(t) + \delta\tilde{\rho}(\vec{k},t) \quad , \quad \overline{P}(t) \to \overline{P}(t) + \delta\tilde{P}(\vec{k},t) \\ ik_j\delta T^0_j = (\overline{\rho}+\overline{P})\theta(\vec{k},t) \quad , \quad (\hat{k}_i\hat{k}_j - \frac{1}{3}\delta_{ij})\delta T^i_j = -(\overline{\rho}+\overline{P})\sigma(\vec{k},t) \end{aligned} \quad (7.30)$$

The perturbation of the energy density is $\delta\tilde{\rho}(\vec{k},t)$ and the pressure perturbation is $\delta\tilde{P}(\vec{k},t)$. $\theta(\vec{k},t)$ describes the longitudinal degree of freedom of the perturbed energy flux δT^0_i, the fluid

1. One can also consider the non-relativistic field and so get rid of the fast time dependence [172]

velocity. $\sigma(\vec{k},t)$ is the scalar anisotropic pressure (or anisotropic stress). In order to determine the behaviour of the axion component of the cosmic fluid we are interested in how these quantities can be related to the axion field. From field theory the energy momentum tensor of a real scalar field is given by

$$T^{\mu}_{\nu} = a^{;\mu}a_{;\nu} - \frac{1}{2}\left(a^{;\alpha}a_{;\alpha} - m_a^2 a^2\right)\delta^{\mu}_{\nu} \quad . \tag{7.31}$$

Comparing this with equation (7.30) we can determine the fluid parameters as a function of the axion field. The homogeneous axion energy density is given by the average of T^0_0. It is therefore the $\vec{p}=0$ Fourier mode of the energy density $\widetilde{\rho}(\vec{p},t)$.

$$\begin{aligned} \overline{\rho}_a(t) &= \int_V \frac{d^3x}{V} T^0_0(\vec{x},t) \\ &\approx \frac{m_a^2}{[R(t)]^3}\sum_q \frac{|\widetilde{a}(\vec{q},t)|^2}{m_a V}\left(1+\frac{q^2}{m_a^2 R(t)^2}\right) \quad . \end{aligned} \tag{7.32}$$

We neglected higher orders of $\frac{q^2}{m_a^2}$ as well as terms containing ϕ, ψ and H and averaged over the fast time dependence. In the following we will only consider the leading order term. As the energy density for the non-relativistic axion field is clearly dominated by the mass density, the average number density of axions is easily obtained by dividing by the mass:

$$n_a(t) = \frac{m_a}{[R(t)]^3}\sum_q \frac{|\widetilde{a}(\vec{q},t)|^2}{m_a V} \quad . \tag{7.33}$$

The Fourier transform of the energy density perturbation can be expressed in the following way

$$\begin{aligned} \delta\widetilde{\rho}_a(\vec{k},t) &= \int \frac{d^3x}{V} e^{-i\vec{k}\cdot\vec{x}}[\rho_a(\vec{x},t) - \overline{\rho}_a(t)] \\ &= \frac{m_a^2}{m_a V[R(t)]^3}\sum_q \widetilde{a}(\vec{q}+\vec{k}/2,t)\widetilde{a}^*(\vec{q}-\vec{k}/2,t) \qquad k \neq 0 \quad . \end{aligned} \tag{7.34}$$

It is important to realize that this expression is quadratic in the axion field and cannot be simplified to the product of the averaged axion field times a fluctuation around it. By consequence the linearised Einstein equations that are linear in $\delta\widetilde{\rho}_a(\vec{k},t)$ are non linear in the axion field. We therefore use the energy density and its perturbation as variables to describe the evolution of the system and not the axion field which would contain more information. This should be an appropriate description as gravity only couples to the energy stress tensor and does not care about what is the origin of the fluid.

The dynamics are described by Einstein's field equations $G_{\mu\nu} = 8\pi G T_{\mu\nu}$ and the energy and momentum conservation equations $T^{\mu}_{\nu;\mu} = 0$. In the homogeneous case the (0,0) component of Einstein's field equations gives the well known first Friedman equation

$$\left(\frac{\dot{R}}{R(t)}\right)^2 \equiv H^2(t) = \frac{8\pi G}{3}(\overline{\rho}_a(t) + \overline{\rho}_{\rm strings}(t) + \overline{\rho}_{\rm rad}(t)) \quad . \tag{7.35}$$

The right hand side contains the averaged densities of all species that are relevant during linear structure formation: axions form misalignment angle mechanism, axions from cosmic string

decays and radiation. The equation describes the expansion of the universe that is driven by the average density of the cosmic fluid. Including small perturbations into Einstein's field equations and separating the homogeneous from the linearised perturbed part gives for the (0,0) component

$$-3H^2(t)\psi(\vec{x},t) - 3H\dot{\phi}(\vec{x},t) + \frac{\Delta\phi(\vec{x},t)}{R^2(t)} = 4\pi G\delta\rho(\vec{x},t). \tag{7.36}$$

Deep inside the casual horizon $|\vec{p}| >> H(t)R(t)$ the first two terms can be neglected

$$-\frac{|\vec{p}|^2}{R^2(t)}\widetilde{\phi}(\vec{p},t) \simeq 4\pi G\delta\widetilde{\rho}(\vec{p},t) \tag{7.37}$$

This is just the Fourier transform of the usual Poisson equation with $\widetilde{\phi}(\vec{p},t)$ being the Newtonian potential of the energy density perturbation. The homogeneous part of the energy density does not contribute to the Newtonian potential.

The off-diagonal part (i,j) of Einstein's field equations vanishes in the homogeneous limit but in the perturbed case it gives

$$k^2(\widetilde{\phi}(\vec{k},t) - \widetilde{\psi}(\vec{k},t)) = 12\pi G R^2(t)(\overline{\rho}+\overline{P})\sigma(\vec{k},t) \quad . \tag{7.38}$$

For a perfect fluid one can show [21] that the anisotropic stress vanishes to first-order [2]. This implies that the two perturbations in the metric can be treated as being equal $\phi = \psi$.

Combining equations from both energy-momentum conservation and Einstein's field equations one gets the usual equation that describes structure growth [171] using $\delta(\vec{k},t) = \delta\widetilde{\rho}_a(\vec{k},t)/\bar{\rho}_a(t)$

$$\ddot{\delta} + 2H\dot{\delta} - 4\pi G\overline{\rho}\delta + c_s^2\frac{k^2}{R^2(t)}\delta = 0 \ . \tag{7.39}$$

The speed of sound is defined as $c_s^2 = \frac{\delta p}{\delta\rho_a}$. This equation is well known in the Newtonian limit and it can be found in [16]. As long as $4\pi G\overline{\rho} > c_s^2\frac{k^2}{R^2(t)}$ the perturbation will grow due to gravitational attraction. In the opposite case the pressure can compensate gravitational attraction and the perturbation oscillates. The wavelength for which both terms are equal is called the Jeans length $\lambda_J \equiv \frac{2\pi R(t)}{k_J}$.

In [171] the speed of sound is calculated in the case that PQ symmetry breaking occurred before inflation and consequently the axion field is homogeneous with small fluctuations: $c_s \approx \frac{k}{2m_a R(t)}$. The Jeans length is then given by

$$\lambda_J(t) \simeq \frac{2\pi}{[16\pi G\overline{\rho}(t)m^2]^{1/4}} \sim \frac{6}{\sqrt{H(t)m}} \quad ; \tag{7.40}$$

It can be checked that the Jeans length is smaller than the size of our solar system, suggesting that axions behave like dust on all cosmologically interesting scales. In the case when inflation happens before PQ symmetry breaking (the case we are interested in) this might be different. However, by dimensional analysis, $\overline{P} \sim \delta P \lesssim \overline{\rho}H^2_{\rm QCD}/m^2$, so naively the differences appear to be insignificant to fluctuation evolution on the comoving scale $H^{-1}_{\rm QCD}$.

2. The energy momentum tensor of a perfect fluid is given by $T^\mu_\nu = -Pg^\mu_\nu + (\rho+P)U^\mu U_\nu$ where U^μ is the four-velocity of the fluid. For a fluid moving with a small coordinate velocity v^i it can be treated as a perturbation of the same order as $\delta\rho$ or ϕ. The expansion of the energy momentum tensor shows that to first order the off diagonal terms are zero and so the anisotropic stress vanishes.

Recall that the fluctuations in the density of the axion field on the scale $H_{\rm QCD}^{-1}$ are of $\mathcal{O}(1)$. After matter-radiation equality, these short-distance fluctuations can grow and promptly decouple from the Hubble flow, to form gravitationally bound axion configurations called "miniclusters" [173]. The position-space perspective on these $\mathcal{O}(1)$ inhomogeneities is instructive. One can estimate that an axion (particle?) with comoving momentum $H_{\rm QCD}$ cannot escape from a fluctuation of comoving size $H_{\rm QCD}^{-1}$ prior to matter-radiation equality. That is, the fluctuations are not damped by free-streaming. If an axion BE condensate should be approximately homogeneous, then it is unclear how the axions making up $\mathcal{O}(1)$ density fluctuations on scales $H_{\rm QCD}^{-1}$ can migrate to the zero-momentum mode, because they do not seem to move fast enough to homogenise in position space.

The two leading order effects of gravity that were described here are: the expansion of the universe equation (7.35) and the growth of small perturbations during matter domination equation (7.39). They are both leading order solutions to time-reversal invariant equations and can therefore not contain dissipation as needed for the formation of a BEC. This means that even though axions interact very quickly, they are not thermalised by their gravitational interactions. In the next paragraph we will try to estimate a process that contains dissipation.

7.2.3 Axion viscosity estimate

In the last section we saw that the off-diagonal entries (i, j) of the energy momentum tensor are not important for the leading order solutions (we have even neglected them claiming axions behave as a perfect fluid). We will therefore try to use these off-diagonal terms to get a hand on dissipative processes. Another observation of the last paragraph is, that to describe the cosmic fluid a perfect fluid was used. Such a fluid does not contain dissipation. If one adds dissipation to a perfect fluid one obtains a so called "imperfect fluid" [174]. On its off diagonal it has a viscosity term. The effect of viscosity is well known: it damps fluctuations on small length scales. Damping fluctuations means to homogenize the axion field and could therefore be a way to condense axions into the zero mode. In this section we will estimate the axion viscosity by comparing the energy momentum tensor of the axion field (including perturbations) with the energy momentum tensor of the imperfect fluid.

The off diagonal entry of the axion energy momentum tensor with a perturbed metric is defined in equation (7.31) and has the form $(i \neq j)$

$$T^i{}_j(\vec{x}, t) = -\frac{(1+2\phi)}{R^2(t)} \partial_i a \partial_j a \quad . \tag{7.41}$$

Writing out the Fourier transform of the axion field and the Newtonian potential yields

$$\begin{aligned} T^i{}_j(\vec{k}, t) \quad = \quad & -\frac{1}{mVR^5(t)} \Bigg[\sum_q (q + k/2)_i (q - k/2)_j \widetilde{a}(\vec{q} + \vec{k}/2, t) \widetilde{a}^*(\vec{q} - \vec{k}/2, t) \\ & + 2 \sum_{p,q} (q + k/2)_i (q + p - k/2)_j \widetilde{\phi}(\vec{p}, t) \widetilde{a}(\vec{q} + \vec{k}/2, t) \widetilde{a}^*(\vec{q} + \vec{p} - \vec{k}/2, t) \Bigg] \end{aligned} \tag{7.42}$$

The first term does not contain the gravitational potential. However we are interested to estimate the axion viscosity arising from gravitational interactions. Therefore in the following we will only focus on the second term that contains $\widetilde{\phi}(\vec{p}, t)$. The only interaction considered here is gravitation. We can therefore be sure that the viscosity estimated in this way has its origin in the gravitational interactions. The energy momentum tensor of an imperfect fluid is given by [174]

$$T^i_j(\vec{x},t) \quad = \quad -\eta(t)(\partial_j U^i(\vec{x},t) + \partial^i U_j(\vec{x},t)) \ . \tag{7.43}$$

Where η is the viscosity coefficient and U_μ is the fluid four velocity that must satisfy the relation $U_\mu U^\mu = 1$. Weinberg defines it from the conserved number current $N^\alpha = nU^\alpha$. However the axion is a real scalar field which does not have a conserved current, so a definition from the energy flux is more convenient: $T^0_i = \rho U^0 U_i$. As discussed with care in Weinberg's paper [174], it is important to use a self-consistent formalism, so we anticipate that our estimate will not have the correct constant factors. We hope that the dependence on physical parameters will nonetheless be correct.

$$U_0 U^i(\vec{x},t) \simeq \frac{-1}{R^2(t)\overline{\rho}(t)} \partial_t a(\vec{x},t)\partial_i a(\vec{x},t) \tag{7.44}$$

Using this definition we obtain the explicit form for the imperfect fluid energy momentum tensor

$$T^i_j(\vec{k},t) \quad = \quad -\frac{\eta(t)}{mVR^5(t)n_a(t)} \sum_q \left[q_i k_j + k_i q_j - k_i k_j\right] \widetilde{a}(\vec{q}+\vec{k}/2,t)\widetilde{a}^*(\vec{q}-\vec{k}/2,t) \ . \tag{7.45}$$

In order to get an approximate analytic expression for η we simply equate the terms in equation (7.45) and equation (7.42) that are proportional to $\sim k_i k_j$. We are not interested in a very accurate value for the viscosity, the order of magnitude is completely sufficient for us. We obtain

$$\frac{\eta(t)}{n_a(t)} \sim -2\pi G \sum_p \frac{\delta\widetilde{\rho}(p,t)R^2(t)}{|\vec{p}|^2} \ . \tag{7.46}$$

The density perturbations $\delta\widetilde{\rho}$ contains contributions from axions as well as radiation and all other species present in the universe. It shows nicely that a viscosity that is caused by gravitational interaction keeps the universal character of gravity.

This estimate used a description of imperfect fluids [174] which can suffer from non-causal information propagation. Such difficulties are avoided with the causal thermodynamics of [175], which adds approximately a factor $(1 + H/\Gamma_g)$ to the right side of equation (7.46), where $\Gamma_g \sim 8\pi G\rho_a m_a R(t)^2/H^2_{\rm QCD}$ is the gravitational interaction rate of axions (see [165]). The correction factor exceeds 2 for $T > 2$keV (for $f_{\rm PQ} \sim 10^{12}$ GeV fixed) and grows linearly with T. However, we neglect this effect, because it never allows the time or length scale of dissipation to reach the horizon, and because axions gravitationally thermalise after $T \sim$ keV in the scenario of Sikivie and collaborators.

The first limiting case that we consider is when the density perturbations are dominated by radiation. Radiation has a scale-invariant power law which means that $\delta\widetilde{\rho}(k,t)/\overline{\rho}(t) = A(k_H/k)^{3/2}$ where $k_H = H(t)\frac{R(t)}{R_{\rm QCD}}$ is the comoving scale at the horizon. One can show that the sum in equation (7.46) is dominated by the infra-red contributions [3]:

$$\left|\frac{\eta(t)}{n_a(t)}\right| \sim 2\pi G \left|\frac{\delta\widetilde{\rho}(H(t)\frac{T_{\rm QCD}}{T},t)}{H^2(t)}\right| \simeq \frac{3}{4}\left|\frac{\delta\widetilde{\rho}(H(t)\frac{T_{\rm QCD}}{T},t)}{\rho(t)}\right| \ . \tag{7.47}$$

One easily sees that $\left|\frac{\eta(t)}{n_a(t)}\right| << 1$ because radiation density perturbations are always much smaller then the radiation background density.

3. The integral gives $V\int_{k_H} d^3p\delta(p,t)/p^2 = 4\pi V k_H A \sim \delta\widetilde{\rho}(k_H,t)/(\overline{\rho}(t)k_H^2)$

In the second case we will assume that the dominant density perturbations come from axions from the misalignment angle mechanism. These perturbations are around the comoving scale of the horizon during the QCD phase transition $H_{\rm QCD}^{-1}$. Therefore the sum in equation (7.46) is dominated by the $p \sim H_{\rm QCD}$:

$$\left|\frac{\eta(t)}{n_a(t)}\right| \sim 2\pi G \left|\frac{\delta\widetilde{\rho}(H_{\rm QCD},t)R^2(t)}{H_{\rm QCD}^2}\right| \lesssim \frac{8\pi G\rho_a(t_{\rm QCD})}{3H_{\rm QCD}^2}\left(\frac{T}{T_{\rm QCD}}\right) = \frac{\rho_a(t_{\rm QCD})}{\rho_{\rm rad}(t_{\rm QCD})}\left(\frac{T}{T_{\rm QCD}}\right) = \frac{T_{\rm eq}T}{T_{\rm QCD}^2} \ . \tag{7.48}$$

where $T_{\rm eq}$ is the temperature at matter radiation equality. Also in this case $\left|\frac{\eta(t)}{n_a(t)}\right| << 1$.

For a given viscosity Weinberg estimates the time-scale that is takes to damp fluctuations of a given length-scale [174].

$$\Gamma \sim \frac{\eta(t)|\vec{p}|^2}{R^2(t)\overline{\rho}(t)} \tag{7.49}$$

Comparing the damping rate to the expansion rate $H(t)$ fixes the length-scale up to which all fluctuaions are damped away within the available time.

$$\ell_{\rm damp}^2(t=1/H) \sim \frac{1}{H(t)m_a}\frac{\eta(t)}{n_a(t)}\frac{\rho_a(t)}{\rho(t)} \tag{7.50}$$

It is not very difficult to see that the damping scale is always smaller than the Jeans length of axions $\lambda_J \sim 1/(\sqrt{H(t)m_a})$. This means that viscosity only damps fluctuations that do not grow during matter domination but the modes that oscillate because of the interplay between gravity and pressure. It is reassuring to know that the damping distance due to viscosity is shorter than the Jeans length.

7.2.4 Discussion

In the following section we will review the basic assumptions and main points of our estimate. After this we will compare our estimate to the calculation done by Saikawa and Yamaguchi in [165] and show how one can make contact between the two estimates.

The question we wanted to answer is if axions from the misalignment angle mechanism condense into a Bose Einstein condensate due to their gravitational interactions. We assume that the PQ symmetry was broken after inflation because in the contrary case almost all axions are already in the same mode with small fluctuations around it. This can already be considered as a BEC. In our case, shortly after the QCD phase transition, the axion field has variations of $\mathcal{O}(1)$ over length-scale $H_{\rm QCD}^{-1}$. As a BEC is the state of maximal entropy we look for dissipative processes in the gravitational interaction of axions. The axions are born as oscillations of a classical field and can be described as a coherent state. From this we infer that the problem can be treated to a very good approximation as a classical problem and all information about gravitational interactions should be given by general relativity. We choose to use the axion energy density as the relevant variable. It is clear that the axion field contains more information but the dynamics are determined by ${T^{\mu\nu}}_{;\mu} = 0$ and Einstein's field equations which only contain the energy momentum tensor and not the field. The advantage of the axion density is that the differential equations that describe the evolution of axions are linear in the axion density (or its perturbations) whereas the equations of motion for the axion field involving gravity are highly non-linear. The leading order solutions tell us that the homogeneous energy density of axions

contributes to the expansion of the universe equation (7.35) whereas its perturbations on scales larger than the Jeans length grow during matter domination equation (7.39). These processes are leading order solutions to time-reversal invariant equations and do therefore not contain dissipative effects. We conclude that dissipation must be a subleading effect in gravitational interactions. To discuss gravitational thermalisation one needs to divide gravity into a leading order part and a dissipative part. We attempt this by looking at the off-diagonal terms of the energy momentum tensor that is normally neglected in the leading order solutions.

The leading order solutions in cosmology are normally obtained by describing the content of the universe as a perfect fluid. If one is interested in dissipation one has to use a imperfect fluid which can still expand the universe and grow density fluctuations but on its off diagonal terms it has viscosity sitting. Viscosity damps fluctuations on small scales and homogenizes the energy density in this way. By estimating the axion viscosity we hope to get our hands on one part of dissipative gravitational interactions. We estimate the axion viscosity by comparing the energy momentum tensor of the axion scalar field with a perturbed metric to the energy momentum tensor of a imperfect fluid. From the viscosity we infer a damping scale up to which perturbations are damped away. We obtain a damping scale that is smaller than the Jeans length and has no influence on cosmological processes. We cannot confirm that gravity creates enough entropy to thermalise axions and to form a BEC.

We want to compare our analysis with the previous papers on this subject [163, 164, 165] to emphasis common points and to explain the differences. We will concentrate on the calculation in [165] because they clearly introduce their formalism for their solid analytical calculation [4] and obtain the same results as the original papers by Sikivie and collaborators. Saikawa and Yamaguchi (SY) calculate the rate of change of the axion number operator in a quantum field theory approach where axions are described as a coherent state of highly populated low-momentum states. Their space time is Minkowski and Gravity is described by Newtonian gravity. The gravitational interaction rate is interpreted as a thermalisation rate that exceeds the expansion rate of the universe at photon temperature ~ 1 keV.

A fist difference is that SY calculate in a Minkowski space with Newtonian gravity in contrast to our general relativity formalism. The gravitational effect of the homogeneous and isotropic axion density is to drive expansion, but since SY calculate with Newtonian gravity in a non-expanding space-time, all the gravitational effects of the axions are included in the "thermalisation" process. However this is not a very important difference because one can simply add scaling factors and replace the axion density by its perturbation in their expression for Newtonian interaction in order to make it consistent with linearised Einstein equations. Recall that also our results are obtained in the limit of fluctuations on scales much smaller then the casual horizon, so the Newtonian limit.

A second difference is that SY use a quantised formalism whereas we use classical field theory. This difference should not be important because SY describe the axions in a coherent state which is usually used to make the limit form quantum field theory to classical field theory. Indeed we can obtain a similar result in our formalism. We calculate the equations of motion in the perturbed universe [5].

$$-m_a^2 a(x) = \Box a(x) = g^{\mu\nu}\nabla_\mu\nabla_\nu a(x) = g^{\mu\nu}(\partial_\mu\partial_\nu a(x) - \partial_\alpha a(x)\Gamma^\alpha_{\mu\nu}) \tag{7.51}$$

where the Christoffel symbols are given by $\Gamma^\alpha_{\mu\nu} = \frac{1}{2}g^{\alpha\beta}(g_{\mu\beta,\nu} + g_{\nu\beta,\mu} - g_{\mu\nu,\beta})$. Plugging the Fourier transform of the field into the equation of motion and keeping only leading order terms

4. In section 7.1 a short overview of this calculation is given
5. We use the metric of equation (7.28) setting $\phi = \psi$.

one obtains

$$i\partial_t \widetilde{a}(\vec{k},t) \approx m_a \sum_{\vec{q}} \widetilde{\phi}(\vec{q},t)\widetilde{a}(\vec{k}-\vec{q},t) \tag{7.52}$$

Using this and the Poisson equation (7.37) to replace $\widetilde{\phi}(\vec{q},t)$ we obtain as similar result as SY:

$$i\frac{\partial}{\partial t}|\widetilde{a}(\vec{q},t)|^2 \simeq 4\pi m G \sum_k \frac{R^2(t)}{|\vec{k}|^2}\delta\rho(\vec{k},t)\left\{\widetilde{a}^*(\vec{q}+\vec{k},t)\widetilde{a}(\vec{q},t) - \widetilde{a}^*(\vec{q},t)\widetilde{a}(\vec{q}-\vec{k},t)\right\} \quad . \tag{7.53}$$

It seems that the difference between a quantum analysis and the our classical analysis can be neglected.

Another difference is that SY find that axions do not interact with photons. This is an important result because a fast interaction of axions with photons would heat axions up to photon temperature. However our analysis shows that the axion viscosity comes form the gravitational interaction of axions with density perturbations including those of photons. This is due to the universal character of gravity that couples to energy densities no matter what their origins are. We interpret that at order G, the axions should have gravitational interactions with the fluctuations in the density of other particles, rather than with the individual particles.

At the end we do not disagree at all with the interaction rate derived by SY, we can even obtain the same rate in our formalism. However we disagree with the interpretation of this rate as a "thermalisation rate". In our interpretation the result of SY means that axions have fast gravitational interactions [6] but does not tell what these interactions do. Whereas the equations of motion for density perturbations tell us that perturbations grow above the Jeans length.

7.2.5 Summary

This work was motivated by the scenario of Sikivie and collaborators which claim that due to gravitational thermalisation axions form a Bose Einstein condensate. Such a BEC develops a different galactic halo structure than WIMPs. This could imply that there exists an observable difference between axions and WIMPs. Our interest focuses on the gravitational thermalisation process.

Our analysis is based prior to non-linear structure formation and we assume that inflation occurs before PQ symmetry breaking. We only consider axions from the misalignment angle mechanism. Therefore shortly after the QCD phase transition the axion density distribution has perturbations of $\mathcal{O}(1)$ on comoving length scales $H_{\rm QCD}^{-1}$ and the typical axion comoving momentum is of the order of $H_{\rm QCD}$. General relativity tells us that the homogeneous axion density participates in the expansion of the universe and the density fluctuations grow. These effects do not contain dissipation and can therefore not drive axions into a BEC, the state of highest entropy. The question is if gravity can in addition to the leading order effects also thermalise axions. To estimate the dissipative gravitational interaction rate of axions we use the off diagonal terms of the energy momentum tensor that is not used for the leading order solutions. Comparing it to the off-diagonal term of the imperfect fluid yields a rough estimate of the axion viscosity. Viscosity is known to damp fluctuations on small scales and could therefore be a way to bring axions into a BEC. The estimated damping scale is however smaller than the Jeans length of axions and we can consequently not confirm the interpretation of [163, 165] that axions migrate to the zero mode (form a Bose Einstein condensate) at a photon temperature $T_\gamma \sim$ keV, due to "gravitational thermalisation". We can reproduce the gravitational interaction rate obtained by [163, 165], but it is unclear to us that this is a thermalisation rate: some of the gravitons should be contributing to the growth of density fluctuations.

6. So to say the emission rate of gravitons by axions is higher than the expansion rate of the universe.

Part IV

Z' project

Chapter 8

Heavy Z': resonant versus non-resonant searches

We turn now to the last research topic of this thesis: new neutral gauge bosons, often called Z'. Collider searches for these new vector particles have mostly been pursued by looking for a peak in the invariant mass spectrum of the decay products. However off-shell Z' exchange may leave an imprint on other kinematic distributions, leading thus to non-resonant searches. The aim of this project is to assess, in the context of the LHC, the interplay between resonant (s-channel) and non-resonant (t-channel) searches for a generic leptophobic Z' model. We show in particular that while non-resonant searches are less sensitive to small couplings, they tend to be more adapted at high masses and large couplings. We discuss our findings both at the level of the current limits and the expectations at higher luminosities.

8.1 Introduction

Additional neutral $U(1)'$ gauge bosons are a well motivated extensions of the SM, appearing in a very large number of different theories. Reviews of new vector particles can be found in [176]. Z' typically appear in extended gauge groups: when the larger gauge group breaks down into the SM gauge groups one often finds additional $U(1)'$ symmetries. However there is a priori no reason that this new symmetry is associated to the TeV scale. If the model is embedded in supersymmetry than the symmetry breaking of the $U(1)'$ is often tied to the soft SUSY breaking scale and expected at the TeV scale. Such a scenario arises naturally in super string theories which involve large symmetry groups that must be broken into the SM gauge groups or in supersymmetric GUT theories, e.g. $SO(10)$ or E_6 based models. Recent examples can be found in [177]. Another possibility are composite models that describe the Higgs as being a pseudo Goldstone boson of a new approximate symmetry. These models often introduce new gauge bosons as well as new fermions around the TeV scale, e.g. [178]. Also in extra dimensional models new neutral gauge bosons can arise. In the simplest case of one extra dimension of radius R which implies the existence of Kaluza-Klein excitations for all states that are allowed to propagate in the bulk. If the SM Z boson propagates in the bulk the presence of a Z' is predicted at mass $\sim 1/R$. Among many other models extra-dimensional frameworks can be found in [179]. The last models we want to mention are connected to dark matter. One assumes a dark matter sector that couples to SM via a Z' boson (see for instance [180]). In this case the Z' can not only be searched for at colliders but can also be constrained by the non-observation of direct detection experiments or indirect dark matter searches.

The range of models involving Z' is large and in almost all models the predicted boson has different couplings to SM particles. Their discovery prospects at the LHC can most often be described in terms of a generic Z' model, which will be our framework for this study. The question we want to address is how can one best constrain Z' particles at the LHC. The number of searches at the LHC is so large that it can be a thorny issue to find the most constraining analysis for a given model of new physics.

In most cases it is assumed that the best chance of catching this vector boson at the LHC is through a resonance search, or in other words by producing directly the particle. This is what we refer to as a s-channel search, since the main diagram is the s-channel one drawn in figure 8.1. In such a case the reach of the LHC will be limited by the probability of the incoming partons to have a center of mass energy higher than the mass of the new particle, which boils down to the pdf (parton distribution functions) of the proton and the beam energy. However, some models can be more elusive to direct production, for instance leptophobic particles escape the cleanest channels at the LHC.

s-channel t-channel

Figure 8.1: s and t channel diagrams mediating the interactions of a Z' particle with SM quarks.

When the vector boson escapes direct production, its exchange may still affect the shape of a given observable, without being produced on-shell. An example is a t-channel exchange, exemplified in the right diagram of figure 8.1, and for this reason we may refer to those searches as t-channel searches [1]. A major point is that processes with many different kinds of initial states can be affected ($uu, ud, \dots$) while direct production requires a particle and its antiparticle as an initial state ($u\bar{u}, d\bar{d}, \dots$), leading thus to higher statistics for t-channel (non-resonant) searches. The aim of this work is to assess, for a generic vector boson, to which extent the t-channel searches can be as powerful, or even better, than s-channel searches. Such attempts have already been carried out in the recent years (see [181]), but either with a specific vector boson or with only part of the relevant analyses at the LHC. Here we have opted for a generic discussion, keeping in mind the aim of comparing the sensitivity of different searches on different regions of the parameter space and what would be their future reach. This chapter is organized as follows: section 8.2 introduces the Z' model that we use, section 8.3 describes the experimental analyses and section 8.4 discusses our results and leads us to the conclusion. More details on how we recast the analyses to constrain our Z' model can be found in the appendix section 8.6.

8.2 Framework

We assume that the new vector boson only decays into SM particles or invisible states, in particular we avoid the case of cascade decays through other exotic particles. Its most generic

1. This dichotomy of s and t searches must be understood as a loose use of the initial word since the diagrams alone are not physically relevant.

definition is then: it is a spin 1 particle with mass M, couplings to all SM particles g_{XX} and width Γ, which only differs from the partial width to SM particles by an invisible width Γ_{inv}. The free parameters are M, g_{XX} and Γ. Such a generic definition does however involve many final states and as such many analyses from the LHC, we have thus decided to consider only couplings to SM fermions, for simplicity. At this point it is known that if the couplings to leptons are not negligible the constraints from LHC resonant searches in dileptons final states (see [182, 183]) are overwhelming: in such a case it is quite unlikely that a non-resonant search could compete. We focus thus on a leptophobic Z' framework, where the only allowed couplings to SM particles are to quarks. It may seem that the framework has been drastically reduced from its initial scope, however it remains an interesting playground for different models, as shown in [184]. A last simplification is to assume that the Dirac structure of the couplings is the same as the Z of the Standard Model, leaving free only one scaling parameter, and to assume this scaling factor to be flavour universal. This restriction allows us to use a minimal set of parameters. Our set-up is summarized by the following Lagrangian :

$$\mathcal{L}_{\text{N.P.}} = \frac{1}{2}F'_{\mu\nu}F'^{\mu\nu} - \frac{1}{2}M^2 Z'_\mu Z'^\nu + \kappa \sum_i \left(g_L^{\text{SM}} \bar{q}_{iL} \not{Z}' q_{iL} + g_R^{\text{SM}} \bar{q}_{iR} \not{Z}' q_{iR} \right) + \mathcal{L}_{\text{inv.}} \tag{8.1}$$

Here, κ refers to the common scaling factor with respect to the Standard Model and $\mathcal{L}_{\text{inv.}}$ deals with the possible interaction with other particles that would be unseen at the LHC. For all practical purposes we will account for this last term simply via a free parameter Γ_{inv}, so that the total width of the Z' can be larger than what would be expected to SM decay modes, making thus its branching fraction to SM particles lower than 100%. Our model is thus fully described by 3 parameters:

$$\kappa,\ M,\ \Gamma_{\text{inv}}.$$

Note that the choice of taking the same Dirac structure as for the standard Z is only made for convenience as it lowers the number of free parameters, and we have checked that taking vector-like couplings would not alter our conclusions. We restrict ourselves to $\kappa > 0$ because in this case the Z' interferes constructively with the SM and the expected signals are stronger. Perturbativity imposes an upper bound on κ, so that the coupling is actually smaller than 4π, which will be the case in our focus range $\kappa < 5$. An important implication of the effective Lagrangian postulated in equation (8.1) is that we do not consider mixing with the standard Z, and consequently there is no constraint coming from electroweak precision tests. This differs from UV-complete models where all the interactions between both Z are taken into account.

Turning now to the LHC analyses, we have considered two representatives of the s-channel: the search for resonances in dijets [185] and in $\bar{t}t$ pairs [186]. Each of them consider the case of a Z' with different widths and variable cross-sections, so that we were able to recast their results as a function of our parameters $(M, \kappa, \Gamma_{\text{inv}})$, up to adjustments that will be addressed in the following section. Those analyses are the most likely to probe a direct production of a leptophobic Z', and are thus a relevant comparison point for the t-channel searches. For the latter we have used the shape analyses of the inclusive jet p_T spectrum [187] and of the dijet angular spectrum [188]. In particular, it is interesting to study the interplay between the p_T spectrum analysis and the angular one, which was solely studied in [181].

The two t-channel analyses focus originally on a model of contact interaction between left handed quarks. We validate our recast of those analyses by re-deriving the bounds on this model. The relevant Lagrangian for the contact interaction between only left handed quarks of

all three families and constructive interference with the SM is

$$\mathcal{L}_{\text{C.I.}} = -\frac{2\pi}{\Lambda^2}(\bar{q}_L\gamma^\mu q_L)(\bar{q}_L\gamma_\mu q_L). \tag{8.2}$$

8.3 Analysis

We will now describe the four experimental analyses on which we have built our results. Since our set-up (defined in equation (8.1)) is not the one used in those analyses, we had to recast them in a consistent way. In this section we describe only very briefly the different analyses, and postpone the details to appendix 8.6.

8.3.1 t-channel: Dijet angular spectrum

The dijet angular distribution has been measured by the ATLAS and CMS collaborations to search for contact interactions between quarks [189, 188]. Both analyses being comparable and giving similar results we considered only one, the CMS angular analysis. CMS uses 2.2 fb^{-1} of $\sqrt{s} = 7$ TeV data. The analysis studies the normalized dijet angular distributions for different invariant mass regions M_{jj}. The used angular variable that is $\chi_{\text{dijet}} = e^{|y_1 - y_2|}$, where y_1 and y_2 are the rapidities of the two highest transverse momentum jets. The normalized angular spectrum is then given by $\frac{1}{\sigma_{\text{dijet}}}\frac{d\sigma_{\text{dijet}}}{d\chi_{\text{dijet}}}$. For the QCD dijet background this normalized angular spectrum is almost flat. New physics like contact interactions or Z' mediated interactions predict a peak of the spectrum at low χ.

We recast the analysis by calculating both background and Z' signal at leading order and consider only events with large invariant mass $M_{jj} > 3$ TeV. Our statistical evaluation follows closely the experimental analysis, as explained in appendix 8.6. We validated our analysis on the same contact interaction model as the CMS study. We find an expected exclusion of $\Lambda^{\text{expct}} = 10.2$ TeV, while the experimental analysis exhibits an expected value of $\Lambda^{\text{expct}} = 10.9$ TeV. We conclude that our analysis is a bit conservative but sufficiently accurate for our goals.

8.3.2 t-channel: Inclusive jet p_T spectrum

Our second t-channel analysis is the search for contact interactions carried by the CMS collaboration in [187]. The aim is to look for a deviation from the QCD prediction in the inclusive jet p_T spectrum, e.g. events as $p + p \to j + X$ where X is any collection of particles, using 5.0 fb^{-1} of $\sqrt{s} = 7$ TeV data. The considered events have a partonic center of mass energy 1 TeV $\lesssim \sqrt{\hat{s}} \lesssim 4$ TeV. While the QCD background happens to be falling exponentially with increasing p_T, the contact interactions will show deviations that are more pronounced at higher p_T.

To adapt the analysis to a Z' search we simulate the Z' signal at leading order (as a difference between Z'+QCD and QCD only cross-sections) and add it to the QCD background calculated at NLO, taken from the experimental analysis. For the statistical evaluation we use a Bayesian method with a flat prior for the Z' mass to calculate the $CL = 95\%$ exclusion mass for a given value of κ. We consider systematic errors from renormalisation/factorisation scale and variations of the pdf sets to construct a covariance matrix that takes correlations between bins into account.

We validate our analysis by comparing once again using the contact interaction model given in equation (8.2). We compute the expected 95% exclusion expected value to be $\Lambda^{\text{expct}} = 15.1$ TeV while the CMS analysis obtains a value of $\Lambda^{\text{expct}} = 13.6$ TeV. Thus, our estimation is slightly more affirmative than its true reach, and we will keep this in mind when turning to the Z' case.

8.3.3 s-channel: Dijet resonance

For our Z' model the most obvious decay channel in a resonant s-channel search is a light quark-antiquark pair, which would manifest itself as a pair of jets with invariant mass equal to M. Such searches have been carried out recently both at ATLAS and CMS, here we will use the analysis described in [189], which searches the dijet invariant mass distribution for peaks. The analysis sets bounds on the quantity $\sigma \times \text{Br} \times \mathcal{A}$ (where $\mathcal{A}$ is the acceptance of the search) on typical Z' particles, the only requirements being that the Z' is produced by $\bar{q}q$ initial states and that its shape is approximately Gaussian. Three different resonance widths are considered, namely $\Gamma/M = 7\%, 10\%, 15\%$. This restricts the recast of our analysis to not too wide Z'. This is to put into perspective with the t-channel case whose reach is independent of the width.

8.3.4 s-channel: $t\bar{t}$ resonance

Both CMS [186, 190] and ATLAS [191, 192] are looking for Z' resonances in the $t\bar{t}$ spectrum. The two top quarks decay into two leptons plus two jets and missing transverse momentum due to neutrinos. We focus on [186] as it uses a similar integrated luminosity than the t-channel analyses. The analysis constrains any massive neutral vector boson that couples to quarks by putting an upper bound on the product of production cross section times branching ratio to tops $\sigma \times \text{Br}$ as a function of the Z' mass M for two different widths $\Gamma/M = 1.2\%$ and $\Gamma/M = 10\%$. This implies that also this analysis can only be used directly for widths that are not much larger than 10%. For larger widths, the exclusion is expected to be weaker, so we have extrapolated an upper bound on the exclusion by taking the limit at $\Gamma/M = 10\%$. For widths in-between 1.2% and 10% we use the less stringent one as a conservative estimate.

8.4 Results

8.4.1 Observed results

We show the observed $CL = 95\%$ exclusion lines in the (M, κ) plane in figure 8.2. This corresponds to the slice $\Gamma_{\text{inv}} = 0$ of our parameter space, the effect of invisible decay channels being discussed later on. We note that the two t-channel analyses give very comparable bounds, which was not granted since they do not yield similar bounds on the contact interaction model. On the s-channel side, the dijet search performs better than the $\bar{t}t$: this is no surprise since it was already the case of a "standard-like" sequential Z'. In the latter case, part of the exclusion line is plotted as dashed, which corresponds to points where the Z' width is larger than the maximal width constrained by the experimental searches. Broader peaks are harder to distinguish from the QCD background and the real limits are probably weaker than our extrapolation. An important point is that low couplings ($\kappa < 2$) are not probed at all by the t-channel analyses, whereas s-channel can be sensitive if the mass is low enough. Overall, a striking feature is that the shape of t and s exclusions stand significantly apart, revealing a different kind of sensitivity.

First, the t-channel limits are best understood by looking at the very high and very low mass regimes. In the limit $M \gg \sqrt{\hat{s}}$ (where $\hat{s}$ is the partonic energy of the events considered), one notices that the exclusion grows linearly with M. This corresponds to the case where the Z' can be integrated out and replaced by a contact interaction, suppressing thus the particular kinematics of a t-channel exchange. In this case the contact interaction is parametrized by only one parameter: κ/M, which justifies the asymptotic behaviour shown in figure 8.2. On the

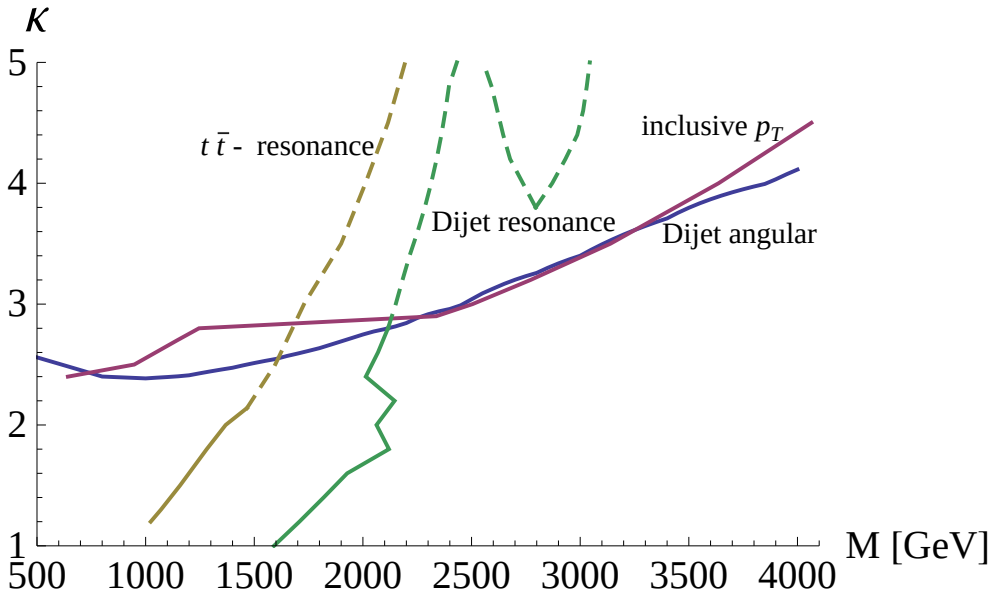

Figure 8.2: The observed exclusion at $CL = 0.95\%$ in the plane $M - \kappa$. The angular dijet and p_t spectrum search correspond to the blue and magenta line, respectively. The brown and green curve are the $t\bar{t}$ and the dijet resonant searches. The dashed lines denote that our extrapolation to large values of κ is done in the best case scenario. In reality the exclusions for large κ are weaker. Points on the left upper side of the lines are excluded.

other hand, for small masses ($M < 1$ TeV) we observe that the exclusion does not improve with decreasing mass. This effect can be tracked down to the kinematics of a t-channel exchange. Unlike the cross section of a contact interaction in the limit $\Lambda \to 0$, the signal cross section of a t-channel Z' exchange does not diverge for $M \to 0$ but saturates to a finite value, as the propagator tends towards $\sim 1/\hat{t}$ ($\hat{t}$ being the Mandelstam variable on partonic level). This is specially relevant for the dijet angular search, since the shape of the distribution becomes flat, just as in QCD, hence the normalized distribution is left unaltered. Since both t-channel analyses have a minimal cut on the $\hat{t}$ variable (through p_T in the inclusive p_T analysis and the angle χ plus the invariant mass $\hat{s}$ in the angular analysis) this also explains that small [2] couplings ($\kappa \sim 1$) are out of reach for the whole mass range, as lowering M under this cut will not increase the signal any more. The first bounds on the Z' mass can be put for $\kappa \geq 2.3$.

The inclusive p_T analysis has a non-trivial feature in the intermediate mass region: the exclusion curve raises suddenly from 1 to 1.2 TeV, and then stays horizontal until 2.0 TeV. This is due to the fact that, even though the jet spectrum is dominated by processes such as $uu \to uu$ due to pdf considerations, a small resonance appears in $\bar{q}q \to \bar{q}q$ for $\frac{1}{4}M \lesssim p_T \lesssim \frac{1}{2}M$. When this resonance falls into one of the first p_T bins of the analysis, the total shape is significantly altered. This occurs since those bins have the largest number of events, so they weight more in the normalization of the shape. The exclusion then gets stronger, all the more since some of those bins have small uncertainties. When M increases again, the resonance goes to higher bins, its effect gets smaller and the exclusion curve goes back to the usual slope.

The s-channel analyses obey quite a different behaviour, in particular at high κ. The sen-

2. Small must be understood here as electroweak-like. This is in contrast with contact interaction models for instance, where κ is much larger than unity.

sitivity is dependent on a subtle mix of theoretical and experimental considerations, which are not obviously deduced from figure 8.2. Indeed the theoretical prediction for mass dependence of the cross-section differs significantly from low κ to high κ: in the first case the width stays small hence the integrated cross-section decreases exactly as the pdf does while in the latter the convolution of a large width resonance with the pdf leads to a much smaller decrease. We reach a similar conclusion here as in [193]. At first glance this would make the s-channels searches quite efficient at high masses, provided κ is large. However, experimental analyses are less sensitive to broad resonances, and in particular the model-independent analysis of ATLAS [194] restricts the integration range to $[0.8, 1.2] \times M$. This reduces the expected signal and thus limits the reach of the s-channel searches. Note that the two experimental s-channel searches only constrain particles with a maximal width $\Gamma/M = 10\%, 15\%$ respectively. For larger widths we extrapolate using a best-case scenario as described in appendix 8.6 but the real exclusion is very likely to be weaker than our estimate (therefore the dashed line).

Comparing s-channel to t-channel searches one finds that for small κ the s-channel searches are more efficient. Due to the small width the signal of a Z' in a resonance search is distributed over very few bins which makes it easy to discriminate against the background. For larger κ the width increases and the signal gets diluted in a resonant search. The t-channel searches are independent of the Z' width and tend to exclude larger masses for larger couplings. In the low mass region s-channel searches are dominant because in this region the t-channel searches are limited by kinematic effects which do not affect the resonant searches. However for large masses the resonant searches are limited by the parton distribution functions. To produce an on-shell resonance one needs an antiquark in the initial state which is highly suppressed for large energies, whereas for a t-channel exchange the Z' does not have to be on-shell and only valence quarks are needed which are less suppressed by pdf.

Extending our conclusion to the whole $(M, \kappa, \Gamma_{\text{inv}})$ space is straightforward. t-channel analyses are blind to Γ_{inv}, so their exclusions stay identical. s-channel analyses will be doubly affected: first because the total width increases and second because the branching ratio to the observable final state decreases. Both effects will contribute to lower the sensitivity of those searches, shifting thus the exclusion lines to lower masses. Note that the second effect occurs only when the width is small as compared to the PDF variation scale, otherwise the narrow-width approximation does not apply and the cross-section starts to be insensitive to the branching ratio. Such an extension does not change the global picture that small values of κ are only constraint by resonant searches whereas for $\kappa \gtrsim 2.5$ non-resonant t-channel searches are more efficient.

8.4.2 Projections at higher luminosities

In figure 8.3 we show the expected exclusions for both t-channel analyses each once with the luminosity used by the experimental study and once with 50 fb^{-1} at the same centre of mass energy $\sqrt{s} = 7$ TeV. A compelling feature is that the angular dijet study can still improve the exclusion at higher luminosity since the dominant uncertainty comes from the low statistics for events with $M_{jj} > 3$ TeV. The inclusive p_T analysis cannot be improved so much by acquiring more statistics since already in its present state the study is dominated by systematic errors. On the s-channel side, the increase of luminosity is expected to have a limited impact since the signal is mainly suppressed by pdf.

Comparing figure 8.2 and figure 8.3 one notices at once that the angular dijet analysis has an observed exclusion that is much more stringent than the expected exclusion. This is consistent with what was observed for contact interactions and is due to the fact that in the two

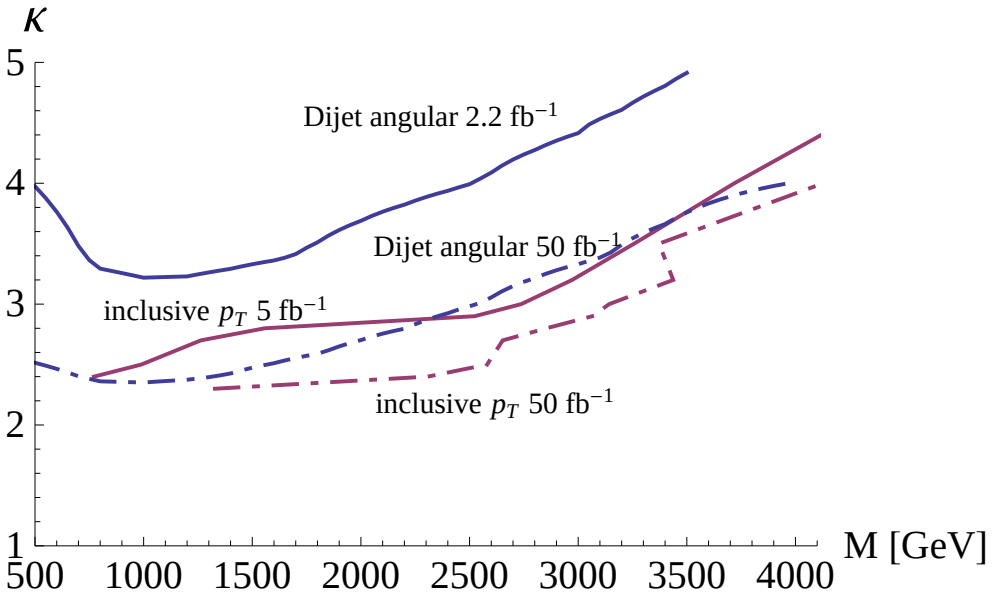

Figure 8.3: The expected exclusions at $CL = 95\%$ for 2.2 fb^{-1} (angular dijet analysis), 5 fb^{-1} (dijet analysis) and the expected exclusions for 50 fb^{-1} (both analysis) with a constant centre of mass energy $\sqrt{s} = 7$ TeV. in the plane M, κ.

lowest χ_{dijet} bins the observed value is below the QCD prediction where new physics gives an enhancement compared to the QCD background.

The expectations at 50 fb^{-1} show, albeit in a very crude way, what could be gained by updating the t-channel searches with the entire dataset of Run I (counting 25 fb^{-1} for ATLAS and CMS each). Although this is already an important indication to what can be gained by taking into account such analyses, it is also tempting to guess what would come from an increase of the center of mass energy such as will occur for the Run II. The gain may seem obvious for s-channels searches since higher invariant masses get accessible, but assessing the ratio of the signal to the background is much more intricate, making a precise prediction tough. For the t-channel analyses, the gain depends on the strategy. For the inclusive p_T study, the deviation of the shape to the QCD background increase with p_T, so that accessing to higher p_T should enhance the sensitivity. This statement must however be qualified, we have noted that for the data presented in [187], most of the exclusion was coming from moderate p_T values, due to statistical and systematic uncertainties in higher bins. The angular dijet analysis can be improved by requiring a higher cut on the invariant mass of the dijet. This will reduce the QCD background but keep the signal constant, in the case where M lies above the cut. If M is lower than the cut, there may not be such enhancement.

8.5 Conclusion

New vector particles appear in many a theory beyond the SM and bear a great discovery potential at the LHC. Such states are traditionally searched for as resonances in the invariant mass spectrum of the decay products. However one can also constrain vector particles by their effect on the shape of a given observable without the need of producing the particle on shell.

These processes involve most of the time a t-channel exchange of the new particle. We compare both methods by testing their exclusion potentials for a sequential Z', with mass M, that only couples to SM quarks with couplings proportional to the SM couplings of the Z boson, κ being the constant of proportionality.

It turns out that the critical variable that determines the strength of the t-channel searches is the coupling strength. Most models proposed in the literature predict Z' couplings to SM quarks of the same order as the SM couplings or even weaker, e.g. in models where the Z' couples to dark matter as well as SM quarks, the couplings to SM must be quite small to avoid exclusion from direct detection experiments. We find that t-channel searches can only constrain Z' models when the couplings are sufficiently large $\kappa \gtrsim 2.3$. For smaller couplings even low masses are not constrained because the propagator then goes like $1/\hat{t}$ and is independent of M. In the case of SM-like or smaller couplings, the s-channel searches are thus more efficient. The situation changes significantly at large couplings since the resonant searches are hampered by the larger width of the Z', which makes it difficult to distinguish from the background. t-channel searches are however independent of the Z' width and tend to exclude larger masses for larger couplings. For couplings $\kappa \gtrsim 2.5$ we find that t-channel searches constrain larger masses than resonant searches. This effect is also due to the pdf suppression for large masses, which is stronger for s-channels than for t-channels because antiquarks in the initial state are not needed in the latter one. The possibility of a coupling to an invisible sector will decrease the reach of s-channel search, leaving t-channel ones unaltered.

8.6 Appendix: Details on analysis recasts

In this section we give more details on the way we recast the experimental analyses in order to constrain our Z' model. For the two t-channel studies we compare our recast to the experimental analyses by constraining the same contact interaction models.

8.6.1 t-channel: Dijet angular spectrum

We recast the CMS analysis [188] that is looking for new physics effects in the normalized dijet angular spectrum. In the case of pure QCD background the normalized dijet angular spectrum is almost flat whereas new physics like contact interactions of Z' are peaked at low χ. As the most stringent bound comes from dijets with high invariant mass $M_{jj} > 3$ TeV, we will only focus on these events. The angular distribution is cut into 7 bins in the region $1 \leq \chi_{\text{dijet}} \leq 16$.

We simulate both our Z' signal and the background at tree level using `CalcHep` [195] and the `CTEQ6L` pdf set [196]. The signal is defined by

$$\sigma^{\text{LO}}_{\text{Signal}} = \sigma^{\text{LO}}_{\text{QCD+Signal}} - \sigma^{\text{LO}}_{\text{QCD}}. \tag{8.3}$$

where the $^{\text{LO}}$ superscript stands for Leading Order, indicating that we used tree-level amplitudes. We do not hadronize our final state and assume that every outgoing quark and gluon produces one jet. Our QCD$^{\text{LO}}$ angular spectrum is in very good agreement with the QCD$^{\text{NLO}}$ spectrum used in the CMS angular analysis.

We follow the statistical procedure of the experimental analysis by using the same statistical test function for a given distribution $dist$ of the data and a given Z' hypothesis Λ consisting of the Z' mass M and the coupling κ (the width is irrelevant in this analysis).

$$Q(dist, \Lambda) = -2 \log \left(\frac{L(dist, \Lambda)}{L(dist, 0)} \right) \tag{8.4}$$

Here 0 is the background only hypothesis, corresponding to $\kappa = 0$. The likelihood L is given by a product of Poisson likelihood functions for each χ_{dijet} bin, with the total number of events kept fixed. To obtain the p-value of our hypothesis, we perform a large number (500 000) of pseudo-experiments for the Λ hypothesis and the 0 hypothesis in order to compute the quantities $P(Q(dist, \Lambda) \geq Q(\text{data}, \Lambda))$ and $P(Q(dist, 0) \geq Q(\text{data}, 0))$ and finally the p-value. The systematic uncertainties are taken from the experimental analysis, up to the correlations between different bins which are not given. We have circumvented the issue by assuming that, since this uncertainty comes mostly from the renormalisation and factorisation scales as indicated by Table 1 of [188], it would be nearly fully correlated, which is supported by the triangular shape of the uncertainty in fig 2 of [188]. In any case, the analysis is clearly dominated by statistical errors, hence the implementation of systematic errors does not change much the exclusion limits. A hypothesis Λ is excluded at 95% confidence level if $CL_s = p < 0.05$.

We validated our analysis on the same contact interaction model as the CMS study. We find an expected (observed) exclusion of $\Lambda^{\text{expct}} = 10.2$ TeV ($\Lambda = 13.4$ TeV), while the experimental analysis exhibits an expected (observed) value of $\Lambda^{\text{expct}} = 10.9$ TeV ($\Lambda = 11.7$ TeV). We conclude that our analysis is sufficiently accurate for our goals.

8.6.2 t-channel: Inclusive jet p_T spectrum

The second t-channel analysis that we use is the search for a deviation in the one jet inclusive p_T spectrum done by CMS [187]. The research is restricted to the region where contact

interactions have the largest effect, $|\eta| < 0.5$. The events are collected in 20 p_t bins in the region 507 GeV $\leq p_T \leq$ 2116 GeV.

We take the QCD$^{\rm NLO}$ background prediction from the CMS p_t analysis which was simulated using `fastNLO` and the `CTEQ6.6` parton distribution functions [197]. We define the Z' signal as previously: $\sigma^{\rm LO}_{Z'} = \sigma^{\rm LO}_{\rm QCD+Z'} - \sigma^{\rm LO}_{\rm QCD}$. This signal is added to the QCD$^{\rm NLO}$ background and then compared to the data.

Our statistical procedure follows the Bayesian method with flat prior used by the experimental analysis as a cross-check. We consider only the shape by normalizing the total number of events to the observed total number of events. We define $\lambda \equiv 1/M^2$ ($\lambda \equiv 1/\Lambda^2$) for the Z' (contact interaction) model. The CL=95% exclusion limit for a fixed value of κ and for a given observed (or expected) distribution *dist* of the data is then defined by

$$\int_0^{\lambda^{95}} \overline{L_{p_t}}(dist|\lambda,\kappa)d\lambda = 0.95 \tag{8.5}$$

where $\overline{L_{p_t}}$ is the marginal likelihood. The likelihood of a distribution *dist* characterized by the number of events in every bin N_j, with $j \in [1, 20]$, given a set of 20 cross section $\vec{\sigma} = (\sigma_j)$, is calculated using the probability density function of a multinomial distribution

$$L_{p_t}(dist, \vec{\sigma}(\lambda,\kappa)) = \frac{N!}{N_1! \cdots N_{20}!} \prod_{j=1}^{20} \left(\frac{\sigma_j(\lambda,\kappa)}{\sigma(\lambda,\kappa)}\right)^{N_j} \tag{8.6}$$

where N is the total number of events and $\sigma(\lambda,\kappa) = \sum_{j=1}^{20} \sigma_j(\lambda,\kappa)$ is the total predicted cross section. The marginal likelihood is then simply the average over $S = 500000$ sets of cross-sections sampled from a multivariate Gaussian distribution incorporating systematic uncertainties

$$\overline{L_{p_t}}(dist|\lambda,\kappa) = \frac{1}{S}\sum_{a=1}^{S} L_{p_t}(dist, \vec{\sigma}_a(\lambda,\kappa)) \quad . \tag{8.7}$$

We construct a 20 dimensional covariance matrix from the errors on the pdfs and from the normalization and factorization scale $\mu_{r,f}$. The latter ones are the dominant source of systematic uncertainties whose effect is to globally shift the predictions in all bins in the same direction. For the variations of $\mu_{r,f}$ we include a k-factor to take into account that we calculate the variations a LO and not at NLO for which the dependence on $\mu_{r,f}$ is smaller than for LO. The value of $k = 0.5$ is determined by fitting our systematic errors to the errors of the CMS analysis on the QCD$^{\rm NLO}$ prediction. Using the covariance matrix we sample S sets of errors that we add to the predicted QCD$^{\rm NLO}$ and Signal cross-sections. These modified cross sections are used to calculate the marginal likelihood.

We validate our analysis by comparing once again using the contact interaction model given in equation (8.2). We compute the expected 95% exclusion (observed) value to be $\Lambda^{\rm expct} = 15.1$ TeV ($\Lambda = 15.6$ TeV). The CMS analysis obtains an expected (observed) exclusion of $\Lambda^{\rm expct} = 13.6$ TeV ($\Lambda = 14.3$ TeV). Thus, our estimation is slightly more affirmative than its true reach, and we will keep this in mind when turning to the Z' case.

8.6.3 s-channel: Dijet resonance

The ATLAS analysis [189] gives the excluded $\sigma \times {\rm Br} \times \mathcal{A}$ as a function of the resonance mass for three different widths, $\Gamma/M = 7\%, 10\%, 15\%$. To set limits on our Z' model we calculate the cross sections for processes of type $pp \to Z' \to q\bar{q}$ using `CalcHep` and the `CTEQ6LL` pdf set. We

apply the same cuts as the experimental analysis and follow their description of how to recast their analysis given in [194] by integrating the cross section only between $0.8M \leq m_{jj} \leq 1.2M$ where m_{jj} is the dijet invariant mass. The intersection of our Z' cross sections with the excluded cross sections from ATLAS gives the $CL = 95\%$ exclusion mass. To give conservative bounds we compare the obtained cross section to the excluded cross section with the next in size width, e.g. models with $7\% < \Gamma/M \leq 10\%$ are constrained using the 10% exclusion values. For models with large widths $\Gamma/M > 15\%$ we can only compare them to 15% exclusion but keeping in mind that the real exclusions will be weaker. Our extrapolation for large widths corresponds to a best case scenario in which the excluded cross section does not change with increasing widths, which is probably much too optimistic.

8.6.4 s-channel: $t\bar{t}$ resonance

To recast the CMS $t\bar{t}$ resonance search [186] we compute the cross section of $pp \to Z' \to t\bar{t}$ using `CalcHep` with the `CTEQ6L` pdf set. In contrast to the CMS analysis we do not include a K-factor for NLO corrections. The way exclusions are extracted is analogue to the dijet resonant analysis. In our Z' model in the case of $\Gamma_{\text{inv}} = 0$, fixing $\Gamma = 0.012\ M$ yields $\kappa = 0.74$ and $\Gamma = 0.1\ M$ yields $\kappa = 2.1$. Couplings smaller than one are not very interesting for our analysis so we do not consider the exclusion line for 1.2% width. The calculated cross sections are compared to the exclusions at 10%. This gives a conservative limit on all widths $\Gamma/M \leq 10\%$. For larger widths the obtained limit is stronger than the real one, corresponding to the best-case scenario.

Conclusion & perspectives

During the three years of my PhD I had the possibility to work on different projects covering a rather large range of extensions of the standard model of particle physics, mostly motivated by cosmological observations. All projects were united in the goal to better constrain these new physics models.

Right-handed neutrinos are a minimal extension of the SM but yet turn out to be potentially very powerful for solving two issues: neutrino masses and the baryon asymmetry of the universe (BAU). By simply adding more than one right-handed neutrino to the SM one can incorporate neutrino masses and naturally explain their smallness compared to other fermion masses via the seesaw mechanism. The seesaw mechanism type I introduces a Dirac mass term m_D but also a Majorana mass term M for the right-handed neutrinos. The diagonalisation of the resulting mass matrix gives light eigenvalues of order m_D^2/M which explain naturally small neutrino masses if M is a large scale. The decays of the heavy right-handed neutrinos can produce a lepton asymmetry which can be transformed into a baryon asymmetry by non-perturbative sphaleron processes. The additional Yukawa couplings introduced for the Dirac mass term are the new source of CP violation needed to produce a large enough asymmetry. In a large number of models among them the simplest ones, the Majorana mass must be far above the TeV scale, which makes observations difficult.

Our aim was to link the BAU to the WIMP relic density. The observed baryon relic density is similar to the dark matter density and the latter one is naturally explained by the WIMP miracle. If the baryon asymmetry is produced in an electroweak-scale-out-of-equilibrium decay and dark matter is made of WIMPs, both relic densities are controlled by electroweak scale interactions going out of equilibrium. This also has the advantage to bring down the scale of leptogenesis to accessible values $\sim$ TeV. We use an inverse seesaw model and extend it by additional light singlets. Our scenario needs CP violation $\mathcal{O}(1)$ to produce a large enough asymmetry. However we can only get such a large asymmetry by fine-tuning the heavy Majorana masses to be degenerate. The interesting property of the inverse-seesaw scenario is that it introduces new particles at the TeV-scale with $\mathcal{O}(1)$ Yukawa couplings making it accessible at collider searches. Unfortunately our scenario requires small Yukawa couplings for wash-out reactions to freeze-out soon enough making our model difficult to test.

Even if the scenario discussed above does not work pretty well, it could still be possible that similar baryon and dark matter densities arise if dark matter is a WIMP and if BAU is produced in out-of-equilibrium decays. When the wash-out reactions that prevent a net baryon asymmetry production freeze-out, the remaining density of baryon-parents is $\sim M/m_W\times$ the WIMP relic density. The similar WIMP and baryon densities could then be explained naturally if the CP violation is of the order m_W/M.

Axions are a very attractive extension of the SM because not only do they solve the strong

CP problem but they can also explain the observed dark matter relic density in the universe. The axion mass and its couplings to SM particles depend only on one parameter f_{PQ}, the scale of the Peccei-Quinn symmetry breaking [1]. Mass and couplings scale like $\sim 1/f_{PQ}$. This makes theoretical predictions of observables quite robust and straight-forward to test. In cosmology a cold axion population can be produced by the misalignment angle mechanism and by cosmic strings that decay into axions. Both give similar contributions to the axion relic density. The axion parameter space is already quite constrained. Astrophysical observations exclude large axion-SM couplings because these would alter the lifetimes of stars. The cosmological relic density constrains small masses because they would produce too much dark matter [2]. The remaining free parameter space is 10^9 GeV $\lesssim f_{PQ} \lesssim 10^{12}$ GeV.

We examined a novel possibility to test the axion dark matter hypothesis against the WIMP hypothesis. Sikivie and collaborators claim that if axions are in a Bose-Einstein condensate (BEC) during non-linear structure formation, they form a different galactic dark matter halo than WIMPs. They further claim that due to fast gravitational interactions axions thermalise at temperatures $T \sim$ keV and form such a condensate. We explored the question whether axions from the misalignment angle mechanism, that can be described as a classical field, form a BEC due to their gravitational interactions. It is well known that a BEC is the state of maximal entropy. Therefore we look for dissipative effects of gravity. Clearly the leading order effects of gravity that are driving expansion and structure formation do not create entropy. We estimate a dissipation scale in the axion fluid due to the anisotropic stress induced by gravitational interactions. We find that this dissipation scale is much too small to be relevant for non-linear structure formation and can therefore not confirm a gravitational thermalisation. Using our formalism we can reproduce the previously estimated fast gravitational interaction rate but we do not see entropy creation associated to it.

The issue of an observable difference in the dark matter halo structure is not yet settled. It is not clear whether an axion BEC is needed for such a difference or if it is sufficient to have non-negligible off-diagonal terms in the axion energy momentum tensor contrary to the dust fluid formed by WIMPs. The classical axion field has such additional terms in the energy momentum tensor. To test if these terms are sufficient one could try to simulate non-linear structure formation taking into account the additional terms in the energy momentum tensor.

Additional heavy neutral gauge bosons like the Z' exist in many extensions of the SM. They typically appear in extensions of the SM gauge group. When the larger gauge group is broken into the SM gauge groups additional $U(1)$ symmetries appear often. Another possibility among many others are extra dimensional models, where those spin 1 particles appear as Kaluza-Klein excitations. The Z' is generally searched for by resonant searches: one looks for a resonance in the invariant mass spectrum of the decay products of the Z'. For this one has to produce the Z' on-shell (s-channel) from a $q\bar{q}$ initial state. However the presence of a Z' can also influence other observables by a non-resonant (t-channel) exchange. This has the advantage that the centre of mass energy can be inferior to the Z' mass and that also qq' initial states contribute. However the cross section is not enhanced by the propagator going on-shell. We compared the exclusion power of both search strategies for a sequential leptophobic Z' with couplings rescaled by a factor κ. We find that for small couplings ($\kappa \lesssim 2.5$) resonant searches are more restrictive but for larger couplings (and larger masses) the situation changes and non-resonant searches are more sensitive. This is not surprising because a large coupling implies a large Z' width

1. There is also a small model dependence that reflects the exact implementation of axions
2. Small masses are possible in the fine tuned case of a very small initial misalignment angle and a vanishing contribution from string decays because the PQ symmetry was broken before inflation.

which makes resonant searches less sensitive whereas non-resonant searches are not affected by the width and are simply more sensitive to larger couplings. Furthermore the pdf suppression of a qq initial state is less important than for a $q\bar{q}$ state which gives another advantage to non-resonant searches.

The non-resonant searches discussed above are not only a powerful tool to search for contact-interactions but they also have a great potential to constrain or to discover heavy Z' with large widths before resonant searches. Once discovered resonant searches are nevertheless essential to determine the exact couplings and mass of the new Z'. Especially the run 2 of the LHC with a larger centre of mass energy will probe new regions in the parameter space with great precision.

These three projects allowed me to study different extensions of the SM of particle physics often motivated by cosmology in a large range of research fields in particle physics, from model-building to experimentally oriented studies. I am very happy that during my PhD I could contribute to current physical research and put my small brick into the great construction that is particle physics.

List of Figures

1.1 Loop contributions to Higgs boson mass 12

2.1 Average binding energy per nucleon 23
2.2 Evolution of the physical wavelength of a perturbation during different stages of expansion 27
2.3 Theoretical sketch of the large scale structure power spectrum 29
2.4 Observed large scale power spectrum 30
2.5 Sketch of the CMB power spectrum and its determining effects 31
2.6 Observed CMB power spectrum by PLANCK 33
2.7 Evidence for dark matter in a galactic rotation curve and the bullet cluster . . . 34
2.8 WIMP freeze-out density 37
2.9 Combined direct dark matter search results 39

3.1 Influence of a non-zero neutrino mass on β-decay spectrum 48
3.2 Neutrinoless double beta decay Feynman digram 54

4.1 Schematic draw of $B + L$ violating processes 63

5.1 Annihilation process 73
5.2 Diagrams contributing to the CP asymmetry with final state $\ell_\alpha + H$. 74
5.3 Diagrams contributing to the CP asymmetry with final state $s_\alpha + \phi$. 74
5.4 Washout scattering process 76
5.5 Parameter space in Majorana case 78
5.6 Parameter space in Dirac case 79

6.1 Axion pion mixing 86
6.2 Axion gluon coupling 87
6.3 Different bounds on the axion parameter space 94
6.4 Constraints on the axion photon coupling 95
6.5 Isocurvature perturbations in the CMB spectrum 96

8.1 s and t channel diagrams mediating the interactions of a Z' particle with SM quarks. 116
8.2 Observed Z' exclusions at $CL = 95\%$ in the plane $M - \kappa$ 120
8.3 Expected Z' exclusions for current and future luminosities 122

Bibliography

[1] S. Davidson and M. Elmer, "Reconstructing Seesaws," Eur. Phys. J. C **71** (2011) 1804 [arXiv:1108.0548 [hep-ph]]. 2

[2] S. Davidson and M. Elmer, "Similar Dark Matter and Baryon abundances with TeV-scale Leptogenesis," JHEP **1210** (2012) 148 [arXiv:1208.0551 [hep-ph]]. 2, 3, 67

[3] S. Davidson and M. Elmer, "Bose Einstein condensation of the classical axion field in cosmology?," JCAP **1312** (2013) 034 [arXiv:1307.8024]. 2, 3

[4] G. D. La Rochelle and M. Elmer, "Heavy Z': resonant versus non-resonant searches," arXiv:1406.2547 [hep-ph]. 2, 3

[5] P. W. Higgs, "Broken symmetries, massless particles and gauge fields," Phys. Lett. **12** (1964) 132. 7

[6] F. Englert and R. Brout, "Broken Symmetry and the Mass of Gauge Vector Mesons," Phys. Rev. Lett. **13** (1964) 321. 7

[7] M. E. Peskin and D. V. Schroeder, "An Introduction to quantum field theory," Reading, USA: Addison-Wesley (1995) 842 p 7

[8] T. P. Cheng and L. F. Li, "Gauge Theory Of Elementary Particle Physics," Oxford, Uk: Clarendon (1984) 536 P. (Oxford Science Publications) 7

[9] C. Itzykson and J. B. Zuber, "Quantum Field Theory," New York, Usa: Mcgraw-hill (1980) 705 P.(International Series In Pure and Applied Physics) 7

[10] S. Chatrchyan *et al.* [CMS Collaboration], "Observation of a new boson at a mass of 125 GeV with the CMS experiment at the LHC," Phys. Lett. B **716** (2012) 30 [arXiv:1207.7235 [hep-ex]]. 10

[11] G. Aad *et al.* [ATLAS Collaboration], "Observation of a new particle in the search for the Standard Model Higgs boson with the ATLAS detector at the LHC," Phys. Lett. B **716** (2012) 1 [arXiv:1207.7214 [hep-ex]]. 10

[12] J. Beringer *et al.* [Particle Data Group Collaboration], "Review of Particle Physics (RPP)," Phys. Rev. D **86** (2012) 010001. 11, 24, 30, 31, 32, 37, 38, 39, 47, 91, 94

[13] E. W. Kolb and M. S. Turner, "The Early universe," Front. Phys. **69** (1990) 1. 15, 20, 27, 28, 35, 57

[14] S. Dodelson, "Modern cosmology," Amsterdam, Netherlands: Academic Pr. (2003) 440 p 15

[15] J. Lesgourgues, "Cosmology, ENS Lyon lecture notes" available on "http://lesgourg.web.cern.ch/lesgourg/courses.html" 15, 26, 27, 28, 29

[16] S. Weinberg, "Gravitation and Cosmology: principles and applications of the general theory of relativity " Jhon Wiley and Sons, Inc. (1972) 657 p 15, 107

[17] P. A. R. Ade *et al.* [Planck Collaboration], "Planck 2013 results. XVI. Cosmological parameters," arXiv:1303.5076 [astro-ph.CO]. 18, 31, 49, 58, 68, 69

[18] S. Sarkar, "Big bang nucleosynthesis and physics beyond the standard model," Rept. Prog. Phys. **59** (1996) 1493 [hep-ph/9602260]. 24

[19] B. D. Fields, "The primordial lithium problem," Ann. Rev. Nucl. Part. Sci. **61** (2011) 47 [arXiv:1203.3551 [astro-ph.CO]]. 24

[20] V. F. Mukhanov, H. A. Feldman and R. H. Brandenberger, "Theory of cosmological perturbations. Part 1. Classical perturbations. Part 2. Quantum theory of perturbations. Part 3. Extensions," Phys. Rept. **215** (1992) 203. 25

[21] C. -P. Ma and E. Bertschinger, "Cosmological perturbation theory in the synchronous and conformal Newtonian gauges," Astrophys. J. **455** (1995) 7 [astro-ph/9506072]. 25, 26, 107

[22] A. D. Linde, "Particle physics and inflationary cosmology," Contemp. Concepts Phys. **5** (1990) 1 [hep-th/0503203]. 28

[23] M. Tegmark *et al.* [SDSS Collaboration], "Cosmological Constraints from the SDSS Luminous Red Galaxies," Phys. Rev. D **74** (2006) 123507 [astro-ph/0608632]. 30

[24] R. K. Sachs and A. M. Wolfe, "Perturbations of a cosmological model and angular variations of the microwave background," Astrophys. J. **147** (1967) 73 [Gen. Rel. Grav. **39** (2007) 1929]. 32

[25] P. A. R. Ade *et al.* [Planck Collaboration], "Planck 2013 results. XV. CMB power spectra and likelihood," arXiv:1303.5075 [astro-ph.CO]. 32, 33

[26] P. A. R. Ade *et al.* [BICEP2 Collaboration], "BICEP2 I: Detection Of B-mode Polarization at Degree Angular Scales," arXiv:1403.3985 [astro-ph.CO]. 33, 96

[27] J.H. Oort. "The force exerted by the stellar system in the direction perpendicular to the galactic plane and some related problems," Bull. Astron. Inst. Netherlands bf 6 (1932) 249 33

[28] F. Zwicky, "Die Rotverschiebung von extragalaktischen Nebeln," Helv. Phys. Acta **6** (1933) 110. 34

[29] K. G. Begeman, A. H. Broeils and R. H. Sanders, "Extended rotation curves of spiral galaxies: Dark haloes and modified dynamics," Mon. Not. Roy. Astron. Soc. **249** (1991) 523. 34

[30] D. Clowe, M. Bradac, A. H. Gonzalez, M. Markevitch, S. W. Randall, C. Jones and D. Zaritsky, "A direct empirical proof of the existence of dark matter," Astrophys. J. **648** (2006) L109 [astro-ph/0608407]. 34

[31] S. 'i. Nojiri and S. D. Odintsov, "Introduction to modified gravity and gravitational alternative for dark energy," eConf C **0602061** (2006) 06 [Int. J. Geom. Meth. Mod. Phys. **4** (2007) 115] [hep-th/0601213]. 35

[32] K. Garrett and G. Duda, "Dark Matter: A Primer," Adv. Astron. **2011** (2011) 968283 [arXiv:1006.2483 [hep-ph]]. 37

[33] B. Kubik "Electroweak symmetry breaking in the light of LHC" PhD Thesis, 2012 38

[34] S. Dodelson and L. M. Widrow, "Sterile-neutrinos as dark matter," Phys. Rev. Lett. **72** (1994) 17 [hep-ph/9303287]. 38

[35] E. Bulbul, M. Markevitch, A. Foster, R. K. Smith, M. Loewenstein and S. W. Randall, "Detection of An Unidentified Emission Line in the Stacked X-ray spectrum of Galaxy Clusters," arXiv:1402.2301 [astro-ph.CO]. 38

[36] A. Boyarsky, O. Ruchayskiy, D. Iakubovskyi and J. Franse, "An unidentified line in X-ray spectra of the Andromeda galaxy and Perseus galaxy cluster," arXiv:1402.4119 [astro-ph.CO]. 38

[37] C. E. Aalseth *et al.* [CoGeNT Collaboration], "CoGeNT: A Search for Low-Mass Dark Matter using p-type Point Contact Germanium Detectors," Phys. Rev. D **88** (2013) 1, 012002 [arXiv:1208.5737 [astro-ph.CO]]. 39

[38] C. E. Aalseth, P. S. Barbeau, J. Colaresi, J. I. Collar, J. Diaz Leon, J. E. Fast, N. Fields and T. W. Hossbach *et al.*, "Search for an Annual Modulation in a P-type Point Contact Germanium Dark Matter Detector," Phys. Rev. Lett. **107** (2011) 141301 [arXiv:1106.0650 [astro-ph.CO]]. 39

[39] R. Bernabei *et al.* [DAMA and LIBRA Collaborations], "New results from DAMA/LIBRA," Eur. Phys. J. C **67** (2010) 39 [arXiv:1002.1028 [astro-ph.GA]]. 39

[40] E. Armengaud *et al.* [EDELWEISS Collaboration], "Final results of the EDELWEISS-II WIMP search using a 4-kg array of cryogenic germanium detectors with interleaved electrodes," Phys. Lett. B **702** (2011) 329 [arXiv:1103.4070 [astro-ph.CO]]. 39

[41] Z. Ahmed *et al.* [CDMS-II Collaboration], "Dark Matter Search Results from the CDMS II Experiment," Science **327** (2010) 1619 [arXiv:0912.3592 [astro-ph.CO]]. 39

[42] R. Agnese *et al.* [SuperCDMSSoudan Collaboration], "CDMSlite: A Search for Low-Mass WIMPs using Voltage-Assisted Calorimetric Ionization Detection in the SuperCDMS Experiment," Phys. Rev. Lett. **112** (2014) 041302 [arXiv:1309.3259 [physics.ins-det]]. 39

[43] E. Armengaud *et al.* [EDELWEISS Collaboration], "A search for low-mass WIMPs with EDELWEISS-II heat-and-ionization detectors," Phys. Rev. D **86** (2012) 051701 [arXiv:1207.1815 [astro-ph.CO]]. 39

[44] Z. Ahmed *et al.* [CDMS and EDELWEISS Collaborations], "Combined Limits on WIMPs from the CDMS and EDELWEISS Experiments," Phys. Rev. D **84** (2011) 011102 [arXiv:1105.3377 [astro-ph.CO]]. 39

[45] R. Agnese *et al.* [CDMS Collaboration], "Silicon Detector Dark Matter Results from the Final Exposure of CDMS II," Phys. Rev. Lett. **111** (2013) 251301 [arXiv:1304.4279 [hep-ex]]. 39

[46] E. Armengaud, Q. Arnaud, C. Augier, A. Benoit, A. Benoit, L. Bergé, T. Bergmann and J. Blümer *et al.*, "Axion searches with the EDELWEISS-II experiment," JCAP **1311** (2013) 067 [arXiv:1307.1488 [astro-ph.CO]]. 39

[47] E. Aprile *et al.* [XENON100 Collaboration], "Dark Matter Results from 225 Live Days of XENON100 Data," Phys. Rev. Lett. **109** (2012) 181301 [arXiv:1207.5988 [astro-ph.CO]]. 40

[48] D. S. Akerib *et al.* [LUX Collaboration], "First results from the LUX dark matter experiment at the Sanford Underground Research Facility," Phys. Rev. Lett. **112** (2014) 091303 [arXiv:1310.8214 [astro-ph.CO]]. 40

[49] C. Weniger, "A Tentative Gamma-Ray Line from Dark Matter Annihilation at the Fermi Large Area Telescope," JCAP **1208** (2012) 007 [arXiv:1204.2797 [hep-ph]]. 40

[50] M. Ackermann *et al.* [Fermi-LAT Collaboration], "Search for Gamma-ray Spectral Lines with the Fermi Large Area Telescope and Dark Matter Implications," Phys. Rev. D **88** (2013) 082002 [arXiv:1305.5597 [astro-ph.HE]]. 40

[51] R. Abbasi *et al.* [ICECUBE Collaboration], "Limits on a muon flux from neutralino annihilations in the Sun with the IceCube 22-string detector," Phys. Rev. Lett. **102** (2009) 201302 [arXiv:0902.2460 [astro-ph.CO]]. 40

[52] O. Adriani *et al.* [PAMELA Collaboration], "Cosmic-Ray Positron Energy Spectrum Measured by PAMELA," Phys. Rev. Lett. **111** (2013) 8, 081102 [arXiv:1308.0133 [astro-ph.HE]]. 40

[53] M. Aguilar *et al.* [AMS Collaboration], "First Result from the Alpha Magnetic Spectrometer on the International Space Station: Precision Measurement of the Positron Fraction in Primary Cosmic Rays of 0.5–350 GeV," Phys. Rev. Lett. **110** (2013) 141102. 40

[54] O. Adriani *et al.* [PAMELA Collaboration], "PAMELA results on the cosmic-ray antiproton flux from 60 MeV to 180 GeV in kinetic energy," Phys. Rev. Lett. **105** (2010) 121101 [arXiv:1007.0821 [astro-ph.HE]]. 40

[55] J. Lesgourgues, G. Mangano, G. Miele and S. Pastor "Neutrino Cosmology," Cambrige University Press (2013) 378 p 41, 44, 49

[56] B. Pontecorvo, "Mesonium and anti-mesonium," Sov. Phys. JETP **6** (1957) 429 [Zh. Eksp. Teor. Fiz. **33** (1957) 549].

[57] B. Pontecorvo, "Inverse beta processes and nonconservation of lepton charge," Sov. Phys. JETP **7** (1958) 172 [Zh. Eksp. Teor. Fiz. **34** (1957) 247]. 42

[58] Z. Maki, M. Nakagawa and S. Sakata, "Remarks on the unified model of elementary particles," Prog. Theor. Phys. **28** (1962) 870. 42

[59] M. Wilking [for the T2K Collaboration], "New Results from the T2K Experiment: Observation of ν_e Appearance in a ν_μ Beam," arXiv:1311.4114 [hep-ex]. 42

[60] L. Wolfenstein, "Neutrino Oscillations in Matter," Phys. Rev. D **17** (1978) 2369.

[61] S. P. Mikheev and A. Y. .Smirnov, "Resonance Amplification of Oscillations in Matter and Spectroscopy of Solar Neutrinos," Sov. J. Nucl. Phys. **42** (1985) 913 [Yad. Fiz. **42** (1985) 1441]. 44

[62] B. T. Cleveland, T. Daily, R. Davis, Jr., J. R. Distel, K. Lande, C. K. Lee, P. S. Wildenhain and J. Ullman, "Measurement of the solar electron neutrino flux with the Homestake chlorine detector," Astrophys. J. **496** (1998) 505. 45

[63] M. Altmann *et al.* [GNO Collaboration], "GNO solar neutrino observations: Results for GNO I," Phys. Lett. B **490** (2000) 16 [hep-ex/0006034]. 45

[64] S. Fukuda *et al.* [Super-Kamiokande Collaboration], "Solar B-8 and hep neutrino measurements from 1258 days of Super-Kamiokande data," Phys. Rev. Lett. **86** (2001) 5651 [hep-ex/0103032]. 45

[65] Q. R. Ahmad *et al.* [SNO Collaboration], "Direct evidence for neutrino flavor transformation from neutral current interactions in the Sudbury Neutrino Observatory," Phys. Rev. Lett. **89** (2002) 011301 [nucl-ex/0204008]. 45

[66] Y. Fukuda *et al.* [Super-Kamiokande Collaboration], "Evidence for oscillation of atmospheric neutrinos," Phys. Rev. Lett. **81** (1998) 1562 [hep-ex/9807003]. 45

[67] Y. Abe *et al.* [DOUBLE-CHOOZ Collaboration], "Indication for the disappearance of reactor electron antineutrinos in the Double Chooz experiment," Phys. Rev. Lett. **108** (2012) 131801 [arXiv:1112.6353 [hep-ex]]. 45

[68] F. P. An *et al.* [DAYA-BAY Collaboration], "Observation of electron-antineutrino disappearance at Daya Bay," Phys. Rev. Lett. **108** (2012) 171803 [arXiv:1203.1669 [hep-ex]]. 46

[69] J. K. Ahn *et al.* [RENO Collaboration], "Observation of Reactor Electron Antineutrino Disappearance in the RENO Experiment," Phys. Rev. Lett. **108** (2012) 191802 [arXiv:1204.0626 [hep-ex]]. 46

[70] M. C. Gonzalez-Garcia, M. Maltoni, J. Salvado and T. Schwetz, "Global fit to three neutrino mixing: critical look at present precision," JHEP **1212** (2012) 123 [arXiv:1209.3023 [hep-ph]]. 46

[71] S. Schael *et al.* [ALEPH and DELPHI and L3 and OPAL and SLD and LEP Electroweak Working Group and SLD Electroweak Group and SLD Heavy Flavour Group Collaborations], "Precision electroweak measurements on the Z resonance," Phys. Rept. **427** (2006) 257 [hep-ex/0509008]. 46

[72] A. Aguilar-Arevalo *et al.* [LSND Collaboration], "Evidence for neutrino oscillations from the observation of anti-neutrino(electron) appearance in a anti-neutrino(muon) beam," Phys. Rev. D **64** (2001) 112007 [hep-ex/0104049]. 47

[73] A. A. Aguilar-Arevalo *et al.* [MiniBooNE Collaboration], "Event Excess in the MiniBooNE Search for $\bar{\nu}_\mu \to \bar{\nu}_e$ Oscillations," Phys. Rev. Lett. **105** (2010) 181801 [arXiv:1007.1150 [hep-ex]]. 46

[74] T. .A. Mueller, D. Lhuillier, M. Fallot, A. Letourneau, S. Cormon, M. Fechner, L. Giot and T. Lasserre *et al.*, "Improved Predictions of Reactor Antineutrino Spectra," Phys. Rev. C **83** (2011) 054615 [arXiv:1101.2663 [hep-ex]].
G. Mention, M. Fechner, T. .Lasserre, T. .A. Mueller, D. Lhuillier, M. Cribier and A. Letourneau, "The Reactor Antineutrino Anomaly," Phys. Rev. D **83** (2011) 073006 [arXiv:1101.2755 [hep-ex]].
P. Huber, "On the determination of anti-neutrino spectra from nuclear reactors," Phys. Rev. C **84** (2011) 024617 [Erratum-ibid. C **85** (2012) 029901] [arXiv:1106.0687 [hep-ph]]. 46

[75] C. Giunti and M. Laveder, "Short-Baseline Electron Neutrino Disappearance, Tritium Beta Decay and Neutrinoless Double-Beta Decay," Phys. Rev. D **82** (2010) 053005 [arXiv:1005.4599 [hep-ph]]. 46

[76] Karlsruhe Tritium Neutrino Experiment, picture from the experiment web page: https://www.katrin.kit.edu/79.php 47, 68, 69

[77] A. van Engelen, R. Keisler, O. Zahn, K. A. Aird, B. A. Benson, L. E. Bleem, J. E. Carlstrom and C. L. Chang *et al.*, "A measurement of gravitational lensing of the microwave background using South Pole Telescope data," Astrophys. J. **756** (2012) 142 [arXiv:1202.0546 [astro-ph.CO]]. 47
48

[78] S. Das, T. Louis, M. R. Nolta, G. E. Addison, E. S. Battistelli, J. R. Bond, E. Calabrese and D. C. M. J. Devlin *et al.*, "The Atacama Cosmology Telescope: temperature and gravitational lensing power spectrum measurements from three seasons of data," JCAP **1404** (2014) 014 [arXiv:1301.1037 [astro-ph.CO]]. 49

[79] J. Hamann, S. Hannestad, G. G. Raffelt and Y. Y. Y. Wong, "Sterile neutrinos with eV masses in cosmology: How disfavoured exactly?," JCAP **1109** (2011) 034 [arXiv:1108.4136 [astro-ph.CO]]. 49

[80] E. Giusarma, E. Di Valentino, M. Lattanzi, A. Melchiorri and O. Mena, "Relic Neutrinos, thermal axions and cosmology in early 2014," arXiv:1403.4852 [astro-ph.CO]. 49, 69

[81] P. Minkowski, "mu –> e gamma at a Rate of One Out of 1-Billion Muon Decays?," Phys. Lett. B **67** (1977) 421. 50

[82] M. Gell-Mann, P. Ramond and R. Slansky, "Complex Spinors and Unified Theories," Conf. Proc. C **790927** (1979) 315 [arXiv:1306.4669 [hep-th]]. 50

[83] T. Yanagida, "Horizontal Symmetry And Masses Of Neutrinos," Conf. Proc. C **7902131** (1979) 95. 50

[84] R. N. Mohapatra and G. Senjanovic, "Neutrino Mass and Spontaneous Parity Violation," Phys. Rev. Lett. **44** (1980) 912. 50

[85] E. Majorana, "Theory of the Symmetry of Electrons and Positrons," Nuovo Cim. **14** (1937) 171. 50

[86] M. C. Gonzalez-Garcia and J. W. F. Valle, "Fast Decaying Neutrinos and Observable Flavor Violation in a New Class of Majoron Models," Phys. Lett. B **216** (1989) 360. 50

[87] J. J. Gomez-Cadenas, J. Martin-Albo, M. Mezzetto, F. Monrabal and M. Sorel, "The Search for neutrinoless double beta decay," Riv. Nuovo Cim. **35** (2012) 29 [arXiv:1109.5515 [hep-ex]]. 53, 67

[88] Sakharov, A. D., "Violation of CP Invariance, C Asymmetry, and Baryon Asymmetry of the Universe", *"Pisma Zh. Eksp. Teor. Fiz."*, **5** (1967) 32-35. 54

[89] S. Davidson, E. Nardi and Y. Nir, "Leptogenesis," Phys. Rept. **466** (2008) 105 [arXiv:0802.2962 [hep-ph]]. 58, 67

[90] A. Y. .Ignatiev, N. V. Krasnikov, V. A. Kuzmin and A. N. Tavkhelidze, "Universal CP Noninvariant Superweak Interaction and Baryon Asymmetry of the Universe," Phys. Lett. B **76** (1978) 436. 59, 63, 65, 66, 67, 138

[91] M. Yoshimura, "Unified Gauge Theories and the Baryon Number of the Universe," Phys. Rev. Lett. **41** (1978) 281 [Erratum-ibid. **42** (1979) 746]. 59

[92] A. Riotto and M. Trodden, "Recent progress in baryogenesis," Ann. Rev. Nucl. Part. Sci. **49** (1999) 35 [hep-ph/9901362]. 59

[93] I. Affleck and M. Dine, "A New Mechanism for Baryogenesis," Nucl. Phys. B **249** (1985) 361. 59

[94] M. Fukugita and T. Yanagida, "Baryogenesis Without Grand Unification," Phys. Lett. B **174** (1986) 45. For a review, see *e.g.* [89]. 59

[95] L. Covi and E. Roulet, "Baryogenesis from mixed particle decays," Phys. Lett. B **399** (1997) 113 [hep-ph/9611425].
A. Pilaftsis, "Heavy Majorana neutrinos and baryogenesis," Int. J. Mod. Phys. A **14** (1999) 1811 [hep-ph/9812256].
A. Pilaftsis and T. E. J. Underwood, "Resonant leptogenesis," Nucl. Phys. B **692** (2004) 303 [hep-ph/0309342]. 59, 68, 70

[96] A. Anisimov, A. Broncano and M. Plumacher, "The CP-asymmetry in resonant leptogenesis," Nucl. Phys. B **737** (2006) 176 [hep-ph/0511248]. 60, 68, 70, 74

[97] V. A. Rubakov and M. E. Shaposhnikov, "Electroweak baryon number nonconservation in the early universe and in high-energy collisions," Usp. Fiz. Nauk **166** (1996) 493 [Phys. Usp. **39** (1996) 461] [hep-ph/9603208]. 60

[98] A. I. Vainshtein, V. I. Zakharov, V. A. Novikov and M. A. Shifman, "ABC's of Instantons," Sov. Phys. Usp. **25** (1982) 195 [Usp. Fiz. Nauk **136** (1982) 553]. 62, 67

[99] Sidney Coleman, "The uses of instantons, in Aspects of Symmetry, " Subnucl. Ser. bf 15 (1979) 805 62

[100] G. 't Hooft, "Symmetry Breaking Through Bell-Jackiw Anomalies," Phys. Rev. Lett. **37** (1976) 8. 62

[101] V. A. Kuzmin, V. A. Rubakov and M. E. Shaposhnikov, "On the Anomalous Electroweak Baryon Number Nonconservation in the Early Universe," Phys. Lett. B **155** (1985) 36. 62, 63

[102] Y. Burnier, M. Laine and M. Shaposhnikov, "Baryon and lepton number violation rates across the electroweak crossover," JCAP **0602** (2006) 007 [hep-ph/0511246].
M. D'Onofrio, K. Rummukainen and A. Tranberg, "The Sphaleron Rate through the Electroweak Cross-over," arXiv:1207.0685 [hep-ph]. 63, 72

[103] S. Weinberg, "The Quantum theory of fields. Vol. 1: Foundations," Cambridge, UK: Univ. Pr. (1995) 609 p 63, 77

[104] S. Davidson and A. Ibarra, "A Lower bound on the right-handed neutrino mass from leptogenesis," Phys. Lett. B **535** (2002) 25 [hep-ph/0202239]. 64

[105] J. R. Ellis, G. B. Gelmini, J. L. Lopez, D. V. Nanopoulos and S. Sarkar, "Astrophysical constraints on massive unstable neutral relic particles," Nucl. Phys. B **373** (1992) 399. 66

[106] T. Asaka, K. Hamaguchi, M. Kawasaki and T. Yanagida, "Leptogenesis in inflaton decay," Phys. Lett. B **464** (1999) 12 [hep-ph/9906366]. 66

[107] A. D. Dolgov, "NonGUT baryogenesis," Phys. Rept. **222** (1992) 309. 66

[108] for a review of cold dark matter, see *e.g.* G. Jungman, M. Kamionkowski and K. Griest, "Supersymmetric dark matter," Phys. Rept. **267** (1996) 195 [hep-ph/9506380].
G. Bertone, D. Hooper and J. Silk, "Particle dark matter: Evidence, candidates and constraints," Phys. Rept. **405** (2005) 279 [hep-ph/0404175]. 67

[109] P. Hut and K. A. Olive, "A Cosmological Upper Limit On The Mass Of Heavy Neutrinos," Phys. Lett. B **87** (1979) 144.
K. Griest and D. Seckel, "Cosmic Asymmetry, Neutrinos and the Sun," Nucl. Phys. B **283** (1987) 681 [Erratum-ibid. B **296** (1988) 1034].
S. Nussinov, "Technocosmology: Could A Technibaryon Excess Provide A 'natural' Missing Mass Candidate?," Phys. Lett. B **165** (1985) 55. 67, 69

[110] D. Hooper, J. March-Russell and S. M. West, "Asymmetric sneutrino dark matter and the Omega(b) / Omega(DM) puzzle," Phys. Lett. B **605** (2005) 228 [hep-ph/0410114].
M. L. Graesser, I. M. Shoemaker and L. Vecchi, "Asymmetric WIMP dark matter," JHEP **1110** (2011) 110 [arXiv:1103.2771 [hep-ph]].
S. B. Gudnason, C. Kouvaris and F. Sannino, "Dark Matter from new Technicolor Theories," Phys. Rev. D **74** (2006) 095008 [hep-ph/0608055].
D. E. Kaplan, M. A. Luty and K. M. Zurek, "Asymmetric Dark Matter," Phys. Rev. D **79** (2009) 115016 [arXiv:0901.4117 [hep-ph]].
A. Belyaev, M. T. Frandsen, S. Sarkar and F. Sannino, "Mixed dark matter from technicolor," Phys. Rev. D **83** (2011) 015007 [arXiv:1007.4839 [hep-ph]].
K. Kamada and M. Yamaguchi, "Asymmetric Dark Matter from Spontaneous Cogenesis in the Supersymmetric Standard Model," Phys. Rev. D **85** (2012) 103530 [arXiv:1201.2636 [hep-ph]]. 67, 69

[111] E. J. Chun, "Minimal Dark Matter and Leptogenesis," JHEP **1103** (2011) 098 [arXiv:1102.3455 [hep-ph]].
Z. Kang, J. Li, T. Li, T. Liu and J. Yang, "Asymmetric Sneutrino Dark Matter in the NMSSM with Minimal Inverse Seesaw," arXiv:1102.5644 [hep-ph].
A. Falkowski, J. T. Ruderman and T. Volansky, "Asymmetric Dark Matter from Leptogenesis," JHEP **1105** (2011) 106 [arXiv:1101.4936 [hep-ph]]. 67, 69

[112] Y. Cui, L. Randall and B. Shuve, "A WIMPy Baryogenesis Miracle," arXiv:1112.2704 [hep-ph]. 67, 69

[113] J. McDonald, "Simultaneous Generation of WIMP Miracle-like Densities of Baryons and Dark Matter," arXiv:1108.4653 [hep-ph].
J. McDonald, "Baryomorphosis: Relating the Baryon Asymmetry to the 'WIMP Miracle'," Phys. Rev. D **83** (2011) 083509 [arXiv:1009.3227 [hep-ph]].
J. McDonald, "Right-handed sneutrino condensate cold dark matter and the baryon-to-dark matter ratio," JCAP **0701** (2007) 001 [hep-ph/0609126]. 67, 69

[114] E. Komatsu *et al.* [WMAP Collaboration], "Seven-Year Wilkinson Microwave Anisotropy Probe (WMAP) Observations: Cosmological Interpretation," Astrophys. J. Suppl. **192** (2011) 18. [arXiv:1001.4538 [astro-ph.CO]]. 67, 69

[115] F. Iocco, G. Mangano, G. Miele, O. Pisanti and P. D. Serpico, "Primordial Nucleosynthesis: from precision cosmology to fundamental physics," Phys. Rept. **472** (2009) 1 [arXiv:0809.0631 [astro-ph]]. 68

[116] A. Mirizzi, N. Saviano, G. Miele and P. D. Serpico, "Light sterile neutrino production in the early universe with dynamical neutrino asymmetries," arXiv:1206.1046 [hep-ph]. 69

[117] G. R. Farrar and G. Zaharijas, "Dark matter and the baryon asymmetry," Phys. Rev. Lett. **96** (2006) 041302 [hep-ph/0510079]. 69

[118] M. T. Frandsen and S. Sarkar, "Light asymmetric dark matter," DESY-PROC-2010-03. M. T. Frandsen at the DMUH11 workshop at CERN; http://indico.cern.ch/conferenceDisplay.py?ovw=True&confId=110992 69

[119] M. Claudson, L. J. Hall and I. Hinchliffe, "Cosmological Baryon Generation At Low Temperatures," Nucl. Phys. B **241** (1984) 309. 69

[120] T. Hambye, "Leptogenesis at the TeV scale," Nucl. Phys. B **633** (2002) 171 [hep-ph/0111089]. 70

[121] S. K. Kang and C. S. Kim, "Extended double seesaw model for neutrino mass spectrum and low scale leptogenesis," Phys. Lett. B **646**, 248 (2007) [hep-ph/0607072].
M. Hirsch, J. W. F. Valle, M. Malinsky, J. C. Romao and U. Sarkar, "Thermal leptogenesis in extended supersymmetric seesaw," Phys. Rev. D **75** (2007) 011701 [hep-ph/0608006].
E. J. Chun, "TeV leptogenesis in Z-prime models and its collider probe," Phys. Rev. D **72** (2005) 095010 [hep-ph/0508050]. 70

[122] M. C. Gonzalez-Garcia, J. Racker and N. Rius, "Leptogenesis without violation of B-L," JHEP **0911** (2009) 079 [arXiv:0909.3518 [hep-ph]]. 70

[123] S. Blanchet, T. Hambye and F. -X. Josse-Michaux, "Reconciling leptogenesis with observable mu $\to$ e gamma rates," JHEP **1004** (2010) 023 [arXiv:0912.3153 [hep-ph]]. 70

[124] J. Garayoa, M. C. Gonzalez-Garcia and N. Rius, "Soft leptogenesis in the inverse seesaw model," JHEP **0702** (2007) 021 [hep-ph/0611311].
S. Blanchet, P. S. B. Dev and R. N. Mohapatra, "Leptogenesis with TeV Scale Inverse Seesaw in SO(10)," Phys. Rev. D **82** (2010) 115025 [arXiv:1010.1471 [hep-ph]]. 70

[125] M. Frigerio, T. Hambye and E. Ma, "Right-handed sector leptogenesis," JCAP **0609** (2006) 009 [hep-ph/0603123]. 70

[126] H. Zhang, "Light Sterile Neutrino in the Minimal Extended Seesaw," arXiv:1110.6838 [hep-ph]. 70

[127] F. del Aguila and J. A. Aguilar-Saavedra, "Distinguishing seesaw models at LHC with multi-lepton signals," Nucl. Phys. B **813** (2009) 22 [arXiv:0808.2468 [hep-ph]].
A. G. Akeroyd, C. -W. Chiang and N. Gaur, "Leptonic signatures of doubly charged Higgs boson production at the LHC," JHEP **1011** (2010) 005 [arXiv:1009.2780 [hep-ph]].
A. Das and N. Okada, "Inverse Seesaw Neutrino Signatures at LHC and ILC," arXiv:1207.3734 [hep-ph]. 70

[128] M. Malinsky, T. Ohlsson, Z. -z. Xing and H. Zhang, "Non-unitary neutrino mixing and CP violation in the minimal inverse seesaw model," Phys. Lett. B **679** (2009) 242 [arXiv:0905.2889 [hep-ph]].
F. Deppisch, T. S. Kosmas and J. W. F. Valle, "Enhanced mu- - e- conversion in nuclei in the inverse seesaw model," Nucl. Phys. B **752** (2006) 80 [hep-ph/0512360].
W. Abdallah, A. Awad, S. Khalil and H. Okada, "Muon Anomalous Magnetic Moment and mu -> e gamma in B-L Model with Inverse Seesaw," arXiv:1105.1047 [hep-ph].
P. S. B. Dev and R. N. Mohapatra, "TeV Scale Inverse Seesaw in SO(10) and Leptonic Non-Unitarity Effects," Phys. Rev. D **81** (2010) 013001 [arXiv:0910.3924 [hep-ph]].
M. Hirsch, T. Kernreiter, J. C. Romao and A. Villanova del Moral, "Minimal Supersymmetric Inverse Seesaw: Neutrino masses, lepton flavour violation and LHC phenomenology," JHEP **1001** (2010) 103 [arXiv:0910.2435 [hep-ph]].
A. Abada, C. Biggio, F. Bonnet, M. B. Gavela and T. Hambye, "Low energy effects of neutrino masses," JHEP **0712** (2007) 061 [arXiv:0707.4058 [hep-ph]]. 70

[129] E. Ma, "Verifiable radiative seesaw mechanism of neutrino mass and dark matter," Phys. Rev. D **73** (2006) 077301 [hep-ph/0601225]. 70, 71

[130] D. Schmidt, T. Schwetz and T. Toma, "Direct Detection of Leptophilic Dark Matter in a Model with Radiative Neutrino Masses," Phys. Rev. D **85** (2012) 073009 [arXiv:1201.0906 [hep-ph]].
R. Bouchand and A. Merle, "Running of Radiative Neutrino Masses: The Scotogenic Model," JHEP **1207** (2012) 084 [arXiv:1205.0008 [hep-ph]].
E. Ma, A. Natale and A. Rashed, "Scotogenic A_4 Neutrino Model for Nonzero θ_{13} and Large δ_{CP}," arXiv:1206.1570 [hep-ph]. 70

[131] C. Arina, F. Bazzocchi, N. Fornengo, J. C. Romao and J. W. F. Valle, "Minimal supergravity sneutrino dark matter and inverse seesaw neutrino masses," Phys. Rev. Lett. **101** (2008) 161802 [arXiv:0806.3225 [hep-ph]].
H. An, P. S. B. Dev, Y. Cai and R. N. Mohapatra, "Sneutrino Dark Matter in Gauged Inverse Seesaw Models for Neutrinos," Phys. Rev. Lett. **108** (2012) 081806 [arXiv:1110.1366 [hep-ph]]. 70

[132] J. E. Kim, "Light Pseudoscalars, Particle Physics and Cosmology," Phys. Rept. **150** (1987) 1. 70

[133] N. Arkani-Hamed, D. P. Finkbeiner, T. R. Slatyer and N. Weiner, "A Theory of Dark Matter," Phys. Rev. D **79** (2009) 015014 [arXiv:0810.0713 [hep-ph]]. 71

[134] S. Y. .Khlebnikov and M. E. Shaposhnikov, "The Statistical Theory of Anomalous Fermion Number Nonconservation," Nucl. Phys. B **308** (1988) 885.
J. A. Harvey and M. S. Turner, "Cosmological baryon and lepton number in the presence of electroweak fermion number violation," Phys. Rev. D **42** (1990) 3344. 73

[135] S. D. Shapiro, S. A. Teukolsky and I. Wasserman "Do Neutrino Rest Masses Affect Cosmological Helium Production?" Phys. Rev. Lett. **45** (1980) 669-672 75, 77

[136] G. G. Raffelt, "Stars as laboratories for fundamental physics: The astrophysics of neutrinos, axions, and other weakly interacting particles," Chicago, USA: Univ. Pr. (1996) 664 p 78

[137] V. Baluni, "CP Violating Effects in QCD," Phys. Rev. D **19** (1979) 2227. 85, 91, 92

[138] H. -Y. Cheng, "The Strong CP Problem Revisited," Phys. Rept. **158** (1988) 1. 85

[139] S. Weinberg, "The U(1) Problem," Phys. Rev. D **11** (1975) 3583. 85

[140] P. Sikivie, "The pooltable analogy to axion physics," [hep-ph/9506229] 86

[141] R. D. Peccei and H. R. Quinn, "Constraints Imposed by CP Conservation in the Presence of Instantons," Phys. Rev. D **16** (1977) 1791. 86

[142] R. D. Peccei, "The Strong CP problem and axions," Lect. Notes Phys. **741** (2008) 3 [hep-ph/0607268]. 86, 89

[143] J. E. Kim, "Weak Interaction Singlet and Strong CP Invariance," Phys. Rev. Lett. **43** (1979) 103. 86

[144] M. A. Shifman, A. I. Vainshtein and V. I. Zakharov, "Can Confinement Ensure Natural CP Invariance of Strong Interactions?," Nucl. Phys. B **166** (1980) 493. 86

[145] S. Weinberg, "A New Light Boson?," Phys. Rev. Lett. **40** (1978) 223. 86

[146] F. Wilczek, "Problem of Strong p and t Invariance in the Presence of Instantons," Phys. Rev. Lett. **40** (1978) 279. 89

[147] A.P. Zhitnitskii, Yad. Fiz. **31** (1980) 497 (Sov. J. Phys. 31, 260). 89

[148] M. Dine, W. Fischler and M. Srednicki, "A Simple Solution to the Strong CP Problem with a Harmless Axion," Phys. Lett. B **104** (1981) 199. 89

[149] E. Masso, F. Rota and G. Zsembinszki, "On axion thermalization in the early universe," Phys. Rev. D **66** (2002) 023004 [hep-ph/0203221]. 89

[150] S. Chang and K. Choi, "Hadronic axion window and the big bang nucleosynthesis," Phys. Lett. B **316** (1993) 51 [hep-ph/9306216]. 90

[151] S. Hannestad, A. Mirizzi and G. Raffelt, "New cosmological mass limit on thermal relic axions," JCAP **0507** (2005) 002 [hep-ph/0504059]. 90

[152] S. Hannestad, A. Mirizzi, G. G. Raffelt and Y. Y. Y. Wong, "Neutrino and axion hot dark matter bounds after WMAP-7," JCAP **1008** (2010) 001 [arXiv:1004.0695 [astro-ph.CO]]. 90

[153] E. Masso and R. Toldra, "New constraints on a light spinless particle coupled to photons," Phys. Rev. D **55** (1997) 7967 [hep-ph/9702275]. 90

[154] T. Hiramatsu, M. Kawasaki, T. Sekiguchi, M. Yamaguchi and J. 'i. Yokoyama, "Improved estimation of radiated axions from cosmological axionic strings," Phys. Rev. D **83** (2011) 123531 [arXiv:1012.5502 [hep-ph]]. 90

[155] P. Sikivie, "Axion Cosmology," Lect. Notes Phys. **741** (2008) 19 [astro-ph/0610440]. 92

[156] G. G. Raffelt, "Astrophysical axion bounds," Lect. Notes Phys. **741** (2008) 51 [hep-ph/0611350]. 92

[157] M. Fouche *et al.* [BMV Collaboration] "Search for photon oscillations into massive particles," Phys. Rev. D **78** (2008) 032013
P. Pugnat *et al.* [OSQAR Collaboration], "First results from the OSQAR photon regeneration experiment: No light shining through a wall," Phys. Rev. D **78** (2008) 092003
K. Ehret *et al.* [ALPS Collaboration] "New ALPS Results on Hidden-Sector Lightweights," Phys. Lett. B **689** (2010) 149 92

[158] E. Arik *et al.* [CAST Collaboration], "Probing eV-scale axions with CAST," JCAP **0902** (2009) 008
S. Aune *et al.* [CAST Collaboration], "CAST search for sub-eV mass solar axions with 3He buffer gas," Phys. Rev. Lett. **107** (2011) 261302 93

[159] G. G. Raffelt, "Axions, Motivation, Cosmological Role and Experimental Searches, " Talk at BLV 2013, MPIK Heidelberg 93

[160] S. J. Asztalos, R. F. Bradley, L. Duffy, C. Hagmann, D. Kinion, D. M. Moltz, L. JRosenberg and P. Sikivie *et al.*, "An Improved RF cavity search for halo axions," Phys. Rev. D **69** (2004) 011101 95

[161] M. Beltran, J. Garcia-Bellido and J. Lesgourgues, "Isocurvature bounds on axions revisited," Phys. Rev. D **75** (2007) 103507 [hep-ph/0606107]. 93

[162] P. A. R. Ade *et al.* [Planck Collaboration], "Planck 2013 results. XXII. Constraints on inflation," arXiv:1303.5082 [astro-ph.CO]. 95

[163] P. Sikivie and Q. Yang, "Bose-Einstein Condensation of Dark Matter Axions," Phys. Rev. Lett. **103** (2009) 111301 [arXiv:0901.1106 [hep-ph]]. 95, 96

[164] O. Erken, P. Sikivie, H. Tam and Q. Yang, "Cosmic axion thermalization," Phys. Rev. D **85** (2012) 063520 [arXiv:1111.1157 [astro-ph.CO]]. 99, 100, 111, 112

[165] K. 'i. Saikawa and M. Yamaguchi, "Evolution and thermalization of dark matter axions in the condensed regime," Phys. Rev. D **87** (2013) 085010 [arXiv:1210.7080 [hep-ph]]. 99, 100, 111

[166] T. Noumi, K. 'i. Saikawa, R. Sato and M. Yamaguchi, "Effective gravitational interactions of dark matter axions," arXiv:1310.0167 [hep-ph]. 99, 100, 109, 110, 111, 112
100

[167] A. J. Leggett, "Bose-Einstein condensation in the alkali gases: Some fundamental concepts," Rev. Mod. Phys. **73** (2001) 307 [Erratum-ibid. **75** (2003) 1083]. 101

[168] J. Berges and D. Sexty, "Bose condensation far from equilibrium," Phys. Rev. Lett. **108** (2012) 161601 [arXiv:1201.0687 [hep-ph]]. 101

[169] N. D. Birrell and P. C. W. Davies, "Quantum Fields in Curved Space," 1982 , Cambridge Monogr.Math.Phys.. 103, 104

[170] M. S. Turner, "Coherent Scalar Field Oscillations in an Expanding Universe," Phys. Rev. D **28** (1983) 1243. 105

[171] J. -c. Hwang and H. Noh, "Axion as a Cold Dark Matter candidate," Phys. Lett. B **680** (2009) 1 [arXiv:0902.4738 [astro-ph.CO]]. 105, 107

[172] Y. Nambu and M. Sasaki, "Quantum Treatment of Cosmological Axion Perturbations," Phys. Rev. D **42** (1990) 3918. 105

[173] C. J. Hogan and M. J. Rees, "Axion Miniclusters," Phys. Lett. B **205** (1988) 228. 108

[174] S. Weinberg, "Entropy generation and the survival of protogalaxies in an expanding universe," Astrophys. J. **168** (1971) 175. 108, 109, 110

[175] R. Maartens, "Causal thermodynamics in relativity," [astro-ph/9609119]. 109

[176] T. Appelquist, B. A. Dobrescu and A. R. Hopper, "Nonexotic neutral gauge bosons," Phys. Rev. D **68** (2003) 035012 [hep-ph/0212073].
P. Langacker, "The Physics of Heavy Z' Gauge Bosons," Rev. Mod. Phys. **81** (2009) 1199 [arXiv:0801.1345 [hep-ph]]. 115

[177] Y. Li, F. Petriello and S. Quackenbush, "Reconstructing a Z-prime Lagrangian using the LHC and low-energy data," Phys. Rev. D **80** (2009) 055018 [arXiv:0906.4132 [hep-ph]].
E. Salvioni, G. Villadoro and F. Zwirner, "Minimal Z-prime models: Present bounds and early LHC reach," JHEP **0911** (2009) 068 [arXiv:0909.1320 [hep-ph]].
L. Basso, A. Belyaev, S. Moretti, G. M. Pruna and C. H. Shepherd-Themistocleous, "Z' discovery potential at the LHC in the minimal $B-L$ extension of the Standard Model," Eur. Phys. J. C **71** (2011) 1613 [arXiv:1002.3586 [hep-ph]].
R. Diener, S. Godfrey and T. A. W. Martin, "Unravelling an Extra Neutral Gauge Boson at the LHC using Third Generation Fermions," Phys. Rev. D **83** (2011) 115008 [arXiv:1006.2845 [hep-ph]].
E. Accomando, A. Belyaev, L. Fedeli, S. F. King and C. Shepherd-Themistocleous, "Z' physics with early LHC data," Phys. Rev. D **83** (2011) 075012 [arXiv:1010.6058 [hep-ph]].
A. Belyaev, S. F. King and P. Svantesson, "Little Z' models," Phys. Rev. D **88** (2013) 3, 035015 [arXiv:1303.0770 [hep-ph]]. 115

[178] R. Contino, T. Kramer, M. Son and R. Sundrum, "Warped/composite phenomenology simplified," JHEP **0705** (2007) 074 [hep-ph/0612180].
D. Barducci, A. Belyaev, S. De Curtis, S. Moretti and G. M. Pruna, "Exploring Drell-Yan signals from the 4D Composite Higgs Model at the LHC," JHEP **1304** (2013) 152 [arXiv:1210.2927 [hep-ph]].
J. de Blas, J. M. Lizana and M. Perez-Victoria, "Combining searches of Z' and W' bosons," JHEP **1301** (2013) 166 [arXiv:1211.2229 [hep-ph]].
D. Barducci, S. De Curtis, K. Mimasu and S. Moretti, "Multiple Z' -> t-tbar signals in a 4D Composite Higgs Model," Phys. Rev. D **88** (2013) 074024 [arXiv:1212.5948 [hep-ph]]. 115

[179] K. Agashe, H. Davoudiasl, S. Gopalakrishna, T. Han, G. -Y. Huang, G. Perez, Z. -G. Si and A. Soni, "LHC Signals for Warped Electroweak Neutral Gauge Bosons," Phys. Rev. D **76** (2007) 115015 [arXiv:0709.0007 [hep-ph]].
G. Cacciapaglia and B. Kubik, "Even tiers and resonances on the Real Projective Plane," JHEP **1302** (2013) 052 [arXiv:1209.6556 [hep-ph]]. 115

[180] A. Alves, S. Profumo and F. S. Queiroz, "The dark $Z^{'}$ portal: direct, indirect and collider searches," JHEP **1404** (2014) 063 [arXiv:1312.5281 [hep-ph]].
G. Arcadi, Y. Mambrini, M. H. G. Tytgat and B. Zaldivar, "Invisible Z' and dark matter: LHC vs LUX constraints," JHEP **1403** (2014) 134 [arXiv:1401.0221 [hep-ph]].
O. Lebedev and Y. Mambrini, "Axial Dark Matter: the case for an invisible Z'," arXiv:1403.4837 [hep-ph]. 115

[181] H. An, X. Ji and L. -T. Wang, "Light Dark Matter and Z' Dark Force at Colliders," JHEP **1207** (2012) 182 [arXiv:1202.2894 [hep-ph]]. 116, 117

[182] S. Chatrchyan *et al.* [CMS Collaboration], "Search for heavy narrow dilepton resonances in pp collisions at $\sqrt{s} = 7$ TeV and $\sqrt{s} = 8$ TeV," Phys. Lett. B **720** (2013) 63 [arXiv:1212.6175 [hep-ex]]. 117

[183] [ATLAS Collaboration], "Search for high-mass dilepton resonances in 20 fb^{-1} of pp collisions at $\sqrt{s} = 8$ TeV with the ATLAS experiment," ATLAS-CONF-2013-017. 117

[184] B. A. Dobrescu and F. Yu, "Coupling-mass mapping of dijet peak searches," Phys. Rev. D **88** (2013) 3, 035021 [arXiv:1306.2629 [hep-ph]]. 117

[185] S. Chatrchyan *et al.* [CMS Collaboration], "Search for narrow resonances using the dijet mass spectrum in pp collisions at $\sqrt{s}$=8 TeV," Phys. Rev. D **87** (2013) 11, 114015 [arXiv:1302.4794 [hep-ex]]. 117

[186] S. Chatrchyan *et al.* [CMS Collaboration], "Search for Z ' resonances decaying to $t\bar{t}$ in dilepton+jets final states in pp collisions at $\sqrt{s} = 7$ TeV," Phys. Rev. D **87** (2013) 072002 [arXiv:1211.3338 [hep-ex]]. 117, 119, 126

[187] S. Chatrchyan *et al.* [CMS Collaboration], "Search for contact interactions using the inclusive jet p_T spectrum in pp collisions at $\sqrt{s} = 7$ TeV," Phys. Rev. D **87** (2013) 5, 052017 [arXiv:1301.5023 [hep-ex]]. 117, 118, 122, 124

[188] S. Chatrchyan *et al.* [CMS Collaboration], "Search for quark compositeness in dijet angular distributions from pp collisions at $\sqrt{s} = 7$ TeV," JHEP **1205** (2012) 055 [arXiv:1202.5535 [hep-ex]]. 117, 118, 124

[189] G. Aad *et al.* [ATLAS Collaboration], "ATLAS search for new phenomena in dijet mass and angular distributions using pp collisions at $\sqrt{s} = 7$ TeV," JHEP **1301** (2013) 029 [arXiv:1210.1718 [hep-ex]]. 118, 119, 125

[190] S. Chatrchyan *et al.* [CMS Collaboration], "Searches for new physics using the $t\bar{t}$ invariant mass distribution in pp collisions at $\sqrt{s} = 8$ TeV," Phys. Rev. Lett. **111** (2013) 211804 [arXiv:1309.2030 [hep-ex]]. 119

[191] G. Aad *et al.* [ATLAS Collaboration], "Search for $t\bar{t}$ resonances in the lepton plus jets final state with ATLAS using 4.7 fb^{-1} of pp collisions at $\sqrt{s} = 7$ TeV," Phys. Rev. D **88** (2013) 1, 012004 [arXiv:1305.2756 [hep-ex]]. 119

[192] The ATLAS collaboration, "A search for $t\bar{t}$ resonances in the lepton plus jets final state with ATLAS using 14 fb^{-1} of pp collisions at $\sqrt{s} = 8$ TeV," ATLAS-CONF-2013-052. 119

[193] B. Díaz and A. R. Zerwekh, "Axigluon Phenomenology using ATLAS dijet data," Int. J. Mod. Phys. A **28** (2013) 1350133 [arXiv:1308.0166 [hep-ph]]. 121

[194] G. Aad *et al.* [ATLAS Collaboration], "Search for New Physics in the Dijet Mass Distribution using 1 fb^{-1} of pp Collision Data at $\sqrt{s} = 7$ TeV collected by the ATLAS Detector," Phys. Lett. B **708** (2012) 37 [arXiv:1108.6311 [hep-ex]]. 121, 126

[195] A. Belyaev, N. D. Christensen and A. Pukhov, "CalcHEP 3.4 for collider physics within and beyond the Standard Model," Comput. Phys. Commun. **184** (2013) 1729 [arXiv:1207.6082 [hep-ph]]. 124

[196] J. Pumplin, D. R. Stump, J. Huston, H. L. Lai, P. M. Nadolsky and W. K. Tung, "New generation of parton distributions with uncertainties from global QCD analysis," JHEP **0207** (2002) 012 [hep-ph/0201195]. 124

[197] P. M. Nadolsky, H. -L. Lai, Q. -H. Cao, J. Huston, J. Pumplin, D. Stump, W. -K. Tung and C. -P. Yuan, "Implications of CTEQ global analysis for collider observables," Phys. Rev. D **78** (2008) 013004 [arXiv:0802.0007 [hep-ph]]. 125